BINDING SERVICES
Tel +44 (0)29 2087 4949
Fax +44 (0)29 20371921
e-mail bindery@cardiff.ac.uk

C A R D I F F
U N I V E R S I T Y

WELSH SCHOOL OF ARCHITECTURE

The Architectural Science Group

Investigations into Mitigating the Heat Island Effect through Green Roofs and Green Walls

Eleftheria Alexandri

13th July, 2005

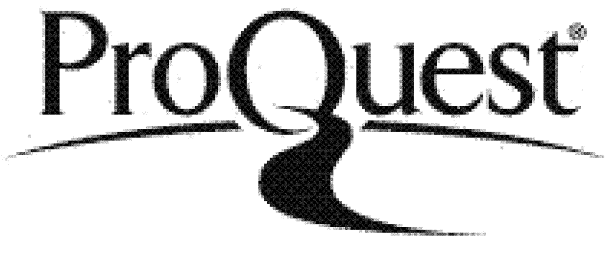

ProQuest LLC
789 East Eisenhower Parkway
P.O. Box 1346
Ann Arbor, MI 48106-1346

Summary

This thesis investigates the thermal effect of green roofs and green walls on the built environment and investigates whether they could be used in existing cities so as mitigate the heat island effect. In order to estimate this for various climates, a prognostic, micro-scale, two-dimensional heat and mass transfer model has been developed. In the first chapter the aim, objectives and methodology of the research are established. In the second chapter a literature review of the causes and the consequences of the heat island effect is made, as well as a critique on the use of urban parks for mitigating raised urban temperatures. In the third chapter, a research is carried on where, when and why roofs and walls were covered with vegetation. In the fourth chapter the development of the one-dimensional model is presented, for heat and mass transfer in building materials, soils, plants and the air. The model is validated with an experiment conducted at a concrete and a vegetated test cell. A comparison is made between green roofs and conventional concrete ones, as well as with white coated roofs for different climates. In the fifth chapter the one-dimensional model is developed into a two-dimensional one and the microclimatic heat and mass transfer model of a typical urban canyon is established. In the sixth chapter, the model is used to investigate the effect of green roofs and green walls for various climates, geometries, canyon orientations and wind directions. From this parametric analysis, an investigation is done on how the raised urban temperatures could lower when the building envelope is covered with vegetation, which could lead to energy savings for cooling and more comfortable outdoor conditions. In the last chapter, conclusions are drawn from the results of this thesis and further research is proposed.

Acknowledgements

I would like to thank Phil Jones for his guidance and everything he has taught me all these years. I would also like to thank Mike Fedeski for our conversations on the subject of my thesis. Sylvia Harris, our Librarian, for always informing me when she came across new articles and books on green roofs and walls. My enormous gratitude to Panagiotis Doussis for his help and contribution in modelling in C and to Vassilios Raptis for checking the algorithms developed in this study. I am indebted to Judi Loach, Norma Roberts, Katrina Lewis, Vicki Stevenson and Toby Adam for proof-reading this thesis. Many thanks to my sister, Eftychia Alexandri, and her husband, André Quicheron, for their hospitality all the times I was visiting libraries in Paris and to Panagiotis Papagiannis for lending me his computer while I was in Athens.

Regarding the experimental part of this work, many thanks to Huw Jenkins for his help, Delta-T for hiring a porometer to us, to Dave Reid for his help with the concrete slabs. My gratitude to the people who carried them to the roof, and to Georgia Alexandri and Orestis Antoniou for helping me construct the test cells.

I would like to thank the State Scholarship Foundation of Greece (IKY), without whose funding this work would have never started. My extreme gratitude to the people working in the Alumni Office of Cardiff University (Sarah Price, Roz Kilcourse, Shân Dawson), for working with them after my funding had finished, and for the beautiful moments we shared together. My gratefulness to the staff of Aberconway Library, especially to Pat Redford, with whom I worked for a year.

Many thanks to the people who believed in my work for giving me strength; to the people who did not believe in it, for making me stronger.

At last, but the most, to my partner, Tasos Lampropoulos, for being an inspiration to anything I do, for his love, support and shelter all these years, to my family for their enormous support and my friends. Many thanks to Gareth Blake and his partner, Patrick Myall, for their support, and for the spiciness that Gareth's cooking added to my life in Cardiff.

This thesis has been funded by the State Scholarship Foundation of Greece (IKY) from 2001 to 2003. Afterwards, through selling my labour force to various places.

Declaration

This work has not previously been accepted in substance for any degree and is not being concurrently submitted in candidature for any degree.

Signed .....

Date 13.7.2005

Statement 1

This thesis is the result of my investigation, except where otherwise stated.

Other sources are acknowledged by footnotes giving explicit references. A bibliography is appended.

Signed .....

Date 13.7.2005

Statement 2

I hereby give consent for my thesis, if accepted, to be available for photocopying and for inter-library loan, and for the title and summary to be made available to outside organisations.

Signed .....

Date 13.7.2005

Il y a des fleurs partout pour qui veut bien les voir.[1]

Henri Matisse

To my grandmother, Eleftheria, and her sisters, who would turn the most unfriendly urban and rural environments into gardens, with their patience, love and determination.

To my parents, Christos and Lamprini.

To my partner, Tasos.

[1] There are flowers everywhere, for those who want to see them.

Table of Contents

List of Tables

List of Figures

Chapter 1

Introduction

1 Introduction

> Let us not, however, flatter ourselves too much as to our victories over nature. For each one of these, it takes its revenge. Initially, each victory certainly has the consequences which we anticipated, but at a second or third move, it has effects that are so different, so unforeseen, that too often the initial achievement is destroyed.
>
> Engels, The Dialectics of Nature

Since the beginning of their existence, human beings have been living together, to protect themselves from dangers from other species and natural hazards. Their homes, either in caves or man-made, have been modified so as to shelter themselves from climatic conditions in which they feel uncomfortable as species (e.g. extreme temperatures, humidity, rainfall). Even from the first evidence of Neolithic houses and settlements, it is obvious that they were not sited in a purely natural environment, but in a part of nature transformed according to a human plan (Benevolo, 1980). With the evolution of human societies, settlements were transformed, evolved into villages, towns or cities, or stayed the same, according to the geographical, economic, social and cultural transformations which took place throughout time.

Cities were formed as fully-fledged places of settlements, where certain categories of work were carried out by people who were not working the land, but were supported by the surplus produced by the cultivators. They were first established around the fertile, well-irrigated areas of the Nile and the Mesopotamia. Cities in these areas date from 4,000 BC and by the beginning of the third millennium BC Sumerian cities contained tens of thousands of people, covering an area of the order of 100 hectares (Benevolo, 1980). As the economy was mostly based on agricultural production, cities evolved mostly in fertile areas, replacing pre-existing forms of life (e.g. vegetation), and altering the environment of those locations, as life moved from agricultural activities to more "urban" ones. According to the geological, historical and economic circumstances, they either faded away or evolved into today's modern urban spaces (Figure 1).

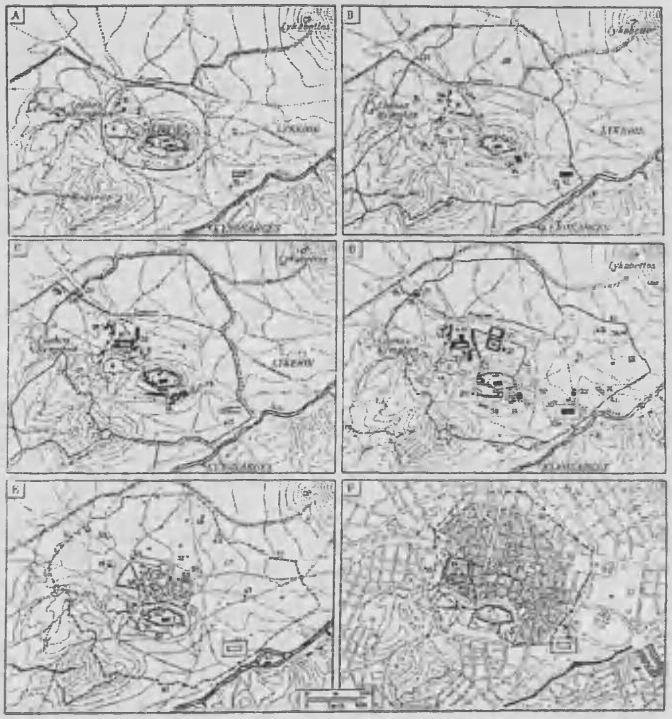

Figure 1. Evolution of the city of Athens; A. Classical era, 6th century BC, B. Classical era, 5th century BC, C. Hellenistic era, D. Roman era, E. Medieval era, F. Modern era (Benevolo, 1980)

Since the Industrial Revolution, urban areas have expanded dramatically as labour was needed in the new working domains located in the cities. New technologies, materials, activities and demands managed to significantly differentiate the urban space from the rural one, displacing most forms of natural habitats and open spaces. In the industrial world, cities evolved much faster in the 19th and 20th century and expanded over larger areas than in previous times. In the instance of the evolution of Athens (Figure 1) it can be noticed that the city's growth in modern times (panel F) is much more different and faster than its evolution from classical ancient to medieval era (panels A to E); the expansion of the city within a single century cannot be compared with any of its previous evolutionary periods. The large areas modern cities occupy, their structure, materials used and the general lack of vegetation cannot but have altered the climatic characteristics of urban spaces.

These changes have a direct effect on the local climate of urban spaces, especially the central parts of the city, causing a significant rise of the urban air temperature and other alterations, known as the *heat island effect*. This temperature rise in the urban environment has a direct effect on the energy consumption for heating and cooling of buildings as well as on the thermal comfort and even the thermal stress of the inhabitants. Especially for cities in climates with a distinct hot season, this may cause serious local climatic and health problems (Koppe et al., 2004; White et al., 2001); the

moderation of extreme heat in the local environment of such climates could mean not only their sustainable survival, but also the potential of occupying them without the morbidity and mortality risks caused by excessive heat (Diaz et al., 2005; Davis et al., 2003). Apart from the health risks, the heat island effect also raises energy demand for cooling to very crucial levels (Santamouris, 2001; Akbari et al., 2001). In the instance, of Athens, where the city centre's temperature is elevated by 12°C in summers, compared to its suburban areas (Santamouris, 2001), it is impossible to talk about passive cooling strategies for urban buildings, before mitigating these extremely raised temperatures.

On prima facie evidence, the general lack of vegetation in existing cities might be one of the factors affecting the formation of raised temperatures. In most cities, appreciable amounts of vegetation exist mostly concentrated in parks or recreational spaces. Depending on the history and development of the city and its relationship with botanic gardens in medieval times and the 19th century naturalist movement (Laurie, 1979), the amount of vegetation and its relationship with the urban fabric varies significantly for cities around the world. These scattered patches of greenery may have a beneficial effect on the local climate of their vicinity (Givoni, 1998; Santamouris, 2001), but not on the whole of the city, as will be examined in the following chapter. With the raised temperatures of the building fabric, there is very little these vegetated pockets can do to lower urban temperatures; the main spaces where people live and work, buildings, are exposed to excessive solar gains and raised temperatures.

However, if vegetation was placed as close to the building fabric as possible, the thermal benefits of plants could be sensed around the building itself. In general, vegetation has a lower temperature than most building materials, due to its responses to weather changes; its surface temperature is not higher than air temperature, being 20-35°C less than commonly used urban materials (Scudo et al., 2004). Plants, being living creatures, tend to keep their temperature within a range which allows them to survive (approximately 5-40°C for most species (Gates, 1980)). For raised surrounding temperatures, most plants maintain their temperature at the desired level through evapotranspiring water. It is estimated that the rate of water loss from leaves is often 50% or more of that from a piece of wet paper with the same size, shape and exposure (Rutter, 1975), although the pores through which evaporation happens, stomata, account only for up to 1% of the total leaf area. In this way they manage to

be very high-tech climatic regulators; the amount of water released into the atmosphere is the exact amount needed to keep their temperatures at desired levels of less than 40°C for most species (Gates, 1980). These temperature levels are closer to the ones characterised as comfortable for the human life than the elevated surface temperatures (up to 80°C) of urban materials (Konopacki et al., 1998).

This technique of placing vegetation as close to the building as possible is a passive cooling strategy used in vernacular architecture of temperate and tropical climates. Vegetation has been used to modify the microclimate around the building in the form of open or courtyard gardens, or in the form of arbours and pergolas (Sullivan, 2002) or as ivies covering walls (Woodell, 1979), or as green roofs (Osmundson, 1999) for centuries. However, in most existing cities, there is not so much free space available to be vegetated, nor would small gardens affect high rise buildings. Therefore this study focuses on the reintroduction of vegetation in the widely available and quite spacious surfaces of most existing cities; roofs and walls.

Due to economic and social factors, the tendency is for urban population to augment significantly. According to statistics, in mid-2004, 48% of the total world population (6.396 billion people) lived in urban spaces (Population Reference Bureau, 2004). By comparison, in the year 1950 only 30% of the 2.5 billion people were urban dwellers (Figure 2) (Population Reference Bureau, 2000). It is estimated that by the year 2030 more than 60% of the world's population will be living in urban spaces (Nash and De Souza, 2002), as there is no sign of the shift from rural to urban spaces of slowing or reversing (Ashford, 2004). As the magnitude of the heat island effect (heat island intensity) strongly depends on the urban population (Oke, 1987), as cities grow larger, more serious manifestations of the heat island effect are expected to occur; cities will expand occupying more of the rural space around them and maybe the green areas inside them, as has been the case of Athens (Kafkoula, 1990). As cities in the developing world, in hot climates are expected to grow significantly (Low et al., 2000), they are bound to suffer from unbearably raised temperatures. A major issue is therefore to manage to alter the physical factors which cause the formation of the heat island effect in the urban environment, in which almost half the population of the planet resides.

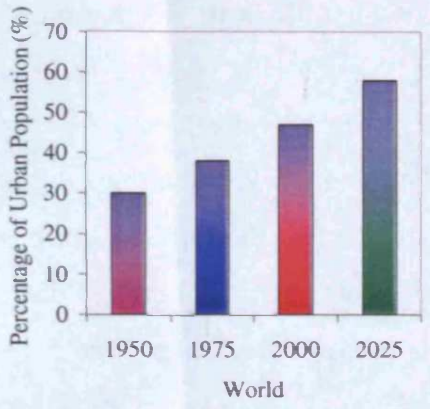

Figure 2. Percentage of population living in urban areas, in 1950, 1975, 2000 and 2025 (after Population Reference Bureau, 2000)

1.1 Aims

The aim of this study is to examine quantitatively how the heat island effect can be reduced in cities if their building fabric, mainly the roofs and walls of buildings, are covered with vegetation. It will assess the potential for cooling urban spaces from ground covering vegetation on the building envelope, which does not add to the static load of the building significantly. This study will examine the effect for different climatic characteristics and urban geometries.

1.2 Objectives

The objectives of this study are:

- Literature review on the heat island effect and how it can be mitigated, and an investigation of how and when buildings have been covered with vegetation throughout time and climates,
- Developing a two-dimensional model which describes in detail heat and mass transfer in a typical urban canyon, when walls and roofs are covered with vegetation,
- Calibration of this model, with an experiment and
- Application of the model to assess the potential of lowering urban temperatures through green roofs and green walls.

A literature review is carried out on the factors which affect the formation of the heat island effect (chapter 2) so as to comprehend how the heat island effect can be tackled. The factors affecting the formation of the heat island effect are analysed, divided into two main categories; physical and chemical ones. Physical factors are the ones affecting the physical phenomena taking place in the urban fabric (e.g. momentum, heat and mass transfer), while chemical factors are the ones produced or affecting chemical processes (e.g. pollutants in the atmosphere, smog). By covering the building fabric with vegetation, most of the physical factors important for the formation of the heat island effect, such as optical properties of the surface, heat capacity, surface roughness, porosity and evaporation can be altered, causing new thermal balances. Existing studies of mitigating the heat island effect and the effect of urban parks on city temperatures are also investigated.

Covering the building fabric with vegetation, in its alive or dry form, is not a novelty of the 21st century, as will be discussed in chapter 3. Since the first man-made structures, vegetation has been used as an element of the building fabric throughout different climates and societies in both vernacular and monumental architecture. Early 20th century utopians had perceived green roofs as an important element of the building, while later 20th century environmental awareness gave a more environmental dimension in the implementation of green roofs and green walls in the urban fabric.

A review of the available tools for quantifying the effect of vegetation in the built environment showed that most tools describing heat transfer from a vegetated roof calculate its thermal effects inside the building and not in its outside vicinity. Tools which describe the effect of vegetation outdoors, in the micro or local climate of buildings, consider vegetation being detached from buildings (e.g. in forms of parks). Most of these available tools do not take into consideration the effect of vapour molecular diffusion in heat transfer, whose significance is discussed in chapter 4. In most simulations of the effect of vegetation on the built environment, a CFD code is used. The raised building and street temperatures are input as heat fluxes and the evapotranspiration rate as a heat sink (Dimoudi and Nikolopoulou, 2000; Santamouris, 2001). This methodology had been used at the early stages of this study (Alexandri, 2001). As the interaction of surface-air temperature and the effect of mass transfer on heat are not fully described with the use of a CFD code (surface temperatures being input as estimated heat fluxes and mass transfer not being taken

into consideration in the heat transfer), a new methodology is investigated for describing the potential of lowering urban temperatures with green roofs and walls.

That is why, in order to validate the climatic effects of covering the building fabric with plants, a model of combined heat and mass transfer has been developed. This tool is based on heat and mass transfer theory in buildings and the atmosphere, as well as on existing studies of quantifying the evapotranspiration rate and heat exchanges in plants. The model is presented in chapters 4 and 5 in its one-dimensional and two-dimensional forms. Its accuracy is validated with an experiment, for both a plain construction material and a vegetated test cell, presented in chapter 4.

This tool is used to assess the potential of lowering urban temperatures through green roofs and green walls for different climates around the globe, different urban geometries and different amounts of ground-covering vegetation. The results from these calculated temperature decreases are presented in chapter 6. A validation is carried out on how these decreases may improve thermal comfort in urban spaces, both at roof level and inside the canyon, for the different climates examined. The energy savings from cooling buildings from these microclimatic alterations are also estimated.

Finally in chapter 7, conclusions are drawn from this study. This is followed by proposals for further research on the subject of mitigating the heat island effect through green roofs and green walls.

1.3 Introduction to Methodology

The quantitative validation of the thermal effect of ground covering plants on roofs and walls is done through a prognostic (dynamic) two dimensional model which is developed in this study, describing heat and mass transfer within an urban canyon. Heat and mass transfer are described within the building materials (capillary-porous bodies), the soil of the green roof, the vegetation of the green roof and the green wall as well as in the air. Across the solids' (building materials, soil, vegetation) width heat and mass transfer is expressed as one-dimensional. In the air in the canyon heat and mass transfer is expressed in its two-dimensional form, across the canyon's height and width. The effect of wind speed on temperature and moisture distributions is also taken into consideration. The differentials describing these exchanges are solved with

finite differences numerical approximations, where finite elements of materials and air are approximated as nodes.

The model is divided into nodes, with two sets of equations for each node; a heat transfer one and a mass transfer one. Momentum in and above the canyon is calculated through a CFD code and input as velocity in each node. Heat and mass transfer is calculated in building materials and asphalt as heat and mass transfer in capillary-porous media, in the soil layer as heat and mass transfer in soils, and in plants as heat and mass transfer in plants, taking into consideration the evapotranspiration rate from stomata. In the air close to the surfaces the molecular diffusion of heat and mass is taken into consideration. The effect of the water vapour gradient on heat transfer is calculated for air nodes in the vicinity of surfaces, where mechanical shear due to wind speed is not so strong.

Temperature and relative humidity are considered to be constant inside the buildings. Temperature and humidity concentration are also considered constant in the layer of the earth under the road. The boundary air nodes, characterised as the "urban" nodes, have as input the climatic characteristics of the city in question (temperature, relative humidity and wind speed), while the solar radiation is input on the surfaces (roofs, walls, street), depending on their orientation and inclination. With those boundaries and inputs, a detailed prediction of temperature and humidity distributions inside and above the urban canyon can be achieved.

The effect of greening roofs and walls is examined for different canyon geometries and for different climates. The climates studied are taken from Koeppen's climatic classification and the urban geometries are chosen according to the wind flow type they produce. The climatic conditions are those of the hottest month for each city examined. For all cases examined, a base case, where no vegetation exists in the urban canyon is first considered. The greening of walls, roofs or both is compared with this base-case, so as to validate how vegetation affects the certain type of urban geometry and climate. The description of temperature and humidity distributions in the air and the fabric are quite detailed; the effect is not only examined near the vegetated surface but also in different heights and widths of the canyon and above it. With the detailed description of humidity as a climatic characteristic affecting temperature distributions and evapotranspiration rate, the phenomenon can be described in detail for climates

with similar temperatures and amounts of solar radiation, but with different relative humidity bands.

The main purpose of this study is to answer the question up to what extent green roofs and green façades can be a solution to the mitigation of the heat island effect for different climates and urban geometries. With the rising urban population around the globe, this thesis wishes to contribute to solutions of sustainable living conditions in cities, with reduced morbidity and mortality risks. Although the reintroduction of nature in the city, especially on the human habitats themselves, buildings, cannot only have thermal benefits, but also social, cultural and psychological, this work focuses on the first aspect, the thermal benefits of greening roofs and walls in urban spaces.

1.4 References

1. H. Akbari, D.M. Kurn, S.E. Bretz, J.W. Hanford (1997) *Peak Power and Cooling Energy Savings of Shade Trees.* Energy and Buildings, Vol. 25 (1997), pp 139–148.
2. E. Alexandri (2001) *The Effect of Green Roofs on the Urban Climate: Case Study: Athens.* MPhil Dissertation, University of Cambridge.
3. L. Ashford (2004) *World Population Highlights 2004.* Bridge Project, Population Reference Bureau. Available from http://www.prb.org [Accessed 4th December 2004].
4. A.P.M. Baede, E. Ahlonsou, Y. Ding, D. Schimel, B. Bolin and S. Pollonais (2001) The Climate System: An Overview. *In:* J.T. Houghton, Y. Ding, D.J. Griggs, M. Noguer, P.J. van der Linden, X. Dai, K. Maskell and C.A. Johnson (eds) *Climate Change 2001: The Scientific Basis.* United Nations' Intergovernmental Panel on Climate Change (IPCC) Cambridge University Press, Cambridge, pp 86-98.
5. L. Benevolo (1980) *The History of the City.* Scolar Press, London.
6. R.E. Davies, P.C. Knappenberger, W.M. Novicoff and P.J. Michaels (2003) *Decadal Changes in Summer Mortality in U.S. Cities.* International Journal of Biometeorology, Vol. 47 (2003), pp 166-175.
7. A. Dimoudi and M. Nikolopoulou (2000) *Vegetation in the Urban Environment: Microclimatic Analysis and Benefits.* PRECis Project, the

European Commission, Directorate General XII, Joule III, Contract JOR3-CT97-0192. Centre for Renewable Energy Sources, Athens.

8. J. Díaz, F. Ballester and R. López-Vélez (2005) Impacts on Human Health. *In:* J.M. Moreno Rodríguez (ed) (2005) *The Preliminary Assessment of the Impacts in Spain due to Effects of Climate Change.* Project ECCE, Ministry of the Environment, Madrid, Spain. Available from: http://www.mma.es/en/oecc [Accessed 4th April 2005].
9. E.R.G. Eckert and R.M. Drake (1959) *Heat and Mass Transfer.* McGraw-Hill Book Company Inc., New York, Toronto, London.
10. D.M. Gates (1980) *Biophysical Ecology.* Springer-Verlag, New York.
11. B. Givoni (1998) *Climate Considerations in Building and Urban Design.* Van Nostrand Reinhold, New York.
12. K. Kafkoula (1990) *The Notion of Garden City in Greek Town-Planning in the Period of 1920-1940.* Ph.D. Thesis, Technical School of Architecture of the Aristotle University of Thessaloniki, Thessaloniki.
13. S. Konopacki, L. Gartland, H. Akbari and L. Rainer (1998) *Demonstration of Energy Savings of Cool Roofs.* A Report Prepared for the U.S. Environmental Protection Agency, Heat Island Project, University of California, Berkeley.
14. C. Koppe, S. Kovats, G. Jendritzky and B. Menne (2004) *Health and Global Environmental Change; Heat-Waves: Risks and Responses.* Series No. 2, Energy, Environment and Sustainable Development, World Health Organization, Copenhagen.
15. M. Laurie (1979) Nature and City Planning in the Nineteenth Century. *In:* I.C. Laurie (ed) (1979) *Nature in Cities.* John Wiley & Sons, Chichester, New York, pp 37-63.
16. N. Low, B. Gleeson, I. Elander and R. Lidskog (2000) *Consuming Cities; The Urban Environment in the Global Economy after the Rio Declaration.* Routledge, London, New York.
17. A.V. Luikov (1961) *Heat and Mass Transfer in Capillary-Porous Bodies.* Pergamon Press, Oxford, London, New York.
18. J.G. Nash and R.-M. De Souza (2002) *Making the Link: Population, Health, Environment.* Measure Communication, Population Reference Bureau. Available from http://www.prb.org [Accessed 5th December 2004].
19. T.R. Oke (1987) *Boundary Layer Climates.* Routledge, London.

20. T. Osmundson (1999) *Roof Gardens: History, Design, and Construction.* W. W. Norton & Company, New York.
21. Population Reference Bureau (2000) *An Urbanizing World: Urban Population Trends.* Population Bulletin, Vol. 55, No 3. Available from http://www.prb.org/pubs/population_bulletin/bu55_3/55_3_urban_population_trends.html#figure1 [Accessed 12th August 2001].
22. Population Reference Bureau (2004) *2004 World Population Data Sheet of the Population Reference Bureau.* Available from http://www.prb.org [Accessed 4th December 2004].
23. A.J. Rutter (1975) The Hydrological Cycle in Vegetation *In:* J. L. Monteith (ed) *Vegetation and the Atmosphere. Volume 1, Principles.* Academic Press, London, New York, San Francisco, pp 111-154.
24. M. Santamouris (ed) (2001) *Energy and Climate in the Urban Built Environment.* James & James, London.
25. G. Scudo, V. Dessi and A. Rogora (2004) Evaluation of Radiant Conditions in Urban Spaces. *In:* M. Nikolopoulou (ed) *Designing Open Spaces in the Urban Environment: A Bioclimatic Approach.* RUROS project, Centre of Renewable Energy Sources, Athens, pp 12-16.
26. C. Sullivan (2002) *Garden and Climate.* McGraw-Hill, New York, Chicago.
27. K.S. White et al. (2001) Technical Summary, Climate Change 2001: Impacts, Adaptation and Vulnerability. *In:* J.J. McCarthy, O.F. Canziani, N.A. Leary, D.J. Dokken and K.S. White (eds) (2001) *Climate Change 2001: Impacts, Adaptation and Vulnerability.* United Nations' Intergovernmental Panel on Climate Change (IPCC) Cambridge University Press, Cambridge, pp 19-73.
28. S. Woodell (1979) The Flora of Walls and Pavings. *In:* I.C. Laurie (ed) (1979) *Nature in Cities.* John Wiley & Sons, Chichester, New York, pp 135-157.

Chapter 2

Human Impacts on Climate in Different Scales

2 Human Impacts on Climate in Different Scales

Before proceeding to the factors which affect or cause climate changes on global or local scales, the term "climate change" is defined and the scientific distinction is made between "weather" and "climate". According to Geiger (1967) climate is an abstract concept, which can be grasped only by means of comprehensive calculations. It includes the sum total meteorological occurrences, called weather processes, at a given space. Climate comprises the average conditions and the regular sequences of weather, as well as repeatedly observed phenomena (e.g. tornadoes, dust storms etc) (ibid.). Baede et al. (2001) give the following distinction between "weather" and "climate": *""Weather" [...] is the fluctuating state of the atmosphere around us, characterised by the temperature, wind, precipitation, clouds and other weather elements. [...] "Climate" refers to the average weather in terms of the mean and its variability over a certain time-span and a certain area"*. In other words, weather is the result of rapid changes in the thermodynamic and momentum exchanges of the planet. It has only limited predictability, upon a certain area and time. Climate on the other hand, refers to the state of the climate system as a whole, including a statistical description of its variations. It is a way of classifying and describing the weather conditions of diverse places on the planet and by times of the year, by averaging weather characteristics. It varies with time and place and is determined by atmospheric circulation and characteristics of the land with such features as vegetation, soil moisture and albedo. Thus, the term "climate change" describes a change in the characteristics which compose the climate and derives from alterations of factors which affect the climatic elements, either on a local or a global scale. These changes might be due to human actions or natural factors, or both.

Climate change is not a characteristic of the last century only, nor has it only been driven from anthropogenic factors. Earth, being a living planet, has experienced many climate changes throughout its history. These changes have been mostly affected by changes of the energy balances on the planet.

2.1 Thermal Balances on the Planet

Before proceeding to presenting climatic alterations in global and smaller scales, a primary examination of the energy balances of the planet is carried out.

Generally, atmosphere is characterised by events whose time and space scales cover a wide range. These events can be classified according to their typical lifetime or period, and the space scales by their typical size or wavelength. The meteorological scale classification is usually related to atmospheric phenomena, mainly associated with motion (Oke, 1987). Its limits are given in the following table.

Table 1. Atmospheric scales and their limits (Oke, 1987)

Scale	Limits (m)
Micro-scale	10^{-2} to 10^{3}
Local scale	10^{2} to $5 \cdot 10^{3}$
Meso-scale	10^{4} to $2 \cdot 10^{5}$
Macro-scale	10^{5} to 10^{8}

The total Earth-Atmosphere (E-A) system can be considered as a close system. This means that no mass transfer takes place to/from exterior (space), but only energy exchanges. The external energy input to the E-A system is solar radiation (short-wave radiation), with wavelengths from 0.15μm (ultra-violet) to 3.00μm (near infra-red), with its peak at 0.48μm. The E-A system's wavelengths are in the band of 3.00μm to 100.00μm (area of long-wave radiation) with a peak at about 10.00μm. As energy can neither be created nor destroyed, according to the First Law of Thermodynamics, only converted from one form to another, the system either does not absorb any energy, or it absorbs and stores energy within it. The first possibility can be expressed as:

$$\text{Energy Input} = \text{Energy Output} \qquad \textbf{Eq. 1}$$

In this case there is no change in the net energy status of the system through which the energy has passed. For the majority of natural systems the equality Input = Output is only valid if values are integrated over a long period of time (e.g. a year). Over shorter periods the energy balance of the system differs significantly from the equality. This difference is accounted for by energy accumulation or depletion in the system's energy storage. In climatic terms, if energy is being accumulated in the earth (soil)-atmosphere system, it probably means an increase in soil and/or air temperature. Thus, the energy balance of the system can be written as:

Energy Input - Energy Output - Energy Storage Change = 0 **Eq. 2**

The energy input to the E-A system, solar irradiation (K_{Ex}), is reflected, absorbed, stored and emitted within the E-A system. The amount of reflected energy from the E-A system is directly related to the value of the system albedo ($\alpha_{E\text{-}A}$). The totally reflected energy from the system is $K_{Ex} \cdot \alpha_{E\text{-}A}$. Since the transmissivity of the E-A system is zero, the rest of the energy input, ($K_{Ex} \cdot (1-\alpha_{E\text{-}A})$), is absorbed within the system and emitted to space, as long-wave radiation. On an annual basis exactly the same amount of energy must be lost from the E-A system to space, otherwise a net energy gain or loss could mean a change of the average E-A system temperature.

Part of the incoming short-wave radiation to the E-A system is scattered, reflected and absorbed in the atmosphere due to clouds and other atmospheric constituents (water vapour, salt crystals, dust particles and various gases). The rest of the heat flux is transmitted to the earth's surface, where it is reflected and absorbed. If the earth and atmosphere are considered as separate sub-systems, then the energy balance equation can be written as:

$$K_{Ex} = K\uparrow_{(Ac)} + K\uparrow_{(Aa)} + K^{*}_{(Ac)} + K^{*}_{(Aa)} + K\uparrow_{(E)} + K^{*}_{(E)} \qquad \textbf{Eq. 3}$$

Where:

$K\uparrow_{(Ac)}$:	Reflected radiation back to space from clouds in the atmosphere	Atmospheric Reflection
$K\uparrow_{(Aa)}$:	Scattered and reflected radiation to space from atmospheric constituents	
$K^{*}_{(Ac)}$:	Absorbed radiation by clouds in the atmosphere	Atmospheric Absorption
$K^{*}_{(Aa)}$:	Absorbed radiation by atmospheric constituents	
$K\uparrow_{(E)}$:	Radiation reflected from earth's surface to space	Earth Reflection
$K^{*}_{(E)}$:	Radiation absorbed by earth's surface	Earth Absorption

The schematic diagram of the annual solar energy cascade of the earth-atmosphere sub-systems is given by Figure 3. Values are expressed as percentages of the average annual solar radiation that reaches the atmosphere, considered equal to 338W/m^2.

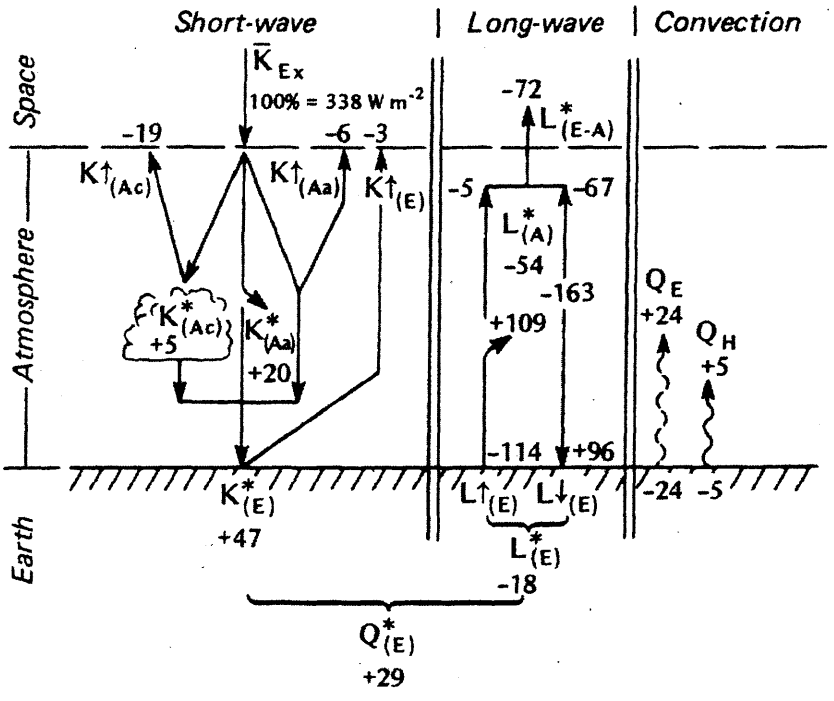

Figure 3. Schematic diagram of the annual solar energy cascade of the Earth-Atmosphere sub-systems (Oke, 1987)

As can be observed in Figure 3, 28% of the solar energy coming to the E-A system is reflected into space from the atmosphere and it does not participate further in the E-A system energy cascade. The atmosphere, being semi-transparent to short-wave radiation, absorbs 25% of the incoming energy. A very small amount of the energy reaching the earth's surface is reflected (3%), depending on the surface's albedo. The largest part of the incoming radiation (47%) is absorbed by the earth's surface (Oke, 1987; Geiger, 1967). This considerable amount of energy is converted from solar radiation to thermal energy and warms the earth's surface.

Most of this emitted long-wave radiation, from the earth's surface is absorbed by clouds and atmospheric constituents in the atmosphere. Only 5% of the heat emitted by the earth's surface is lost directly to space. The absorption (α) spectrum of the atmosphere and some of its most influential atmospheric constituent gases are given in Figure 4.

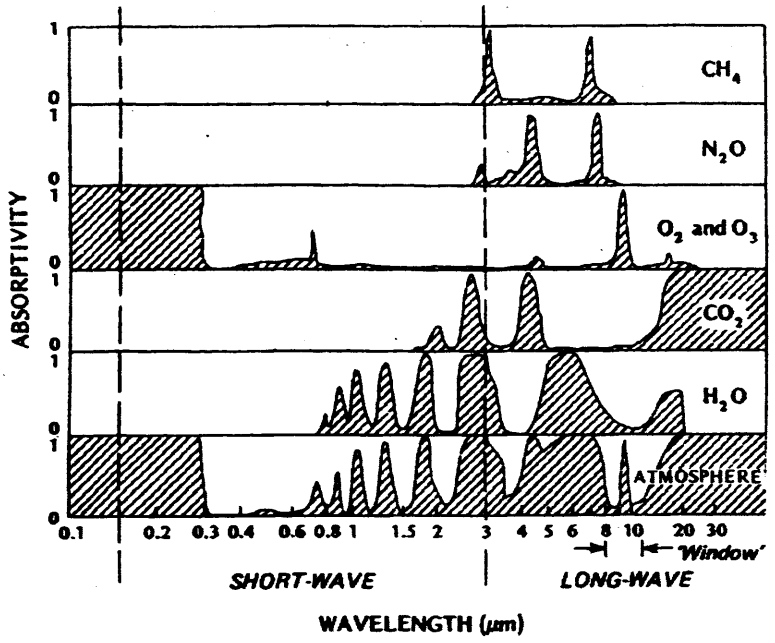

Figure 4. Absorption of certain constituents, at various wavelengths (Oke, 1987)

It is obvious from Figure 4 that the atmosphere is a poor absorber of short-wave radiation, but a very good absorber of long-wave radiation. In the band of 0.30μm to 0.80μm, where the intensity of solar radiation is at its highest, the atmosphere is relatively transparent. Regarding long-wave radiation, mainly because of the absorptivity of water vapour (H_2O), carbon dioxide (CO_2), ozone (O_3), methane (CH_4) and nitrous oxides (N_xO_y), referred to as *"greenhouse gases"*, the atmosphere is almost opaque. If the atmosphere is cloudless, there is an important gap in its absorption spectrum. The atmosphere is then open to the transmission of long-wave radiation to space in the band from 8.00μm to 11.00μm, know as the "atmospheric window"[1]. Thus, solar energy can penetrate easily to the earth's surface, but the heat emitted by the earth's surface cannot get out of the atmosphere easily. This opaqueness to long wave radiation due to greenhouse gases is quite important for life on the planet; in the absence of greenhouse gases from the atmosphere the average surface temperature of the earth would be over 30°C cooler than it is today (Cotton and Pielke, 1995). However, as the energy exchanges of the planet relies on the balances of the factors which take part in this process, an increase or decrease of any of these factors might cause a new order balance, characterised as "climate change" which may or may not be so favourable for human and natural habitats.

[1] Apart from a narrow band of ozone absorption (9.60μm to 9.80μm).

2.2 Climate Change; Global Scale

Climate change during human's presence on Earth is not only a phenomenon of the post-industrial era, nor are humans responsible for all the global climate changes which have occurred on the planet. Volcanic eruptions, or solar irradiance variability are natural factors which are responsible for climate changes. Even before the 18th century establishment of instrumentation for the observation of weather characteristics, there has been evidence of climate change. During the Roman period, in the early part of the first century BC there is written evidence of warming in areas of northern Italy which allowed for the cultivation of olives and grapes, an impossibility in earlier times (Lamb, 1995). Palaeoclimatic analysis also verifies that it is likely that the temperatures of the Northern Hemisphere were relatively warm during the earlier centuries of the millennium (Folland et al., 2001). After that period, Europe experienced colder weather up until the late 11th - 12th century when higher temperatures were noticed, perhaps approaching the level of the warmest millennia of post-glacial times[2]. It is estimated that average summer temperatures were about 0.7°C to 1.0°C higher in Britain and 1.0°C to 1.4°C in central Europe (Lamb, 1995). This rise of global temperature is characterised as the "Medieval warmth" and is comparable to the near global warmth of the late 20th century (Folland et al., 2001). The climate then started cooling again in the late 13th century, leading to a colder period in the 16th and 17th century, also referred to as the little ice age. The temperature started rising again from the early 18th century, stabilising during the 19th century to warmer temperatures and leading to the 20th century notion of global warming, with probably the highest temperatures of the last millennium.

These changes, over the pre-industrial centuries occurred on a much larger time-scale than post-industrial climate changes. Observations of climatic parameters were instituted from the late 18th century in cities in Western Europe and North America. The climate observed until the late 19th century was very similar for the 100 years for which data existed, establishing the notion of the constancy of climate (Lamb, 1995). During the first fifty years of the 20th century global warming was recorded, followed by some cooling and then recently another period of warming. It was only during the

[2] During that period there were vineyards in Southwest Britain, indicating a much warmer climate (Lamb, 1995).

1980's that the possibility of the occurrence of rapid climatic changes during the time-span of human life was recognised (Folland et al., 2001).

To what extend climate is stable is really a question of scale. From its beginning the planet's climate has gone through many changes of completely different temperatures, relative humidity and constituents in the atmosphere, allowing different forms of life to develop. Over the last million years, the earth's climate has been very unstable, with repeated swings from ice age to warm inter-glacial conditions and back again (Lamb, 1995). These alterations are the result of changes in the energy balance of the planet (input, output and absorbed energy, as briefly discussed in paragraph 2.1).

There are several theories explaining why these climate changes have occurred. Milankovitch established the theory of relating the variations in the ellipticity of the orbit of earth's movement around the sun (Santamouris, 2001). This affects the incoming radiation, which leads to climatic change, occurring within a period of 100,000 years which coincides with the repeated alterations between ice ages and warm interglacial periods (Lamb, 1995).

Also, recent measurements by satellites suggest that the outgoing energy from the sun can vary significantly. Until the 1970's, the notion that the amount of energy reaching the external layers of the atmosphere was constant dominated thinking. With the evolution of satellite measurements of the total solar irradiance, it was obvious that the "solar constant" does, in fact, vary. Sunspot activity on the sun's surface can be responsible for alterations on its surface. Satellite measurements suggest that there is a variation in the annual mean total solar irradiance of the order of 0.08% (about 1.1 W/m^2) between minimum and maximum of the 11-year solar cycle (Ramaswamy et al., 2001). This affects the climate of the earth, as the input energy is altered. It has been estimated that a decrease in solar energy of the order of 1% can lead to a decrease of the magnitude of 1.0°C in the earth's average temperature (Santamouris, 2001). In addition, especially the changes of the solar irradiation in the ultraviolet of the electromagnetic spectrum, result in changes in the stratospheric ozone concentrations, which cause stratosphere warming. However, the response of ozone to solar variability and its affects on the climate are not well established (Ramaswamy et al., 2001). Nevertheless, the effect on climate change in the 20th century due to solar variations are less significant than the effect of greenhouse gases (discussed below); it

has been shown (Mitchell et al., 2001) that the change in forcing to solar variation is of the magnitude of 20-25% of the change in forcing due to increases in greenhouse gases.

A factor which influences the amount of solar irradiation reaching the earth's surface is the concentration of stratospheric ozone. Due to human activities, the concentration of stratospheric ozone is declining. The observed stratospheric ozone losses over the 1980's and 1990's have caused a negative forcing of the surface-troposphere system. Ozone depletion in the lower stratosphere causes an increase in the solar forcing on the surface-troposphere system. Models calculating the temperature change due to observed stratospheric ozone changes have estimated a force of the magnitude of -0.05 to -0.19 W/m^2 per decade. It has been estimated that 1% decrease in global total ozone leads to a global increase in ozone photolysis rate of the magnitude of 1.4% (Ramaswamy et al., 2001). However, the reliability of these estimates is affected by the fact that the ozone changes in the lower stratosphere, the tropopause, and the upper troposphere are all poorly quantified around the globe in general which makes difficult to derive more precise predictions (ibid.).

Another important factor which, according to tectonic plates theory, has an important effect on climate change on a global scale is that the earth's surface has changed significantly through time because of the movement of tectonic plates underneath its surface, thereby changing the position of the land and oceans (Santamouris, 2001). This affects the transport of heat and the wind system of the planet. Also, other changes on the surface of the earth such as changes in the surface albedo of huge areas of land (e.g. desertification, deforestation) has a significant effect on energy balances for the local climate (Lamb, 1995). This is the issue on which this study is going to focus in the following chapters, emphasising the climatic alterations which are caused mainly on a local scale due to changes of land surface characteristics.

There are also other theories which explain climate changes, taking into consideration atmospheric particulates. As was discussed in paragraph 2.1, the green house gases are responsible for absorbing long wave radiation, therefore raising the system's temperature. For about 1,000 years before the Industrial Revolution, the amount of greenhouse gases in the atmosphere remained relatively constant. Since then, industrialisation has increased the concentration of these gases in the

tropospheric zone. In general, the tropospheric chemical processes determining the indirect greenhouse effects are highly complex and not fully understood (Ramaswamy et al., 2001). This makes it almost impossible to predict the radiative balances through indirect effects relating to chemical transformation or change in the distribution of radiatively active species. The estimations presented here are the ones derived from models describing the direct effects of each greenhouse gas, leaving its indirect effects aside.

Observations show that the amount of carbon dioxide in the atmosphere has increased by more than 30% since pre-industrial times and is still increasing at an average rate of 0.4% per year, mainly due to the combustion of fossil fuels and deforestation (Baede et al., 2001). The concentration of substances such as nitrogen oxides (mainly NO and NO_2) and carbon monoxide (CO) have also increased. Although these gases are not greenhouse gases, they have caused a 40% increase in tropospheric ozone since pre-industrial times (Ehhalt and Prather, 2001). Changes in the proportions of greenhouse gases cause alterations in the heat balance of the system. Climatic models have estimated that a doubling of the CO_2 concentration in the atmosphere can lead to an increase of the global average temperature by 1.5°C to 4.0°C (Lamb, 1995). Tropospheric ozone is mostly observed in urban areas, where it is a major component of "*smog*"[3]. It has been estimated that the concentration of tropospheric ozone influences the ground's surface temperature, depending on the height at which the ozone concentration changes. Model studies have shown that for total sky conditions the range in globally and annual averaged tropospheric ozone forcing is from 0.23 to 0.43 W/m^2 (Ramaswamy et al., 2001). In general, tropospheric ozone is increasing around the globe, but its observed upward trends in Europe and North America appear to be less steep than in the 1980's. It is expected that the largest future increases of tropospheric ozone will occur in Asia, due to its population and city growth. It has been estimated that this will cause a globally averaged radiative forcing from pre-industrial times to 2050 of the magnitude of 0.43 to 0.66 W/m^2 (ibid.).

[3] Discussed in paragraph 2.3.1.8.

2.2.1 Climate Change in the 20th century

There has been evident climate change from the early 20th century and onwards, as can be observed in Figure 5. As discussed in the previous paragraph, from the beginning of the century up until the 1950's there have been indications of global warming, followed by a period of cooling and then a further temperature increase in the 1990's. Apart from natural activities which may take place and affect the energy balances in the system of the planet (e.g. volcanic dust in the atmosphere), human intervention in the 20th century has been playing a very crucial role on the factors which affect the climate. These two most dominant factors are land-use changes and green house gases.

The term "land-use" change refers to a change in the use or management of land. Such change may result from various human activities such as changes in agriculture and irrigation, deforestation, reforestation and afforestation, but also from urbanisation or traffic (Baede et al., 2001). Land-use change results in changing the physical and biological properties of the land surface and thus the climate system. The changes of land surface albedo are especially the most significant (Ramaswamy et al., 2001). Land-use change may contribute significantly to changing the local, regional and even global climate and has an important impact on the carbon cycle (Stoker et al., 2001).

One of the greatest land-use changes on the Earth's surface due to human activity has been the deforestation of the Northern Hemisphere's temperate forest zone. It began on a small scale more than 5,000 years ago. Forests were converted to land for cultivating grasses and this was responsible for causing climate change at that time (Lamb, 1995). This influence of land-use change on the weather and climate has been known in a qualitative manner for several years; even Thomas Jefferson, in 1861, was commenting on the alterations of wind patterns in the State of Virginia, North America, due to the deforestation of the land (Cotton and Pielke, 1995).

There are potential local and global climatic impacts associated with land-use changes. Two of the most important ones are the changes in the fraction of solar radiation reflected back to space (albedo) and the changes in the fraction of heat used to evaporate and transpire water in the atmosphere. It has been estimated (Ramaswamy et al., 2001) that due to land-use change a forcing of -0.4 W/m^2 has resulted, about half of which is estimated to have occurred in the Industrial Era.

Deforestation in lower latitudes, as is happening today in the Amazon basin, can have serious effects on global climate, especially on rainfall. It has been estimated that if the tropical rain forests that cover 34% of the equatorial zone are completely replaced this could cool the Earth by 0.2°C-0.3°C and rainfall would be reduced by 10% in the zone and by 1% for the earth as a whole (Lamb, 1995). Apart from such alterations in temperature and rainfall, land-use change is responsible for changes in roughness length, and turbulent fluxes thus causing changes in the local winds near the ground level, soil moisture and heat budgets in general.

According to the United Nations' Intergovernmental Panel on Climate Change (IPCC) report, published in July 2001, the global average surface temperature (the average near the surface air temperature over land, and sea surface temperature) has increased since 1861. Over the 20th century this increase has been of the magnitude of 0.6±0.2°C (Figure 5), including the influence of the heat island effects on the global temperature (Houghton et al., 2001).

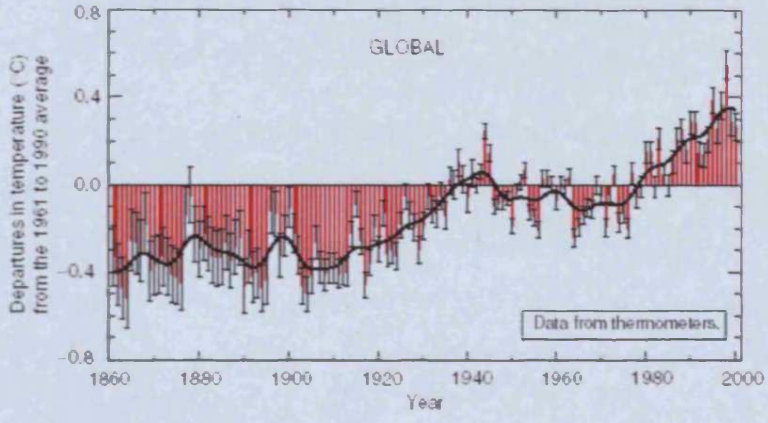

Figure 5. Variation of the Earth's surface temperature, based on measurements, for the past 140 years (Houghton et al., 2001)

Another very important factor, which has altered the climate since the Industrial Revolution, is the emission of greenhouse gases which are released into the atmosphere due to the combustion of fossil fuels and especially CO_2. Since the Industrial Revolution the concentration of CO_2 in the earth's atmosphere has augmented significantly (Figure 6). Alterations in its concentration may rise temperature to unbearable levels for most of the existing forms of life on the planet. Its effect on warming the planet had been mentioned since 1896 by the Swedish scientist Svante Arrhenius (Cotton and Pielke, 1995; Godrej, 2001), when he estimated that a 2.5- to 3-fold increase in CO_2 would increase temperatures in the Arctic regions by 8-9°C. However, it was in 1938 that Callendar clearly stated his

concerns about the impact of anthropogenic emissions on global temperatures (Cotton and Pielke, 1995) and awareness about greenhouse gases only started in the late 20th century.

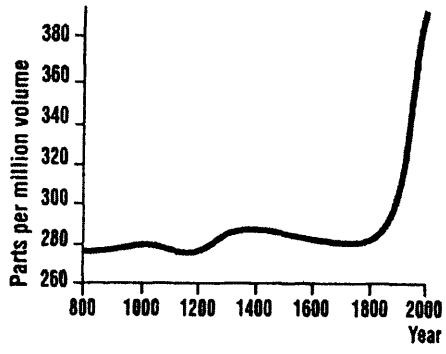

Figure 6. Growth in CO2 concentration from 800 AD up to date (Godrej, 2001)

2.2.1.1 Climate Change in the 20th Century; Anthropogenic or Natural?

There are two main natural sources to which climate change can be attributed; solar irradiance variability (discussed in paragraph 2.2) and volcanic eruptions.

Volcanic eruptions are able to affect the planet's climate on a global scale due to the aerosols they release. After a volcanic eruption, the stratosphere warms and the annual mean surface and tropospheric temperatures decrease for the following two to three years. It has been estimated that the radiative forcing due to volcanic aerosols from the recent El Chichon and Mt. Pinatubo eruptions is of the magnitude of -3W/m^2 (Mitchell et al., 2001). However, the variability from other sources makes the assessment of the observed climatic response quite difficult, particularly when these two most recent volcanic eruptions coincided with the El Niño warm years (ibid.).

The United Nations' IPCC modelled the climate change experienced in the last century due to natural and anthropogenic forces (Figure 7). As is obvious from Figure 7a natural forcings alone do not explain the warming in the second half of the 20th century. However, natural forces may have contributed to the observed warming in the first half of the 20th century, which is not embodied in the model of anthropogenic forces (comparison of Figure 7b and c). Generally, it is concluded (Mitchell et al., 2001) that although natural forces do have an impact on the observed global warming, they are too small to explain the change trends. The global warming due to solar variations cannot be more than 0.7W/m^2, while the largest force is estimated to be due

to well mixed greenhouse gases (of the magnitude of 2.3W/m^2), followed by other anthropogenic causes, such as tropospheric ozone (0.3W/m^2), increases in sulphate aerosols (-0.4W/m^2) and decreases in stratospheric ozone (-0.2W/m^2) (Ramaswamy et al., 2001). The effects on global climate change of other factors, such as changes in land use and mineral dust are very poorly known and not yet incorporated into simulation studies. It is believed (ibid.) that their contribution is small compared to greenhouse gases, though they could be of importance in local scales (paragraph 2.3.1.8).

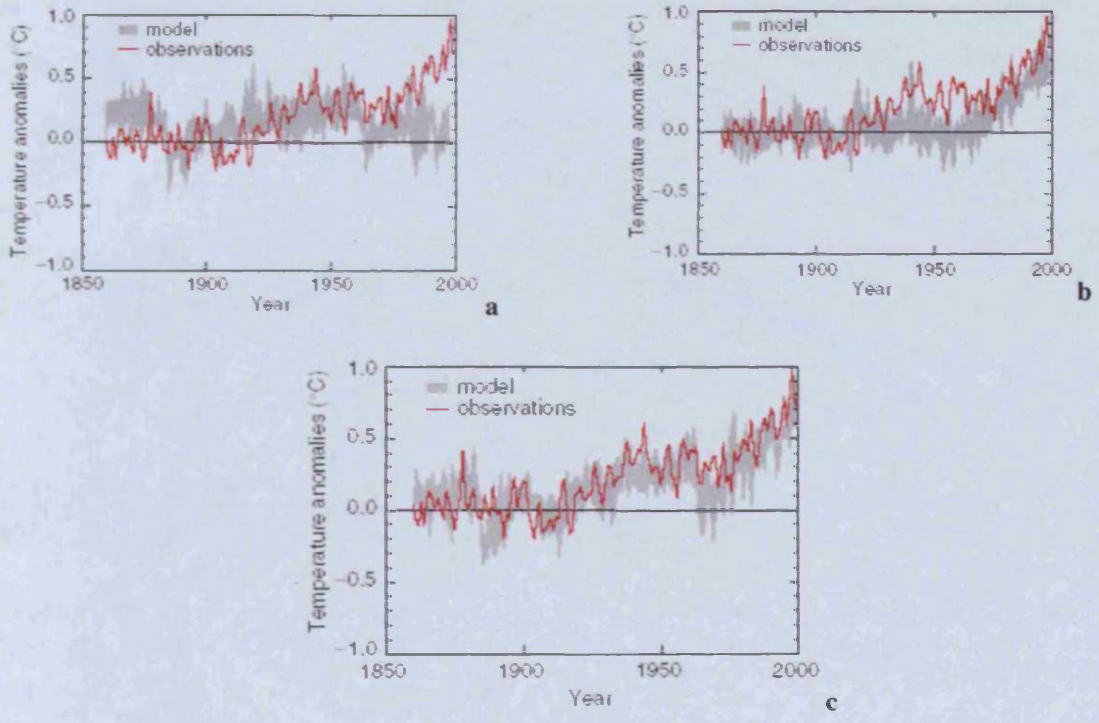

Figure 7. Observed and simulated annual global mean surface temperature anomalies relative to the 1880 to 1920 mean compared with simulations of coupled ocean-atmosphere climate model with (a) only natural forces (solar variation and volcanic activity) (b) only anthropogenic forces (well mixed greenhouse gases, changes in stratospheric and tropospheric ozone and the direct and indirect effects of sulphate aerosols) and (c) both natural and anthropogenic forces (Houghton et al., 2001)

Through the United Nations' Intergovernmental Panel on Climate Change, it is made clear that the climate change the planet is going through is mostly due to anthropogenic reasons. Various climatic scenarios have been developed describing what the trends of climatic characteristics of the planet are going to be, under different assumptions. Under the assumption that there is a global 1% increase of carbon dioxide and that CO_2 is doubled after 70 years, it has been estimated (Cubasch et al., 2001) that a mean global temperature change of the magnitude of 1.1 to 3.1°C, with an average of 1.8°C and a standard deviation of 0.4°C is expected. Another type of climatic scenario uses specified time-evolving future forcing where the simulations

start in the 19th century, are run with estimates of observed forcing through the 20th century and is continued with estimated forcings of greenhouse gases or with the additional contribution from the direct and indirect effects of sulphate aerosols. For the 30-year average 2021 to 2050 compared with 1961 to 1990, the temperature change due to both greenhouse gases and sulphate aerosols is 1.3°C with a range from 0.8°C to 1.7°C, while for greenhouse gases only the temperature change is 1.7°C ranging from 1.0 to 2.1°C (Cubasch et al., 2001). A maximum warming is expected in the high latitudes of the Northern Hemisphere and a minimum in the Southern Ocean (due to the ocean heat uptake). In general, if carbon dioxide emissions are not reduced, temperatures will be about 2°C higher than today in 2050 (Hadley Centre, 2002). This could be delayed by 50 years if CO_2 concentrations drop to 750ppm and by 100 if CO_2 concentrations drop to 550ppm (Figure 8).

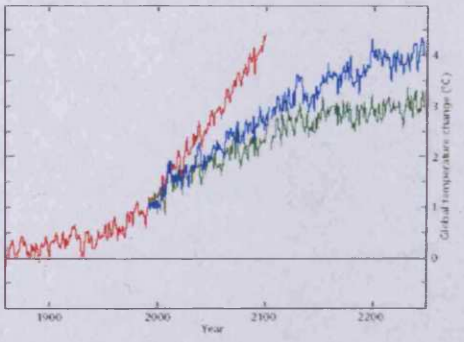

Figure 8. Global average temperature rise resulting from the unmitigated CO_2 emissions scenario (red), and emissions scenarios which stabilise CO_2 concentrations at 750 ppm (blue) and at 550 ppm (green) (Hadley Centre, 2002)

These global changes cannot but affect the already altered climate of cities. In fact, there is evidence that cities contribute to the global change trends. Due to the change of land surface temperatures that they cause, urbanised land has an effect on global land temperature trends. When taking into consideration only urban stations of the period 1951 to 1989, the pattern of temperature increase is 0.10°C per decade, while for rural stations the trend is 0.80°C per century (Folland et al., 2001). Over the Northern Hemisphere land areas, where urban heat islands are more apparent, the trend of temperature increase is of the magnitude of 0.28°C per decade (over North America) and the surface temperature trend is slightly less (0.27°C per decade) (ibid.). Apart from their global effect, cities alter the local climate of their area very markedly, sometimes making living conditions unbearable for their inhabitants. The local alterations of the climate of cities, generally known as the heat island effect, are analysed in the following paragraphs.

2.3 Climate Change on a Local Scale; the Heat Island Effect

As was discussed above, any alteration on the earth's surface can lead to quite significant transformations of the local climate. The formation of cities in places which were usually covered with vegetation fatally causes alterations of the climatic characteristics of its area, generally known as the *heat island effect.*

This is not only a phenomenon of the recent centuries. Even from ancient times the difference between the urban and the rural environment, from an air quality point of view, was quite obvious. About 2000 years ago, Seneca compared the *"heavy air of Rome with its stench from smoky chimneys"* to the air outside Rome, in the open country, observing air quality differences between urban and rural areas (Watkins, 2000). Yet there is no clear evidence that temperature differences could have been noted in antiquity. In 1820, for the first time, Luke Howard published a comparison of ten years temperature measurements of urban London and the rural area around it, establishing the existence of the heat island effect in London. He observed that the urban temperature was higher than the rural one by 0.6°C in July for the mean 24-hour temperature and by 1.2°C in November. He concluded that *"the temperature of the city is not to be considered as that of the climate: it partakes too much of artificial warmth, induced by its structure, by a crowded population and the consumption of great quantities of fuel"*. This work of Howard's is the first scientific evidence of the temperature irregularities of the urban climatology (Chandler, 1965).

The heat island effect is formed by alterations of the factors which affect the heat energy balances at the local scale of the city. These are summarised in the following paragraphs.

2.3.1 Factors Affecting the Formation of the Heat Island Effect

The main differences between an urban environment and a rural one are governed, in general, by altered factors which take part in the formation of local heat balances. These are factors such as optical and thermal properties of materials (albedo, emissivity and heat capacity) which are of different magnitudes for materials in rural and urban areas. In addition, urban areas are characterised by lack of evapotranspiring surfaces (vegetation) and materials of low porosity. The geometry between a

vegetated area and the density-morphology of an urban area are completely different, which has a direct effect on wind and shade distributions. The human activities which take place in the urban areas are responsible for anthropogenic heat release (transport, space and water heating, cooling etc) and air pollution, the latter affecting cloud cover.

The combination of these factors determines the way in which heat is absorbed, stored, released and dispersed in the urban environment, expressed as temperature difference between the urban and rural environment. This difference varies for different urban environments, according to the exact combination of these factors. Before proceeding to the analysis of this thesis it is useful to examine briefly these factors in order to estimate if covering urban surfaces with vegetation could be expected to have a significant impact on the heat island effect.

2.3.1.1 Albedo

The albedo (α) of a surface, or its reflectivity, is the ratio of the reflected part of the incoming radiation on a medium of finite thickness to the total incoming radiation.

$$\alpha = \frac{\text{reflected part of incoming radiation}}{\text{total incoming radiation}} \qquad \textbf{Eq. 4}$$

Albedo depends on the wavelength of the incoming radiation, the elevation of the radiating source (the sun) and the nature of the surface. It is a fundamental surface property which determines how much solar energy is absorbed by the system. The higher the albedo of a surface, the lower the energy absorbed by the medium. In the following table a comparison of the albedo of selected surfaces is given.

Table 2. Typical albedo of selected surfaces (adapted from Oke, 1987; Watkins, 2000)

Surface	Albedo	Surface	Albedo
Concrete	0.10 - 0.35	Snow	0.79 - 0.95
Brick	0.20 - 0.40	Ice	0.30 - 0.40
Asphalt	0.05 - 0.20	Still Water	0.09 - 0.10
Tar & Gravel	0.03 - 0.18	Thick Clouds	0.60 - 0.90
White Paint	0.50 - 0.90	Thin Clouds	0.30 - 0.50
Coloured Paint	0.15 - 0.35	Corrugated Roof	0.10 - 0.15

Surface	Albedo	Surface	Albedo
Highly Reflective Roof	0.60 - 0.70	Dark Soil	0.05 - 0.15
Dry, Black Earth	0.14	Wet, Black Earth	0.08
Dry, Grey Earth	0.25 - 0.30	Wet, Grey Earth	0.10 - 0.12
Dry Sand	0.35 - 0.45	Wet Sand	0.20 - 0.30
Desert	0.34 - 0.52	Crops	0.15 - 0.25
Trees	0.15 - 0.18	Green Grass	0.26
Dry Grass wizened by sun	0.19	Wet Grass	0.33 - 0.37
Deciduous Forest	0.10 -0. 20	Coniferous forest	0.05 - 0.15

Surfaces in the urban environment are different from surfaces in the rural one. Generally, urban surfaces tend to have lower albedo than surfaces in rural environment (such as vegetation), thus absorb more solar radiation. This causes higher surface temperatures than air temperature; they can become 30°-40°C higher than ambient air temperature (Akbari et al., 2001). Thus, the ambient air temperature is increased, due to the heat which is convected and radiated by them.

The albedo of urban surfaces is quite responsible for the cooling energy consumption within cities. On the urban scale, Rosenfeld et al. (1995) simulated the effects of raising average urban albedo in the Los Angeles Basin. The average albedo that was identified as 0.13 increased to 0.26. The results showed that central Los Angeles became 2-4°C cooler at midday in summer. As less energy is introduced to the system with an increase in albedo, there is a significant impact on air-conditioning energy use. Peak power consumption for Los Angeles can then be reduced by 0.6-1.2GW (Konopacki et al., 1998).

2.3.1.2 Emissivity

Emissivity (ε) is the ability of a body to emit thermal radiation. At a given temperature, the maximum possible thermal radiation is the one emitted by a black body, thus the emissivity of a surface is defined as:

$$\varepsilon = \frac{\text{energy emitted from a surface}}{\text{energy emitted from a black surface at same temperature}} \qquad \text{Eq. 5}$$

Emissivity defines the long-wave radiation (thermal radiation) from a body, of a specific temperature. The higher the emissivity is the larger the thermal radiation emitted from the body. It is therefore important for the redistribution of the heat inside the system and for its radiative heat exchanges with the atmosphere. Urban materials may have both low (e.g. aluminum foil 0.10) and high emissivity (e.g. asphalt 0.95), while vegetation has generally high emissivity (0.94-0.99). The radiative heat emitted between bodies is conversely proportional to the square of the distance between them. Thus, if bodies are quite far away, relatively to their surface temperatures, the radiated heat exchange could be negligible, no matter which their emissivities are. Thus the role of emissivity on the formation of heat island depends on the geometry of the urban structure and its view factor to the sky.

Systematic urban-rural differences in surface emissivity have been reported to be the potential cause of part of the heat-island effect (Watkins, 2000). On the other hand, Grimmond et al. (1991) simulated the effect of optical and thermal characteristics of materials responsible for the heat island intensity and found that the role of emissivity is minor. As emissivity increased from 0.85 to 1.00 there was a slight increase of 0.4K in the temperature difference between the urban and rural environment, during night, for very tight canyons. For canyons with higher view factors there was practically no change.

2.3.1.3 Heat Capacity

Heat capacity is the ability of a body to store heat. It is defined as the amount of heat necessary to raise the temperature of a given mass by 1K. Numerically it is the density of the body, multiplied by its specific heat. Structures in the urban environment tend to have quite high thermal capacity. On the other hand, the thermal capacity of vegetation is almost negligible, so generally is its mass. Due to the high heat capacity of building materials, the energy received in the urban structure is primarily stored in its mass and released when the ambient temperature is lower than the surface one. A vegetated surface stores practically no heat. This causes a diurnal difference in the rural and urban temperature fluctuation, described in paragraph 2.3.2.1.

The extensive heat storage in the urban environment can block night cooling on extremely hot days with high irradiance and a clear sky. Heat stored in the urban fabric during the day is released into the environment at night, raising the ambient temperature. This results in slower night cooling of surfaces or, in extreme circumstances in no night cooling at all.[4] In dense urban structures with limited plantation and shade, this phenomenon is quite usual.

2.3.1.4 Vegetation

In rural areas, if they are not desert or rocky, their main characteristic is the existence of vegetation, which tends to be a secondary characteristic in the urban environment. As will be discussed in paragraph 2.4 and in the following chapters, the existence of vegetation modifies the local climate, due to the latent heat flux produced by plants. If vegetation is eliminated significantly and replaced by waterproof materials (such as in the urban environment), then latent heat will decrease, thus most radiation will be converted to sensible heat. This is one of the reasons why, in general, especially during summers, the air temperature is much higher in urban areas which lack vegetation, compared to rural, vegetated ones, but also compared to urban vegetated spaces (discussed in paragraphs 2.4 and 2.5).

2.3.1.5 Porosity

Apart from plants and water surfaces, porous surfaces, which absorb water (e.g. soil) account for quite significant latent heat flux in the atmosphere. If the porosity of a material is high, it can absorb more water, thus be responsible for the release of more latent heat into the atmosphere. Materials mostly used in the urban texture are generally waterproof. Rainwater in cities is mostly channelled away from the city system through sewers and not through latent flux from the surface.

---

[4] This is a quite typical phenomenon during very hot days, in ancient open theatres in Athens, which are made of stone. Exposed to solar gains and raised urban temperatures all day, the heat stored in their stone is released during the early night hours, giving an uncomfortable feeling of thermal stress to both audience and performers.

2.3.1.6 Shade

Generally, in rural environments shading is determined by the characteristics of the features of the rural environment and their density. In the example of trees, their shading can reduce the radiation stored in soil, according to their density. In very dense forests air temperature in a hot, sunny day may be much lower in the core of the forest than in its surrounding area.

Shading of urban surfaces which tend to store heat from direct solar gains can lead to noticeable reduction of surface temperatures, especially in hot periods when solar radiation is at its highest. This shading depends on the morphology of the urban structure and orientation, as well as on the existence of trees which shade urban surfaces. Measurements carried out in Tel Aviv (Givoni, 1998), correlated the ratio of the Building's Envelope to the Site Area (BESA) and the ratio of the Permanently Shaded area around the building (PSHA) to the plot area to the maximum air temperature and range in the urban environment. It was found out that in summer both BESA and PSHA have a significant effect on temperatures, while in winter temperatures are affected only by BESA. The following relationships were attained:

For summer:

$$T_{max} = 32.93 - 0.155(PSHA) - 0.0061(BESA) \quad \textbf{Eq. 6}$$

$$Range = 11.05 - 0.148(PSHA) - 0.0011(BESA) \quad \textbf{Eq. 7}$$

For winter:

$$T_{max} = 19.1 - 0.011(BESA) \quad \textbf{Eq. 8}$$

$$Range = 10.7 - 0.023(BESA) \quad \textbf{Eq. 9}$$

From equations 6 and 7 it is quite obvious that the effect of the permanently shaded areas on lowering the maximum air temperature in the hot summer and dense structure of Tel Aviv is very significant, of a much larger order of magnitude (10^{-1}) than the building's envelope (10^{-3}).

2.3.1.7 Anthropogenic Heat Release

Anthropogenic heat release is the concentrated heat that is produced by human activities in urban areas all year-round. It is the heat released by the combustion of

fuels from either mobile sources (means of transportation), or by stationary sources (buildings, industrial activities etc). Anthropogenic heat is a quite crucial factor in the heat island effect when both the per capita energy use and the population density are high (Watkins, 2000). In certain high density areas, anthropogenic heat release can be equal to or even more than the solar input in winter and on some occasions in summer also, because of the high use of air conditioning systems.

Harrison and McGoldrick (1981) determined the anthropogenic heat fluxes (transport, service, industry and domestic sectors) for the United Kingdom. For the city of London, the results showed a wide range of heat release from less than $1W/m^2$ on the outskirts to more than $300W/m^2$ at the centre of London.[5] It was found that in the centre of London (a diameter of 5 km) the artificial heat flux exceeds the natural flux for every month of the year. Oke (1987) also compared summertime anthropogenic heat release from all sources within certain cities with the net radiation (short-wave and long-wave) received from the sky. The results of these studies are summarized in Figure 9.

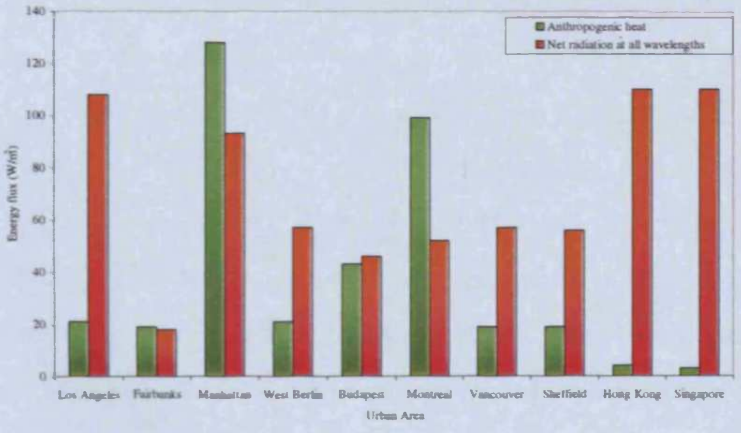

Figure 9. Anthropogenic heat and net radiation at all wavelengths for selected urban areas (adapted from data from Oke, 1987; Santamouris, 2001; Watkins, 2000)

It can be observed in Figure 9 that anthropogenic heat can be of similar or higher magnitude to net sky radiation. Thus a measurable temperature rise due to anthropogenic heat should be expected. Meteorological simulations conducted by Taha (1997), showed that anthropogenic heat emissions in a large city core can be responsible for a temperature increase of 2-3°C both during day and night.

[5] Comparatively, the average global solar radiation on a horizontal plane in London, in June, is $455W/m^2$ (Page and Lebens, 1985).

2.3.1.8 Air Pollution

Atmospheric pollution is a very significant factor for the air quality of the urban environment. Some atmospheric pollutants, such as sulphur dioxide, carbon monoxide, carbon dioxide, nitrous oxides tend to affect the temperature in the urban area (Moussiopoulos, 2003).

Due to human activities in the urban environment a lot of particulates are produced, mostly by industry, vehicles and the burning of fossil fuels for heating, cooling or electricity generation. The significance of each source varies according to the characteristics of each city. In the instance of Mumbai and Delhi, in India, the major source is vehicles (Singh and Kumar, 2001). For Paris, the major source had been the industry, but since the 1980ies, Sundays are equivalently polluted as the rest of the weekdays, leading to the conclusion that cars are also a major source of urban air pollution (Escourrou, 1991). The level of the particulates concentration depends on several factors, such as the type and amount of fuels consumed, geographic and topographic particularities, town planning, meteorological factors, etc. Those particulates, under solar radiation and certain humidity concentrations react and cause numerous problems in the urban environment, such as sulphurous dioxide, smoke (suspended particulates with a diameter less than 2μm), which can be responsible for the loss of lives and deterioration of health (Chandler, 1965) as was dramatically experienced with 4,000 deaths in London in December 1952 (Figure 10). Cities in lower latitudes also experience photochemical smog, chemical substances formed in the atmosphere under the influence of solar radiation, when nitrogen oxides and hydrocarbons are present, which is also fatal for human lives (Moussiopoulos et al., 1995; Diaz et al., 2005).

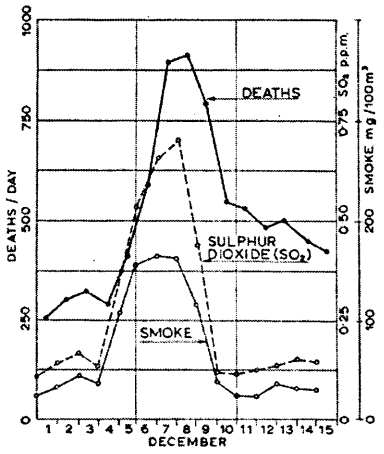

Figure 10. Daily air pollution and deaths in London in December 1952 (Chandler, 1965)

Some of those pollutants are greenhouse gasses; they are not transparent to long-wave radiation, as shown in Figure 4. Higher concentrations of these particulates locally or globally can be responsible for temperature rise, on the level of the earth's surface, as radiative heat loss is reduced by them. In addition, some particulates tend to absorb, reflect and scatter short-wave radiation. Their high concentration influences the solar radiation that reaches the surface, by decreasing the direct, and increasing the diffuse radiation (Sachsamanoglou, 1999). Generally their high concentration leads to higher air temperatures.

2.3.2 Urban Air Temperature

All these altered factors discussed above, lead to new energy balances in urban areas, which lead to different air temperature distributions in the urban areas. It can be said that in general the differences of the air temperature between urban and rural area, regarding distance, for a large city with clear sky, exhibit a steep temperature gradient to the centre of the urban area, forming an "island profile" (Oke, 1987), as can be seen in Figure 11.

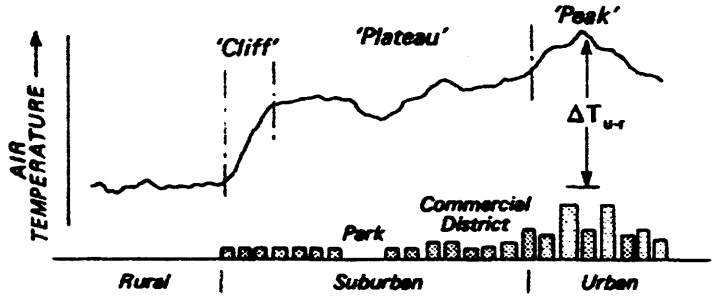

Figure 11. Typical sketch of an urban heat-island profile (Oke, 1987)

It is quite difficult to define the size of the heat island effect. Theoretically it could derive from a set of pre-urban measurements of the climate of the area before urbanisation and present measurements and after urbanisation (Oke, 1987). In most cases this is an impossibility, as most cities have been founded before the establishment of meteorological measurements. Instead, it is common to compare climatic data from the centre of the urban area with those from a rural or a non-urban station in its surrounding area. The temperature difference between the urban and rural environments is called the *heat island intensity* and it is an indicator of the

magnitude of the heat island effect. It is usually calculated from the maximum urban temperature at the canopy layer and its respective rural temperature (ibid.).

In the instance of Paris, the average annual heat island intensity is of the magnitude of +2°C to +3°C compared to the countryside. It is estimated that only a very strong wind with an average speed of more than 11m/s or a very intense rain can eliminate the heat island effect of Paris almost completely but even then only temporarily (Cantat, 1989). Chandler (1965), when examining the heat island effect of London came to the conclusion that there were more days with exceptionally high temperatures and fewer days with lower temperatures in the city centre. The estimated London heat island density is of the magnitude of +1.4°C (ibid). For the hotter climate of Athens and its more significant absence of vegetation the heat island effect becomes larger; reaching the magnitude of +10°C (Santamouris, 2001). For Hong Kong, the day-time heat island intensity reaches +1.5°C in summer (Giridharam et al., 2004), and Tel-Aviv's heat island intensity is of a similar magnitude (+1.5 to +2.5°C) (Saaroni et al., 2000). A summary of heat island intensities for various cities can be observed in Figure 18 and Figure 19 (page 62).

There are differences between the urban and rural areas both on a time and space scale. On the time basis two different patterns can be distinguished; the diurnal and the seasonal pattern. A brief description of those three patterns is presented in the following section.

2.3.2.1 Diurnal Pattern

Typically, during the night, urban environments are warmer than rural ones, as they cool down at a slower rate than rural areas; solar radiation stored as heat in their thermal mass during the day is released to the environment with a lower frequency than in rural areas. As the sun rises, solar radiation does not immediately heat up the rural environment, as it is consumed in evaporating the dew. By comparison, the urban fabric starts heating up immediately. When the dew has evaporated from plants rural surfaces start warming up faster than urban ones, as they have lower heat capacity. The temperature difference between the urban and rural environment at midday depends then on the urban density, the wind speed, the anthropogenic heat release in the city, the concentration of pollutants. During sunset, rural surfaces cool

down very rapidly because of their low heat capacity. At the same time, urban surfaces cool down more slowly. Thus, the largest differences are normally noticed during the night, as can be observed in Figure 12. In the instance of London, the average day-time heat island effect is of the magnitude of 1.1°C, while at night it reaches 1.9°C (Chandler, 1965).

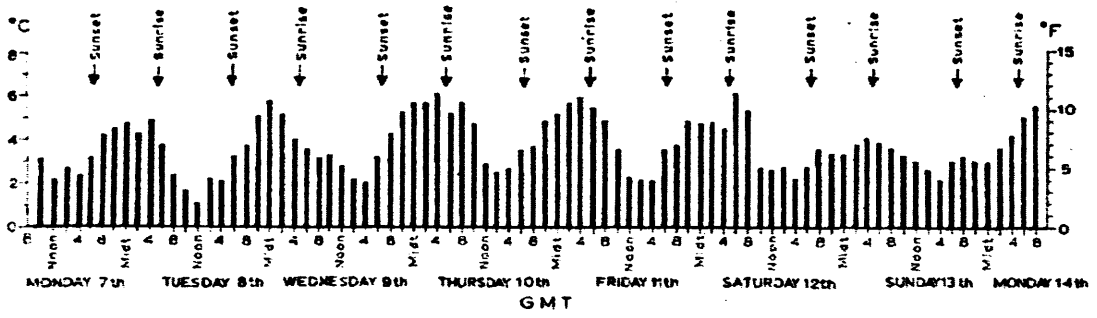

Figure 12. Diurnal heat island intensity in September 1959 in London (Chandler, 1965)

A typical diurnal temperature pattern for urban and rural areas is presented in Figure 13.

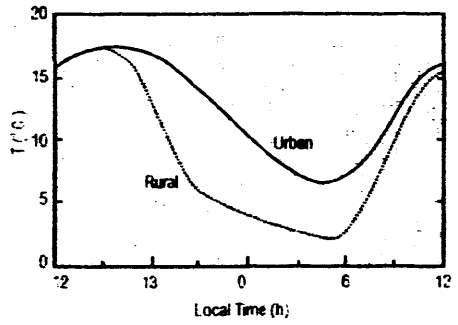

Figure 13. Typical temperature diurnal pattern for urban and rural area (Santamouris, 2001)

2.3.2.2 Seasonal Pattern

The seasonal pattern of the heat island effect depends on the climate and the local characteristics of the area of the city. Generally, for cities with warm and hot climates, the heat island intensity is usually larger in summer than in winter. This happens because the solar input is larger, therefore urban fabric stores more heat and urban materials raise their temperatures more. Wind speeds are usually lower thus less heat is removed from the urban environment. There is less rainfall, consequently urban surfaces remain dry.

This seasonal difference applies in most European cities, especially those in the south. In the example of Athens, the heat island intensity in summer has a mean value

of 12°C, while in winter it is 8°C, with 4°C difference between the two seasons (Santamouris, 2001). In central and northern European cities there is little difference between summer and winter intensities (Watkins, 2000), as solar radiation and air temperatures are not as high as in southern parts. In the instance of London, the winter heat island intensity is 1.2°C, while the summer one is 1.6°C, with only 0.4°C difference between the two seasons (Chandler, 1965). As can be observed in Figure 16 (page 60) the heat island intensity of Paris is 2.9°C in summer and 1.9°C in winter (Cantat, 1989), with 1°C seasonal difference, slightly higher than London's but lower than Athens'. In Figure 14 the monthly variation of the heat island intensity of the city of Szeged, in Hungary is given, where the monthly variations of the heat island intensity within the same season can be observed.

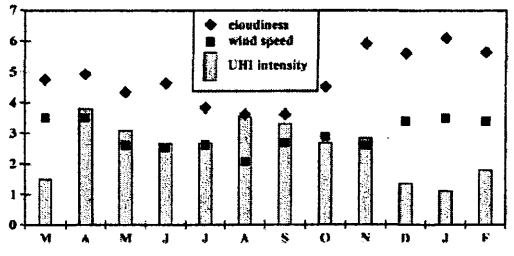

Figure 14. Monthly variations of the urban heat island intensity for the city of Szeged, Hungary (Unger et al., 2001)

2.3.2.3 Spatial Pattern

Heat islands are not uniform across a city. Air temperature is determined by the microclimate of different areas of the city, which is defined by their density, geometry, materials, and the existence of vegetation. The idealised profile of a city described in Figure 11 (page 56), shows that for a large city with clear sky, the air temperature rises sharply on the outskirts of the urban area, exhibiting a steep temperature gradient forming a "cliff". Across suburbia the temperature gradient is gentler, forming a "plateau". It rises more significantly to a peak on the urban core. The presence of vegetation or water produces a local temperature reduction.

In practice, this simple visual concept of the heat island effect is not very realistic; urban climate is generally made up of smaller microclimates, microclimates made up from the characteristics of urban canyons, the existence of vegetation, open spaces and their relationships. All these microclimates can have significantly different temperature distributions, depending on their surface temperatures, which are affected

by materials, geometries and vegetation. An example of the spatial distribution of air temperatures of the heat island of London is given in the following figure.

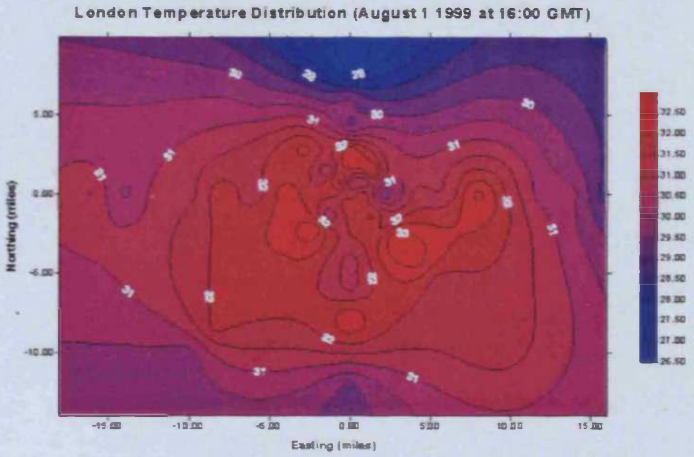

Figure 15. London heat island, as was recorded in August 1999 (Kolokotroni, 2001)

Generally, as was mentioned above, the city centre tends to be hotter than the suburban area. In the instance of the wider area of Paris, the isotherms show that the "pole" of the heat island is at the centre of the city in a zone which corresponds approximately to the areas which are the most densely and the most anciently urbanised (Cantat, 1989). In the following figure a comparison of average air temperatures for different areas of Paris and its suburbs for the period 1971-1980 are given.

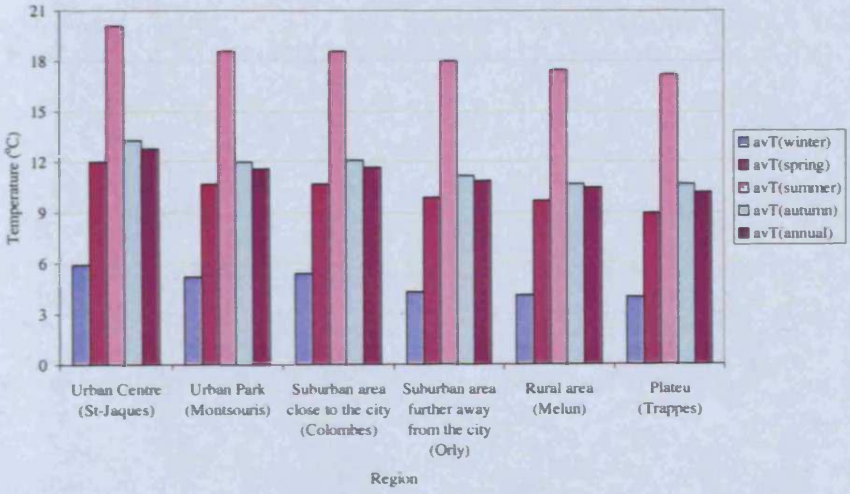

Figure 16. Average seasonal air temperatures for the period 1971-1980 for different areas of Paris and its surroundings (adapted from data by Cantat, 1989)

It is obvious in Figure 16 that as one moves away from the city centre, average air temperatures are lower. It is interesting to mention in Figure 16 that the urban park

Montsouris is cooler than the suburban area Colombes, built close to the city, by an annual average of 0.1-0.2°C.

The heat island effect does not only apply to surfaces and the air above them; it extends well above the ground up to the city's boundary air layer. Ca et al. (1999), developing a three-dimensional local scale model for describing temperature distributions within the built environment, simulated various areas of the city of Tokyo. According to their estimations, temperatures in the city centre (Figure 17b) were higher than those in the suburban area (Figure 17a) not only near the ground, but well away from it as well. It can be observed that at 150m height, most suburban temperatures are between 28.0-28.5°C, while at the same height for the city centre they are in the band of 28.5-29.0°C.

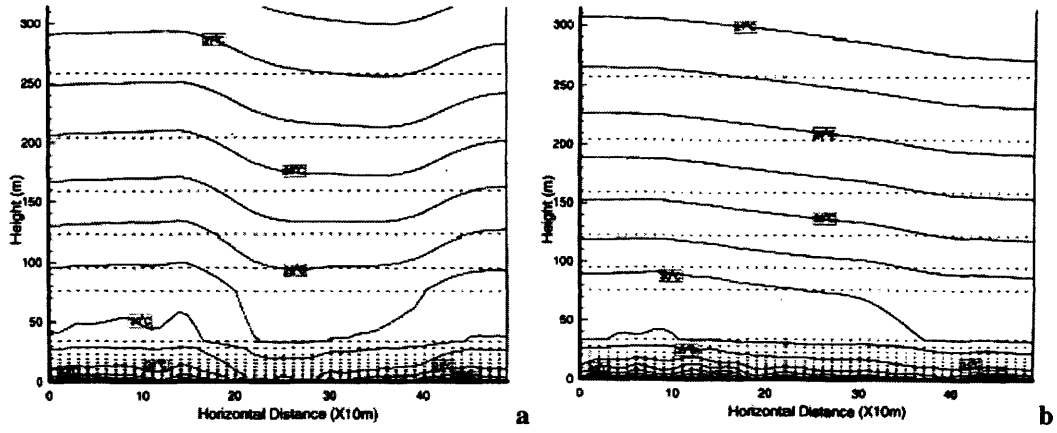

Figure 17. Calculated vertical distribution of air temperature at 14:00 (a) in Kamiigusa (suburban area) and (b) in Kojimachi (city centre) of Tokyo Metropolitan area (Ca et al., 1999)

2.3.2.4 Determining the Heat Island Intensity

Studies have been carried out in order to identify and examine the heat island intensity and pattern. Oke (1987) has suggested the following formula, which correlates the heat-island intensity to the size of the urban population and the wind speed, based on data from North American cities:

$$\Delta T = \frac{P^{1/4}}{(4U)^{1/2}} \qquad \textbf{Eq. 10}$$

Where:

ΔT: heat island intensity (°C)

P: population (number of inhabitants)

U: regional wind speed (m/s)

For European cities Oke (1987) suggested the following formula:

$$\Delta T = 2.01 \cdot \log P - 4.06 \qquad \text{Eq. 11}$$

It has been observed that cities with populations of thousands have maximum heat island intensities of 2 to 3°C, while cities with population of one million the intensities can be 8 to 12°C (Watkins, 2000). As Givoni (1998) concludes, the larger and denser the city the greater the difference which is commonly observed between the city centre and its surrounding area.

In the following figures measurements of the heat island intensity, compared to the population from cities in Europe, North America, Japan and Korea (Figure 18) as well as cities in tropical latitudes (Figure 19) are given.

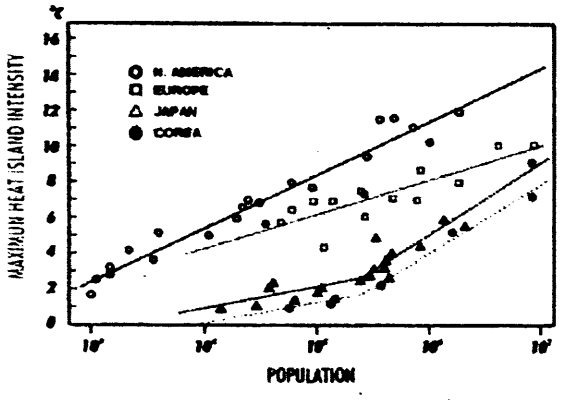

Figure 18. Relationship of the maximum heat island intensity with urban population in European, North American, Japanese and Korean cities (Santamouris, 2001)

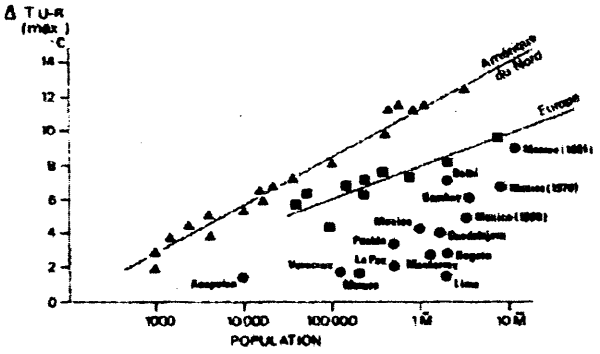

Figure 19. Relationship of the maximum heat island intensity with urban population in European, North American and tropical cities (Escourrou, 1991)

It is obvious from Figure 18 and Figure 19 that regardless of the climatic zone of a city the higher its population is (which makes the city larger and/or denser) the greater is the heat island density. Urbanisation can therefore be considered to be a major factor affecting the heat island effect. In most cities that have expanded dramatically in the 20th century, a significant rise of air temperature has been noticed. In the instance of Paris, from measurements for the period from 1891 to 1968 it is found out that there has been a 1.1°C raise for the maximum temperatures and a 1.9°C rise for the minimum temperatures with a 0.8°C reduction for the diurnal amplitude. During this period the city expanded significantly, particularly after the second half of the 19th century when the surface of its inhabited area increased from 100 km^2 to 2300 km^2 (Cantat, 1989). With the expected further expansion of urban population (Nash and

De Souza, 2002; Ashford, 2004), discussed in chapter 1, heat island intensities might rise even more in the future, unless action is taken to lower the raised urban temperatures.

The thermal consequences of the urban development seem to be more important for the centre than for the zone where the extension of the city has taken place. In the example of the area of Montsouris in Paris (outskirts of Paris), despite the fact that urbanisation was stabilised even before 1951, its temperatures appear to rise as there is quite important urban development around it (Cantat, 1989). The temperature pattern in Paris since 1950 show that urbanisation in zones on the periphery of the city reinforces the heat island effect at the urban centre. When there is a wind speed of the magnitude of 2-5m/s the heat island effect is "removed" and is made apparent in the suburban areas at the wind direction as an "urban shadow". When the wind speed is of the magnitude of 10m/s the thermal exchanges between the air and the ground are only sensible but the heat island effect is totally dispersed (ibid.). Wind speed and urban population are very important factors for the intensity of the heat island as has been concluded by many researchers (Oke, 1987; Givoni, 1998; Escourrou, 1991).

Regarding the geometric characteristics of the city (density, rise) Oke (1987) has also correlated the heat island intensity with the geometry of the urban canyon, the building height, H, and the street width, W, with the following relationship:

$$\Delta T_{max} = 7.45 + 3.97 \ln \frac{H}{W} \qquad \textbf{Eq. 12}$$

A fairly significant factor that describes the heat exchanges of the urban canyon with the sky is the Sky View Factor (SVF). SVF expresses the geometric relations between a surface and the sky in order to determine the radiative heat exchange between them.[6] The higher the sky view factor, the lower the street surface temperature becomes. Oke (1987) has suggested a formula, correlating the heat island intensity with the SVF:

$$\Delta T_{max} = 15.27 - 13.88 \cdot SVF \qquad \textbf{Eq. 13}$$

[6] For an unobstructed, horizontal surface the SVF is equal to 1.0. For a surface surrounded by close, very high buildings, or a very narrow street, it can be 0.1.

2.3.3 Urban Surface Temperatures

As explained in paragraphs 2.3.1.1 to 2.3.1.6, the thermal properties and geometric relationships of urban surfaces are responsible for raised surface temperatures. Due to the complexity of urban geometry and variation of materials, spatial variation is noticed in surface temperatures as well. This spatial variation has been observed quite clearly in the area of Paris from a thermogram taken by a satellite on 30th April 1984 at 11:30 Paris time. Cantat (1989) observed the following regarding surface temperature: the hottest zones (24-30°C) were zones of very high industrialisation, the highways and railways, certain agricultural areas which had plain soil and very little vegetation and the centre of Paris, which is densely built. The coldest zones (10-20°C) were places with water or parks with dense vegetation within the city, forests around the city and agricultural areas. The zones with a "temperate" surface temperature (20-24°C) were mixed spaces with the presence of significant areas of water and vegetation. Radiometer images in Paris also showed diurnal variations, as well as a correlation between urban density and surface temperatures (Dousset and Gourmelon, 2003). It was found that in most cases, the denser the area the higher its surface temperatures are. At night there is a stronger correlation between surface temperatures and urban density (Figure 20), while for day-time the variance is larger, presumably due to larger fluctuations of heat fluxes.

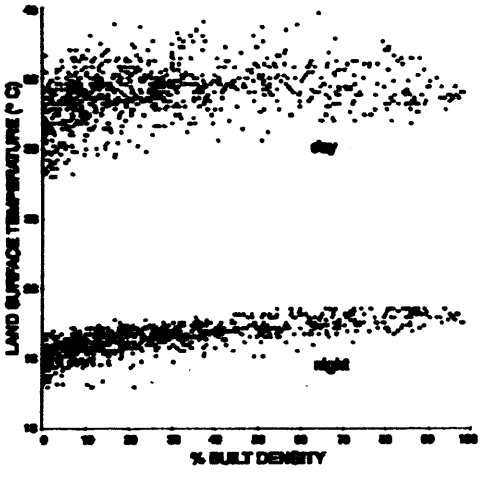

Figure 20. Nighttime and daytime averaged Land Surface Temperature images as a distribution of percentage of the urban density for Paris (Dousset and Gourmelon, 2003)

Urban surface temperatures, focusing on the variety of temperatures on different construction materials in the urban texture of Athens were measured by Santamouris et al., in the summertime of 1996-1999 (Santamouris, 2001) (Figure 21). The surface temperature of asphalt, white and dark pavement slabs was measured. It was found

that the maximum peak for asphalt was 57°C, while for white and dark pavement slabs was 45°C and 52°C respectively. This was carried forward to a study of classifying urban materials as "cold" and "warm" (Doulos et al., 2004), where it was pointed out that materials which do not raise their temperature so much are materials with smooth and light coloured surfaces, made of marble, mosaic or stone, while materials with rough and dark surfaces made of pebble, pave stone and asphalt are responsible for raised surface temperatures.

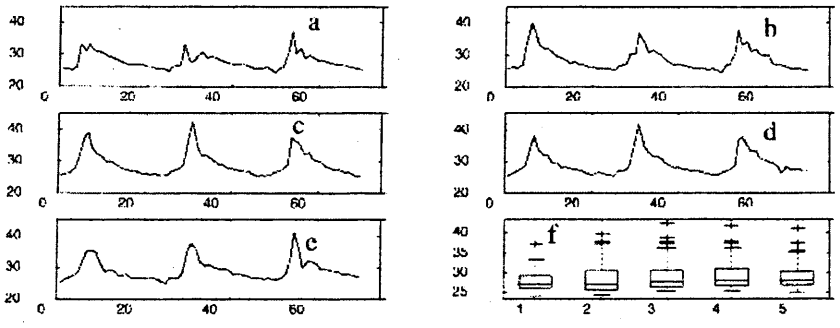

Figure 21. Three-day hourly measurements of surface temperature in an urban canyon of the pavements and the street in the centre of Athens, with temperature being plotted in the y-axis and time in the x-axis, for a) the SE-oriented façade, b), c) and d) the street, e) the NW-oriented façade and f) boxplot of the measured temperatures for the whole period of measurements (Santamouris, 2001)

Apart from surface materials, in the soil itself, the existence of concrete building foundations results in raising the temperature and homogenising the vertical thermal gradient compared with measurements carried out underneath a normal, green surface. In the centre of Paris green areas are characterised by the formation of a microclimatic nocturnal frigidity of the ground in contrast with the vertical homothermality under the urban materials (Cantat, 1989). On the 17th January 1985 when Paris was covered with snow (approximately the same albedo for all the surfaces), at a depth of 10cm below the surface of the ground the soil temperature was -19.0°C in the urban park Montsouris and at the same level and time in the suburban area Melun it was -21.1°C (giving an urban-rural soil temperature difference of +2.2°C). At 50cm below the surface of the ground the urban-rural soil temperature difference because of the heat island effect was even more noticeable, reaching +4.3°C (-15.5°C at Montsouris and -21.2°C in Melun) (ibid.).

2.3.4 Urban Humidity

Generally relative humidity is lower in urban centres than in their surroundings. Due to the raised temperatures, the air can contain larger amounts of water vapour. The analogy between the water vapour that is contained in the air and the water vapour which should be contained so that it is saturated, increases. Thus, relative humidity decreases. Chandler (1965) when measuring relative humidity distributions in the greater area of London, showed that regarding relative humidity the heat island effect has an inverse effect than for temperatures; the centre of the city shows minimum relative humidities, compared to suburban and rural areas (Figure 22). For a night in October 1961, the measured relative humidity in the centre of London was 74%, while for the suburban areas it was as high as 90-100%. In the instance of Paris for the period 1951-1980, the relative humidity at the centre of the city was 72%, in a park at the edge of Paris it was 75% and at the sub-urban area it was higher, reaching 79% (Cantat, 1989). In other cities where relative humidity has been measured both in the centre and in the periphery the results are similar. For Mexico City, which is very densely built and without a lot of vegetation at its centre, the discrepancy is even more significant (Figure 23); relative humidity is 50% in the centre of the city and more than 75% in the suburban areas (Escourrou, 1991).

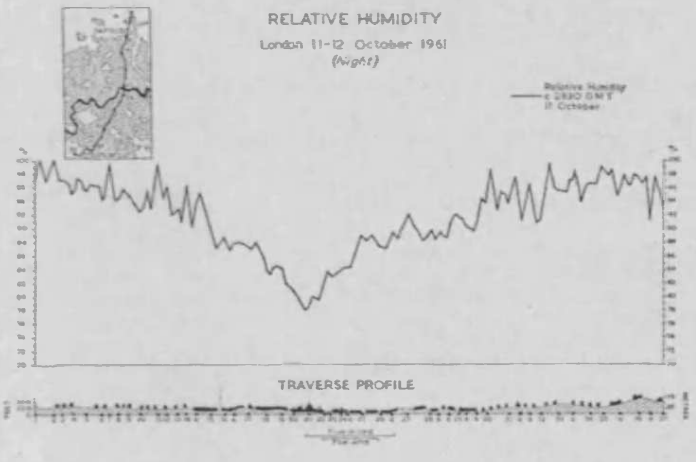

Figure 22. London relative humidity spatial variation as an inverse temperature heat island effect; the traverse for the night 11-12 October 1961 (Chandler, 1965)

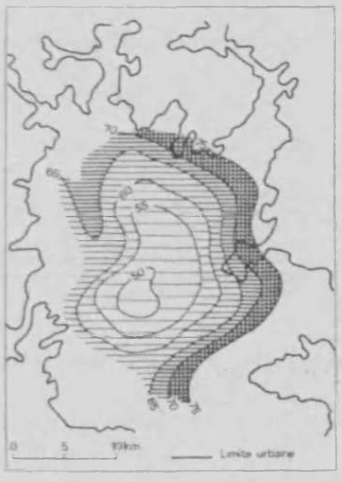

Figure 23. Relative humidity contour map for Mexico City (Escourrou, 1991)

The reduction of air relative humidity due to the heat island effect result in dispersing fogs and the faster disappearance of lower clouds in the centre of large cities which are not so polluted (Cantat, 1989). The following graph shows the seasonal variations of water vapour tension in the area of Paris for 1983.

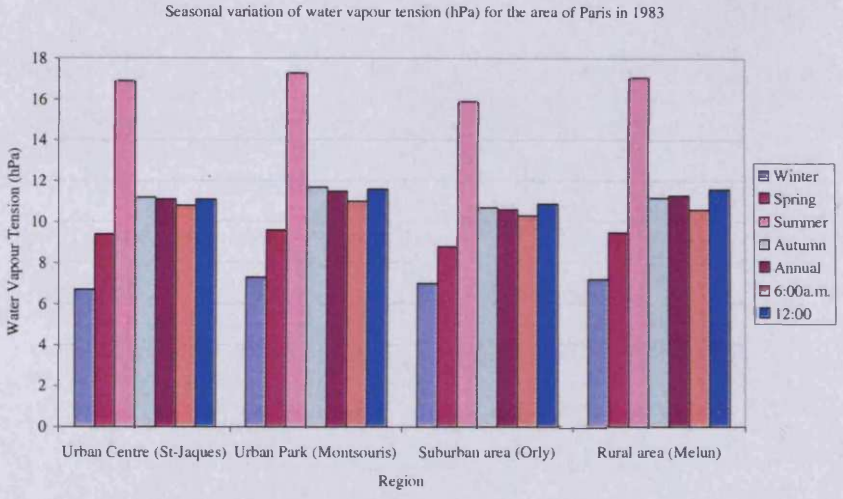

Figure 24. Seasonal variation of water vapour tension for the area of Paris in 1983 (Adapted from data by Cantat, 1989)

According to the graph the urban park Montsouris raises local vapour concentration of soil and vegetation. The difference in the humidity between the park and its surrounding urban area is more noticeable in the middle of the day than at night. This is due to the fact that the water vapour released from evaporation from soil and plants is absorbed during the day by the diurnal rise in temperature and solar radiation. Therefore there are significant differences concerning relative humidity in the air of the urban canopy in a diurnal scale also. In summer daytime the content of moisture in the air in urban areas is much less than in the surrounding countryside. This happens because the evapotranspiration rate decreases in the city; the amount of water that is released to the air by combustion is very small. However, at night in summer, especially in calm clear weather, the city air may be slightly moister, forming a humidity "island" or "plume" (Escourrou, 1991).

2.3.5 Urban Precipitation

The urban characteristics described above contribute to the reinforcement of the instability of air masses. In 1980, Escourrou (1991) observed that the stability of the air mass seems to play a determinant role in explaining the influence of urbanisation on precipitation. It is quite difficult to identify the exact influence of the heat island effect in urban precipitation due to the complexity of the influence of external elements (such as topography) and to the very large geographical range and variety of rainfall pattern. Generally within cities, there is a tendency for lower rainfall.

Nonetheless, there are exceptions; in large industrial centres such as The Port (at the east of Chicago) it is estimated that the acid production from factories must be responsible for a 20-30% raise of precipitation (Cantat, 1989). In 1957, Pédelaborde noted that *"generally cities have rains a little superior to those ones in the country. It is possible that the main reason for this might be the existence of so many clouds of condensation"* (cited in Escourrou, 1991), without commending on the total amount of rainfall itself. It has been observed that in the city of Athens rainfall has generally decreased as a result of urbanisation (Fidas and Lalas, 2000). Since 1925 (period when the city expanded dramatically and the number of buildings increased by 335.82% in the area of Athens and by 664.51%[7] in the greater area of the city) the rainfall in the area of Athens has decreased by 10% (Fidas and Lalas, 2000) (Figure 25). This urban precipitation decrease has been observed in Paris as well, where, for the period 1961-1980 the average duration of rainfall was 529 hours in Paris (Montsouris), 818 hours in the North suburban area Bourget and 840 in the South suburban area Orly (Escourrou, 1991).

The general tendency of cities is to have decreased rainfalls, due to the impermeable materials. However, there can be exceptions, depending on the industrial activity and the specific characteristics of the city, where the heat island effect might increase rainfall.

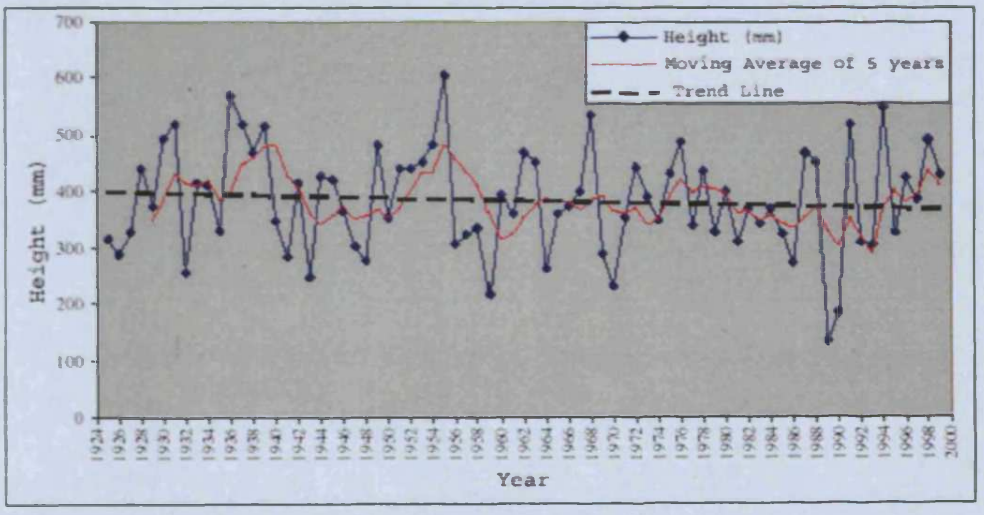

Figure 25. Average annual rainfall in Athens from year 1924 to year 2000 (adapted from Fidas and Lalas, 2000)

[7] According to data from the National Statistical Service of Greece (1990), up to 1919 there were 3,138 buildings in Athens and 6,263 in the greater area, while in the period of 1919-1945 buildings in the area of Athens increased to 10,538 and in the greater area to 41,618.

2.3.6 Urban Radiation

The differences in radiation between urban and rural areas are mostly due to atmospheric pollutants and vary for different climates and topographies. In general, photochemical smog may prevent solar radiation from reaching the ground and green house gases may reduce heat losses from long-wave radiation. As was observed in Paris, the phenomena of alteration of solar radiation are more important during the cold period (Cantat, 1989). In December, one hour of solar radiation brings an average flux of 14.4W/m^2 in Trappes (rural area) and 11.4W/m^2 in Paris, with an average 20.8% less solar radiation in the city centre. In summer these numbers become 26.6W/m^2 and 22.8W/m^2, respectively, with 13.0% less solar radiation in the urban area (Cantat, 1989). On an annual basis Trappes receives 21.9W/m^2/h while this is 18.8W/m^2/h for Paris (14.1% less for the urban area).

On the other hand, for the lower latitude of Athens solar radiation is reported to be increasing mainly due to scattering of pollutants accompanied by a parallel decrease in the amount of sunlight. According to Sachsamanoglou (1999) there seems to be a raise of irradiation in Athens by 5.2% in recent years (Figure 26). If it is also taken into account that, at the same time, sunlight is reduced at a rate of change of 3.034h/year, due to more intense cloud cover, then the total rise of the global solar radiation is 9.7%. During hot months there is a quite significant rise of irradiation but at the same time there is a decrease in sunlight. This is due to the high concentration of atmospheric pollutants in the atmosphere of Athens from anthropogenic activities which increase in summer due to the extensive use of air-conditioning systems (ibid.).

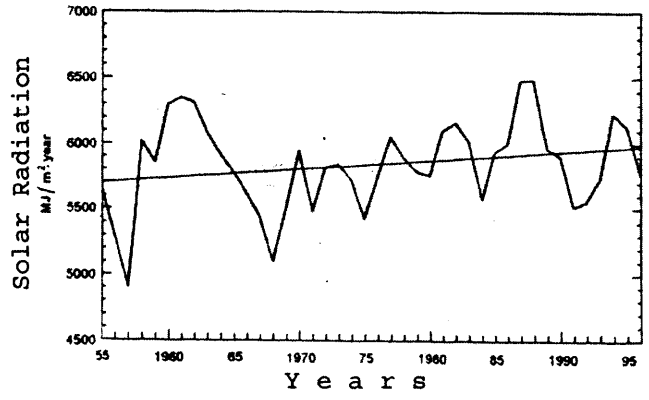

Figure 26. Increase of irradiation in Athens in the last years (adapted from Sachsamanoglou, 1999)

2.3.7 Urban Wind Speed

Generally the wind flow pattern near a surface is determined by the geometry of the surface and its characteristics (e.g. roughness). When a fluid flows along a surface, particles close to the surface are slowed down, because of viscous forces. Particles in contact with the surface adhere to it and have virtually zero velocity. Fluid particles flowing over the adhering particles are slowed down, because of the interaction of faster and slower moving particles. This causes shearing forces to occur. When flow is laminar, the interaction, called viscous shear, takes place on a submicroscopic level. In turbulent flow the interaction is between lumps of the fluid, called turbulent shear. The effect of shearing stress at the boundary extends into the fluid, but at some distance from the surface the velocity of the fluid particles is near that of the undisturbed stream. The boundary layer is the layer in which the fluid is affected by the shearing forces originating at the surface.

In lower parts of the atmosphere, the wind flow is influenced by the surface of the earth. When air flows over a region, the effect of the earth's friction forces creates a boundary layer at the wind flow. The boundary layer extends, by definition, to the height at which wind velocity is about 99% of that in free air movement. This height can be considered to be the *external boundary layer*. Each field or surface feature of varying roughness or height has its own effect and an *internal boundary layer* equilibrated to each surface develops within the external boundary layer. Those two layers are not completely independent. Usually, after some length, the external boundary layer adjusts to the increasing height of the internal boundary layer. These layers are also observed in the wind flow around a city (Rosenberg, 1974). Oke (1987) described the external boundary layer of the flow over an urban area as the *urban boundary layer*, or the *urban air dome*. It is classified as an atmospheric phenomenon which happens in local or meso-scale, whose characteristics are governed by the nature of the general urban "surface". The internal boundary layer is called the *urban canopy layer*, which is identified by phenomena in the micro-scale, in the streets between buildings in which this study is mainly focused. According to Oke (1987), the difference between the urban boundary layer and the rural boundary layer is identified as the *urban plume* (Figure 27).

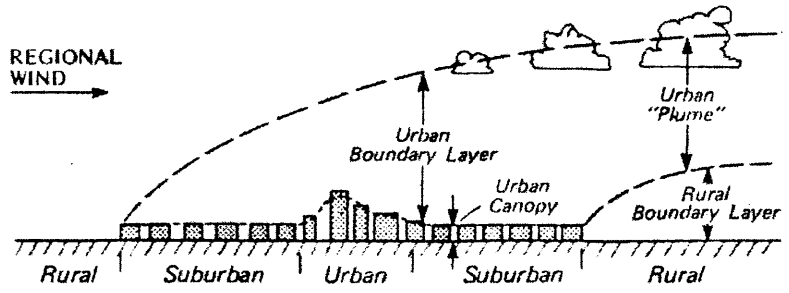

Figure 27. Schematic representation of internal and external boundary layers in the urban environment (Oke, 1987)

This alteration of wind flow in the area of cities has direct effect on wind speed. Chandler (1965) gave a comparative scale of the logarithmic profile of wind speed over urban, rural and sea surfaces showing that the effect of urban geometries on wind flow is generally higher than that of rural and sea surfaces (Figure 28).

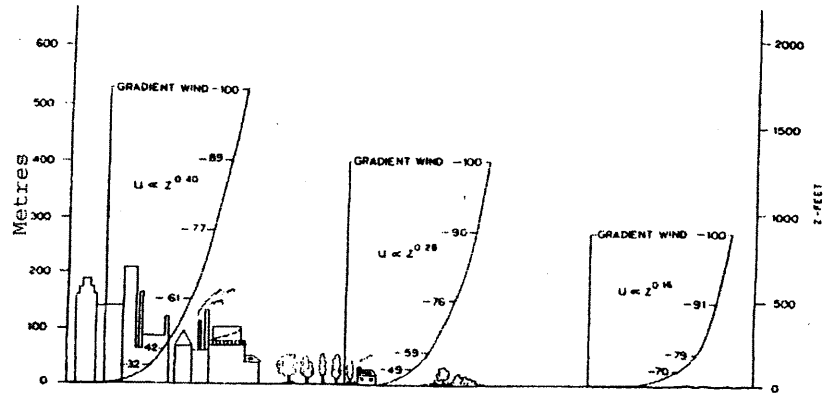

Figure 28. Schematic horizontal wind velocity profiles, above urban, rural and sea surfaces as percentages of gradient wind (Givoni, 1989)

It is evident from Figure 28, that because of the more complex geometries and generally increased heights in the urban environment, wind flow is affected by the urban texture much more than the rural one. Generally wind speeds are much lowered in urban areas than in rural ones. This has a direct effect on the way sensible heat is redistributed and driven away from the two spaces. Lower wind speeds cannot drive it away from the urban texture therefore raising the urban air temperature.

Escourrou (1991) studied the wind effect on the heat island intensity for the city of Paris. By measuring wind speeds at the top of the Tours Saint-Jaques, she found that heat island intensity decreases when wind speed increases. For wind speeds higher than 5m/s the heat island intensity was not important. The results of her study are summarized in Table 3.

Table 3. Wind effect on the heat island intensity of the city of Paris (Escourrou, 1991)

Wind speed (m/s)	Heat island intensity in Paris (K)
1.00	4.5
2.00	3.4
3.00	3.4
4.00	2.6
5.00	2.2

Apart from the alterations in the city meso-scale, the wind flow is dramatically altered in the urban canyon micro scale. In general, due to the canyon geometry of urban blocks, air velocities within the canyon tend to be much smaller than at roof level. From measurements conducted in Athens (Santamouris, 2001), it was found that wind speed above the canyon might reach values more than 5m/s, while, within the canyon the air velocity never exceeds 1m/s (Figure 29).

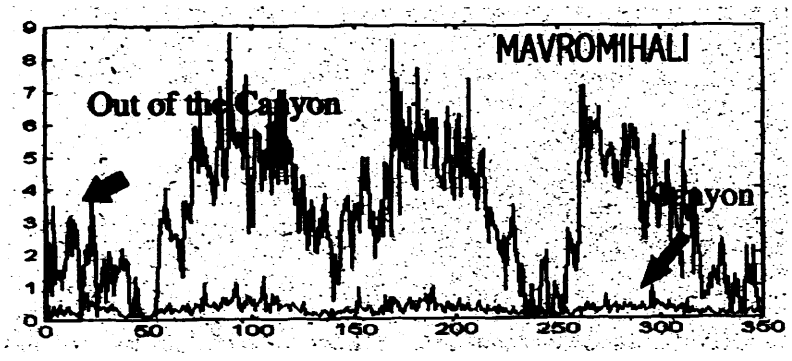

Figure 29. Wind speed (m/s) in and above a typical urban canyon in the city centre, in Athens (Santamouris, 2001)

2.3.8 Should the Heat Island Effect Be Mitigated?

In cold climates the heat island effect may influence beneficially the heating energy demand of buildings (Givoni, 1998). As higher ambient air temperature is produced, less energy is required for heating. As Cantat (1989) concludes *"if it was not for the atmospheric pollution, the heat island effect in the area of Paris would be a pleasant effect for the inhabitants by creating a local climate warmer, less humid and less windy"*. Chandler (1965) also points out that thanks to the raised temperatures of London, the active growing season of crops and the frost-free periods are extended. However, due to global warming becoming a sensitive issue over the last few years, this perspective has changed. It is estimated that the combination of global warming and the heat island effect of London might be responsible for more

energy being expended for cooling the city than the energy saved for heating and it could also lead to a parallel increase in summer stress and mortality (Clarke et al., 2002). With a rising trend, especially in nocturnal heat island intensity (Figure 30), and with the combined warming experienced in Britain in the recent years, these raised urban temperatures cannot be as beneficial as believed in the past, even for the high latitude of London.

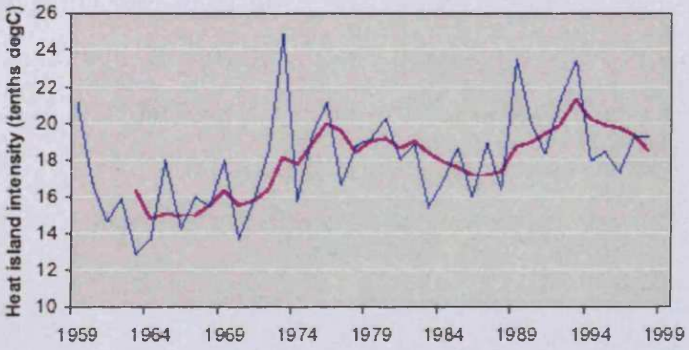

Figure 30. Annual average nocturnal heat island intensity, with rising trends, in London (Clarke et al., 2002)

For warm and hot climates, the resulting higher temperature can lead to increasing demands for air-conditioning during hot period which exceeds by far the energy savings in winter (Santamouris, 2001) and may cause unbearable levels of heat stress. The amount of energy consumed for heating and cooling buildings in cities in western and southern Europe has increased significantly in the last two decades (Dimoudi and Nikolopoulou, 2000). Due to the heat island effect, the cooling degree hours in the central area of Athens are approximately 350% greater than in the suburban areas and the heating degree hours are 40-60% less (Santamouris, 2001). Rosenfeld et al. (1995) showed that in American cities for each 1°C rise in daily maximum temperature above a threshold of 15°C to 20°C, the peak urban electric demand rises by 2–4%. The additional use of air-conditioning caused by this urban air temperature increase is responsible for 5–10% of urban peak electricity demand. The use of air-conditioning for cooling buildings removes the heat from the building to the urban environment. In very dense areas with excessive use of air-conditioning systems this leads to a significant rise of the ambient air temperature (Papadopoulos, 2001), and thus to a rise of the cooling demand, leading to a vicious cycle of rising ambient air temperature and energy demand.

Also, this extensive need for cooling energy leads to increasing emission of pollutants from power plants and air-conditioning systems such as sulphur dioxide,

carbon monoxide, nitrous oxides and suspended particulates. Especially in cities with hot climates, during summer, this combination of extreme temperatures and pollutants can even be responsible for high rates of morbidity and mortality. With the future climate change expecting to increase the number and intensity of extreme events, such as heat waves, and increased maximum and minimum temperatures (White et al., 2001), urban dwellers are bound to suffer from excessive heat stress. With most deaths caused by heat waves occurring in urban centres (Koppe et al., 2004), urban populations morbidity and mortality is bound to be at risk (White et al., 2001; Koppe et al., 2004). In the instance of the population of New York City, the death rates are higher on days when the 4:00 p.m. city temperature exceeds 30°C (Davis et al., 2003). The heat waves experienced in Europe in 2003 cost the lives of not only the most vulnerable groups of the population but also of parts of the population classified as healthy people under heavy activity (Diaz et al., 2005).

With the global trends of urban growth, analysed in chapter 1, and the fact that as urban centres grow, the heat island intensity becomes higher, as discussed in paragraph 2.3.2.4, it is expected that the heat island effect and its consequences will be stronger in the future. As spatial rearrangements envisaged in the early 20th century (discussed in chapter 3) might be unrealistic suggestions for our times, a solution is sought, which could be implemented to existing cities, regardless of their growing trends; a solution which could offer a better and safer quality of life to all layers of urban dwellers and ensure the viability of urban spaces.

This thesis focuses on how the heat island could be mitigated by changing the surface materials of urban areas; by covering urban surfaces with rural materials - vegetation- the physical factors influencing the heat island effect, summarised in paragraphs 2.3.1.1-2.3.1.6 will be altered, leading to new thermal balances with lower temperatures in summer. Lower temperatures can lead to less demand for cooling, which may alter the factors presented in paragraphs 2.3.1.7-2.3.1.8. Vegetation, by lowering pollution indirectly can lead to further temperature decreases (reduction of anthropogenic heat, alterations of solar radiation) and improvement of the air quality of urban spaces.

2.4 Urban Vegetation

When vegetation is placed on urban surfaces, thermal balances might shift to new conditions, closer to the cooler conditions of rural areas. The benefits of vegetation, apart from shading and that its surface temperatures are not significantly different to ambient air temperature, is also able to cause further cooling through the procedure of evapotranspiration, the combined procedure of evaporation and transpiration happening simultaneously at the vegetal surface (analysed in paragraph 4.6, chapter 4). When evapotranspiration occurs, a certain amount of water is lost from a cropped surface. The energy (heat) required to vaporise water is known as the latent heat of vaporization (λ), and is a function of the water temperature. This energy consumed during evapotranspiration is responsible for lowering air temperature.

It is estimated that 1460kg of water is evaporated from an average tree during a sunny summer day, consuming about 860MJ of energy; this offers a cooling effect outside a building that is equal to five average air conditioners (Santamouris, 2001). Measurements were carried out in order to investigate the cooling effect of trees on the microclimate of buildings by Rosenfeld et al. (1995) in Sacramedo, by Papadakis et al. (2001) in Athens and by Lay et al. in Singapore (2000). The results of all three studies were that trees can reduce surface temperatures through shading and air temperature through the combination of evapotranspiration and the shading of surfaces. Rosenfeld et al. (1995) measured the effect of shading two houses in Sacramedo with trees. They found that trees placed in front of south and south-west façades, as well as in front of the air-conditioner's condenser units, lead to a 30-35% drop in the air-conditioning energy use. On a vertical wall with south east orientation in Athens the peak solar radiation that was measured at the exposed parts of the wall to direct solar radiation in August was 600W/m^2 while at the same time at the shaded by trees parts it was under 100W/m^2 with a surface temperature difference of 8.5°C. Relative humidity was higher by 7% in the area with trees, due to transpiration, keeping air temperature in this area lower by 0.5°C to 3.0°C during daytime (Papadakis et al., 2001). Similarly, Lay et al. (2000) measured an 11.0°C peak surface temperature difference between shaded and unshaded parts of a vertical wall with west orientation in Singapore, in September. They went on to measure the thermal effect of potted plants on the built environment. They found out that they were responsible for an average 1.0°C air temperature decrease and a maximum of 4.0°C.

This technique, of lowering temperatures near a building by the use of vegetation has been applied since antiquity and might be one of the most efficient methods. Fylaktou-Cataneo (2002), when investigating the microclimate of three courtyards of the Alhamra palace in Granada, found that the most vegetated courtyard (Lindaraja) shows the lowest temperatures in summer, than the courtyards which only had water features. It can be observed in Figure 31 that the vegetated courtyard Lindaraja, shows lower temperatures than the external air temperature by 3.5°C, while the rest of the courtyards have practically the same air temperature as the external, unmodified space. Similar results were reached by Shashua-Bar and Hoffman (2002), when conducting experiments in courtyards in Tel-Aviv. They estimated that the thermal effect of trees in courtyards causes a 3.0°C temperature difference in the afternoon between a courtyard with and without trees.

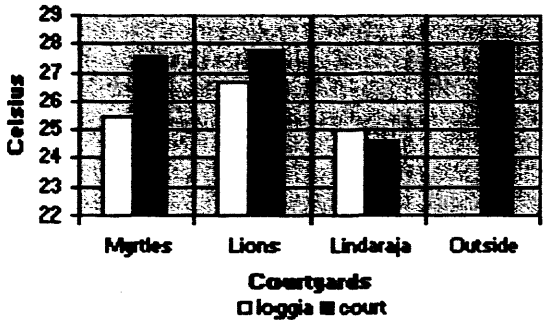

Figure 31. Comparison of measured air temperature (y-axis) in courtyard with vegetation (Lindaraja) and courtyards without vegetation in Alhamra palace in Granada (Fyalaktou-Cataneo, 2002)

Shashua-Bar and Hoffman (1999) when studying the effect of trees in Tel-Aviv found that in streets with heavy traffic and anthropogenic heat release, existing trees were responsible for a cooling effect of 1K. Taking into consideration that road make up 25% of the city's surface, they concluded that if trees are put in Tel-Aviv's streets, they will reduce the effects of anthropogenic heat due to traffic. They carried their research further to show how trees affect different geometries and canyon orientations (Shashua-Bar and Hoffman, 2003). They found that through the shading of trees, the role of the orientation of the canyon and its geometry are greatly minimised (ibid.).

Takahashi et al. (2004) carried out measurements in the city of Kyoto, comparing vegetated (site C) and non-vegetated (site U) urban areas (Figure 32). They found out that for days when the prevailing winds were from a direction where no vegetation existed (Figure 32a), the differences between the day-time average air temperatures between site U and site C away from the trees were negligible, while for site C, near

the trees, they were of the magnitude of 1°C difference. On days when the wind was passing from vegetated areas first in cite C (Figure 32b), the differences between the day-time average temperatures of the vegetated and the non-vegetated parts of site C were of the magnitude of 0.5°C and the differences between the non-vegetated parts of site C and site U also reached 0.5°C.

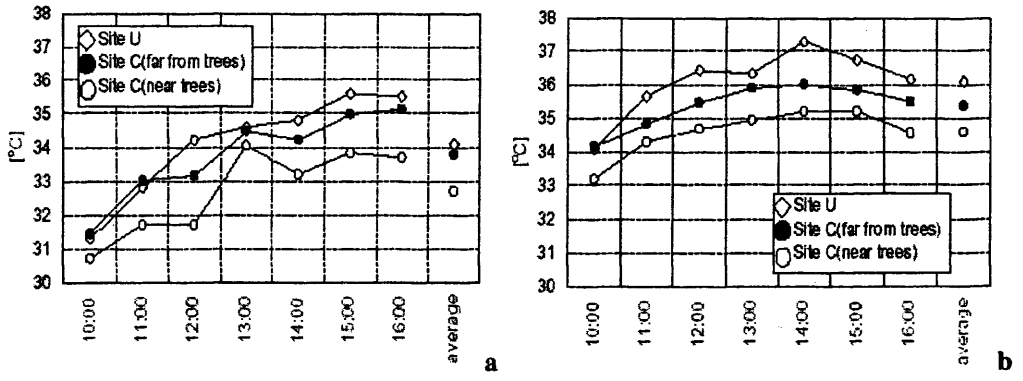

Figure 32. Air temperature measurements 1.5m above the ground in Kyoto in a central part of the city with medium height commercial buildings and scarce vegetation (site U) and a university campus with much greenery (site C) for (a) 21st July, with south prevailing winds, where not so much green area exists and (b) 28th July, with eastern winds, coming from the vegetated area (Takahashi et al., 2004)

The benefits of urban vegetation have been summarised by Akbari et al. (1992) in Figure 33. Apart from energy savings, vegetation offers much better thermal conditions in urban spaces, and makes them more attractive to use. In the RUROS project, a project for assessing thermal comfort models for open urban spaces, interviews took place in various open urban spaces in different climatic zones of Europe. 49% of the interviewees stated that vegetation is an important factor for using open urban spaces (Nikolopoulou, 2004).

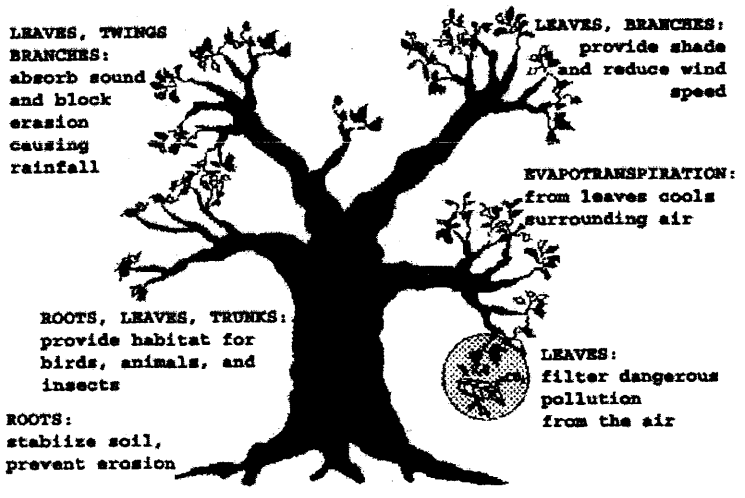

Figure 33. Ecological qualities of trees (Akbari et al., 1992)

2.5 Urban Parks

Lately there has been quite some interest in urban parks, in the question of how they could lower the global urban air temperature. Although urban parks can be extremely beneficial for a city from a social and city planning point of view, from a thermal point of view they can mitigate the heat island effect only at their micro or meso scale, rather than the local scale of the city. The air temperature is reduced significantly inside the park, but only the few buildings which are in the neighbouring area of the park can benefit from the reduction of air temperature due to the park's vegetation. The rest of the city is not affected thermally by the presence of the park. This has been proved both theoretically and through in situ measurements and experiments.

Measurements carried by Santamouris et al. in parks in the centre of Athens in the summer of 1998, showed that the air temperature inside the park is significantly lower than for the densely built city centre, with a peak difference in the afternoon, of the magnitude of 13°C (Figure 34). They pointed out that temperatures in these parks present almost 40% fewer cooling degrees hours than their surrounding urban stations (Santamouris, 2001). From measurement in the urban park *Ethnikos Kipos* (National Garden), it was found that air temperature is lower at the core of the park by 3°C compared to its surrounding built environment (Figure 35). Buildings right next to the park experience a 1°C rise, compared to the core of the park. It was also found out that the air temperature around the park is mainly influenced by parameters other than the presence of the park's vegetation, such as the density of buildings, the rate of anthropogenic heat release, the shading of canyons and so forth (ibid.) and not so much by the park itself.

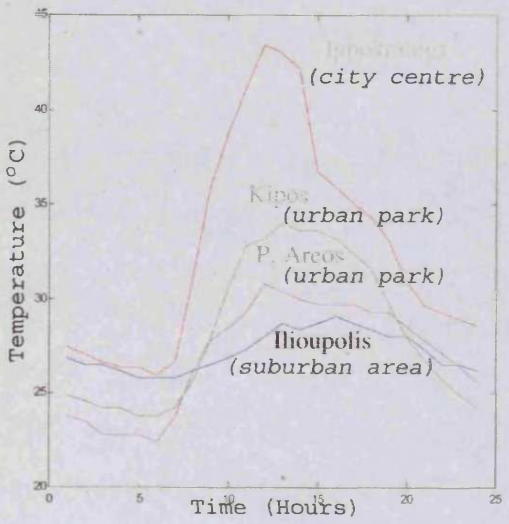

Figure 34. Diurnal pattern of temperature distributions in two urban parks, the city centre and a suburban area in Athens (adapted from Santamouris, 2001)

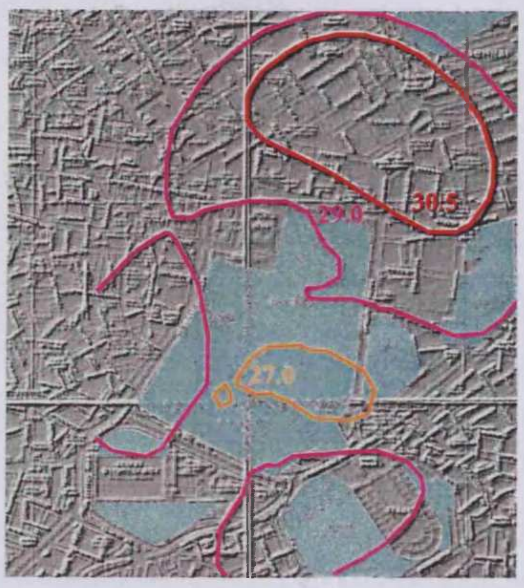

Figure 35. Temperature distribution in and around a park in Athens (adapted from Santamouris, 2001)

Computational modelling for the effect of parks on the air temperature at the centre of Athens was carried out by Dimoudi and Nikolopoulou (2000). The modelling was performed with the use of the Computational Fluid Dynamics programme PHOENICS, inputting evapotranspiration from vegetation as heat sink in the area of the park. Through their study they showed that the buildings which could have a thermal benefit from the existence of a park were only those which were contiguous to it. Heat stored on buildings fabric affects immediately the cool air of the park, raising the ambient air temperature immediately (Dimoudi and Nikolopoulou, 2000).

In the tropical hot and humid climate of Dhaka, Bangladesh, measurements were carried out by Ahemed in 1995 in different urban layouts of the city. It was found that 300m away from a large park of a high-density modern built part of the city (the Motijheel commercial area) there was practically no cooling effect from the park. On the contrary at the Ramna area, which dates from the beginning of the 20th century and is characterised by its low density and mature trees lining each road and with a fairly high distribution of vegetal covering in general, air temperature at these urban canyons was noticeably lower because of the existence of vegetation (Ahemed, 1995). Ahemed came to the conclusion that for tropical climates a number of small parks in an area of the city can be more effective in moderating the microclimate of the area than a large park.

Ca et al. (1998) measured and simulated the thermal effects of parks in the Tama New Town, in the west of Tokyo, in summer. Tama, being characterised with several green areas and a central park, it was found that the scattered small parks of the Tama area can have a thermal effect on a radius of almost 500m and that they can lead to almost 15% cooling savings at noon.

Bruse and Fleer (1998) calculated the effect of an urban park on the urban climate with the use of the ENVI-met software. They also come to the conclusion that the thermal effect of parks is quite local. Giridharam et al. (2004) when evaluating the heat island effect in residential high-rise and high-density areas of Hong Kong also come to the conclusion that pockets of green area are more advisable for mitigating the heat island effect than a single large green area. For densely built, tropical Hong Kong they estimate that these green areas should be placed every 20-30m distance of built area and that they should be at least of an area of 600-700m^2.

With the existence of an urban park, the heat island effect is therefore moderated quite locally, basically inside the park and at its surrounding buildings. A local oasis is formed, but only in the core of the park and its immediate surroundings. The rest of the buildings and the city itself remain practically unaffected by the presence of the park from a thermal point of view. Urban parks can have a quite important effect on the urban air temperature if they are spread across the city and they are quite densely placed (Dimoudi and Nikolopoulou, 2000; Ahemed, 1995; Giridharam et al., 2004; Bruse and Fleer, 1998). From an exaggerated thermal point of view, parks in the city could thus be paralleled to oases in the desert; no matter how many oases there are, the temperature is still high in the desert, away from the oases. Numerous oases could have a larger thermal impact on the desert enclosing them, but they could not lower its temperature as much as if they were part of the desert, if the oases and the desert could not be so separated. Although this cannot happen in the desert, it could happen quite easily in existing cities, by covering its impermeable, hot surfaces, such as the walls and roofs of buildings, with vegetation.

2.6 References

1. K.S. Ahemed (1995) *Approaches to Bioclimatic Urban Design for the Tropics with Special Reference to Dhaka, Bangladesh.* Ph.D. Dissertation. Environment & Energy Studies Programme. Architectural Association Graduate School. London.
2. H. Akbari, S. Davis, S. Dorsano, J. Huang and S. Winnett (eds) (1992) *Cooling our Communities; a Guidebook on Tree Plnating and Light-Colored Surfaces.* U.S. Environmental Protection Agancy.
3. H. Akbari, D.M. Kurn, S.E. Bretz, J.W. Hanford (1997) *Peak Power and Cooling Energy Savings of Shade Trees.* Energy and Buildings, Vol. 25 (1997), pp 139–148.
4. H. Akbari, M. Pomerantz, and H. Taha (2001) *Cool Surfaces and Shade Trees to Reduce Energy Use and Improve Air Quality in Urban Areas.* Solar Energy Vol. 70 (2001), No. 3, p. 295–310.
5. R.G. Allen, L.S. Pereira, D. Raes and M. Smith (1998) *Crop Evapotranspiration - Guidelines for Computing Crop Water Requirements - FAO Irrigation and Drainage Paper 56. FAO* - Food and Agriculture Organization of the United Nations, Rome. Available from http://www.fao.org/docrep/X0490E [Accessed 10th June 2001].
6. L. Ashford (2004) *World Population Highlights 2004.* Bridge Project, Population Reference Bureau. Available from http://www.prb.org [Accessed 4th December 2004].
7. A.P.M. Baede, E. Ahlonsou, Y. Ding, D. Schimel, B. Bolin and S. Pollonais (2001) The Climate System: An Overview. *In:* J.T. Houghton, Y. Ding, D.J. Griggs, M. Noguer, P.J. van der Linden, X. Dai, K. Maskell and C.A. Johnson (eds) *Climate Change 2001: The Scientific Basis.* United Nations' Intergovernmental Panel on Climate Change (IPCC) Cambridge University Press, Cambridge, pp 86-98.
8. M. Bruse and H. Fleer (1998) *Simulating Surface-Plant-Air Interactions inside Urban Environments with a Three Dimensional Numerical Model.* Environmental Modelling & Software, Vol. 13 (1998), pp 373-384.
9. V.T. Ca, T. Ashaeda and E.M. Abu (1998) *Reduction in Air Conditioning Energy caused by a Nearby Park.* Energy and Buildings, Vol. 29 (1998), pp 83-92.

10. V.T. Ca, T. Ashaeda and Y. Ashie (1999) *Development of a Numerical Model for the Evaluation of the Urban Thermal Environment.* Journal of Wind Engineering and Industrial Aerodynamics, Vol. 81 (1999), pp 181-196.
11. O. Cantat (1989) *Contribution à l'Étude des Variations du Bilan d'Énergie en Région Parisienne.* Ph.D. Dissertation, Université Paris-Sorbonne.
12. W.R. Cotton and R.A. Pielke (1995) *Human Impacts on Weather and Climate.* Cambridge University Press, Cambridge.
13. T.J. Chandler (1965) *The Climate of London.* Hutchinson & Co, London.
14. S. Clarke, J. Kersey, E. Trevorrow, R. Wilby, S. Shackley, J. Turnpenny, A. Wright, A. Hunt and D. Crichton (2002) *A Climate Change Impacts in London Evaluation Study, Final Report.* London Climate Change Partnership.
15. U. Cubasch et al. (2001) Projections of Future Climate Change. *In:* J.T. Houghton, Y. Ding, D.J. Griggs, M. Noguer, P.J. van der Linden, X. Dai, K. Maskell and C.A. Johnson (eds) *Climate Change 2001: The Scientific Basis.* United Nations' Intergovernmental Panel on Climate Change (IPCC) Cambridge University Press, Cambridge, pp 527-582.
16. R.E. Davies, P.C. Knappenberger, W.M. Novicoff and P.J. Michaels (2003) *Decadal Changes in Summer Mortality in U.S. Cities.* International Journal of Biometeorology, Vol. 47 (2003), pp 166-175.
17. J. Díaz, F. Ballester and R. López-Vélez (2005) Impacts on Human Health. *In:* J.M. Moreno Rodríguez (ed) (2005) *The Preliminary Assessment of the Impacts in Spain due to Effects of Climate Change.* Project ECCE, Ministry of the Environment, Madrid, Spain. Available from: http://www.mma.es/en/oecc [Accessed 4th April 2005].
18. A. Dimoudi and M. Nikolopoulou (2000) *Vegetation in the Urban Environment: Microclimatic Analysis and Benefits.* PRECis Project, the European Commission, Directorate General XII, Joule III, Contract JOR3-CT97-0192. Centre for Renewable Energy Sources, Athens.
19. L. Doulos, M. Santamouris and I. Livada (2004) *Passive cooling of Outdoor Urban Spaces. The Role of Materials.* Solar Energy, Vol. 77 (2004), pp 231–249.
20. B. Dousset and F. Gourmelon (2003) Satellite Multi-Sensor Data Analysis of Urban Surface Temperatures and Landcover. ISPRS Journal of Photogrammetry & Remote Sensing, Vol. 58 (2003), pp 43– 54.

21. D. Ehhalt and M. Prather (2001) Atmospheric Chemistry and Greenhouse Gases. *In:* J.T. Houghton, Y. Ding, D.J. Griggs, M. Noguer, P.J. van der Linden, X. Dai, K. Maskell and C.A. Johnson (eds) *Climate Change 2001: The Scientific Basis.* United Nations' Intergovernmental Panel on Climate Change (IPCC) Cambridge University Press, Cambridge, pp 239-288.
22. G. Escourrou (1991) *Le Climat et la Ville.* Nathan Editions, Paris.
23. C. Fidas and D. Lalas (2000) *Climatic Changes in the Mediterranean.* National Observatory of Athens, Ministry for the Environment, Physical Planning and Public Works, Athens.
24. C.K. Folland et al. (2001) Observed Climate Variability and Change. *In:* J.T. Houghton, Y. Ding, D.J. Griggs, M. Noguer, P.J. van der Linden, X. Dai, K. Maskell and C.A. Johnson (eds) *Climate Change 2001: The Scientific Basis.* United Nations' Intergovernmental Panel on Climate Change (IPCC) Cambridge University Press, Cambridge, pp 99-181.
25. A. Fylaktou-Cattaneo (2002) *Palace Courtyards; a Case Study of Microclimates.* PLEA2002, Toulouse.
26. R. Geiger (1967) *The Climate Near the Ground.* Harvard University Press, Cambridge Massachusetts.
27. R. Giridharam, S. Ganasan, and S.S.Y. Lau (2004) *Daytime Urban Heat Island in High-Rise and High-Density Residential Developments in Hong Kong.* Energy and Buildings, Vol. 36 (2004), pp 525–534.
28. B. Givoni (1989) *Urban Design in Different Climates.* University of California, Los Angeles, World Climate Programme Applications.
29. B. Givoni (1998) *Climate Considerations in Building and Urban Design.* Van Nostrand Reinhold, New York.
30. D. Godrej (2001) *The No-Nonsense Guide to Climate Change.* New Internationalist Publications Ltd, Oxford.
31. C.S.B. Grimmond, H.A. Cleugh and T.R. Oke (1991) *An Objective Urban Heat Storage Model and its Comparison with Other Schemes.* Atmospheric Environment Vol. 25B (1991), No. 3, pp. 311 326.
32. Hadley Centre (2002) *Stabilisation and Commitment to Future Climate Change.* Met Office, Hadley Centre, Bracknell.
33. R. Harrison and B. McGoldrick (1981) *Mapping Artificial Heat Release in Great Britain.* Atmospheric Environment Vol. 15. (1981) No 5, pp 667-674.

34. J.T. Houghton, Y. Ding, D.J. Griggs, M. Noguer, P.J. van der Linden, X. Dai, K. Maskell and C.A. Johnson (2001) *Climate Change 2001: The Scientific Basis.* United Nations' Intergovernmental Panel on Climate Change (IPCC) Cambridge University Press, Cambridge.
35. M. Kolokotroni (2001) *Urban Heat Island.* Brunel University. Available from http://www.brunel.ac.uk/research/solvent/island.htm [Accessed 25th May 2001].
36. S. Konopacki, L. Gartland, H. Akbàri and L. Rainer (1998) *Demonstration of Energy Savings of Cool Roofs.* A Report Prepared for the U.S. Environmental Protection Agency, Heat Island Project, University of California, Berkeley.
37. C. Koppe, S. Kovats, G. Jendritzky and B. Menne (2004) *Health and Global Environmental Change; Heat-Waves: Risks and Responses.* Series No. 2, Energy, Environment and Sustainable Development, World Health Organization, Copenhagen.
38. H.H. Lamb (1995) *Climate, History and the Modern World.* Routledge, 2nd edition, London and New York.
39. O.B. Lay, L.G. Tiong and C. Yu (2000) *A Survey of the Thermal Effect of Plants on the Vertical Sides of Tall Buildings in Singapore.* PLEA 2000, Cambridge.
40. J.F.B. Mitchell et al. (2001) Detection of Climate Change and Attribution of Causes. *In:* J.T. Houghton, Y. Ding, D.J. Griggs, M. Noguer, P.J. van der Linden, X. Dai, K. Maskell and C.A. Johnson (eds) *Climate Change 2001: The Scientific Basis.* United Nations' Intergovernmental Panel on Climate Change (IPCC) Cambridge University Press, Cambridge, pp 695-738.
41. N. Moussiopoulos, P. Sahm and C. Kessler (1995) *Numerical Simulation of Photochemical Smog Formation in Athens, Greece – A Case Study.* Atmospheric Environment, Vol. 29 (1995), No. 24, pp 3619-3632.
42. N. Moussiopoulos (ed) (2003) *Air Quality in Cities.* Springer, Berlin.
43. J.G. Nash and R.-M. De Souza (2002) *Making the Link: Population, Health, Environment.* Measure Communication, Population Reference Bureau. Available from http://www.prb.org [Accessed 5th December 2004].
44. National Statistical Service of Greece (1990) *Results of the Census of Buildings.* National Statistical Service of Greece, Athens.
45. M. Nikolopoulou (ed) (2004) *Designing Open Spaces in the Urban Environment: A Bioclimatic Approach.* RUROS project, Centre of Renewable Energy Sources, Athens.

46. T.R. Oke (1987) *Boundary Layer Climates.* Routledge, London.

47. P.A. O'Rourke and W.H. Terjung (1981) *Urban Parks, Energy Budgets, and Surface Temperatures.* Archives for Meteorology, Geophysics, and Bioclimatology, Series B, Part 29, pp 327-344.

48. J. Page and R. Lebens (1986) *Climate in the United Kingdom.* Her Majesty's Stationary Office, London.

49. G. Papadakis, P. Tsamis and S. Kyritsis (2001) *An Experimental Investigation of the Effect of Shading with Plants for Solar Control of Buildings.* Energy and Buildings, Vol. 33 (2001), pp 831-836.

50. A.M. Papadopoulos (2001) *The Influence of Street Canyons on the Cooling Loads and the Performance of Air Conditioning Systems.* Energy and Buildings, Vol. 33 (2001), pp 601-607.

51. Population Reference Bureau (2000) *An Urbanizing World: Urban Population Trends.* Population Bulletin, Vol. 55, No 3. Available from http://www.prb.org/pubs/population_bulletin/bu55_3/55_3_urban_population_trends.html#figure1 [Accessed 12th August 2001].

52. V. Ramaswamy et al. (2001) Radiating Forcing of Climate Change. *In:* J.T. Houghton, Y. Ding, D.J. Griggs, M. Noguer, P.J. van der Linden, X. Dai, K. Maskell and C.A. Johnson (eds) *Climate Change 2001: The Scientific Basis.* United Nations' Intergovernmental Panel on Climate Change (IPCC) Cambridge University Press, Cambridge, pp 249-416.

53. N.J. Rosenberg (1974) *Microclimate: The biological Environment.* John Wiley & Sons, New York.

54. A.H. Rosenfeld, H. Akbari, S. Bretz, B.L. Fishman, D.M. Kurn, D. Sailor, H. Taha (1995) *Mitigation of Urban Heat Islands: Materials, Utility Programs, Updates.* Energy and Buildings, Vol. 22 (1995), pp 255-265.

55. H. Saaroni, E. Ben-Dor, A. Bitan and O. Potchter (2000) *Spatial Distribution and Microscale Characteristics of the Urban Heat Island in Tel-Aviv, Israel.* Landscape and Urban Planning, Vol. 48 (2000), pp1-18.

56. Ch. Sachsamanoglou (1999) *Solar Radiation in Athens the Last 40 Years.* Sixth National Conference for Renewable Energy Sources, Vol. A, pp1-8, Volos, Greece.

57. M. Santamouris (ed) (2001) *Energy and Climate in the Urban Built Environment.* James & James, London.

58. L. Shashua-Bar, and M.E. Hoffman (1999) *Vegetation as a Climatic Component in the Design of an Urban Street. An Empirical Model for Predicting the Cooling Effect of Urban Green Areas with Trees.* Energy and Buildings, Vol. 31 (1999), pp 221–235.

59. L. Shashua-Bar, and M.E. Hoffman (2002) *Quantitative Evaluation of the Effects of Built-Up Geometry and Trees on Diurnal Air Temperature in Canyon-Type Courtyards.* Advances in Building Technology, 2002, Hong Kong, Vol. 2, pp 1493–1500.

60. L. Shashua-Bar, and M.E. Hoffman (2003) *Geometry and Orientation Aspects in Passive Cooling Canyon Streets with Trees.* Energy and Buildings, Vol. 35 (2003), pp 61–68.

61. R.B. Singh and B. Kumar (2001) Sources of Air Pollution Emissions in Selected Metropolitan Cities in India. *In:* R.B. Singh (ed) *Urban Sustainability in the Context of Global Change.* Science Publishers Inc., Plymouth, pp 29-48.

62. T.F. Stocker et al. (2001) Physical Climate Processes and Feedbacks. *In:* J.T. Houghton, Y. Ding, D.J. Griggs, M. Noguer, P.J. van der Linden, X. Dai, K. Maskell and C.A. Johnson (eds) *Climate Change 2001: The Scientific Basis.* United Nations' Intergovernmental Panel on Climate Change (IPCC) Cambridge University Press, Cambridge, pp 417-470.

63. H. Taha (1997) *Urban Climates and Heat Islands: Albedo, Evapotranspiration, and Anthropogenic Heat.* Energy and Buildings, Vol. 25 (1997), pp 99–103.

64. K. Takahashi, H. Yoshida, Y. Tanaka, N. Aotake, F. Wang (2004) *Measurement of Thermal Environment in Kyoto City and its Prediction by CFD Simulation.* Energy and Buildings, Vol. 36 (2004), pp 771–779.

65. J. Unger, Z. Sumeghy and J. Zoboki (2001) *Temperature Cross-Section Features in an Urban Area.* Atmospheric Research , Vol. 58 (2001), pp 117–127.

66. R. Watkins (2000) *The Impact of the Urban Environment on the Energy Demand for Cooling Buildings. Literature Review.* Report, written as part of a research project carried out at Brunel University and the Building Research Establishment Ltd. Available from http://www.brunel.ac.uk/research/solvent/ [Accessed 25th May 2001].

67. K.S. White et al. (2001) Technical Summary, Climate Change 2001: Impacts, Adaptation and Vulnerability. *In:* J.J. McCarthy, O.F. Canziani, N.A. Leary, D.J. Dokken and K.S. White (eds) (2001) *Climate Change 2001: Impacts, Adaptation*

and Vulnerability. United Nations' Intergovernmental Panel on Climate Change (IPCC) Cambridge University Press, Cambridge, pp 19-73.

Chapter 3

Green Roofs and Green Walls; History and Potential

3 Green Roofs and Green Walls; History and Potential

On city buildings there are vast surfaces which are not used as functional spaces, mainly their roofs and walls. These surfaces could be covered with vegetation (grass, small crops, pergolas, or even trees) and change significantly the microclimate around them. If this is applied on an urban scale, the thermal effect could be noticeable for the whole city. If this is done, there would be a direct effect on energy savings from air conditioning buildings, on outdoors thermal comfort, in addition to the air quality improvements (Dunnett and Kingsbury, 2004), psychological benefits for urban dwellers (Palmer-Wilson, 2003) and, if designed properly, aesthetics.

3.1 Green Roofs; Definitions

The term "green roof" is used to describe both intensive roof gardens and extensive roofs with naturalistic or self-established vegetation. "Green roof" is defined either as a roof garden of usually ornamented planting or a fertile area which has been allowed to colonise and develop naturally, with a substrate isolated from the natural ground by a man-made structure, of at least one floor (Grant et al., 2003). The categories of green roofs which have been identified by the German Landscape Development Research Society are three according to their use, construction method and maintenance requirements of the roof; the intensive, the extensive and the simple intensive roof (Grant et al, 2003; Dunnet and Kingsbury, 2004). Intensive green roofs, usually referred to as roof gardens, are the equivalent of parks and gardens at a roof level (Figure 36). Their soil layer is generally at least 15cm deep and vegetation on them might vary from grasses to shrubs and trees. They are usually constructed on flat roofs, reinforced to bear the weight of vegetation and normally they are accessible. They are usually more expensive to construct and maintain than extensive roofs. Extensive green roofs are vegetated with grass and, in general, ground covering plants (Figure 37). Their soil layer depth is between 2 and 15 cm. Normally they are not intended for regular human usage. Their static loads are not so large –approximately 0.50kN/m^2 (Eumorfopoulou, 1992)– and can be either plane or tilted roofs. Generally, they are less expensive to built and maintain. The final classification, which did not exist in older bibliographies, is the simple intensive green roof (Figure 38), which is in-between the intensive and the extensive roof. Usually it is covered with grasses and

ground covering plants, which require more regular maintenance than extensive roofs. Their loading structure and cost is not as large as the intensive ones, but they are more complex constructions than extensive roofs.

Figure 36. Intensive green roof of Kaiser Resources in Vancouver, designed by Theodore Osmundson (Osmundson, 1999)

Figure 37. Residency of the architect Eli Georgiadou with extensive green roofs, in Thessalonica, (author)

Figure 38. Simple intensive green roof in the Centre for Alternative Technologies, in Machynlleth (author)

Figure 39. Vine pergola[8] at the entrance of a dwelling, creating an outdoors sun protected space, in Nea Ionia, Athens (author)

For reasons of completeness, the term "green sky" is introduced here; with this term, the formation of a pergola is described, which creates a shaded space on the roof or at the building's yard (Figure 39). The soil layer is not on the roof itself, but inside containers, or even on the ground for low level constructions. From a construction point of view, these elements could not be described as green roofs. However, from a microclimatic point of view, they act as a horizontal layer of green above the roof, creating an outdoors shaded space in between.

[8] This kind of vine pergola, placed at the main entrance of dwellings is a characteristic of vernacular architecture in the mainland parts of Greece.

There are also the earth-sheltered structures, which could be considered as extensive green constructions. These structures are set into the ground, with a continuous earth cover where the walls and roofs of a conventional building would be. Usually they are found in rural locations (Grant et al., 2003). For reasons of thoroughness, such constructions are also taken into consideration[9] in the following paragraphs, where the history of green roofs is examined.

3.2 Green Walls; Definitions

Green walls or green façades describe cases where vegetation is applied to the vertical elements of a building. The planting medium is usually not adjacent to the building element, but to another surface, either the ground or a container. Green walls can be beneficial for both the construction itself and the thermal conditions of both the interior and the exterior of the building. Although they might not be applicable for all buildings (e.g. historic, or of architectural importance buildings) they could improve the aesthetics of a large proportion of urban buildings. They could also protect the construction from high amounts of solar radiation, strong winds and rain. Although there has been a notion of plants damaging the wall of a building, according to Johnston and Newton (2003) this is only true in cases where decay has already set in and plants can then indeed accelerate the process of deterioration. Doernach (1998) has noticed that for plants clinging directly to the wall, they can act as a protective layer, with the exception of west and north oriented walls. Also, they can be extremely beneficial from a thermal point of view for both the interior and the exterior of the building; for the interior, in summer, they provide shading, evapotranspiration and their leaves create a ventilation blind. This is beneficial, especially for poorly-insulated structures. For winter an insulation effect of 30% has been recorded, although such a high percentage is likely to occur only when temperatures drop to freezing (Johnston and Newton, 2003; Doernach, 1998). For the exterior of urban buildings, their beneficial effects on lowering urban canyon temperatures is analysed in detail in chapter 6.

[9] Man-made mounds such as Silbury Hill are not taken into consideration here. The cases of earth-sheltered structures examined are the ones where a man-made structure with at least one chamber exists within the man-made hill.

For reasons of classification, three types of green walls have been distinctive; the green wall, where creepers and ivies climb directly on the wall, covering the wall layer (Figure 40). The green wall adjacent to the building, where creepers, ivies and plants generally climb over a construction adjusted to the wall, leaving an air gap between the wall and the construction (e.g. Figure 42). The last type is the green curtain, used in this study to describe the case where greenery is not climbing on the wall or an adjacent construction, but plants hang loose in front of the building, without any structural support (e.g. Figure 41, Figure 43).

Figure 40. Green wall in Cardiff (author)

Figure 41. Yeang's Boustead building in Malaysia, with plants hanging from the balconies as "curtains"[10] (Yeang, 1992)

Figure 42. Green wall adjusted to the building with a metal frame, creating an intermediate exterior living space, protected from the summer sun, in Athens (author)

Figure 43. Green curtains hanging in the entrance of a building apartment in Athens (author)

[10] Although in Figure 41 the plants are not long enough, to creating the "hanging green curtain effect", when in full growth they cover the exterior walls of the building as curtains (personal communication with P. Jones).

3.3 Examples of Existence of Green Roofs through History

Before proceeding to analyse the climatic benefits of green roofs and green façades, a historical investigation is carried out, to trace where and why green roofs and green walls have been applied in previous eras. In order to facilitate this study, two categories are examined; one based on the climatic characteristics of the place where forms of green building elements were found, with the general division of cold and hot climates and a second category, based on the characteristics of the buildings with greenery, with the distinction between vernacular and monumental architecture.

The cases examined are only those where vegetation is used as a distinct element of the building envelope, whether in its living or dry form. Although from a thermal point of view dried plants behave differently from the living ones (they do not evapotranspire, therefore they cannot act as efficient "climatic regulators"), thatched roofs have been classified as green ones by several authors (Osmundson, 1999; Pedersen, 2000). In addition, the distinction of dried grasses and live turf in many cases of vernacular architecture is not so clear (turf, grasses and ivies growing up on thatched roofs), thus it should not be left uninvestigated. The cases in which parts of plants are used as construction elements (e.g. reeds being plastered, timber or the case of straw bale constructions) are not examined; they do not have any effect on the building's microclimate.

3.3.1 Microclimatic Behaviour of Thatches

Before examining the history of green roofs and green walls, a short reference is carried out about the performance of dried turfs and thatches. Although dried grass does not evapotranspire, it can have lower surface temperatures than most construction materials, due to its light colour, and its structural texture (air cavity inside the thatches), which allows for a lower specific heat capacity. Despite the fact that green roofs show lower surface temperature distributions than thatched roofs, the latter also have much lower temperatures than for example, a concrete roof. From an experiment conducted in Cardiff[11], on the roof of the Bute Building (where the Welsh School of Architecture is accommodated), during the first week of August 2004, it

[11] Details about the experiment are given in chapter 4.

was noticed that for clear sky conditions dried grass had lower surface temperatures than concrete (Figure 44). As is obvious from Figure 44, grass has lower surface temperature than concrete of the magnitude from 4.0°C to 19.0°C, under clear sky conditions (days 4/8 and 5/8). The temperature difference between concrete and dried grass surface temperatures reaches 18.0°C under clear sky conditions, while the difference between dried grass and grass reaches a maximum of the magnitude of 5.5°C. Under overcast conditions (6/8/04) the differences between concrete and grass become lower, reaching a maximum of 9.0°C, while the maximum temperature difference between the concrete and the dried grass reaches 8.0°C. For night-time conditions (measurements taken from 23:40pm to 2:45am), under a clear sky and after a warm day with high solar radiation levels (Figure 160 and Figure 161, chapter 4) the temperature difference between concrete and grass and between concrete and dried grass reaches a maximum of 9.0°C, with an average of 7.0°C.

Due to its light colour, thus its higher albedo, and its texture, which lets the air penetrate and ventilate its fabric, and the fact that its thermal capacity is not as large as construction materials, dried grass has much lower surface temperatures than concrete. Its surface temperatures are much closer to grass surface temperatures than concrete, under the same climatic conditions. Thus, especially in dry and arid areas, where irrigation of gardens and green roofs is a preventive issue, plants in their dry form have been applied on the building envelope, especially in vernacular architecture, as will be examined in the following paragraphs.

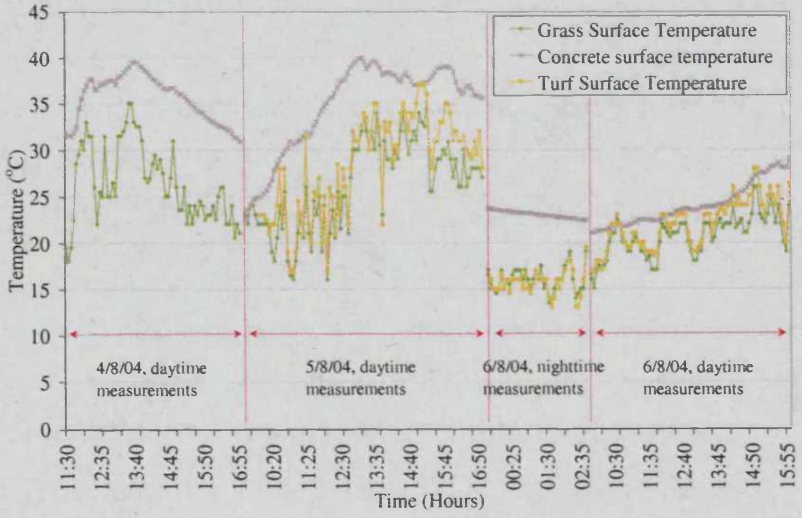

Figure 44. Measurements of surface temperatures of concrete, grass and dried grass for Cardiff, from the 4th until the 6th of August, 2004, under clear sky (4th and 5th August 2004) and cloud sky conditions (6th August 2004)

3.3.2 Definitions and Classifications

Before proceeding to the analysis, the definitions of "monumental", "vernacular", "hot" and "cold" are clarified. Monumental is defined as *"building intended as a monument, or looking like one"*[12]. As temples and religious spaces are, in most cultures, intended for standing aside, they are examined under this category, even when, from a structural or aesthetical point of view, they might belong to vernacular architecture. Vernacular architecture is defined as *"unpretentious, simple, indigenous, traditional structures made of local materials and following well-tried forms and types, normally considered in three categories: agricultural (barns, farms, etc.), domestic, and industrial (foundries, potteries)"*[13]. In this study of vernacular architecture mostly the second category (domestic) will be examined and, where necessary, some reference will be made to the first category (agricultural).

The general classification of "hot" and "cold" distinguishes between climates with generally high and generally low temperatures, respectively. According to the climatic classification used in chapter 6, the Mediterranean, arid, steppe and the tropical climates are classified as "hot" climates in this section. The subarctic, temperate, continental cool summer, ice cap and tundra climates are classified as generally "cold" ones.

Plants have been used as building materials, especially as roofing ones in both monumental and vernacular architecture in diverse climates and cultures. Although vegetation is not the easiest material to be found as archaeological evidence, a quite important number of descriptions, excavations or ruins shows the existence of green roofs on buildings, even 6,000 years ago. Both as gardening elements and as dried thatches, plants and reeds have been part of the building envelope for centuries.

Either for climatic necessities or merely as the only building materials available, people have been using vegetation to construct shelters, houses and settlements before recorded history. Mostly palms, bamboos, reeds and grasses have been used in buildings (Oliver, 1997a)[14]. They are easy to find, collect, work, replace and renew (by being replanted by humans or through natural growth). Dried parts of plants and

---

[12] Source: *A Dictionary of Architecture in Art & Architecture*, Oxford Reference on Line.

[13] ibid.

[14] I would like to express my gratitude to Jacob Hotz-Hung for lending me his Encyclopedia of Vernacular Architecture of the World.

trees, such as reeds, grasses and leaves are quick and easy to put together to make a simple construction without the use of advanced technology, thanks to their lightness and elasticity.

Evidence of gardens on roofs have been traced on monumental buildings, in places of power or worship, such as palaces and temples. Traces of green roofs on monumental architecture have been found or the information has reached us through ancient texts and works of art. One cannot be certain that green roofs might have been more or less popular than the evidence that exists; time and historical circumstances may or may not have made them disappear into oblivion.

A summary of the places and periods for which evidence exists for the use of green building elements for both vernacular and monumental architecture, hot and cold climates, is given in Figure 45.

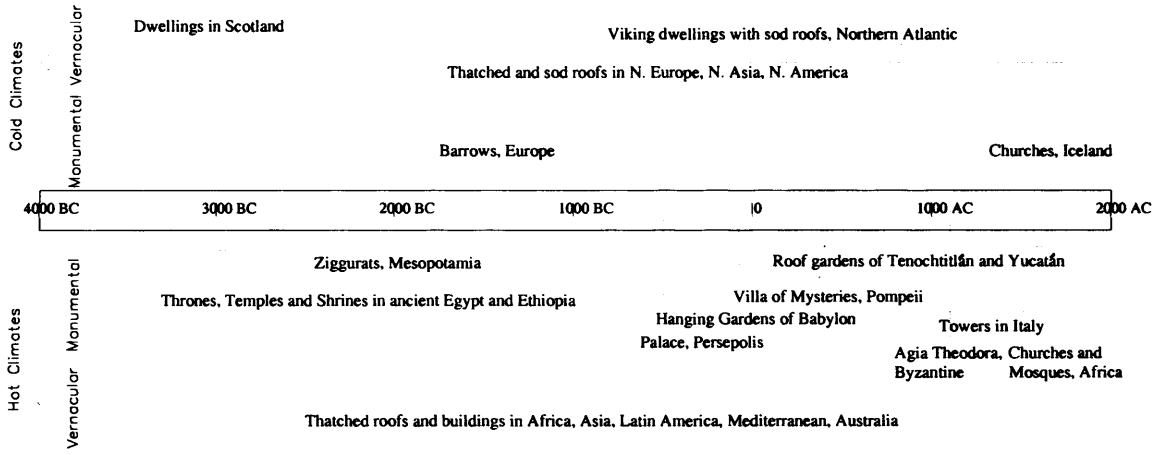

Figure 45. Diagram of evidence of the existence of green roofs throughout history for diverse climates (author)

3.3.3 The Use of Green Roofs in Hot Climates

Green roofs and walls have been elements of both vernacular and monumental architecture in hot climates. Either in the form of subterestrial gardens or as construction elements of the building envelope, they can be found on buildings from Eurasia to Africa, Australia and America. In the following paragraph, evidence of their use in monumental architecture is presented.

3.3.3.1 Monumental Architecture

Roofs have been planted and used as ways of mitigating extremely hot conditions since antiquity in hot areas. The first known man made gardens above ground level, are the Ziggurats of Ancient Mesopotamia (Osmundson, 1999). They were built from the 4th millennium until about 600 BC, located in the courtyards of temples, with a form of grand stepped pyramid tower of stone. Trees and shrubs were planted at the terraces formed by these steps (Figure 46). In this way the extreme heat of the Babylonian plain was lowered locally through evapotranspiration and shading.

In general, gardens in ancient Mesopotamia were a significant element of the houses of the nobles and the palace. In the ruins of Persepolis, chambers were found on both the roofs and the squares in front of the palace, where it is believed that trees were planted in their soil, forming a garden at the palace's entrance (Contenau, 1989) at two levels; one at the entrance level and one above it. Apart from the element of grandeur that a garden adds to a place, these gardens, in front of the palace might have also acted as climatic modifiers, mitigating the heat of the area.

At the same extremely hot area, the Hanging Gardens of Babylon, one of the Seven Wonders of the World, was possibly a tiered terraced stone construction, within the palace, on a small hill near the palace's Istar Gate (Contenau, 1989). This stone construction, constructed at about 500 BC, was full of vegetation in order to resemble the mountainous landscape (Figure 47), where the Queen came from (Osmundson, 1999). The archeological excavations showed evidence of wells underneath the construction, from which the gardens must have been watered (Contenau, 1989). The existence of vegetation on the building itself moderated the extreme heat, locally, through shading and the evapotranspirational process from the trees and plants, which lowered air temperature. Also, the gradated construction of the gardens provided a very good view of the vegetation from outside the palace. The kings of Assyria were keen on having botanic gardens, where vegetation which did not normally exist in the area was cultivated, as trophies from their campaigns. An elevated intensive garden, whose rare trees could be seen from outside the palace's walls, could have been a very good way for the king to keep his subject's faith to tradition (ibid.) as well as to remind them of his wealth, power and the superiority of his social position.

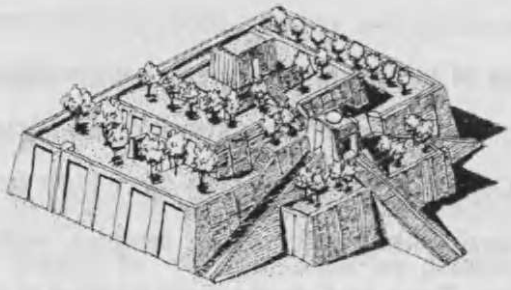

Figure 46. The ziggurat of Nanna, in today southern Iraq (Osmundson, 1999)

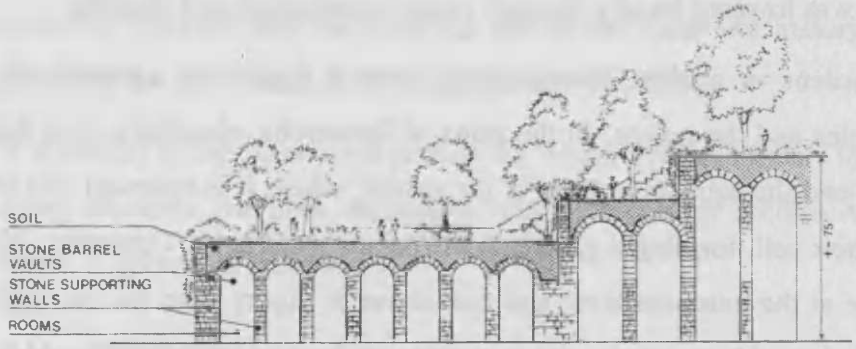

Figure 47. Section of the Hanging Gardens of Babylon (Osmundson, 1999)

In the Mediterranean area, with its milder climate, compared to the heat of the Mesopotamian area, little is known about the role of green roofs, in ancient times. Although roofs and terraces were used as outdoor living spaces in both Greek and Roman times -as they still are across the Mediterranean- there is no archeological evidence about their being planted. From the ruins of Pompeii, where the urban planning of the city has survived, evidence of the importance of the vegetated element exists; gardens and parks were not only important for public spaces and buildings, but also for dwellings. Gardens could be large or small, according to the property, but a patch of green was a basic part of the Roman character. The heart of the Pompeian house was the garden, in the form of atrium, which furnished air and light to the various rooms arranged around it (Jashemski, 1979).

In the Villa dei Misteri (Villa of the Mysteries) evidence exists of roof gardens. The villa is located in the outskirts of Pompeii, near the Porta Ercolano. Mostly aristocrats lived in the villas in the outskirts of Pompeii (Robinson, 1977; Wallace-Hadrill, 1994) and the Villa of the Mysteries with its roof gardens and intensive gardens, its large spaces and impressive wall paintings definitely used to belong to a noble Pompeiian (Maiuri, 1960). At the U-shaped terrace along the northern, western and southern perimeters of the villa, at the entrance of the house, clear evidence of plants growing directly in soil is observed (Osmundson, 1999). According to

Jashemski (1979) the villa has a *"quasi-monumental"* character in relation to the landscape, with its outer façade and its hanging gardens as a dominating factor of its theme. The vegetation which existed on the roofs of the Villa of the Mysteries has been reconstructed, based on the evidence of the roots of the plants found in its soil layer (Figure 48). Although it is more famous for its interior murals of Mystery Ceremonies (from where its name derives), its hanging gardens must have made it an outstanding villa at the time.

Figure 48. The reconstructed green roofs at the ruins of the Villa of the Mysteries in Pompeii (Jashemski, 1979)

Figure 49. View of the villa Medici Fiesole, near Florence, with its vegetated viale (Van der Ree et al., 1992)

Figure 50. View of the church of Ayia Theodora, with trees on its roof (University of Patras, 2001)

In the Middle Ages and Renaissance Italy special interest was shown in roof gardens by people with wealth and power. Such examples can be found in the Italian villas, which were dwellings with gardens, intended for the social elite to enjoy the countryside (Van der Ree et al., 1992), for example, the Palazzo Piccoliomini in Pienza, the Tower of the Guinigis in Lucca, the Cosimo de' Medici Roof Garden in Careggi (Osmundson, 1999). In the instance of the Villa Medici Fiesole, built between 1458 to 1462, outside Florence, its intensive terraces are constructed according to the inclination of the ground, connected with a fully covered with vegetation *viale* (Figure 49). As the rural parts of the Mediterranean are not extremely hot, these examples of green roofs are mostly the expression of the wealth of their owners, a design challenge

for a garden above ground level, with probably much better view, rather than a climatic necessity.

At the same period, in the Byzantine Empire, not so much interest is shown in roof gardens, in monumental architecture. An accidental exception is the church of Ayia Theodora, near the village Vasta, in Arcadia, Greece. It is a typical small church, built between 1050 and 1100 (University of Patras, 2001). Its uniqueness is due to the fact that its roof bears seventeen trees (Figure 50), while there was no such intention when it was first built. This accidental "green roof" is due to the fact that the church was built with masonry, stones and plenty of soil, in which trees managed to root, allowing popular folk-lore to create stories about the "miracle" of Ayia (Saint) Theodora (ibid.).

Apart from the Mesopotamian and the Mediterranean civilizations, the Aztecs in the hot area where Mexico is today, used green roofs on their buildings. Although none of the roof gardens of the city of Tenochtitlán (today Mexico City) survived when the Spanish conquistadores invaded it, in 1521, written evidence can be found of the Spanish invaders describing the gardens of city dwellings. In the highly stratified society of the Aztecs, the houses of the elite, placed in the city centre, were the only residencies allowed to be two-stored and have roof gardens (Robertson, 1968). Although extensive gardens within the city were a characteristic of both upper and lower classes dwellings (Hardoy, 1973), only the nobles could have an extensive garden on their roof, a garden above ground level being a privilege of the elite of Aztec society. According to Cortés[15], these elite dwellings consisted of *"very exquisite flower gardens both on the upper apartments as well as down below"* (Yampolsky and Sayer, 1993), with roof gardens acting as an expression of the social status of their inhabitants. Whether this was also applied for climatic reasons, as the noble houses were in the centre of the densely built Tenochtitlán, one cannot tell with certainty.

Evidence of intensive green roofs exists in Maya buildings as well. The Mayas in the Yucatán peninsula (the jungles between today's Mexico and Guatemala) were accustomed to having roof gardens (Yampolsky and Sayer, 1993), on their much

[15] Hernàn Cortés (1485-1547): leader of the Spanish *conquistadores* who reached Mexico in 1519. In his five letters addressing to Charles V (king of Spain, emperor of the Holy Roman Empire) information is given about the architecture of Tenochtitlán.

decorated buildings, again expressing the strong position of the upper class. Monuments in Chichén Itzá, like the Monjas Annexe –known otherwisely as the Nunnery (Figure 51 and Figure 52)– were found in the 19th century with tropical intensive gardens on their roofs.

Figure 51. Nineteenth-century engraving showing the main façade with tropical, intensive roof of the Monjas Annexe (the Nunnery) at the Maya site of Chichén Itzá, Yucatán (Yampolsky and Sayer, 1993)

Figure 52. Late nineteenth-century photograph of the upper part of the Monjas Annexe (the Nunnery), with the remains of its tropical, intensive green roof, at Chichén Itzá, Yucatán [source: http://www.rose-hulman.edu]

In rural areas, where the surplus wealth of cities is not available, sacred and buildings of monumental character were made out of the same materials and typology as the rest of the buildings, with only very few elements to give them an almost monumental character within the rural society. Thatching, being an important element of the building envelope in vernacular architecture (paragraph 3.3.3.2) was also used in its monumental-intended buildings. In the instance of the Wewewa corral village (Figure 53) in Indonesia, the sacred building is distinct from the residential huts, through its roof shape, being a high-peaked roof, nonetheless thatched, as are the rest of the village buildings. Similarly, the monumental character of the chief's house in the Fijian islands is expressed through its elevation (Figure 54), while dried vegetation covers its roof, as is the case in most Fijian houses (Figure 80, page 107).

Figure 53. Wewewa corral village in Indonesia, with thatched roofs and thatched, high-picked sacred house (Oliver, 1997c)

Figure 54. A Fijian chief's house with thatched roofs, on elevated platform (Oliver, 1997c)

Africa has a strong tradition of using grass roofs since antiquity, in both monumental and vernacular architecture. Most of the evidence shows that plants have

been used in their dried form. There is evidence of an ebony table of King Menes dating from 3100 BC which has a woven thatch house carved on it (Nnamdi, 1996). The throne of Aksumite kings in Ethiopia was sheltered with a reed construction bound together to form a thatched, hoop roof at the top (Figure 55). Shrines of the God Mene in ancient Egypt were also built in the form of the round hut, with a thatched conical roof (Figure 56). As Nnamdi (1996) concludes, traditional architecture in archaic Egypt did not begin with the pyramids; it began with thatched constructions and it later evolved to the pyramids.

Monumental architecture in Africa continued to use thatched roofs until recently. The round Aksumite churches with thatched roofs in Ethiopia are quite characteristic African monumental buildings (Figure 57). Mosques were also built with grass roofs. Of the most famous ones are the Seno Palel Mosque in Senegal (Figure 58) and the mosque in Kabe, Futa Jallon, in Guinea (Figure 59). The Seno Palel Mosque was built in the 1770s, during the period of Islamic reform. It demonstrates *"the interplay between several cultures"* (Nnamdi, 1996). Its square plan, the portico to the east and the three entrances to the Prophet's courtyard are elements of Islamic architecture. The thatched roof, the lighting systems, additional corridors, transitional spaces, doors and windows are African modifications (ibid.). A very different mosque is the Kabe mosque, dating from the 1730s. It is the oldest mosque in beehive style architecture (ibid). Here, Islam has adapted to the culture of West African people and the Islamic sacred place was built according to the ancestral places of worship; a round construction with beehive, thatched roof.

Figure 55. Reconstructed throne of an Aksumite king in Ethiopia (Nnamdi, 1996)

Figure 56. Shrine of God Mene, in ancient Egypt, with thatched roofs on round buildings (Nnamdi, 1996)

Figure 57. Round church with thatched roof at the village of Mishuk, Ethiopia (Nnamdi, 1996)

Figure 58. Seno Palel Mosque in Senegal, with square form and thatched roofs (Nnamdi, 1996)

Figure 59. Mosque in beehive style in Kabe, Futa Jallon, Guinea (Nnamdi, 1996)

3.3.3.2 Vernacular Architecture

Thatches and dried plants have been an elementary construction material of vernacular architecture in most places of the world from prehistoric times until today. In settlements and villages in many parts of Africa dried parts of plants are still used as construction materials. Reeds, bamboo stems, grasses, leaves (especially palm leaves) are vital construction elements. The grass roof is an element of African architecture which has spread throughout the continent (Nnamdi, 1996). Either in round plans (Figure 60) or more complicated geometrical forms (Figure 62), on the top of clay walls, stone houses or grass houses (Figure 63), domes (Figure 61), on individual dwellings or in settlements (Figure 60) most of the roofs are thatched in offshore, lowland and mountainous areas of Africa, from antiquity to the present time.

Figure 60. Aerial view of a Kikuyu village in Kenya, with round buildings with thatched roofs (Nnamdi, 1996)

Figure 61. Natal Nguni dome shaped dwellings (indlu) in Zulu land (Oliver, 1997b)

Figure 62. Linked cone-on-cylinder Xhosa house with thatched roofs in Cape Nguni in Southern Africa (Oliver, 1997b)

Figure 63. Lesotho (South Africa) traditional round grass hut (Nnamdi, 1996)

From the Sudan to the Congo, from Egypt to South Africa, thatched roofs are an important element of vernacular African architecture. They are used in simple one-unit huts and houses (e.g. Figure 63) to more complicated dwellings, such as the impluvium house style in forest areas in West Africa Ashanti, Benin, Ibos, Yoruba houses), and especially in the more complex Joola impleviums in Joolaland, Senegal, which combine both thatched roofs and terraces (Oliver, 1997b) (Figure 65), and the Ndebele houses in Zimbabwe or the Konkomba dwellings in Togo. The impluvium house style is a four-house unit, which face one another and enclose a courtyard (Figure 64). These houses are usually with thatched roofs, either separately or together. The Ndebele houses in Zimbabwe are characterised by their elliptical and round forms (Figure 66); their complexity is due to the fact that they try to combine communal and private spaces with respect and link to the ancestors of the family (Nnamdi, 1996).

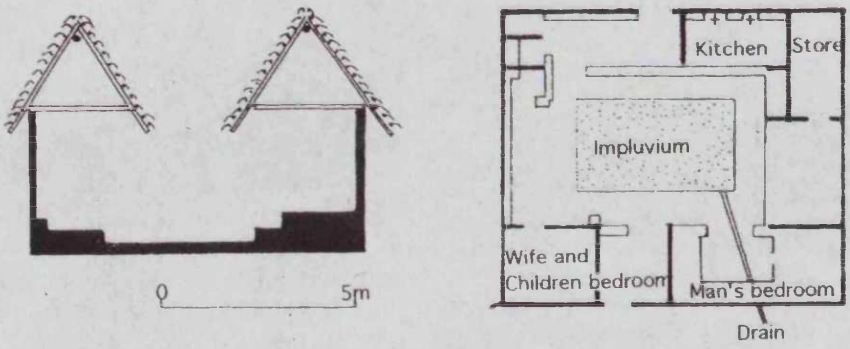

Figure 64. Impluvium house style with thatched roofs and courtyard in forest areas of West Africa (Nnamdi, 1996)

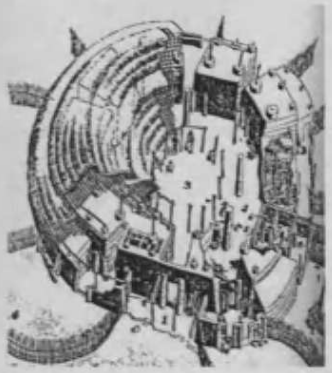

Figure 65. Axonometric of a Joola impluvium dwelling in the savanna grasslands of Senegal (Oliver, 1997b)

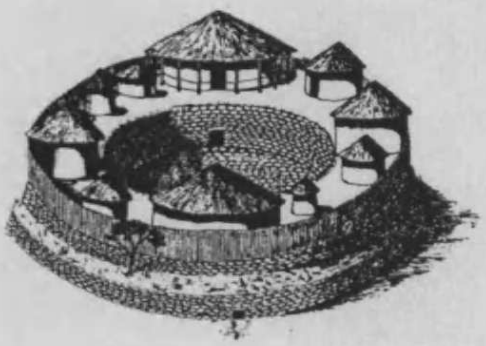

Figure 66. Ndebele house with thatched roofs in Zimbabwe (Nnamdi, 1996)

Turf huts and thatched roofs have not only been used in Africa, but also, in Europe, the Americas and Asia (Oliver, 1997a). They have been found mostly in places where grasses and palms can be cultivated, while in areas where these crops are difficult to cultivate (e.g. the Kyklades islands in Greece) other roofing techniques have been applied[16]. In the mountainous parts of Epirus, Greece, in the Mediterranean area, up until the 1950's-1960's grass huts were used only as temporary shelters, by rural populations who had to move between places due to farming, or groups like the Vlachs, who lived a nomadic life. Either as dwellings or as barns, all-grass huts were usually made of canes, *louria*, where usually rye (sycale cereale) was weaved. These huts were usually twin huts, one for habitation and one for storing food and other goods[17]. A sketch of a typical hut of the area is given in Figure 67. Quite often the roofs of these huts turned green in spring, from the grasses and weeds growing naturally on these materials[18].

Apart from the western parts of Greece, in the Mediterranean, thatching has been used as roofing construction of permanent dwellings, in areas where there are sufficient amounts of rain and adequate soil to allow for the growth of grasses and reeds. In the instance of Galicia, in northeast Spain, its circular *palloza* houses are covered with thatched roofs (Figure 68). In Sicily, Italy, in Val Demone, whole houses can be found, covered with thatching (Oliver, 1997c) (Figure 69), maybe for not allowing heat to be stored in the building fabric.

---

[16] In the example of the Kyklades island, again vegetation is mixed with clay and soils to form a roofing layer, but it is mostly vegetation derived from the sea (seaweeds).

[17] Information derived from elder villagers and craftsmen of the area.

[18] Information derived from elder villagers.

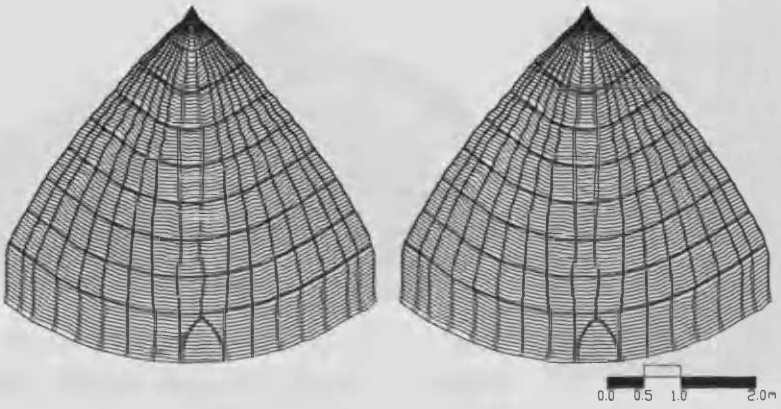

Figure 67. Twin thatched huts of the western parts of Greece, according to the descriptions of elder craftsmen and villagers (author)

Figure 68. Thatched roof house (palloza) in Galicia, northeast Spain (Oliver, 1997c)

Figure 69. A Sicilian house all covered with thatch house, in Val Demone (Oliver, 1997c)

In the pre-Colombian civilizations of America, not only the Aztec and Maya elite, but also the peasantry living in rural areas used turf for constructing their roofs. It was used merely as a building material and not as a garden; grass (thatch) was used to construct very steep roofs (Yampolsky and Sayer, 1993), in order to protect the sub layers of the roof (leaves of palm) from rain. This was carried on in vernacular architecture, after the Spanish invasion. Despite the restrictive planning options of towns due to European legislation, self-built houses away from urban centres were not discouraged (Oliver, 1997b). Continuing with the indigenous techniques, thatched dwellings are still used by Native Americans, in the instance of the *chozas* (huts) in Ecuador (Figure 70). American vernacular architecture has received further influences, especially African ones –in the instance of the "*redondo*" round hut, in South Mexico (Figure 71), (ibid.). Thatching has been an important element of the vernacular building envelope all around Latin America, either in forms without distinctive walls (Figure 70), with thatched roofs on stone walls (Figure 72), or reeds and woods (Figure 73).

Figure 70. Quechua Indian thatched *choza* (hut) in Ecuador (Oliver, 1997c)

Figure 71. Structural sketch of the *redondo* house, in Cuajuincuilapa, Mexico (Oliver, 1997c)

Figure 72. Thatched roofs on stone walls in typical Quechua dwellings (area between Argentina, Bolivia and Chile) (Oliver, 1997c)

Figure 73. Nineteenth-century huts with thatched roofs and reed or wood walls in Saint Elizabeth, Jamaica (Buisseret, 1980)

Dried plants have been one of the major construction materials in most parts of Asia, especially in rural areas. Throughout the whole continent, villages and rural settlements are formed with raw materials which can be found in abundance and can be easily worked and replaced. From India to China, Indonesia to Japan, thatched roofs with grasses or palms, have been used in rural buildings, either in curved (Figure 74), straight (Figure 75) forms, or in pyramid shapes (Figure 76), for habitats in settlements (Figure 75, Figure 77) or as shelters for animals or water (Figure 78). Thatched roofs have been since prehistory and continue to be an important component of vernacular architecture in Asia.

Thatching is also a technique found in Australasia, Polynesia, and New Zealand in the rural settlements of the indigenous people (Figure 79, Figure 80). The Bedouins in the Arab peninsula also used thatches to construct their temporary shelters, made of *barasti*, which is the leaf of the palm tree cut in various ways (Figure 81).

Figure 74. Namoshudra dwellings with curved thatched roofs in Bangladesh (Oliver, 1997c)

Figure 75. Village with thatched roof in Japan (Kahn, 1973)

Figure 76. Thatched Onge winter hut with pyramid shape in Bay of Bengal (Oliver, 1997c)

Figure 77. Village with thatched roofs in Yunnan Province, in China (Microsoft Atlas, 1997)

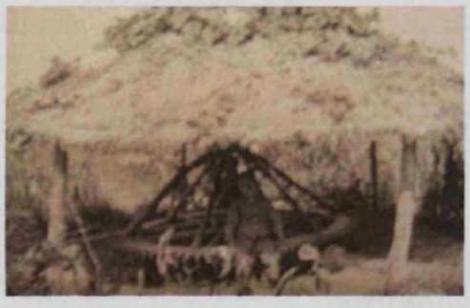

Figure 78. Shelter of a well with thatched roof and ivies in China, early 20th century (Cornet and Verdier, 2004)

Figure 79. Typical Meriam house with woven coconut leaf walls and grass roof in Australia (Oliver, 1997c)

Figure 80. Traditional Fijian house, with palm roof, in Taveuni island (Oliver, 1997c)

Figure 81. Bedouin *barasti* house in the Arab Gulf (Oliver, 1997c)

Green and thatched roofs have been used in monumental and the latter in vernacular architecture of hot climates around the globe. Either for mitigating extremely hot conditions, or merely as a recreational or of an expression of social

status, gardens have been placed on top of monumental buildings since prehistory. In vernacular architecture in hot conditions mostly the dry forms of plants have been used, as water for irrigation may be an issue for populations in hot climates. Dried plants have been an important element of the building envelope in places where vegetation could be easily found. Merely as the only construction material available, or as an insulator from excessive heat from solar radiation, roofs and walls have been made out of grasses, palms, leaves and reeds in different times, places and civilizations. With varying inclinations and shapes, thatched roofs can be found in rural areas all around the globe, from the first man-made structures up to present time.

3.3.4 The Use of Green Roofs in Cold Climates

Apart from their effect of lowering the external temperature in hot areas, green roofs in their living form (referred as turf or sod roofs) have been used in cold climates as an insulating layer, to mitigate the heat losses of the heated interior to the colder exterior. The roof, regardless of its construction material, has been covered with soil and then planted with grass and other plants in order to stabilise it (Osmundson, 1999) in many parts of the world with very high latitudes. In cold climates, where the scarcity of water usually is not an issue, there are plenty of examples of vegetation being used in its living form. However, its dried form has also been popular in cold climates, as presented in the following paragraphs.

3.3.4.1 Monumental Architecture

Grass has been used as an element of primitive European constructions of monumental character from prehistoric times; barrows in central Europe, such as in Poland, Germany and France, but also in Britain, Ireland and the Scandinavian countries today, are examples of a construction destined to survive through centuries and make their footprint on the landscape (Figure 82). Barrows were earth-sheltered, mostly dome shaped structures, where one or more burials were accommodated. They consisted of the burial chamber, which might also contain a passage gallery to the chamber or chambers. In some cases, the chamber might be inaccessible, depending on the period and the type of the barrow. They were either long (Figure 83) or round (Figure 82, Figure 84), large or small, single, twin, triple or more, depending on the

burial type they sheltered. Earth covered the burial construction and turfs, grasses and plants of the area covered the earth. A section of a round barrow can be seen in Figure 85, where its structure can be observed; the chamber and the gallery were constructed with stones and covered with gravel, on which the earth and the plants were laid. They used to impose on the landscape (Donelly, 1992) of the flat lands where they were constructed. As early man was closer to nature, he needed to shelter his dead ones into the ground, which nourished his life, and cover it with life itself, in the form of vegetation. Yet alone, it had to stand aside and dominate the landscape, making it obvious that his ancestors were accommodated under these man-made hills.

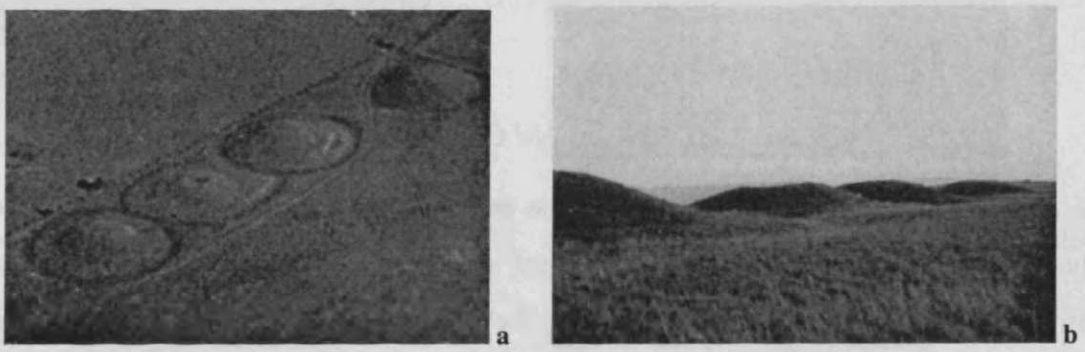

Figure 82. The Four Barrows, of round shape in Aldbourne, Britain, from (a) the air and (b) the ground (right) (Grinsell, 1953)

These large man-made hills, covered with grass, were used by many ethnic groups, such as the Celts, the Pagan Saxons, the Vikings and the central-European people. They date from 1500 to 800 BC for Scandinavia and Germany (Donnelly, 1992), and are estimated to be of about the same period (1400 to 1200 BC) for the South of France (Daniel, 1960), but date from older times for Brittany (2200-1900 BC) (ibid.). In Britain they date from the Neolithic times (from 3500 BC to 2000 BC) (Ashbee, 1970) until the Roman period (in the instance of barrows in Mersea Island and Youngsbury, dating in the first half of the period of Roman domination) and up to 655 AD (Pagan Saxon barrows) (Grinsell, 1953).

Figure 83. Reconstruction of the Fussell's Lodge long barrow, Britain (Ashbee, 1970)

Figure 84. Round barrow in Germany (Donnelly, 1992)

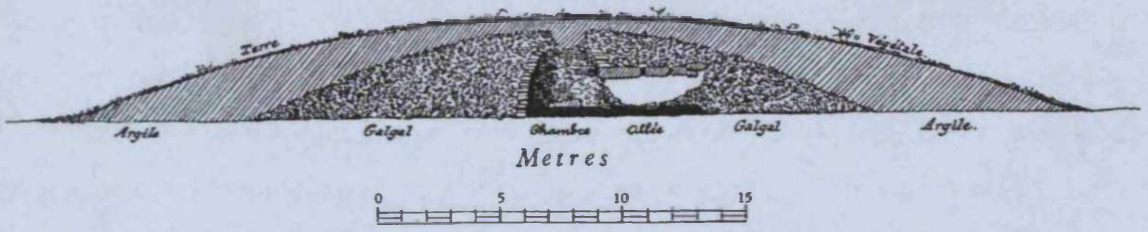

Figure 85. Section of the Tossen-ar-Run round barrow, in Yvias, in Côte du Nord, Bretagne, France (Daniel, 1960)

The use of turf on man-made structures continued in Europe into the Christian period, especially in areas of Viking domination. In Iceland, turf has been used to shelter holy places, such as Christian churches, as has also been the case for churches and mosques in Africa; The first church built in Reykjavik was built with a turf roof, to be replaced by the present Cathedral in 1796 (Donnelly, 1992). Grass-roof churches had been quite popular in rural Iceland; in the instance of the Thingvellir church, according to the description of the English traveller John Barrow, in 1835, it was covered with a green roof. Also the Sifrastadir church (Figure 86), which was built in 1842 in Northern Iceland, had stone walls and green roofs (ibid.) and the Vidmyri Church's roofs and walls were covered with turf (Figure 87) (Velazquez, 2000). Apart from Iceland, the monastery in Mont Saint Michel in Normandy, rebuilt in the 13th century had also green roofs (Grant et al., 2003).

Figure 86. The Sifrastadir church with its turf roof in Iceland (Donnelly, 1992)

Figure 87. The turf roof of Vidmyri Church, Iceland (Velazquez, 2000)

3.3.4.2 Vernacular Architecture

Vernacular architecture in cold climates does not only use thatching on its roofs, but also extensive green roofs, as the ones on Icelandic churches. The higher the rainfall and the colder the climate is, the more likely it is that grasses will be used in their living forms on the roofs, as will be examined in this paragraph.

Thatching has been a very popular technique up until the 19th century in most parts of central Europe, from France to Russia and the British Isles. In the Northern Isles of Scotland, the Orkneys, an extremely cold area without any trees, whose soil is sandstone where only turf grows, masonry walls of houses have been excavated, dating from 3600 to 2500 BC. From the technique of roofing of later, similar constructions of the area, archaeologists have come to the conclusion that these structures were thatched with straw or turf (Pedersen, 2000). Either on stone, brickwalls, or straw bale, thatched roofs were popular in rural areas around Wales, Scotland, England and Ireland from prehistory (Figure 88) until the 19th century (Figure 89, Figure 95). In France, Germany, Austria, Switzerland, Poland Russia and all around central Europe, thatch was once by far the most common form of roof covering (Oliver, 1997c), in the mountainous or lowland areas of the continent (Figure 90-Figure 93). Thatching was not only used for housing, but also for sheltering temporary industries, as the charcoal burner's hut (Figure 94), frequently found in Britain and central Europe.

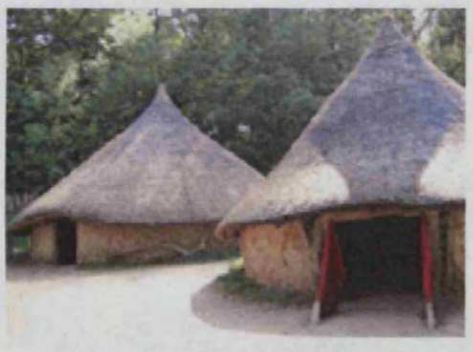

Figure 88. Reconstruction of prehistoric Celtic huts with thatched roofs, in the Museum of Welsh Life, Saint Fagans, Wales (author)

Figure 89. 17th-18th century building with thatched roofs from Llangennydd, Gower, in the Museum of Welsh Life, Saint Fagans, Wales (author)

Figure 90. Multi-purpose residence with straw thatched roof in Koelliken Aargau, Switzerland (Oliver, 1997c)

Figure 91. Early 20th century house with thatched roof in Kursk Province, south Russia (Oliver, 1997c)

Figure 92. L-shaped 18th century farmhouse with thatched roofs in the Netherlands (Oliver, 1997c)

Figure 93. Enclosed four-sided farm with thatched roofs from St Ulrich, Austrian Open Air Museum, Stübing (Oliver, 1997c)

Figure 94. Charcoal burner's hut covered with earth and grasses in England (source: www.yeoldsussexpages.co.uk)

Figure 95. Simple thatched roof in Ireland (Kahn, 1973)

The use of grass on roofs and walls, in both its living and dry form, was a common practice in Scandinavian countries (Finland, Sweden, Norway) since prehistory. Turf was used for millennia for insulating structures from the cold; it was maybe the only primary insulating material easy to find in the area. In addition, the high rainfall levels of the area ensured the survival of plants used on a building. Remains of hunters' and fishers' huts dating from 7500-6000 BC (known as the Maglemose period) at lakesides such as Ulkestrup and Holmegård in Zealand and Ringsjö in Skåne, suggest that walls and roofs were covered with rushes and reeds woven into mats without clay daubing (Donnelly, 1992). As people shifted towards agriculture, settlements of villages started appearing. The remains of their huts dating from 3900-3600 BC, at Stengade on Lakeland, Denmark, suggests that no walls existed, but the rafters sloping to the ground were covered with some kind of thatching material (ibid.). With the evolution of building techniques, walls started appearing, while roofs remained pitched, covered with thatches or turf (Figure 96, Figure 97). This technique was continued and building structures dating from the Middle Ages in the Scandinavian area suggest that no matter what the house type was (farm or town building, fisherman's cottage or post house etc), or what the wall technique was (half timbered, full-timbered, stone etc), roofs were always thatched or turf (Donnelly, 1992;

Osmundson, 1999). Settlements with green roofs were characteristic of Scandinavian tradition, as can be seen in the example of the town of Røros in Sør-Trøndelag (Figure 98), which was founded in 1644 as a copper mining town (Donnelly, 1992). Apart from the Scandinavian people, the Barabinskiy Tartars in also cold and well-watered Siberia used to cover their roofs with turf (Figure 99) (Oliver, 1997c), for insulating purposes as well.

The Viking period in the Northern Atlantic is very much characterised by turf pitched roofs and turf walls in order to insulate buildings from the cold. These constructions date from 800 AD in settlement sites at Jarlshof on the main Sheltland Island. The Vikings passed this "turfing" technique to Iceland in the late 9th century, know as "*sperruthack*" or spar-construction (Pedersen, 2000), which was used in all settlements until the 19th century (Oliver, 1997c) (Figure 100).

Figure 96. Outbuildings under one, turf roof, in the Island of Muhu, in the Baltic area (Oliver, 1997c)

Figure 97. Sod roofed houses in the Mallhaugen Open Air Museum, Lillehammer, Norway (Pedersen, 2000)

Figure 98. Miners' houses with turf roofs dating from the 17th to the 19th century in Røros, in Sør-Trøndelag, Scandinavia (Donelly, 1992)

Figure 99. Typical turfed roof house of the Siberian Tartars (Oliver, 1997c)

Figure 100. Turf farm in North Iceland (Oliver, 1997c)

It is believed that the Vikings founded settlements with similar huts, made of turf roofs and turf walls, in North America as well, in Newfoundland, at L'Anse aux Meadows, off L'Epaves Bay (Donnelly, 1992). This may have been the impact of Northern European people's construction techniques, which were passed to indigenous American people (Oliver, 1997b). In the instance of the Yup'ik Eskimo people in Alaska, they started covering the roofs of their semi-subterranean winter houses with turf, after European contact, as well as covering their above the ground multi-family oval dwellings (Figure 101). Turf roofs have also been found on buildings in 19th century miners settlements in North America, like the Thompson river valley (Figure 102) and vegetation can be spotted on the Doukhobor –of Russian origin– immigrants' roofs, in Canada (Figure 103).

Figure 101. Multi family vertical log dwellings with sod roofs on the banks of the Yukon River, Alaska (Oliver, 1997b)

Figure 102. Miner's turf roofed log house in Wallahachin, Thompson river valley (Oliver, 1997b)

Figure 103. Doukhobor houses with plants on their roofs in Canada (Oliver, 1997b)

Turf roofs have been used in most parts of Northern climates until the mid-nineteenth century when they were replaced with increasingly popular tiles

(Osmundson, 1999). Thatched roofs were also replaced by tiles or slates in most parts of Europe during the 20th century, due to the increasing costs and fire regulations (Oliver, 1997a).

As has been examined here, grass and vegetation have been playing a significant role as materials of the building envelope before the beginning of history, all around the planet, in different civilisations and climates. Either for mitigating high temperatures in hot climates, or acting as an insulating layer in cold ones, or merely as a construction material easily available and worked, grasses and turfs have been used in both their living and dry form, in both vernacular and monumental architecture. In monumental architecture, green roofs have been used as elements of admiration, and in some cultures as manifestations of superiority. They could express social status and, in some cases, they were forbidden to "lower" classes. On the other hand, in vernacular architecture grasses and reeds have been used purely as construction materials, without symbolising anything of the grandeur and power of monumental roof gardens. Thatched roofs can be found in both primitive and sophisticated types of vernacular construction, in temporary or permanent buildings.

3.3.5 The 20th Century

As has been shown in the previous section, the notion of green roofs is not a novelty of the 21st century, but something that has existed in human structures, in different cultures and climates, from prehistoric times. With the Industrial Revolution and the massive production of prefabricated structural materials and especially tiles, turf and thatched roofs, started being replaced by prefabricated roofing materials. The 20th century, with its diverse theories would find new definitions and justifications for the use of vegetation on the building envelope.

At the end of the 19th century, when tiles had replaced most turf and thatched roofs in Northern Europe and North America, the green roof started being used on urban buildings of an "entertaining" or commercial character. Their first use was to accommodate gardens on the buildings themselves, due to the high costs of land in cities. Those gardens were firstly used to accommodate theatrical performances and variety shows in summers. Summer performances on green roofs were firstly established by R. Aronson, in New York in the 1880's, when he had a garden built on

the terrace of the winter "Casino theatre" (Osmundson, 1999). The term "*roof garden*" dates from 1893 as roof garden theatres were gaining popularity. The popularity of roof gardens spread to other sectors in New York, such as restaurants and hotels, offering an agreeable and quite exotic environment to the inhabitants of the city. In Europe, the most famous roof garden of a commercial building of the early 20th century was the "Derry and Toms" roof garden, in London (Figure 104). Built on the art deco building, which accommodated the department store "Derry and Toms", in 1936-38, with more than 500 different varieties of trees and shrubs, it was the place to accommodate the social events of the aristocracy and royalty (ibid.).

The trend passed quickly to dwellings and offices during the art deco movement. Wealthy New Yorkers could express their ability to afford green roofs by adding a roof garden at their penthouses in the new high-rise apartment buildings. Of the most famous roof gardens of the United States are the ones on the Rockefeller Centre, constructed in 1933-36, in New York (Figure 105). During the same period, green roofs were flourishing in the art deco sky scrapers of New York, such as the gardens of the Palazzo d'Italia, the International Building North, the RCA building (Osmundson, 1999), expressing the power and wealth of their owners.

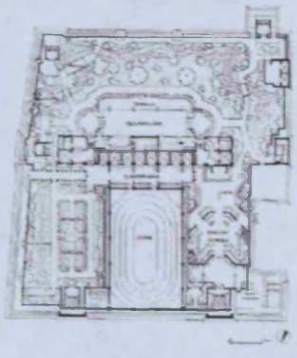

Figure 104. Plan of the Derry and Toms garden in London, in 1938 (Osmundson, 1999)

Figure 105. Roof gardens at the Rockefeller Centre in New York (Osmundson, 1999)

Green roofs were also implemented by the pioneers of Soviet architecture in the late twenties and early thirties, intended as communal spaces in residential buildings. Soviet architects showed great interest in experimenting with new forms of architecture and the creation of a socialist form of spatial life. This was seen as a necessity, as the Pan-Russian executive comity, held in February 1918, had abolished private property and proclaimed the socialisation of the soil (Curtis, 1982). These new

ideas took the form of theories and were implemented in buildings, especially through the constructivists and the OSA (Union[19] of Contemporary Architects) group (Cooke, 1995). One of the attempts of the constructivists was to create buildings where the users would be able to socialise and participate in a communal way of life. Some of the most important architects of OSA, such as Moisei Ginzburg implemented Le Corbusier's ideas of roof terraces, as a further communal space for use in summer months (Curtis, 1982). Gardens were placed on the roofs of many of Ginzburg's designs, such as the Narkomfin apartments[20] which Ginzburg and Milinis built in Moscow in 1928-1930. Strong emphasis had been given to designing for socialising, thus its two-tired roof had a solarium and a garden, with a beautiful view at that time. The residents are known to have spent a lot of time in the roof gardens of the Narkomfin apartments in summers (Ryabushin and Smolina, 1992). Ginzburg had also used vegetation on the roofs of other dwellings, such as the apartment and communal housing block for the state insurance bureau "*Gostrakh*", built in 1926-1927 in Moscow (Figure 106), again with the intension of improving urban life and offering communal spaces for socialising to the dwellers. Apart from dwellings, Ginzburg and Milinis placed green roofs on office buildings as well, for example the House of Government of the Kazakh Republic, in Alma-Ata, Kazakhstan, built in 1929-1931 (Cooke, 1995).

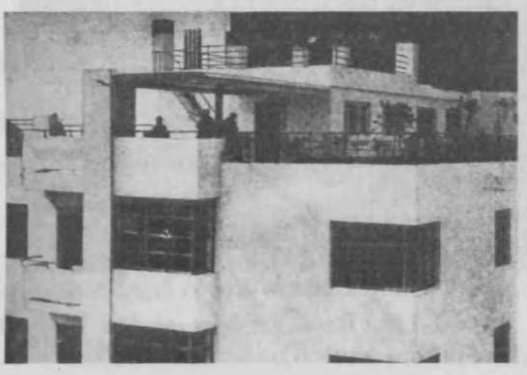

Figure 106. 1927 photograph of the roof garden of Ginzburg's Apartment and communal housing block for the State Insurance Bureau "Gostrakh", Moscow, 1926-1927 (Cooke, 1995)

The tendency of using rooftops as gardens is also expressed in the work of two of the most influential architects of the 20th century; Frank Lloyd Wright and Le

[19] In some texts (e.g. Curtis, 1982; Ryabushin and Smolina, 1992) OSA is translated as "Association of Contemporary Architects".

[20] The Narkomfin apartments were designed as a residential building for fifty families, for housing the employees of the People's Commissariat of Finance (Narkomfin).

Corbusier, as well as by the work of the very important Finnish architect, Alvar Aalto. Although of diverse philosophical perspectives, these architects designed a number of buildings where green spaces were placed on the roofs or the walls of buildings.

Le Corbusier had strong feelings about green roofs. Having considered them as one of the *"five points"* for a *"new architecture"*, he regarded them as an exterior room. Green roofs are a characteristic element of his designs at both the individual building and urban level. With his trip to the East, inspired by the flat roofs of the Kyklades Islands, he put forward the idea of flat roofs, where gardens could be placed, and expansion of living spaces could happen, giving up the idea of sloping roofs, of his homeland, Switzerland (Curtis, 1982; Baker, 1996), which, nevertheless, may have inspired his notion of vegetated roofs. He incorporated the "*jardin suspendu*" (hanging garden) on the roofs of a lot of his work such as the Villa Savoye (Poussy, 1928-31), the Villa Shodhan (Ahmedabad, India, 1954) (Figure 108), the Monastery of La Tourette (Eveux-sur-Arbresle, France, 1957-60) (Figure 107). At an urban level, his views of vegetation on buildings are examined in paragraph 3.3.6.

Figure 107. Green roofs at the courtyard of Le Corbusier's Monastery of La Tourette (Baker, 1996)

Figure 108. Green roofs in Le Corbusier's Villa Shodhan (Baker, 1996)

Figure 109. Perspective of the Millard House, by Frank Lloyd Wright (Levine, 1996)

Figure 110. Terrace with green elements, by Frank Lloyd Wright, in the house of Robert Llewellyn Wright (Brooks Pfeiffer and Futagawa, 1991)

Frank Lloyd Wright expressed a belief in the roots of architecture and society in a natural order. Breaking up with the traditionally closed volume, he mostly used green

roofs as extensions of the interior function of a building (Curtis, 1982), rather than a central space of itself, the way Le Corbusier had perceived it. Green roofs and green terraces had been incorporated into many of his works, as in the instance of the Millard House (Pasadena, California, 1923-24) (Figure 109), the house for Robert Llewellyn Wright (Bethesda, Maryland, 1953) (Figure 110), and the Imperial Hotel (Tokyo, 1922). Apart from individual buildings, he was also concerned about the relationship of nature with the city and he expressed these ideas in Broadacre City, which is discussed in paragraph 3.3.6.

Alvar Aalto, on the other hand, expressed his "naturalistic" concerns (Curtis, 1982), in projects, such as the green roofs in the Villa Mairea, (Noormakku, Finland, 1938-39). The sauna of the villa was covered with turf (Figure 111), mixing modernism with traditional Scandinavian turf roofs. In general, Alvar Aalto was trying to represent through his work the Finnish primitive to western modern architecture, and he used elements of traditional Finnish architecture. Not specifically seeking intellectual justification for his work, but mostly interested in drawing on the variability at the heart of nature (Menin and Samuel, 2003), Aalto saw green roofs as an expression of bringing traditional Finnish culture into the modern world (Trensher, 1996). Either on roofs, or on walls –in the form of trellises in his own house (Munkkiniemi, Helsinki, 1934-36, Figure 112) and ivies (Figure 113), in the instance of Villa Mairea– vegetation and nature were an important element to Aalto (Menin and Samuel, 2003), both detached and attached to the building surfaces.

Figure 111. Sod roofs by Alvar Aalto, on the sauna of the Villa Mairea (Curtis, 1982)

Figure 112. Trellises on Aalto's own house (Menin and Samuel, 2003)

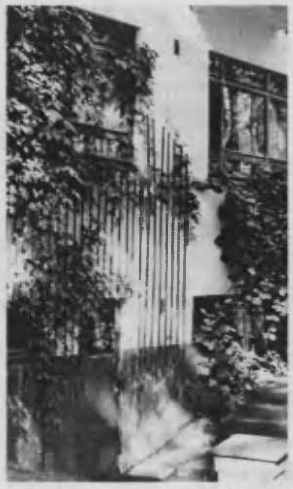

Figure 113. Ivies at the basement entrance of the Villa Mairea, by Alvar Aalto (Menin and Samuel, 2003)

In the early 20th century green roofs were seen by pioneer architects either merely as a recreational space, or a space with its own identity, or a symbolism of nature on the building, regardless of whether they were used as a means of reforming social structures or expressing individual tastes or wealth. The concept of covering building surfaces with plants, purely as a climatic necessity had not yet been put forward.

The notion of greening building roofs and façades in the urban environment for environmental purposes (mitigation of the heat island effect, air filtration etc) is a rediscovery of the late 20th century, as people became more aware of environmental issues. In the 1970's Hundertwasser was even talking about "tree tenants"; trees which would "occupy" an apartment in a building, having their roots inside the building and their branches growing out of its window (Figure 114, Figure 115). He even claimed that "tree tenants" should not pay rent for the space they occupy, as they pay off with the environmental benefits with which they provide the building and its surroundings as they act as *"oxygen suppliers, climatic regulators, dust hoovers, echo dampers, beauty dispensers, mood regulators for urban-damaged people, symbols and regulators of the reorientation of our society and as an example of forestation of cities and even -and in particular- on vertical façades"* (Rand, 1993). He went on to bring his theory to reality first in the Via Manzoni in Milano in 1974 (ibid.) and later, in 1986, in the Hundertwasser Haus Wien in Vienna (Figure 115). In Hundertwasser Haus Wien, trees, apart from being planted in the interior of the building, are also placed on its intensive green roofs (Figure 116, Figure 117). With its 900 tonnes of soil, 250 trees and shrubs (Dunnett and Kingsbury, 2004), the Hundertwasser Haus in Vienna is perhaps one of the most famous European buildings with intensive green roofs, designed as such with an environmental consciousness.

Figure 114. Hundertwasser's model of buildings with "tree tenants" (Rand, 1993)

Figure 115. "Tree tenant" in the Hundertwasser Haus Wien [Source: www.hundertwasser hauswien.com]

Figure 116. View of the Hundertwasser Haus Wien, where trees can be seen on its intensive green roofs (Rand, 1993)

Figure 117. View of the trees of the green roofs in Hundertwasser Haus (Rand, 1993)

In the same radical context, the German architect Rudolf Doernach and the French botanologist Patrick Blanc[21] put forward the idea of transforming the walls of urban buildings into green. Green walls are easier to make than green roofs from a construction point of view; no vapour insulating layers are needed to protect the wall for the plants and no soil layer needs to be adjacent to the construction. Many works of Doernach, suggest that plants should be incorporated in the façade as an *"active building material with the ability to reproduce itself"* (Johnston and Newton, 2003). He has proposed many construction details on how to adjust the plants on walls, with vertical pergolas and trellises adjacent to the structure (e.g. Figure 118). He has also carried it further to suggest which species should be combined in order to maximise the thermal benefits of plants for the interior of the buildings (Doernach, 1998).

Patrick Blanc, having spent a lot of time researching in the tropical forests, where "vertical" vegetation (such as species of ivies and creepers) grow up the trunks of trees, became interested in the technology of "*murs végétaux*"[22]. He considers green walls as "*vertical gardens*" and suggests the formation of "*urban jungles*", with the adoption of vertical gardens on buildings, in the same way that plants grow on trees in the tropical forests. As plants on the ground of tropical forests have adapted to climatic characteristics similar to the ground of an urban canyon, such as lack of light and wind (Blanc, 2002), he believes that the same tropical plants can adapt in the

[21] Many thanks to Emmanuelle Berni for introducing me to the work of Patrick Blanc.

[22] Green walls.

urban environment. His ideas have started being applied in buildings in Paris, such as Fondation Cartier[23], Orangerie du Sénat, Musée du Quai Branly (Figure 119). Trying to introduce biodiversity into the cities, a large variation of plants compose Blanc's green walls, which, in the instance of the Musée du Quai Branly, reach the magnitude of 800m^2 with a variation of more than 15,000 plants from 150 different species, with origins from Japan, China, Northern America and central Europe (Musée du Quai Branly, 2004).

Figure 118. Construction detail of a green wall adjacent to the building (Doernach, 1998)

Figure 119. View of Patrick Blanc's newly formed (summer 2004) *"mur végétal"* in the Musée du Quai Branly (Musée du Quai Branly, 2004)

3.3.6 Greenery as a Primary Urban Utopian Concern in the 20th Century

Vegetation in the vicinity of buildings was not only an important theoretical element of individual buildings for the 20th century, but also on an urban scale. After the expansion of cities with the Industrial Revolutions, architects, scientists and utopians were putting forward ideas for ideal cities for the new era. These cities would provide a solution to the unpleasant and unhealthy living conditions of rapidly growing urban spaces. Either as vehicles of transformation, reformation or overthrow of the existing social system, these ideal cities could not leave the notion of vegetation in the urban environment out of the picture.

Even before the burst of the Industrial Revolution, with the expansion of cities, utopians were dreaming of urban spaces where vegetation would not be a privilege, but a right. Even, from the Renaissance period, Thomas More, the inventor of the

[23] Designed by Jean Nouvel.

word *"utopia"* dreamt of the ideal capital, where all houses would have back gardens in which *"vine, fruits, flowers and any kind of plants"* would be cultivated by the inhabitants (Paquot and Bedarida, 2003). Robert Owen, at the beginning of the Industrial Revolution also pointed out the importance of vegetation in the urban environment, either in the form of gardens attached to dwellings, as public parks, or as trees in the streets. As the phenomenon of elevated urban temperatures was not so well known, and there was still the notion that social reforms could occur through architecture and urban planning, the notion of greening the roofs and façades of buildings was not as central as spatial forms of the utopians concerns in the 20th century.

One of the most important utopians, expressing the necessity of vegetation on an urban scale was Ebenezer Howard, with his idea of "garden cities", suggested in his book *"To-morrow: A Peaceful Path to Real Reform"*, published in 1898 and its revised and re-titled edition *"Garden Cities of To-morrow"*, published in 1902. His idea of garden cities would play an important role around the globe as a solution to the problem of industrialised cities and would influence the urban planning of the first quarter of the 20th century around the world (Figure 120) (Kafkoula, 1990).

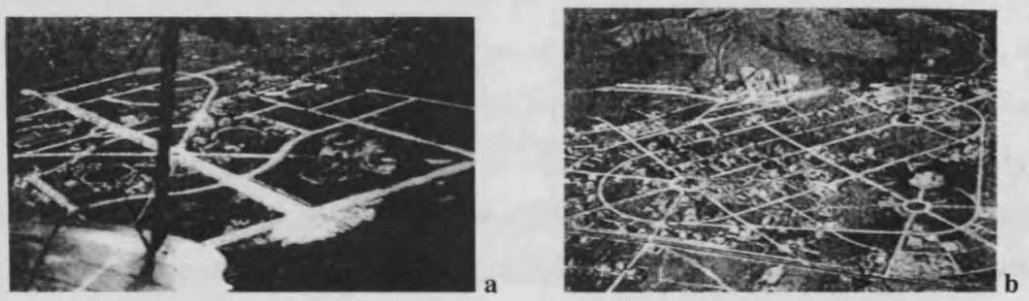

Figure 120. Aerial view of garden cities (a) Jardim America, Sao Paolo in 1921 and (b) Psychiko, Athens in 1930s (Kafkoula, 1990)

In its strict definition the term "garden city" describes "*a town designed for healthy living and industry; of a size that makes possible a full measure of social life, but not larger; surrounded by a rural belt, the whole of the land being in public ownership or held in trust for the community*" (Lancaster and Slaughter, 2000). Similarly, the "garden suburb" is defined as *"the outer part of an urban area, but separated from it by country, with a well planned open layout containing houses or houses plus businesses and/or industry"* and the "garden village" as *"a small development separate from an urban area containing a factory with an associated openly planned housing estate"* (ibid.). However, the definition and implementation of the Garden

City in practice around the world at the early twentieth century was distorted or degenerated; Garden City theories and practice were transformed/deformed and adjusted to the needs or perceptions of cultures, social and historical circumstances around the globe.

Howard's garden city theory envisioned a planning system where the pros of both urban and rural environments could be combined, as summarised in his diagram "the three magnets" (Figure 121). To the concentrated vast city, he proposed an alternative social city with a network of garden cities with their own industries, around a slightly larger city, the central city (Figure 122). His principles were the conscious control of the size of towns, existence of large parks in the city and gardens next to houses, farmlands surrounding the urban areas, and communal land ownership, in order to protect the living environment from individual interests and profits (Howard, 1970). However, he never brought this last principle further to communal ownership of the means of production (Ward, 1992).

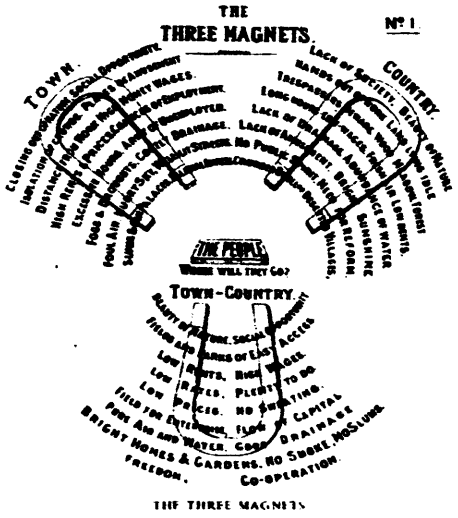

Figure 121. "The three magnets", Howard's diagram, summarizing the pros and cons of city and country which could turn in only pros in garden cities (Howard, 1970)

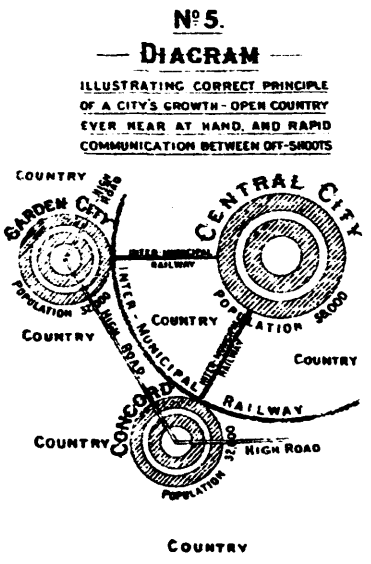

Figure 122. Howard's diagram of correct principle of a city's growth (Howard 1970)

The world's first garden city, which was designed according to Howard's vision, was Letchworth, in England. Built in 1903, it was designed by Unwin and Parker to be an industrial town, with a population of about 32,000 people, drawn from a variety of social backgrounds. It would be free from overcrowding, slum housing and pollution. The countryside would be brought into the town by providing parks and open spaces, low-density housing and extensive landscaping (Miller, 2002). However, Howard's vital principle of communal land ownership was not implemented in a

manner that approached his own ideal (Ward, 1992). The patronage of important industrialists such as Cadbury and the newspaper proprietor Harmsworth were crucially important in the establishment of a bridgehead of middle-class tolerance and sympathy (ibid.) and a primary distortion of Howard's vision. Despite the fact that no suggestion of green roofs and green walls had been made in any of Howard's visions or Unwin and Parker's designs, there were some buildings in Letchworth with green walls (Figure 123) and thatched roofs (Figure 124).

Figure 123. Letchworth Hall with its ivy-covered wall, in the early 1930s (Miller, 2002)

Figure 124. Thatched roof building in Leitchworth, built as the Oarker and Unwin offices in 1907, today sheltering the first Garden City Heritage Museum (Miller, 2002)

Howard's vision of the garden city was not implemented completely anywhere in the world, apart from perhaps the former Soviet Union. The theories of garden cities had been very popular among the modernists in Russia even before the Revolution. After the Revolution, Markovnikov believed that due to the primitive conditions of mass housing in the Soviet Union, there should be a rationalisation of the traditional low-rise housing. He went on to bring these theories into reality in 1922, in the Sokol Garden Suburb, which was designed outside Moscow, by Vesnin and Markovnikov. It was the first Garden Suburb that was designed and built in the USSR and soon it became very popular as an idea of solving the problems of cities and also providing them with food (Papadopoulou-Symeonidou, 1995). The idea of vegetated areas surrounding urban housing was adhere to in settlements built in the former Eastern block (Figure 125), but in the form of Le Corbusier's vertical garden cities (Figure 126, page 127).

Figure 125. Former Soviet Union typical urban block, surrounded by vegetation (courtesy of P. Doussis)

In its distorted context, the garden city theory was implemented in very different social and political contexts and aims, all around the globe. The greatest possible distance from Howard's concept of the garden city was the Nazi garden city (Fehl, 1992). In the 1910s the garden city in Germany had turned into a mere spatial reform model for town planning, where the ruling, bourgeois "caste" would be living in different areas than the inferior labour "castes", separated by green belts of countryside. The Nazis pushed this social order of space, to a concept of racial order (ibid.). Wanting to enforce the "Eastern provinces" (occupied Poland), and to "germanise" them, Nazi planners were allowed to demolish anything related to the Prussian past and allowed "the total freedom to plan", implementing these distorted spatial principles of the garden city. With the Polish resistance and the failure of communication among populations of "Germanic" origin transferred there, in addition to the German defeat in Stalingrad in 1943, most of these plans remained blueprints.

Apart from the Nazi approach, the garden city was perceived as a means of separating classes and populations in other parts of the world, as well, but in a less "orderly" sense than the German concept. In the instance of Athens, despite the attempts of Plato Drakoulis to bring into practice the ideas of Howard as the solution of the housing and social problems that had arisen from the exchange of populations between Greece and Turkey in 1922[24] (Benakis, 2000), garden cities had finally been used as a vehicle of the elite classes to escape from the housing and social problems of the city centre. The first Greek settlement that defined itself as "*kipoupolis*"[25], was the suburban area Psychiko, designed for the elite of Athenian society in 1924

[24] Athens's population had more than doubled because of the immigrants from Turkey, that year (National Statistical Service of Greece, 1990)

[25] Literal translation of "garden city", introduced by Dracoulis.

(Papapanagiotou, 1992) and, for the same reason the garden city of Ekali was established later the same year (Kafkoula, 1990). Both areas were only used as low density housing, with large parks and private gardens, where any industrial or agricultural activity were strictly forbidden. Other "kipoupolis" which were designed with the principle of open, vegetated spaces to accommodate the doubled population of Athens, failed to materialise, due to land costs and profit-driven building. Today the "*kipoupolis*" which had been designed for the elite, are in the very scarce areas of the Greek capital, which are cooler in summer, with buildings surrounded by green, still accommodating the economic elite of the Athenian society.

Apart from Ebenezer Howard, vegetation was a central element in urban transformations proposed by Le Corbusier and Frank Lloyd Wright. Le Corbusier criticised "horizontal" garden cities and proposed "vertical" garden cities, instead. Looking down on suburbanism, he divided the population into two sections; the citizens, who inhabited the city and the *"suburbanites"* who could only live in the suburban areas (Le Corbusier, 1929). With his great belief in the "Machine Age" and the spatial instability that "mechanized speeds" had introduced, he suggested that society was becoming "nomadic", making the settled stability of the family house of low rise "horizontal" garden cities, an echo of the previous era, which was dangerous of dragging *"society into universal waste land of garden cities. Universal, for the crisis is world-wide."* (Le Corbusier, 1948). Instead, his "vertical" garden cities could be applied, which he considered to be *"the fruit of modern techniques adapted to the conditions of modern life"* (ibid.). The "vertical" garden city composed of "superimposed" apartments in an elevated, Dom-Ino type skyscraper, in the middle of a park, in which commodity buildings (maternity homes, clubs, schools etc) could be found (Figure 126). In this way, dwellers would be overlooking a garden from their homes, instead of roads and vehicles.

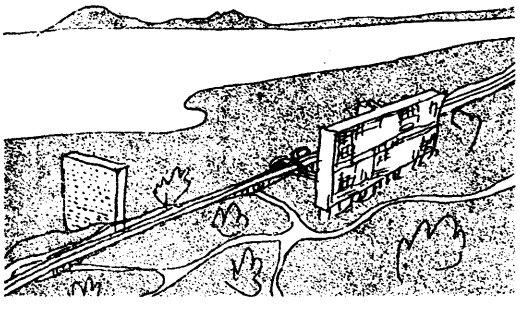

Figure 126. Vertical garden city, as suggested by Le Corbusier, where the vertical use of space "liberates" green spaces around it (Le Corbusier, 1948)

Le Corbusier had incorporated these ideas into his Contemporary and Radiant City. In his Contemporary City, in 1922, with a similar social zoning as in the pre-Nazi Germany interpretation of garden cities, he proposed "vertical" garden cities within the centralised city for the ruling elite of *"large organisations to put this world in order"* (Fishman, 1982) to work and live –in separated zones, though– and "horizontal" ones in the outskirts for the labouring class. Each apartment of the elite skyscraper dwelling had a green veranda (a "hanging garden" as he called it). The roofs of the office skyscrapers were covered with vegetation, for the elite's entertainment at night. The outskirts where the labouring classes would be kept, would consist of smaller building apartments, also surrounded by gardens, where entertainment for the workers could be found. Green roofs and vegetation on buildings were not placed on the residences of the working class, but only in the dwellings, work and entertaining buildings of the ruling class, while the working class dwellings had a detached relationship with it (seeing it in the park next to them, but not on the building itself).

Eleven years later, the social structure of his Radiant City changed dramatically, compared to his earlier Contemporary City. For a city organised around syndicates, in which workers, white-collar employees and engineers run their own factory and regional leaders administer the plants in their region and a national council is in control of the whole area, Le Corbusier now proclaimed that *"if a city were to become a human city, it would be a city without classes"* (Fishman, 1982). Being critical as always of suburbs, he exclaimed, from a different perspective than Howard's that suburbs must be eliminated and that nature should be brought into the cities themselves, creating the *"Ville Verte"*, the "Green City". Doing away with streets, high-rise apartment blocks, now called "*Unités*", surrounded by parks and gardens as in the Contemporary City, were designed for every citizen of the unstratified society of the new civilisation in the Radiant City. The roofs of the *Unités* where covered with gardens, for the inhabitants' recreation (Figure 128). For the right of every urban dweller to vegetation he exclaims *"flowers... for all of us!"* (Le Corbusier, 1933).

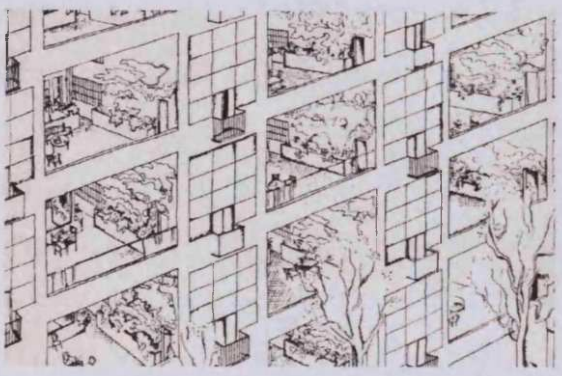

Figure 127. "Hanging gardens" in the apartments of the elite of Le Corbusier's Contemporary City (Fishman, 1982)

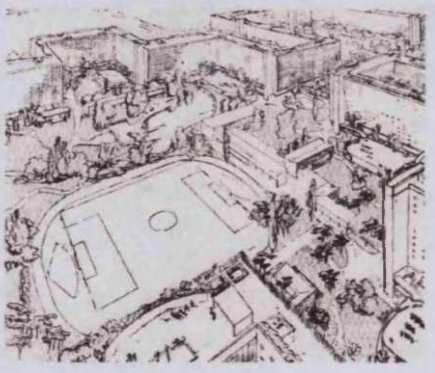

Figure 128. Building apartments with roof gardens inside parks in the Radiant City (Le Corbusier, 1933)

Frank Lloyd Wright, with a more individualist perspective, proposed the ideal city of Broadacre (Figure 129), in 1935, where *"the city had gone to the countryside"* (Fishman, 1982). In a much more decentralised concept than Howard's garden city, in Broadacre, the city disappeared into nature, with vast distances between individual buildings, covered by highways. Frank Lloyd Wright believed that man would reap the benefits of the Machine Age, only when he returned to his natural home, the land, and do away with the big city, which was the representation of greed and destruction. Without any spatial distinction between rural and urban life, Broadacre City achieved a no physical distinction between the two. With buildings "lost" into nature, some of them covered with green (Figure 130), the thermal issues of cities on which this study is focused would not be an issue in such an "urban-rural" layout.

Figure 129. Frank Lloyd Wright's Broadacre City, seen from above (De Long, 1998)

Figure 130. Building with green terraces in the reconstructed model of Frank Lloyd Wright's Broadacre City (De Long, 1998)

Were these horizontal or vertical garden cities or the complete disappearance of the city into nature to have been implemented, this thesis would have no validity. With vegetation being a crucial factor and a central element of design, either on the buildings themselves or right next to them, either in decentralised towns or in cities

where parks would be the most dominant spaces, the heat island effect would have not been demonstrated to the extend it has now. Nonetheless, cities have evolved in a different way than these utopians were envisaging; the thermal effect of concentrated building and street masses combined with the lack of vegetation in urban spaces causes the local environmental issues discussed in chapter 2. The solution of demolishing existing urban forms, for the sake of the now established "Machine Age" is not an option any more. For more "attainable utopias"[26], from an environmental point of view and the well-being of humans from a strictly thermal point of view, in urban spaces, this very utopian concept of "vegetation for everybody" should be applied. By not trying to create new spaces for vegetation, but by placing vegetation in the already available urban surfaces, such as roofs and walls, urban dwellers could have the right to vegetation of which most utopians were dreaming. Also, urban temperatures can be mitigated, as will be discussed in chapters 4, 5 and 6, when the majority of building surfaces are covered with green. By treating vegetated building elements as a privilege only for the social elite, as roof gardens had been used in past civilisations or were envisaged in the Contemporary City, or in the way that the notion of the garden city was used by the wealthy in Athens, and not as a right for the whole urban society, no real thermal benefit can be achieved for anybody. Solutions for mitigating environmental issues cannot be treated in an elitist way, otherwise, they are bound to fail.

3.4 Tendency of Using Green Roofs and Green Walls on an Urban Scale

As green roof technology has advanced and layers which protect the construction of the roof are more reliable than in the past, green roofs can be used much more easily and people can start trusting them as reliable construction means. Especially extensive green roofs, whose static loads are not so large (paragraph 3.1) can be easily put on existing buildings, within the limits of their bearing capacity. On an individual scale, green roofs and walls can be found everywhere on the planet where any form of vegetation is available, in any of its forms. On an urban scale, the first signs of preference towards green roofs as a solution to environmental issues and to the heat island effect has started being manifested. Although there is awareness that covering

[26] Phrase derived from discussions with Phil Jones.

roofs and walls on an urban scale with vegetation might cause water problems, cautious design, irrigation techniques, reuse and recycling of the already consumed water in cities can prove beneficial, as shown in appendix 1.

Of late, the city of Chicago has shown a lot of interest in the thermal effect of green roofs on the city when all of them are covered with green. A study made by Weston Design Consultants (2000) showed that during hot period in the city of Chicago cooling savings of the magnitude of 6,357kWh per 1000ft^2 of green roof can be achieved. The city of Toronto, Canada, has also been interested in modelling the effect of green roofs on the urban climate. The modelling has been performed with the use of a mesoscale model in the MC2 software (Bass et al, 2002). It has been found that a reduction of 1-2°C of urban temperature is expected when roofs in Toronto are covered with green (Peck, 2003).

Oke, when asked about the effect of green roofs on the heat island of Vancouver, Canada, suggested that the greatest effect would be on the urban air quality, which would significantly improve the area's urban heat island issues. He also suggested that the majority of cooling benefits through green roofs in Vancouver would be mostly because of shading, by preventing the creation of extreme surface temperatures and not because of the evapotranspiration of plants (Pedersen, 2000). In the cold and humid climate of Vancouver there are only a few weeks of uncomfortably high temperatures. On the other hand, in cities in hotter areas the mitigation of the heat island effect due to the evapotranspiration of green roofs should be more noticeable, as will be examined in chapter 6.

Germany, being the pioneer in establishing green roofs as a solution to the environmental problems that contemporary cities face, has put into practice laws that promote the implementation of green roofs. Since the 1960's-70's "greening" roofs has been perceived as a way of dealing with run-off water and air pollution issues. Now, 29 of its largest cities (including Berlin, Frankfurt, Stuttgart and Kassel) offer financial support for converting roofs into green ones (Osmundson, 1999), of the magnitude of 25-100% of the installation cost (Grant et al., 2003). Twenty-one of the German cities have added roof greening requirements in their Local Development Plans (Stender, 2002). In the instance of Stuttgart, planning permission is not given to buildings intended to occupy too much ground, unless green roof infrastructures are implemented (ibid.). It is estimated that by 2002 one in every ten flat-roofed buildings

in Germany had a green roof (Dunnett and Kingsbury, 2004), and that 13,000,000m^2 of roofs had been turned into green ones throughout the country (Burdloff and Lassalle, 2005).

Switzerland has also applied laws for the implementation of green roofs. The Swiss federal law requires that the facilities of all federal agencies must be compatible with natural settings and landscape. After 10 years of public education, roof greening now receives an equal level of importance as other construction regulations, such as thermal insulation and fire protection (Brenneisen, 2004). The Swiss federal law also states that 25% of all new commercial developments are "greened" in an attempt to maintain favourable microclimates (Grant et al., 2003). It has been estimated that up to 20% of flat roof area in Switzerland is already greened and this amount is estimated to increase by 1% per year (Brenneisen, 2004).

Recently Belgium, especially its Flemish cities, have started implementing policies which encourage the promotion of green roofs. From a research conducted by Mentens et al. (2003)[27] it has been found that there is a strong tendency to construct green roofs in Belgium (Figure 131); from only 15 roofs that were constructed in 1996, 97 green roofs were constructed in 2001 in Flanders and Brussels. Financial support is given to the inhabitants of Flanders for converting their roofs into green ones in order to encourage urban dwellers with lower incomes to turn their roofs into extensive green ones.

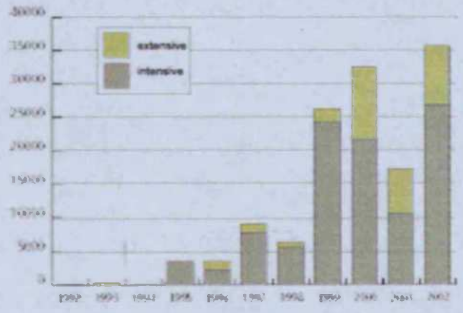

Figure 131. Cumulative number of extensive and intensive green roofs in Flanders and Brussels (adapted from Mentens et al., 2003)

In France, 150,000 m^2 of green roofs have been established up to 2002 (Burdloff and Lassalle, 2005). Throughout the country a potential of 22 million m^2 of roofs which could be easily converted into green ones exists. Lately, places like the Nord-

[27] I would like to thank André Quicheron for finding this article for me and translating it from Flemish.

Pas-de-Calais introduce green roofs in the construction and regeneration of athletic areas (ibid). Paris, in an attempt to offer more green spaces to its inhabitants is putting forward the implementation of vegetated areas in both newly constructed and existing buildings in its PLU (Plan Local d'Urbanism – Local Urban Plan) (Mairie de Paris, 2005).

The city of Tokyo in Japan, has already begun attempts to mitigate the heat island effect with the use of green roofs. The number of hours when Tokyo's temperature was 30°C or more in 2000 was more than double the 1980 figures. These increasing temperatures, being a symptom of the city's heat island effect, made the municipality government of Tokyo aim to establish 1,200 hectares of green roofs in ten years time, with an estimated resulting temperature reduction of at least 1°C (Unknown, 2001). As of April 2000, new public and private commercial buildings, in Tokyo, with roof areas over 250 m^2 and 1,000 m^2 respectively, have to green at least 20% of their flat roofs (Leng and Sia, 2002). In the same year (2000), the Hong Kong government also issued a standard for promoting green features, such as green roofs (ibid.).

The city of Singapore is also considering the implementation of green roofs and green walls and, in general, green balconies, for the sustainable development of its urban character (Leng and Sia, 2002). Green roofs have already been developed in commercial and hotel buildings. As 78% of the land in Singapore is owned by the state and 86% of Singaporeans live in public flats (Savage et al., 2001), this *"garden city image"* (Leng and Sia, 2002) that Singapore wishes to keep, will depend on the government's policies and implementation in macro land use planning.

There have also been quite a few examples of the implementation of green roofs in urban regeneration projects. In the example of the City of Amsterdam, which initiated a number of urban renewal projects in the 1980s, the regeneration of the Wilhelmina Hospital Grounds was put forward, as an eco-village district. One of the most important issues was to *"preserve the green and open character of the site"* (Bekker and Meeder, 1998) which, in 1994, with the addition of new buildings in the site, was turned into a *"roof landscape"* orientation; flat roofs were turned into vegetated areas, covered with grass and plants, and were even cultivated with vegetables (Spitthöver, 1997).

Although green roofs and green walls have not yet been used on a large scale in the UK (Dunnett and Kingsbury, 2004), there are some examples of use of green roofs

and walls more on a community scale than on individual buildings. The most famous project implementing green roofs might be the BedZED (Beddington Zero Energy Development) sustainable urban project, where issues of energy and water conservation have been implemented in the design of both buildings and the urban layout. On the roofs of buildings, vegetation and solar panels are placed (Figure 132), forming gardens for the apartments. In addition, vegetation on the building envelope has been used in renovation projects, as well. The Lambeth Council, being very receptive to sustainability issues, encourages the formation of green roofs and walls in many of its projects. In the example of the renovation of a dwelling block in south London by Lambeth Council, ivies, climbing plants and thorns were used to cover the existing walls of the block, for reasons of *"colour, scent, wildlife resource and security"* (Bradshaw, 2002). The Waterloo Living Space, in north Lambeth, has been designed as a youth resource centre with "living" green roofs (Lake, 2001; Houlihan, 2004). Recently, the Ethelred Estate in Lambeth, is undergoing development to create the largest green roof in Great Britain, by converting the roofs of buildings accommodating 253 flats into green ones[28] (Unknown, 2005).

Figure 132. View of green roofs in BedZED [source: http://www.zedfactory.com]

There seems to be the beginning of an obvious trend of interest towards the thermal effects of green roofs on an urban scale. It is thus quite important to investigate the phenomenon of mitigating the heat island effect through green roofs and walls quite thoroughly. In the following paragraph existing studies of the thermal effect of green roofs are presented.

[28] I would like to thank Jo Patterson for sharing this information with me.

3.5 Existing Studies of the Thermal Effect of Green Roofs

As was mentioned in the previous chapter, existing studies about vegetation in the urban environment have shown that vegetation placed near buildings reduces surface temperatures by shading and air temperature by evapotranspiration and the shading of surfaces as well.

Existing studies of the thermal effect of green roofs have mostly focused on their effect on the internal temperature of the building and not on the external temperature. On this point, the theoretical study of Palomo Del Barrio (1998) is quite important, investigating the thermal performance of the green roof by building an analytical one-dimensional mathematical model for simulating the heat transfer on green roofs (canopy, soil and roof support layers). She went on to simplify it with statistical linearization and model reduction techniques (Palomo Del Barrio, 1999). She concluded that for moderate climates a green roof acts as an insulation layer to the interior of a building and not as a cooling layer of the roof. She also added that the most important role of plants during summer is that of shading construction roof materials, for achieving a lower solar transmission to the interior of the building.

Eumorfopoulou and Aravantinos (1998) came to the same results for the climate of Greece and they summed up that green roofs can contribute positively to the thermal performance of the roof but they cannot replace the insulation layer. They also pointed out that the size of plants plays an important role on the thermal insulation that the green roof can offer. As they noted, roofs with large plants plus an insulation layer have the least heat losses. Aravantinos et al. (1999) have done an experiment comparing an insulated concrete roof with an insulated green roof on two similar constructions in Thessaloniki, Greece. They point out that the existence of plants on the roof plays an important role in lowering the discrepancies of external surface temperatures during extreme climatic conditions. According to their measurements, a conventional roof has a daily external surface temperature range of the magnitude of 25°C during hot period and 10°C during the cold one. For the green roof the range is approximately 5°C for both the hot and cold period (Figure 133). This has a direct impact both on the life and maintenance of construction layers and also on the internal temperature of the building, thus its energy consumption, especially for cooling during the hot period. In addition, from the outdoors climate perspective, on which this study is focused, the extreme surface temperatures of the concrete roof can only

add to the heat island effect, while the lower surface temperatures of green roofs can mitigate it.

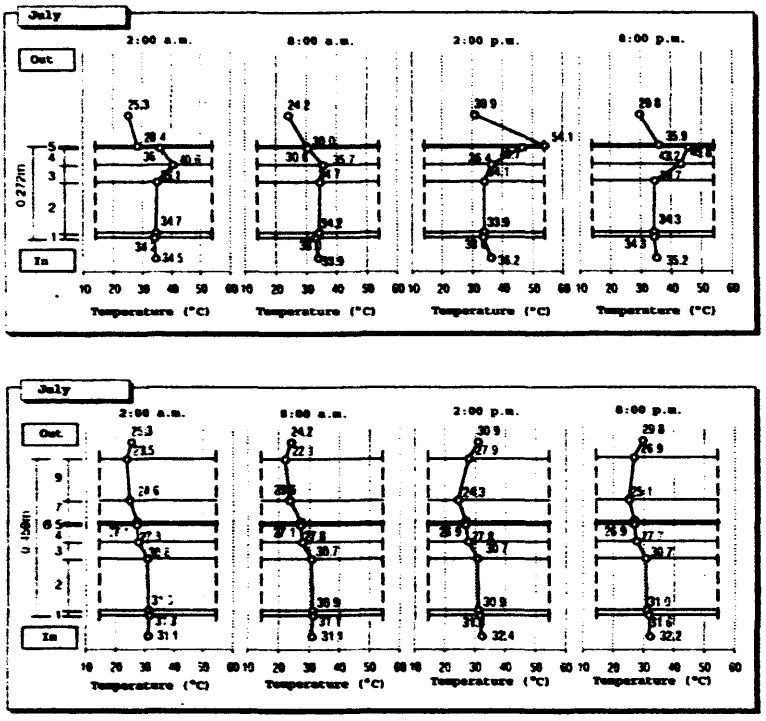

(conventional roof)

(green roof)

Figure 133. Temperature distribution in layers of conventional and green roof, on a typical July day in Thessaloniki, Greece (adapted from Aravantinos et al., 1999)

Niachou et al. (2001) carried out measurements in Loutraki, Greece, on green and bare roofs in the summer of 2000. The surface temperatures of grass and roofing materials were measured with the use of an infrared camera. The surface temperatures of the grass placed on the roof varied from 30°C to 38°C, close to the air's temperature, while the surface temperature of other roofing materials was much higher, varying according to their albedo and time of the day. The difference of the surface temperatures between green and concrete roofs was of the magnitude of 10°C, when the thermography was taken (Figure 134). They noticed that well maintained parts of the green roof with dark green areas had lower surface temperatures, while dry grass had higher temperatures, with the bare soil of the roof reaching the highest peaks. After experimental and theoretical investigation of the green roof as a factor affecting the indoor air temperature, they also reached the conclusion that when greenery is applied on roofs without any insulation layer there is a significant effect on mitigating heat transfer phenomena through the roof. When the roof is insulated the thermal effect of its being planted is much smaller on the internal air temperature of the building.

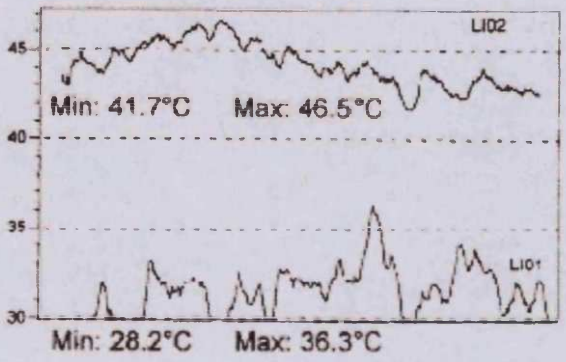

Figure 134. Thermography of surface temperatures on green roof (line LI01) and concrete roof (line LI02), in Loutraki, Greece (adapted from Niachou et al, 2001)

In the City of Chicago there has been interest in investigating the thermal effect of rooftops on the urban environment. As was mentioned above, a study made by Weston Design Consultants (2000) showed that during hot periods in the city of Chicago there can be cooling savings of the magnitude of 6,357 kWh per 1000ft^2 of green roof, due to its evapotranspiration rate. The method they used in order to evaluate the thermal effect of green roofs on the city was by calculating the evapotranspiration from a green area and then by converting it into available cooling effect (Weston Design Consultants, 2000).

Figure 135. The green roof of the City Hall of Chicago (Laberge, 2001)

The City Hall of Chicago has already transformed its roof into a green one (Figure 135), where monitoring of the air temperature at 0.30m above the green roof[29] takes place (Laberge, 2001). It is compared with the air temperature above the black tar roof of the Cook County Building (Figure 136), which is adjacent to the City Hall (both roofs being at the same level). As can be noted in Figure 136, at 11:00 a.m., when the air above the black roof reaches its peak temperature (45.2°C), the air temperature above the green roof is less than 30.3°C, with an air temperature difference of the order of 13.0°C between the two roofs. Regarding the maximum values of air temperature above both roofs a 3.8°C difference is measured. An infrared thermometer is also used to measure surface temperatures. On 9th August 2001, at 1:45 p.m., when the air temperature in the centre of Chicago is about 32.0°C, the

[29] Information derived from personal communication with K. Laberge, environmental engineer at the Chicago Department of Environment.

paved part of the City Hall Roof surface temperatures are between 52.2°C and 54.4°C, and the surface temperatures of its planted area are from 32.8°C to 48.3°C. The surface temperature at the black tar roof of the Cook County Building is 76.1°C (ibid.), leading to a surface temperature difference of the order of 35.0°C between the green and the black roof.

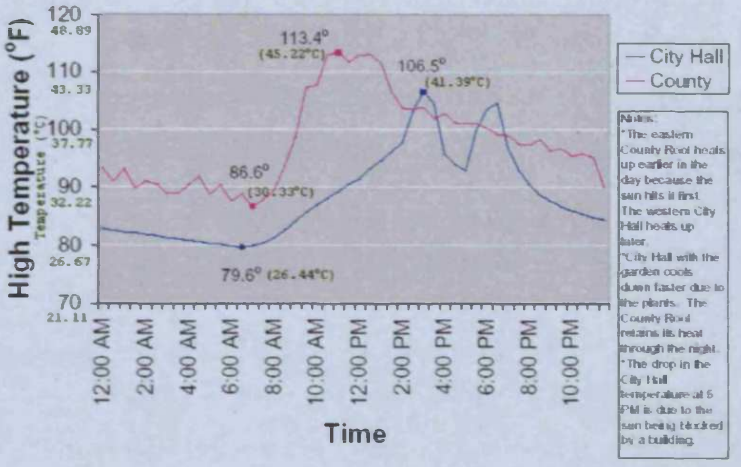

Figure 136. Comparison of the air above the Green Roof of the City Hall of Chicago and the air above the black roof of the Cook County Building for 8th August, 2001 (adapted from Laberge, 2001)

Nyuk Hien et al. (2002) have contributed to the knowledge of the thermal effect of green roofs on the external air temperatures of the built environment, by carrying out measurements in the tropical climate of Singapore. Measurements were carried out on the roof of a low-rise commercial building with intensive green roof comprising a variety of vegetation (grass, shrubs and trees) and other surfaces as well as paved areas and bare soil. The measurements took place during October and November 2001, a quite hot period for Singapore. A comparison was made between the thermal effects (air temperature and relative humidity) of different types of vegetation as well as of the hard building surface on the roof. It was noticed that plants, regardless of their species and their Leaf Area Index[30] have much lower surface temperatures than bare soil and the construction hard surface of the roof. The hard surface reached a maximum surface temperature of 57°C, bare soil 42°C and the plants do not exceed 36°C (Figure 137). Furthermore, comparing the plants themselves, higher surface temperatures were measured under the foliage of the plants with sparse foliages (cases A, C and F) while lower temperatures were found under plants with dense foliage

[30] Term explained in chapter 4.

(cases B, D and E) with maximum surface temperatures measured of the magnitude of 36°C and 26.5°C, respectively.

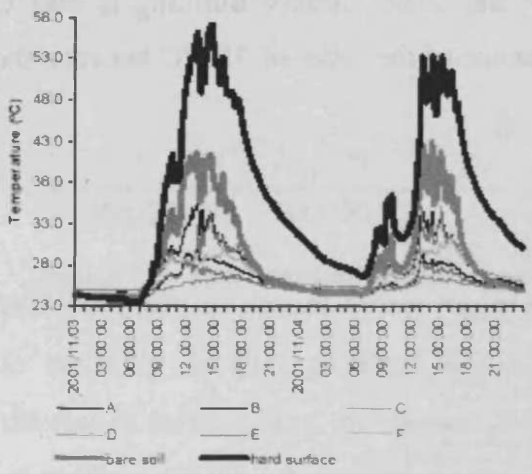

A. Surface temperature measured under Heliconia;
B. Surface temperature measured under Spider lily;
C. Surface temperature measured under Ophiopogon;
D. Surface temperature measured under Raphis palm;
E. Surface temperature measured under Pandanus;
F. Surface temperature measured under Erythrina.

Figure 137. Surface temperatures measured on various surfaces on a green roof in Singapore (Nyuk Hien et al, 2002)

In addition, they also measured the ambient air temperature above vegetation and the hard surface at different heights (0.30m, 0.60m and 1.00m). The results showed that even in the tropical, humid environment of Singapore a 4.2°C temperature difference is measured between the air 0.30m above a green roof and the air above an ordinary terrace (Figure 138). At 1.00m height the effect of vegetation on air temperature is not as strong as at 0.30m height (Figure 138).

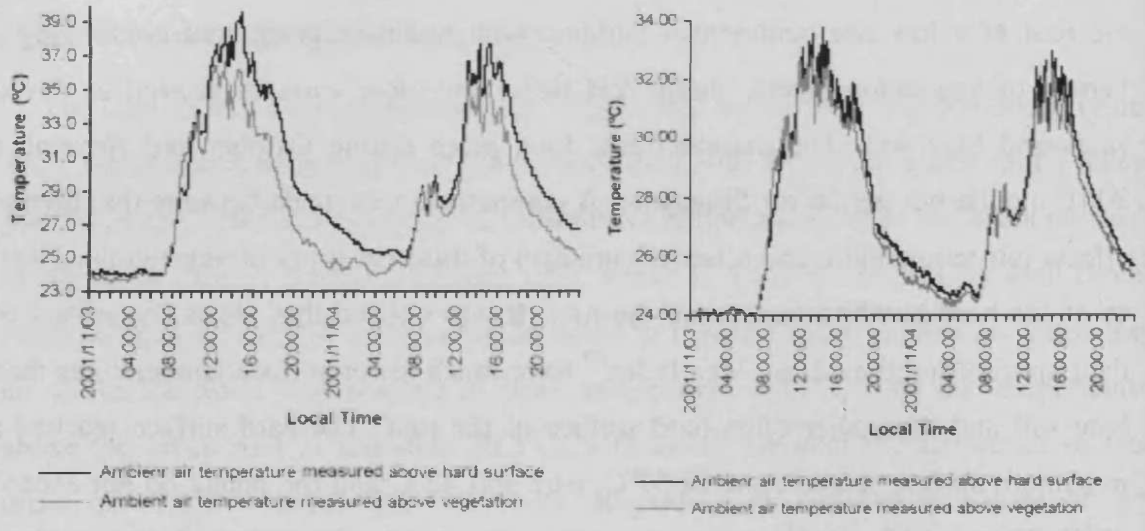

Figure 138: Comparison of air temperatures measured above surfaces with and without plants at 0.30m and 1.00m height respectively (Nyuk Hien et al, 2002)

In measurements carried out in Cardiff, by thet author, in August 2004, a significant difference for clear sky conditions was measured between boundary air temperatures above a grey concrete and a green test cell (chapter 4). For clear sky

conditions, the temperature difference between the two boundary air layers reaches a peak of 1.9°C, with a 0.8°C day-time average. However, for overcast sky this difference reaches a maximum of only 0.6°C, with a 0.3°C day-time average.

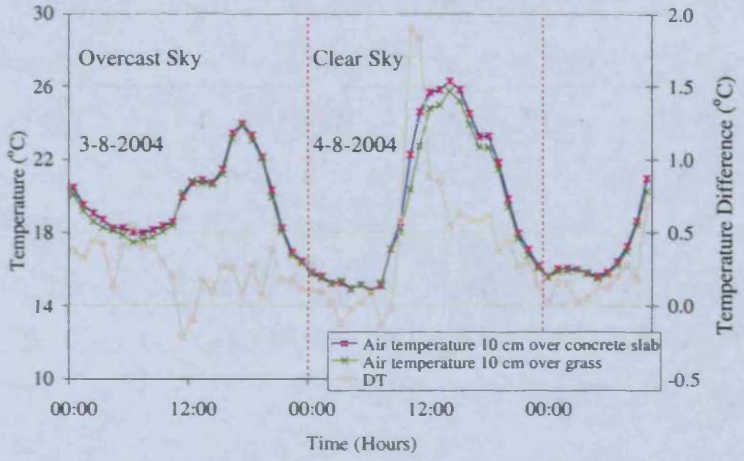

Figure 139. Comparison of measured air temperature 10cm above the concrete slab test cell and the grass test cell, for an overcast and a clear day in Cardiff, in August

It is obvious from all these experiments that surface temperatures measured on green roofs, exposed to solar radiation are much lower than surface temperatures measured on roofs with roof finishing materials. This effect might not be so important for the interior of well insulated buildings, but the external boundary air layer is directly affected by these temperature differences. The Chicago experiment shows that vegetation on the roof is responsible for lowering maximum air temperature by 3.8°C and reaching a peak temperature difference of 13.0°C in its boundary layer (0.30m height), compared to the air temperature above a black roof. In the more humid environment of Singapore there is also a significant difference between air temperature over a green and a conventional roof at the boundary layer (0.30m height), of the magnitude of 4.2°C. In the milder summer of Cardiff the temperature decrease at the boundary air layer reaches a peak of 1.9°C. Although none of these three experiments are directly comparable (test cells, measuring methods and materials are not the same), they show evidence of the potential that exists for lowering urban temperatures with the use of vegetation.

3.6 Summary

It is proved in this chapter that greening building façades for improving environmental and social life in cities is not merely a scientific vision of the 21st

century. Since the early 20th century, visionaries have been trying to find solutions to improve the life of urban dwellers. Despite their approach and social beliefs, vegetation was a central element for the well being of the inhabitants. At the beginning of the 20th century the concerns were more about people and the society rather than the environment itself. With rising environmental awareness, the concerns have moved to protecting the environment as well as its inhabitants. More planners, scientists and authorities are convinced that measures should be taken for mitigating the heat island effect. As the replacement of vegetation with impermeable, hot surfaces seems to be the major factor of the raised urban temperatures, covering them with vegetation could mitigate these temperatures. It is seen as the most realistic solution for tackling the heat island effect.

Vegetation has been an element of the building envelope since prehistory, for different climates, cultures and social status. No matter what the type of construction, structure frame, inclination and shape of the roof, the type of vegetation used, dry or living plants have been elements of the building envelope and especially the roof, in all longitudes and latitudes of the planet. Either as a construction element of the poor or rural dwellers or a triumphal expression of the powerful and the elites, plants have been a vital part of the building envelope. Expressing poverty or expressing wealth and power, used as purely elements of construction or philosophical elements of symbolism or recreational spaces for the wealthy or communal spaces in egalitarian societies, thatched and green roofs have been found around the globe, serving diverse purposes. More recently, with the increase in environmental awareness and the issues which cities have to face, there is a trend toward perceiving them as a possible solution to mitigating raised urban temperatures. Whether or not this could be right, is examined in the following chapters.

3.7 References

1. D. Aravantinos, F. Psomas and N. Tsakiris (1999) *Experimental Test of the Temperature Fluctuation on the Layers of a Green and a Conventional Roof and Evaluation of its Effect on their Thermal Performance.* Sixth National Conference for Renewable Energy Sources, Vol A, pp111-126, Volos.

2. P. Ashbee (1970) *The Earthen Long Barrow in Britain: An Introduction to the Study of the Funeral Practice and Culture of the Neolithic People of the Third Millennium B.C.* J.M. Dent & Sons Ltd, London.
3. G. Asimakopoulou (1996) *The Garden City of Filothei.* Diploma dissertation in the National Technical University of Athens, Department of Architecture, Athens.
4. G.H. Baker (1996) *Le Corbusier, An Analysis of Form.* Van Nostrand Reinhold Co. Ltd, London, New York.
5. B. Bass, R. Stull, S. Krayenjoff, and A. Martilli (2002) *Modelling the Impact of Green Roof Infrastructure on the Urban Heat Island in Toronto.* The Green Roof Infrastructure Monitor, Vol. 4, No. 1 (2002), pp 1-3.
6. F. Bekker and D. Meeder (1998) Amsterdam: *Ecological Urban Renewal at the Wilhelmina Hospital Grounds.* Available from: http://www.eaue.de [Accessed: 29th January 2005].
7. T. Benakis (2000) Introduction to the Life and Work of Plato Drakoulis. In: P. Drakoulis (1893) *Worker's Manual.* Kourier Editions, Athens, pp 7-29.
8. P. Blanc (2002) *Etre Plante a l'Ombre des Forets Tropicales.* Nathan, Paris.
9. F. Bradshaw (2002) *Greening the Flats of London.* Building for a Future, Vol. 11 (2002), pp 22-26.
10. S. Brenneisen (2004) *Swiss Green Roof Innovations and Market.* The Green Roof Infrastructure Monitor, Vol. 6, No. 1 (2004), pp 7.
11. B. Brooks Pfeiffer and Y. Futagawa (1991) *Frank Lloyd Wright Selected Houses, 7.* A.D.A. Edita, Tokyo.
12. D. Buisseret (1980) *Historical Achitecture of the Caribbean.* Heinman, London.
13. J.-C. Burdloff and F. Lassalle (2005) *Un Jardin sur le Toit.* Actualité du CSTB–Webzine, Centre Scientifique et Technique du Bâtiment, Paris. Available from: http://webzine.cstb.fr/webzine [Accessed: 2nd February 2005].
14. G. Contenau (1989) *Everyday Life in Babylon and Assyria.* Papadimas Editions, Athens.
15. C. Cooke (1995) *Russian Avant-Garde, Theories of Art, Architecture and the City.* Academy Editions, London.
16. C. Cornet and F. Verdier (2004) *Paysans de l'Eau, Chine, 1932. Photographies du Père Joseph de Reviers de Mauny.* Actes Sud/Bleu de Chine, Arles.
17. W.J.R. Curtis (1982) *Modern Architecture, Since 1900.* Phaidon, Oxford.

18. G. Daniel (1960) *The Prehistoric Chamber Tombs of France: A Geographical, Morphological and Chronological Survey.* Thames and Hudson, London.
19. D.G. De Long (ed) (1998) *Frank Lloyd Wright and the Living City.* Vitra Design Museum/ Skira Editore, Weil am Rhein, Milan.
20. R. Doernach (1988) *Biotecture I: Living Houses.* The Rainforest Information Centre Good Wood Guide. Available from: http://www.rainforestinfo.org.au [Accessed 25th October 2004].
21. M.C. Donnelly (1992) *Architecture in the Scandinavian Countries.* The MIT Press, Cambridge Massachusetts, London England.
22. N. Dunnett and N. Kingsbury (2004) *Planting Green Roofs and Living Walls.* Timber Press, Portland, Oregon.
23. E. Eumorfopoulou (1992) *Planted Roofs on Buildings, their Contribution to the Ecosystem of Cities, Constructive Solutions and Methods of Application in Greece.* Ph.D. Dissertation, Department of Civil Engineering, Aristotle University, Thessaloniki.
24. E. Eumorfopoulou and D. Aravantinos (1998) *The Contribution of a Planted Roof to the Thermal Protection of Buildings in Greece.* Energy and Buildings, Vol. 27 (1998), pp 29–36.
25. G. Fehl (1992) The Nazi Garden City. In: S. V. Ward (1992) *The Garden City: Past, Present and Future.* pp 88-106. E & FN Spon, London.
26. R. Fishman (1982*) Urban Utopias in the Twentieth Century; Ebenezer Howard, Frank Lloyd Wright and Le Corbusier.* The MIT Press, Cambridge, Massachusetts.
27. G. Grant, L. Engleback and B. Nicholson (2003) *Green Roofs: Their Existing Status and Potential for Conserving Biodiversity in Urban Areas.* Report No 498, English Nature Research Reports, Peterborough.
28. L.V. Grinsell (1953) *The Ancient Burial-Mounds of England.* Methuen & Co Ltd, London.
29. J.E. Hardoy (1973) *Pre-Columbian Cities.* George Allen & Unwin Ltd., London.
30. J. Houlihan (2004) *Waterloo Space.* Available from: http://www.crossriverpartnership.org/page.asp?id=1250 [Accessed 21st June 2005]
31. E. Howard (1970) *Garden Cities of To-morrow.* Faber and Faber Ltd, London.
32. W.F. Jashemski (1979) *The Gardens of Pompeii: Herculaneum and the Villas Destroyed by Vesuvius.* Caratzas Brothers, New York.

33. J. Johnston and J. Newton (2003) *Building Green; A Guide to Using Plants on Roofs, Walls and Pavements.* London Ecology Unit, London.
34. K. Kafkoula (1990) *The Notion of Garden City in Greek Town-Planning in the Period of 1920-1940.* Ph.D. Thesis, Technical School of Architecture of the Aristotle University of Thessaloniki, Thessaloniki.
35. L. Kahn (ed) (1973) *Shelter.* Shelter Publications Inc., Bolinas, California.
36. H.U. Khan (1995) Contemporary Asian Architects. Taschen, Köln, Lisboa, London, New York.
37. K. Laberge (2001) *Monitoring. Compare Temperature, Stormwater Run-off and Other Data Measurements Taken from the Garden Rooftop on City Hall and the Black Roof of the Cook County Building.* City of Chicago. Available from: http://www.ci.chi.il.us/Environment/rooftopgarden/monitoringpage.html [Accessed 22nd October 2002]
38. A. Lake (2001) *Press Release: Green Building 'Topped Out'.* Available from: http://www.lambeth.gov.uk/intradoc/groups/public/documents/pressrelease/010503.htm [Accessed 21st June 2005]
39. R. Lancaster and D. Slaughter (2000) *Garden Cities Worldwide. First Garden City Heritage Museum.* Available from: http://www.hmcm.co.uk/letweb/ [Accessed 29th November 2003]
40. Le Corbusier (1929) *The City of To-morrow.* The Architectural Press, London.
41. Le Corbusier (1933) *The Radiant City; Elements of a Doctrine to be Used as the Basis of our Machine-Age Civilization.* Faber and Faber Limited, London.
42. Le Corbusier (1948) *Concerning Town Planning.* The Architectural Press, London.
43. O.C. Leng and A. Sia (eds) (2002) *Handbook on Skyrise Greening in Singapore.* National Parks Board and Centre for Total Building Performance, School of Design and Environment, National University of Singapore.
44. N. Levine (1996) *The Architecture of Frank Lloyd Wright.* Princeton University Press, Princeton.
45. Mairie de Paris (2005) *L'Embellissement de la Ville, La végétation dans la Ville.* Available from: http://www.paris.fr/fr/urbanisme/plu/ [Accessed 8th March 2005]
46. A. Maiuri (1960) *Pompeii.* Instituto Geografico De Agostini, Novara.
47. S. Menin and F. Samuel (2003) *Nature and Space: Aalto and Le Corbusier.* Routledge, London.

48. J. Mentens, E. Goeminne, M. Verlaek, M. Hermy, and D. Raes, (2003) *Groendaken in Vlaanderen & Brussel: Nichemarkt met Potenties?* Groencontact, Vol. 5 (2003), pp 24-26. Available from: http://www.agr.kuleuven.ac.be/lbh/lbnl/ecology/download.htm [Accessed 1st February 2003]
49. Microsoft Atlas (1997) *Atlas.* Cd-rom.
50. M. Miller (2002) *Letchworth, the First Garden City.* Phillimore, Chichester.
51. Musée du Quai Branly (2004) *Le Mur Végétal: Un Concept et une Réalisation de Patrick Blanc.* Musée du Quai Branly. Available from: http://www.quaibranly.fr/article.php3?id_article=3601&R=2 [Accessed 4th December 2004].
52. National Statistical Service of Greece (1990) *Results of the Census of Buildings.* National Statistical Service of Greece, Athens.
53. A. Niachou, K. Papakonstantinou, M. Santamouris, A. Tsangarassoulis and G. Mihalakakou (2001) *Analysis of the Green Roof Thermal Properties and Investigation of its Energy Performance.* Energy and Buildings, Vol. 33 (2001), pp 719–729.
54. E. Nnamdi (1996) *African Architecture. Evolution and Transformation.* McGraw-Hill, New York, San Francisco.
55. W. Nyuk Hien, L. Siew Eang, O. Chui Leng, L. Guan Tiong, T. Kwok Wai, C. Sekhar, D. Cheong, A. Sia and C. Yu (2002) *Investigation of Thermal Benefits of Rooftop Garden in the Tropical Environment.* PLEA 2002, Toulouse.
56. P. Oliver (1997a) (ed.) *Encyclopedia of Vernacular Architecture of the World. Volume 1, Theories and Principles.* Cambridge University Press, Cambridge.
57. P. Oliver (1997b) (ed.) *Encyclopedia of Vernacular Architecture of the World. Volume 3, Cultures and Habitats, Latin America, North America, Sub-Saharan Africa.* Cambridge University Press, Cambridge.
58. P. Oliver (1997c) (ed.) *Encyclopedia of Vernacular Architecture of the World. Volume 2, Cultures and Habitats, Asia, East and Central, Australasia and Oceania, Europe and Eurasia, Mediterranean and Southwest Asia.* Cambridge University Press, Cambridge.
59. T. Osmundson (1999) *Roof Gardens: History, Design, and Construction.* W.W. Norton & Company, New York.
60. K. Palmer-Wilson (2003) *Introduction to Horticultural Therapy and Green Roofs.* The Green Roof Infrastructure Monitor, Vol 5 (2003), No 1, pp 10-11.

61. E. Palomo Del Barrio (1998) *Analysis of the Green Roofs Cooling Potential in Buildings.* Energy and Buildings, Vol. 27 (1998), pp 179-193.

62. E. Palomo Del Barrio (1999) *Roof Components Models Simplification via Statistical Linearisation and Model Reduction Techniques.* Energy and Buildings, Vol. 29 (1999), pp 259-281.

63. P. Papadopoulou-Symeonidou (1995) *Town and Town-Planning in the Ex-Soviet Union [1917-1985].* Kyriakidis Editions, Thessaloniki.

64. D. Papapanagiotou (1992) *The Kipoupolis of Psychiko during 1920-1940: Establishment, Architects, First Dwellings.* Diploma dissertation in the National Technical University of Athens, Department of Architecture, Athens.

65. T. Paquot and M. Bédarida (2003) *Habiter l'Utopie. Le Familistère Godin à Guise.* Editions de la Villette, Paris.

66. S. Peck (2003) *Towards an Integrated Green Roof Infrastructure Evaluation for Toronto.* The Green Roof Infrastructure Monitor, Vol 5 (2003), No 1, pp 4-5.

67. K. Pedersen (2000) *Meadows in the Sky: Contemporary Applications for Eco-roofs in the Vancouver Region.* MASA dissertation in the UBC School of Architecture. Available from http://www.sustainable-communities.agsci.ubc.ca/thesis/ [Accessed 3rd August 2001].

68. H. Rand (1993) *Hundertwasser.* Taschen, Köln.

69. A. Ryabushin and N. Smolina (1992) *Landmarks of Soviet Architecture 1917-1991.* Passigli Progetti, Milan.

70. D. Robertson (1968) *Pre-Columbian Architecture.* Studio Vista Limited, London.

71. D.J. Robinson (1997) The Social Texture of Pompeii. In: S. E. Bon and R. Jones (eds) *Sequence and Space in Pompeii.* Oxbow Books, Oxford, pp 135-144.

72. V.R. Savage, S. Huang, L. Kong and B. Yeoh (2001) Global Environmental Change: The Singapore Response. In: R.B. Singh (ed) *Urban Sustainability in the Context of Global Change.* Science Publishers Inc., Plymouth, pp 1-16.

73. M. Spitthöver (1997) Open Space. In: M. Kennedy and D. Kennedy (eds) *The Urban Environment in Europe, Designing Ecological Settlements.* Dietrich Reimer Varlag, Berlin, pp 39-52.

74. I. Stender (2002) *Policy Incentives for Green Roofs in Germany.* The Green Roof Infrastructure Monitor, Vol 4 (2002), No 1, pp 10-11.

75. R. Stulz (2000) *Roofing Primer, A Catalogue of Potential Solutions.* Swiss Centre for Development Cooperation in Technology and Management, St. Gallen.

76. M. Trencher (1996) *The Alvar Aalto Guide.* Princeton Architectural Press, New York.

77. University of Patras (2001) *Temple of Agia Theodora.* Arcadia Group, University of Patras. Available from: http://arcadia.ceid.upatras.gr/arkadia/index.html [Accessed 30th November 2003].

78. Unknown (2001) *Tokyo Begins to Tackle Urban Heat with Green Roofs.* The Green Roof Infrastructure Monitor, Vol. 3, No. 2 (2001), pp 4. Available from: www.greenroofs.ca [Accessed 12th December 2001].

79. Unknown (2005) *UK's Biggest Green Roof Project.* Available from: http://www.est.org.uk/aboutest/news/eenews/index.cfm?mode=view&articleid=8692034 [Accessed 21st June 2005].

80. P. Van der Ree, G. Smienk and C. Steenbergen (1992) *Italian Villas and Gardens.* Prestel, Amsterdam.

81. L. Velazquez (2000) *Exploring the Ecology of Organic Green Roof Architecture.* Dissertation submitted for Bachelor of Landscape Architecture Degree, School of Environmental Design, University of Georgia. Available from http://www.greenroofs.com [Accessed 20th October 2002].

82. A. Wallace-Hadrill (1994) *Houses and Society in Pompeii and Herculaneum.* Princeton University Press, Princeton.

83. S.V. Ward (1992) *The Garden City: Past, Present and Future.* E & FN Spon, London.

84. Weston Design Consultants (2000) *Chicago Green Roof Study. Section 7. Task 600/700. Energy Efficiency Analysis and Air Quality Benefits Discussion.* City of Chicago.

85. M. Yampolsky and C. Sayer (1993) *The Traditional Architecture of Mexico.* Thames and Hudson Ltd, London.

86. K. Yeang (1992) *The Architecture of Malaysia.* The Pepin Press, Amsterdam, Kuala Lumpur.

Chapter 4

One Dimensional Model

4 One Dimensional Model

4.1 Meteorological Scales

Generally, the atmosphere is characterised by events whose time and space scales cover a wide range. These events can be classified according to their typical lifetime or period, and the space scales by their typical size or wavelength. Atmospheric phenomena have been classified mainly associated with motion, according to Table 1, chapter 2. Cities' atmospheric phenomena extend from meso to micro scale (Figure 140). In order to understand urban climates, the scale in which they are going to be examined should be chosen first (Oke, 1999). As can be observed in Figure 140c, the smallest scale is that of individual elements, according to which each element creates its own microclimate. As the city usually possesses repetitive structures, such as blocks of buildings and streets, these elements are recombined into larger microscale climate units such as street canyons which generate their own microclimatic characteristics. These characteristics exist beneath the roof-level, to the urban canopy layer (UCL) (Oke, 1987). A larger neighbourhood set of several urban canyons, with their intervening buildings, open spaces and parks creates a larger scale climate, namely the local scale climate (Figure 140b). If there are distinct urban terrain zones (i.e. areas of different physical character, such as the type and density of buildings) in the city, new internal boundary layers will form at each zone border (Oke, 1999). These are mixed together to form the urban boundary layer (UBL) of the whole city. This is a mesoscale phenomenon (Figure 140a) within which the air shows the integrated presence of the city.

This thesis focuses on the development of a two-dimensional microclimatic description of heat and mass exchanges in an urban canyon. In this chapter the presentation of the one-dimensional model takes place, focusing on the theory on which it is based, the assumptions and solutions of its governing equations. An experiment has been carried out in order to calibrate and validate the one-dimensional model and some results comparing the microclimatic behaviour of green roofs with concrete ones are presented and discussed. In paragraphs 4.2 to 4.8.10 the theory on which the model is based and the mathematical solution of the equations describing heat and mass transfer in the one-dimensional model are presented. The model is summarised in paragraph 4.10.

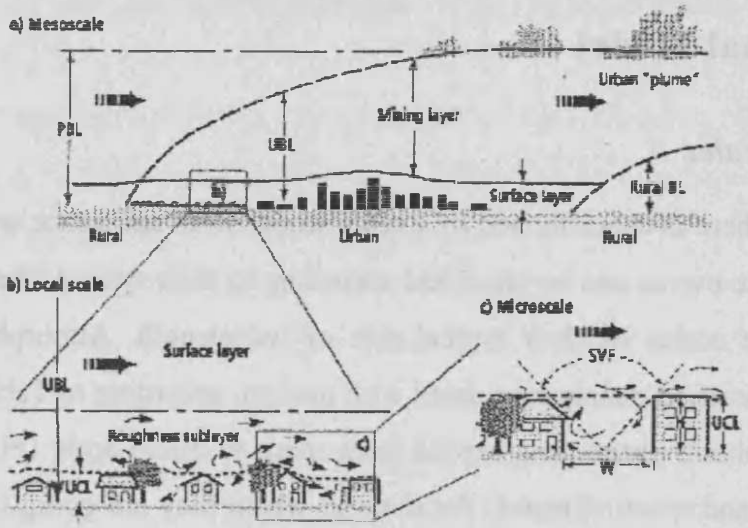

Figure 140. Scales of examining urban climatic characteristics (a) for the whole city (meso-scale), (b) a single urban terrain zone (local scale) and (c) a single street canyon (micro-scale) (Oke, 1999)

4.2 Fundamentals of Heat and Mass Transfer

Heat and mass transfer is described by a system of differential equations obtained from the laws of conservation of mass and energy. When a temperature gradient exists in a body, experience has shown that there is an energy transfer from the high-temperature region to the low-temperature one. By introducing a proportionality constant (K), the heat transfer rate per unit area (Q/A, in W/m^2) is proportional to the normal temperature (T, in K) gradient and, in a one-dimension system, across the z axis expressed by:

$$\frac{Q}{A} = -K\frac{\partial T}{\partial z} \qquad \textbf{Eq. 14}$$

Where K is the thermal conductivity of the material (in W/mK) and the minus sign is a mathematical convention to show that the flux is in the direction of decreasing temperature. Equation 14 is known as the one-dimensional form of Fourier's Law of heat conduction or steady state conduction.

When conduction is not only examined in space but in time as well, the derivative of time (t) is taken into consideration in the one-dimensional expression:

$$\frac{dT}{dt} = -\alpha\frac{\partial^2 T}{\partial z^2} \qquad \textbf{Eq. 15}$$

Where α is the material's thermal diffusion coefficient (in m^2/s), equal to:

$$\alpha = \frac{K}{\rho c_p} \qquad \textbf{Eq. 16}$$

Where ρ is the material's density (in kg/m^3) and c_p its isobaric specific heat capacity (J/kgK). Equation 15 is known as the unsteady-state or dynamic heat conduction.

Similarly to heat transfer, mass transfer (diffusion) in a motionless fluid occurs as a result of the net movement of molecules of one species from any area of high concentration to one of lower concentration. In a one-dimensional system, the flux density or rate of mass transfer (J_i) of an entity i per unit area through a plane is directly related to the concentration gradient ($\partial q/\partial z$) of i across the plane by a proportionality constant (D_i). This is expressed mathematically as:

$$J_i = -D_i \frac{\partial q_i}{\partial z} \qquad \textbf{Eq. 17}$$

Where D_i is the diffusion coefficient of the entity i and the minus sign is a mathematical convention to show that the flux is in the direction of decreasing concentration. This equation is known as the one-dimensional form of Fick's First Law of Diffusion.

When diffusion is expressed in both space and time in one-dimension, it is given by the relationship:

$$\frac{dq}{dt} = -D\frac{\partial^2 q}{\partial z^2} \qquad \textbf{Eq. 18}$$

which is the dynamic expression of mass transfer.

The model developed for predicting the effect of green roofs on the built environment is a prognostic (dynamic) model and not a diagnostic (steady-state) model. In other words, the time derivative is taken into consideration in the solution of the governing heat and mass transfer equations.

Heat and mass transfer, apart from their obvious similarities, affect each other quite significantly, as will be discussed below. Their interaction depends on the type of medium (solid, fluid) and its properties. As Luikov (1961) points out *"mass transfer in wet bodies cannot be separated from heat transfer and the phenomena of heat and mass transfer must be considered in their inseparable association"*. For describing heat and mass transfer in the built environment with green roofs four areas can be distinguished; the construction material, the air, the soil (planting medium) and the

vegetated canopy. Heat and mass transfer expressions in each of these areas are analysed in the paragraphs bellow.

4.3 Heat and Mass Transfer in the Construction Material

Most commonly used structural materials behave as capillary-porous bodies; their technological properties (including hygrothermic ones) are determined, to an important degree, by the form of bonding of the water contained in them. Luikov (1961) first described heat and mass transfer in capillary-porous bodies.

If a system, consisting of a capillary-porous building material (wall or roof) in the medium of wet air and in a region of positive temperatures (no ice), is considered, equations describing the one-dimensional heat and mass transfer can be expressed by (Luikov, 1961):

$$\frac{dT}{dt} = a_c \frac{\partial^2 T}{\partial z^2} + \frac{\varepsilon\lambda}{c_c}\frac{\partial q}{\partial t} \qquad \textbf{Eq. 19}$$

$$\frac{dq}{dt} = a_m \frac{\partial^2 q}{\partial z^2} + a_m \delta \frac{\partial^2 T}{\partial z^2} \qquad \textbf{Eq. 20}$$

Where:

T: building material temperature (K)

t: time (sec)

c_c: building material specific heat capacity (J/kgK)

a_c: building material thermal diffusion coefficient (m^2/s)

ε: ratio of vapour diffusion coefficient to total moisture diffusion coefficient or evaporation number of building material

λ: heat of phase change (latent heat of evaporation of water) (J/kg)

a_m: diffusion coefficient of moisture in the building material (m^2/s)

δ: building material thermogradient coefficient (°M/K)

q: building material moisture content (kg of the substance /kg of the dry body)

The first term in the heat transfer equation 19 expresses the change of enthalpy with time. The first term on the right hand side represents the heat transfer inside the body by molecular conduction. The second term expresses the heat source / sink caused when water changes state (evaporates or condenses). Regarding the mass transfer equation, its left hand side term expresses the water vapour concentration changes with time. The first term on the right hand side represents the molecular diffusion of vapour inside the body and the second one the vapour diffusion due to molecular thermal conduction. It can be assumed (Luikov, 1961) that $a_m \delta \approx 0$. Thus:

$$\frac{dq}{dt} = a_m \frac{\partial^2 q}{\partial z^2} \qquad \textbf{Eq. 21}$$

In other words, inside a capillary-porous body, whose thermal conductivity is considered to be constant[31], temperature distributions are altered by vapour diffusion only when phase change occurs (evaporation or condensation for positive temperatures), due to the energy absorbed / released during the phase change.

4.4 Heat and Mass Transfer in the Air

In this section heat and mass transfer in the air close to the building surface is analysed. For the one-dimensional model heat and mass transfer will be considered only across one dimension is space (z axis), without the influence of any air velocity. The latter will be examined in chapter 5.

If humid air in the urban canyon is considered to be a binary gas mixture (air and moisture[32]), with moisture being component 1 and air, component 2, in a system of zonal calculation, with constant properties of both components, then, the system of differential equations which describe heat and mass transfer in this binary gas mixture are (Luikov, 1961; Eckert and Drake, 1959):

$$\frac{dT}{dt} = a_a \frac{\partial^2 T}{\partial z^2} + \frac{DQ^*}{c_{pa}} \frac{\partial^2 q}{\partial z^2} + \frac{(h_a - h_b)}{c_{pa}\rho_a} I_1 - \left(\frac{c_1 - c_2}{c_{pa}} \right) \left(D \frac{\partial q}{\partial z} \frac{\partial T}{\partial z} \right) \qquad \textbf{Eq. 22}$$

[31] For most building materials, their thermal conductivity is proportional to their humidity concentration (Luikov, 1961; Lü, 2002). Since this study is not focused on the material, but on the phenomena outside the building and it is a common practice in building thermal modelling to consider the thermal conductivity of materials as constant, this has been applied here, apart from the soil layer's thermal conductivity, as will be discussed in paragraph 4.5.

[32] In this study water contained in air is considered to be only in its vapour state. Its liquid or solid state are not taken into consideration.

$$\frac{dq}{dt} = D\frac{\partial^2 q}{\partial z^2} + \frac{Dc_{m1}Q^*}{T}\frac{\partial^2 T}{\partial z^2} + \frac{1}{\rho_a} I_1 \qquad \textbf{Eq. 23}$$

Where:

T: air temperature (temperature of the mixture) (K)

t: time (sec)

α_a: coefficient of thermal diffusivity of air (m^2/s)

D: binary diffusion coefficient (m^2/s)

Q^*: heat of the isothermal mass transfer (J/kg)

c_{pa}: isobaric specific heat capacity of air (J/kgK)

q: relative concentration of component 1, expressed as specific humidity (kg/kg)

h_a: specific enthalpy of phase a (water) (J/kg)

h_b: specific enthalpy of phase b (steam) (J/kg)

I_1: source of component 1 (moisture) of mass (kg/m^3sec)

ρ_α: total concentration of the mixture (kg/m^3)

c_1: isobaric specific heat of component 1 (moisture) of the mixture (J/kgK)

c_2: isobaric specific heat of component 2 (air) of the mixture (J/kgK)

c_{m1}: specific mass capacity of component 1 (moisture, dimensionless)

c_{m1} can be expressed as:

$$c_{m1} = \frac{M_1}{M_1 p_{10} + M_2 p_{20}} \qquad \textbf{Eq. 24}$$

Where M_1 and M_2 are the molar weights of the components (in kg/mol) of the binary mixture (moisture and air respectively) and p_{10} and p_{20} are the relative partial pressures (dimensionless) of component 1 (moisture) and component 2 (air) respectively. Q^* is defined as:

$$Q^* = \frac{K_T}{c_m} \qquad \textbf{Eq. 25}$$

Where K_T is a coefficient experimentally defined by the relation[33]:

$$K_T = -\frac{(\rho_{10})'' - \rho_{10}'}{\ln \frac{T''}{T'}} \qquad \text{Eq. 26}$$

The left-hand side term of the heat transfer equation 22 represents the change of enthalpy with time. The first term of the right-hand side represents the heat transfer by molecular conduction inside the air. The second term expresses the heat transfer by means of diffusion thermal conductivity (Dufour or diffusion-thermo effect) and the third the heat source / sink caused by the chemical reaction of water condensation / evaporation. The fourth term shows the enthalpy transfer resulting from vapour diffusion. Regarding the mass transfer equation 23, its left-hand side term expresses moisture concentration changes with time. The first term on the right hand side represents the molecular diffusion of moisture inside the air, the second one the result of thermal diffusion (Soret effect) and the third one the moisture losses/gains occurring in the air.

Both the Dufour and the Soret effect express the fact that heat and mass transfer do not only depend on the direct effect of conduction and diffusion, respectively, but reciprocally affect one another; heat flow occurs not only because of the temperature gradient but also because of vapour concentration gradients and the flow of moisture is also caused by temperature gradients (Onsager's theorem). Both effects happen simultaneously, in the existence of a temperature or concentration gradient. Both of them are much smaller quantities, compared to the other heat and mass transfer mechanisms and can be omitted (Luikov, 1961). The effect of vapour concentration gradient on air temperature can be expressed by the fourth term of equation 22 (ibid.). More recent studies (Hurt et al., 1992; Bois, 2002; Coelho and Tells, 2002) have pointed out that the Dufour effect is more significant in gases than in liquids and that it should be taken into consideration when a change of phase takes place in the air itself (for example, clouds) (Bois, 2002). However, in this study, as the phase of change takes place in plants and not in the air, nor are clouds modelled, the Dufour and Soret effect are not taken into account because they are too small, compared to the other components of the heat and mass transfer equations. Thus, equations 22 and 23 can be rewritten as:

[33] Where ' and " refer to the first and the second derivative, respectively.

$$\frac{dT}{dt} = \alpha_a \frac{\partial^2 T}{\partial z^2} + \frac{(h_a - h_b)}{c_{pa}\rho_a} I_1 - \left(\frac{c_1 - c_2}{c_p}\right)\left(D \frac{\partial q}{\partial z}\frac{\partial T}{\partial z}\right) \qquad \textbf{Eq. 27}$$

$$\frac{dq}{dt} = D\frac{\partial^2 q}{\partial z^2} + \frac{1}{\rho_a} I_1 \qquad \textbf{Eq. 28}$$

In equation 27 the combined effect of temperature and moisture concentration gradient is expressed in enthalpy changes. According to Eckert and Drake (1959), the effect of thermal diffusion on heat transfer can be neglected in normal engineering mass-transfer processes. However, they point out (ibid.) that it contributes essentially when temperature gradients are extremely large. In the description of the thermal exchanges in the built environment, where temperature gradients in the boundary layer of surfaces exposed to direct solar radiation are relatively large, it will be proved in paragraphs 4.11.1.9 and 4.12.1, that the inclusion of thermal diffusion is essential.

It should be pointed out here that molecular heat conduction through the air, as described in the first term of the right-hand side of equation 27, is important only for the air layer very close to the ground (Jacobson, 1999; Geiger, 1965). As will be discussed more thoroughly in chapter 5, within the air layer, the role of molecular conduction is insignificant compared with eddy diffusion (Geiger, 1965; Sachsamanoglou and Makrogiannis, 1998).

Before proceeding, it is important to establish a relationship between relative humidity and specific humidity, as most meteorological data available are for the former. From their definitions, if air relative humidity, ϕ, is expressed not as a percentage, but as the ratio of water density (ρ_v) to saturation density ($\rho_{s,a}$) ($\varphi=\rho_v/\rho_{s,a}$) and q (specific humidity) is defined as the ratio of water density to the total density ($q=\rho_v/\rho_a$), then q can be expressed as:

$$q = \frac{\varphi\rho_{s,a}}{\varphi\rho_{s,a} + \rho_a} \qquad \textbf{Eq. 29}$$

Similarly, relative humidity can be expressed as:

$$\varphi = \frac{\rho_a q}{\rho_{s,a}(1-q)} \qquad \textbf{Eq. 30}$$

Therefore relative humidity as a percentage (RH), can be given by:

$$RH = \frac{\rho_a q}{\rho_{s,a}(1-q)} \cdot 100 \qquad \text{Eq. 31}$$

4.5 Heat and Mass Transfer in the Soil

Soil is a porous medium which has three fundamentally different components; the solid matrix, consisting of chemical and organic substances of a certain density and specific heat, the liquid phase, which is free available water, not chemically bound to the soil and the gaseous one, air and water vapour occupying the spaces between the soil particles. In dry soil only the solid (soil) and gaseous (air) states can be detected. The liquid water which is added to soil replaces air. In unsaturated soils heat transfer happens in these three phases (solid, liquid and gas). Heat is therefore conducted in solid and liquid phases, convected in liquid and gaseous ones and is transferred through latent heat by vapour diffusion in pores. Consequently heat transfer in soils strongly depends on the water content and temperature, making the assumption of a constant thermal conductivity, used in capillary-porous building materials, invalid.

All three of the most dominant thermal properties of a material (thermal capacity, density and thermal conductivity) are referred to the mixture of the solid soil, water and air. The heat capacity of air is smaller than the heat capacity of soil, making the heat capacity of the soil-air mixture smaller than the heat capacity of solid soil. The heat capacity of liquid water is much larger than the heat capacity of air, thus the heat capacity of the mixture soil-water-air is larger than the heat capacity of the soil-air mixture (Jacobson, 1999).

Temperature changes due to conduction in a homogenous soil below the ground can be estimated with the heat conduction equation:

$$\frac{dT_s}{dt} = \frac{1}{\rho_g c_G} \frac{\partial}{\partial z}\left(K_s \frac{\partial T_s}{\partial z}\right) \qquad \text{Eq. 32}$$

Where:

T_s: soil temperature (K)

K_s: thermal conductivity of the soil-water-air mixture (W/mK)

ρ_g: density of the mixture (kg/m^3)

c_G: specific heat of the mixture (J/kgK)

$K_s \partial T_s / \partial z$: conductive heat flux through the soil-water-air mixture (W/m^2)

It is proved (Jacobson, 1999; Pielke, 2002) that soil's thermal conductivity can be given by the relationship:

$$K_s = \max\left\{418\exp\left(-\log_{10}|\psi_p| - 2.7\right), 0.172\right\} \quad \textbf{Eq. 33}$$

Where:

ψ_p: moisture potential of soil tension (cm)

The moisture potential of soil tension is the potential energy required to extract water from capillary and adhesive forces in the soil. It is given by the relationship:

$$\psi_p = \psi_{p,s}\left(\frac{\omega_{g,s}}{\omega_g}\right)^b \quad \textbf{Eq. 34}$$

Where:

ω_g: volumetric water content of the soil (soil moisture) (m^3 of liquid water/m^3 of the soil-water-air mixture)

$\omega_{g,s}$: maximum volumetric water content that a given soil type can hold (m^3/m^3)

$\psi_{p,s}$: moisture potential when soil is saturated (cm)

b: coefficient, depending on the soil type

The product of soil density and heat capacity is defined as (Jacobson, 1999):

$$\rho_g c_G = (1-\omega_{g,s})\rho_s c_s + \omega_g \rho_w c_w \quad \textbf{Eq. 35}$$

Where:

ρ_s: density of solid soil (kg/m^3)

c_s: specific heat of solid soil (J/kgK)

ρ_w: density of liquid water (kg/m^3)

c_w: specific heat of liquid water (J/kgK)

$(1-\omega_{g,s})$: volumetric content of solid soil (m^3/m^3)

For describing mass transfer in the soil-water-air mixture, the volumetric water content of soil (ω_g) is used as soil moisture expression. Mass transfer in soil is given by:

$$\frac{d\omega_g}{dt} = \frac{\partial}{\partial z}\left(K_g\left(\frac{\partial \psi_p}{\partial z}+1\right)\right) = \frac{\partial}{\partial z}\left(D_g\frac{\partial \omega_g}{\partial z}+K_g\right) \qquad \text{Eq. 36}$$

Where:

K_g: coefficient of permeability of liquid water through soil (hydraulic conductivity) (m/s)

D_g: diffusion coefficient of water through soil (m^2/s)

The term $K_g\left(\partial\psi_p/\partial z+1\right)$ represents the kinematic flux of liquid water through the soil ($m[m^3m^{-3}]s^{-1}$). K_g and D_g are given by the relationships:

$$K_g = K_{g,s}\left(\frac{\omega_g}{\omega_{g,s}}\right)^{2b+3} \qquad \text{Eq. 37}$$

Where:

$K_{g,s}$: hydraulic conductivity at saturation (m/s)

And:

$$D_g = -\frac{bK_{g,s}\psi_{p,s}}{\omega_{g,s}}\left(\frac{\omega_g}{\omega_{g,s}}\right)^{b+2} \qquad \text{Eq. 38}$$

4.6 Heat and Mass Transfer in the Canopy

Before proceeding to the presentation of heat and mass transfer equations of plants, a brief description of the physiology of plants is presented, in order to understand the factors which influence heat and mass transfer in the vegetated medium. Plants, being living creatures, respond to environmental changes, in contrast to building materials, which accept them passively. Since they are rooted to their environment and cannot escape climatic extremes (Gates, 1980), they have adapted quite sophisticated climatic responses. Their most important processes are photosynthesis and evapotranspiration, this study being interested in the latter.

Evapotranspiration, by definition, is the combined process of evaporation, from both soil and plant surfaces and transpiration, through plant surfaces. The evaporation process depends on climatic parameters, such as direct solar radiation, air temperature, air humidity, and wind speed. In order to change the state of molecules of water from liquid to vapour, a certain amount of energy is required. This energy is derived from solar radiation and, to some extend, from the ambient air temperature. Because of the difference between the water vapour pressure on the evaporating surface and that of the surrounding atmosphere, water vapour is removed from the evaporating surface. As evaporation proceeds, the surrounding air becomes gradually saturated. If moist air is not transferred further away from the evaporating surface, the process slows down and might stop. The replacement of saturated air with drier air depends a lot on wind speed. Transpiration, like evaporation, depends on the energy supply (solar radiation and air temperature), vapour pressure gradient (which depends on air humidity) and wind speed (Gates, 1980; Jones, 1992). It also depends on the soil water content and the ability of soil to conduct water to roots, the soil water salinity, the way the plant is watered and the plant itself (Allen et al., 1998). Plants lose water basically through stomata. Stomata, as will be analysed in paragraph 4.6.1, are small pores on the leaves of plants, through which gases and water vapour pass. Water, together with nutrients for the plant, is taken up by roots and transported through the plant. The transformation of liquid water to water vapour takes place within the leaf, in the intercellular spaces. The amount of vapour that is exchanged with the environment is controlled by the stomata aperture. Thus different kinds of plants may have different transpiration rates. Almost all the amount of water that is taken up by the roots is lost by transpiration to the environment (Gates, 1980). Only a very small portion (about 1%) of the water taken up by plants is consumed in their metabolic activity (Allen et al., 1998). Evaporation and transpiration occur simultaneously and it is quite difficult to distinguish the two processes. That is why the term of evapotranspiration is introduced, through which the phenomena are studied and quantified.

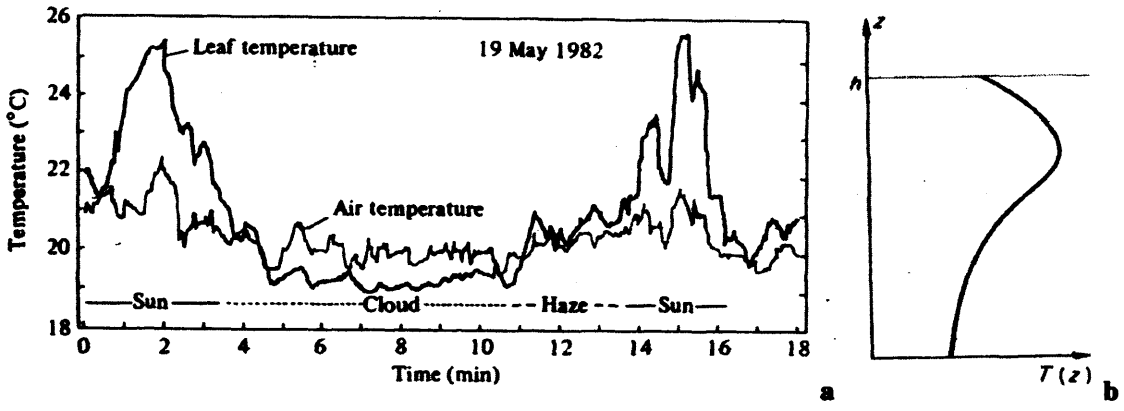

Figure 141. (a) Temperature fluctuations of an apple leaf for a day with diverse sky conditions (Jones, 1992) and (b) Typical vertical, day-time temperature profile within a plant community (Thom, 1975)

Leaf temperature strongly depends on the air temperature in the vicinity of plants. As leaves do not have a thermal mass, they raise their surface temperature with solar radiation and lower it immediately when the radiation reaching them is reduced (Figure 141a). In most species, when the vertical temperature profile is considered, the part of vegetation a short distance away from the more exposed surface has higher temperatures than the upper and the lower part during day-time (Figure 141b). This is due to the fact that this part of vegetation receives some significant amounts of solar radiation (discussed in paragraph 4.6.3.1), yet, it is more insulated, thanks to the upper and lower parts of the plant.

4.6.1 Stomata

Stomata[34] are structural features of aerial organs in most plants (Zeiger et al., 1987). They are microscopic pores formed by a pair of specialised cells, the guard cells, which are found in the surface (epidermis) of most plants (Figure 142). They are involved in the control of two of the most important plant processes: photosynthesis and transpiration.

[34] "Stomata" is the plural of "stoma", which means "mouth" in Greek, therefore "stoma" is used to describe the single pore. This term was first used by Link and de Candolle, in 1827 (Willmer, 1983).

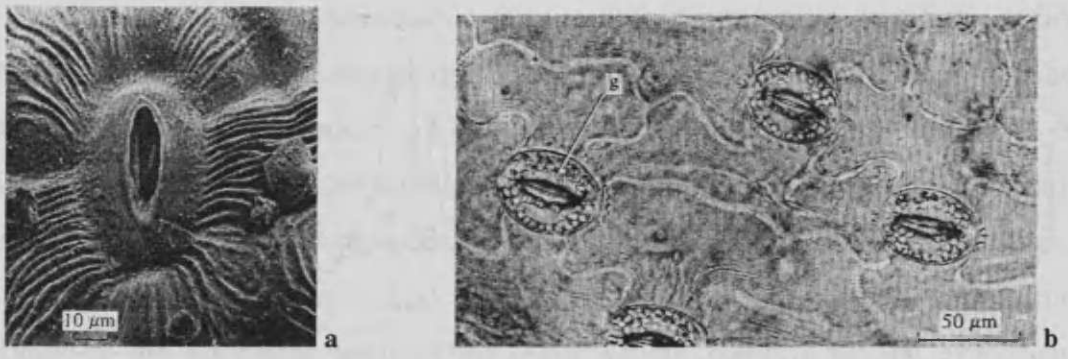

Figure 142. (a) Scanning electron micrograph of a stoma (echinops echinatus species) (b) gramiceous type stomata (triticum aestivum species) with guard cells (g) (Jones, 1992)

The exchange of water vapour and carbon dioxide between plants and the atmosphere happens through stomata. Stomata act as valves to this exchange; the two guard cells which surround the stomatal pores change their shape, in order to control the vapour and carbon dioxide exchanges. In some plants the function of stomata occurs on both leaf surfaces (amphistomatous leaves), in others only on the lower surface (hypostomatous leaves). They are also found on unthickened stems, parts of fruits and parts of inflorescences (e.g. awns of grasses and sepals of angiosperms).

In most species stomata are randomly scattered within the epidermis (Willmer, 1983). Their frequency on a leaf ranges from 50 to 500 per mm^2 (Rutter, 1975). The length of a stoma varies from 10 to 30 μm and its mean width varies from zero when closed, up to approximately 10μm when fully open (ibid.). Both frequency and size vary as a function of leaf position and growth conditions. It can be said in general, that the smaller the stomatal size, the higher their frequency (Willmer, 1983). Even within one species there may be a large genetic component of the variation between different cultivars or ecotypes (Jones, 1992). The total pore area when the stomata are open is from 0.3 to 1% of the total leaf area (Rutter, 1975; Allen et al., 1998). According to Jones (1992) this proportion is quite larger, from 0.5 to 5%.

Stomatal frequencies often vary according to cell size (smaller stomata producing highest stomatal frequencies); therefore the term "stomatal index" is introduced, relating the number of stomata per unit leaf area to the number of epidermal cells per unit leaf area. Thus:

$$\text{Stomatal Index} = \frac{\text{No. of stomata per unit leaf area}}{\text{No. of stomata per unit leaf area} + \text{No. of epidermal cells per unit leaf area}} 100 \quad \textbf{Eq. 39}$$

Stomatal index was considered to be fairly constant within leaves of a single plant. However, this has not been confirmed in all species investigated. In some species, the

light intensity and quality received by mature leaves can affect the stomatal index of still developing leaves (Willmer, 1983).

Stomatal movements depend on changes in turgor pressure inside the guard cells and in the adjacent epidermal cells. The changes in turgor can result either from a change in the total osmotic potential of the guard cells as the supply or loss of water changes, or from active changes in osmotic potential.

Guard cells (Figure 142b) are quite important for defining the stomatal function and resistance, as they are the cells which control the opening and closing of stomata. They are the most complicated cells within the epidermal layer both from a biochemical and anatomical point of view. They possess a specialised set of metabolic pathways able to bring about rapid changes in osmotic potential within the cells when stimulated by relatively minor changes in the external environment. Although they are relatively small cells, there is a considerable variation in their size. Their dimensions may vary from under 10 μm to 80 μm in length and from a few μm to 50 μm in width (Willmer, 1983).

4.6.2 Stomatal Responses to Environmental Factors

As was discussed above, the major role of stomata is to control the entry of carbon dioxide into a leaf for photosynthesis and, at the same time, allow the exit of water vapour which evaporates from the cell walls in contact with air spaces within the leaves. Some of the water loss serves for evaporative cooling of the leaf when exposed to high temperatures, but much is unnecessarily lost when the stomata are open. It has been estimated that several hundred molecules of water are lost from a plant for each molecule of carbon dioxide taken up (Willmer, 1983).

Stomata respond extremely rapidly to changes in environmental factors. Their movements are directly affected by light, water availability (plant-soil water status), water vapour pressure deficit (atmospheric humidity), carbon dioxide concentration, and temperature. Some of these factors and wind movement may also affect stomata in an indirect manner. All these factors tend to interact, making the study of stomatal response to each factor difficult. In general, due to the huge amount of interactions, direct and indirect effects each factor has on stomata and guard cells, the control of

stomatal aperture has not been understood holistically. Several experiments and observations have reached conclusions about how each factor affects directly or indirectly stomatal aperture, but due to the biological and chemical complexity of plants, some aspects and functions are still not fully understood. In the following paragraphs a summary is presented on how the most important environmental factors affect stomatal responses.

4.6.2.1 Light

Light is a very important determining factor for stomatal function. The normal response of stomata is to open with light and to close with darkness. This response varies according to the species, the age of the leaf or the plant and other factors. The stomatal response to light is both direct and indirect. The direct response occurs when the light is absorbed by pigments within the guard cells. The indirect response is triggered by carbon dioxide concentrations within the plant; an increase in irradiance can cause an increase in photosynthesis, leading to a decreased level of carbon dioxide in the intercellular spaces. Stomata then open in response to the decrease in carbon dioxide (Zeiger et al., 1987).

Small amounts of light are able to open stomata. It has been reported that light levels between 1 and 10 per cent of full sunlight are enough to saturate the opening response (Willmer, 1983). According to Jones (1992) maximum aperture is usually achieved with irradiances greater than 200W/m^2, though this value depends on species and on the natural radiation environment. Stomata on shade-grown leaves open at lower light levels than those on sun-adapted leaves. The species of the plant and its growing conditions affect stomatal responses to light and the degree to which these responses are direct or indirect (Zeiger et al., 1987).

In most species, stomata of the abaxial (lower) leaf surface are more sensitive to light than the adaxial (upper) stomata; they open at lower levels of light and are wider open at all light levels than the adaxial ones. Generally, in most species, the closing of stomata happens much faster than the opening in response to light quantity changes.

Light has a direct effect on stomatal aperture, even when carbon dioxide concentration remains constant. In this way light has a direct effect on diurnal stomatal resistance. From a number of studies it has been found out that blue light is

two to twenty times more effective at causing stomatal opening than red light (Willmer, 1983), while other wavelengths have little or no effect. Different species show a different response to light wave lengths, which is believed to be due to the stomatal anatomy.

4.6.2.2 Carbon Dioxide

Stomata respond to carbon dioxide concentrations in both light and dark. Although carbon dioxide concentrations in the natural environment are relatively constant (Jones, 1992), stomata are sensitive to carbon dioxide, responding to the carbon dioxide mole fraction in the intercellular spaces. In general, stomata tend to open as the carbon dioxide mole fraction in the intercellular spaces decreases.

Generally, as ambient carbon dioxide concentrations increase over the physiological range (atmospheric carbon dioxide concentrations being about 320 µl/l) stomata close (Willmer, 1983). As carbon dioxide concentrations decrease over the same range, stomata open. Thus high carbon dioxide concentrations can close stomata, even in the light, while reduced CO_2 concentrations can open stomata, even in the dark.

4.6.2.3 Temperature

As the leaf temperature is raised, the metabolic activity within the guard cells and the leaf as a whole will increase, reaching an optimum, and then decrease. The effect of the increased metabolic activity within the guard cells is to stimulate stomatal aperture.

The effects of temperature on stomatal behaviour can also be indirect. There is a possibility that temperature increases affect the internal carbon dioxide concentrations, which, in turn, affect stomatal movements.

4.6.2.4 Humidity and Plant Water Status

Stomata respond to bulk leaf water potential by closing when the leaf water content becomes too low and opening as the leaf water content increases. In addition, stomata

respond to changes in the soil water status, as well. There is evidence of stomatal closure in response to soil drying (Jones, 1992).

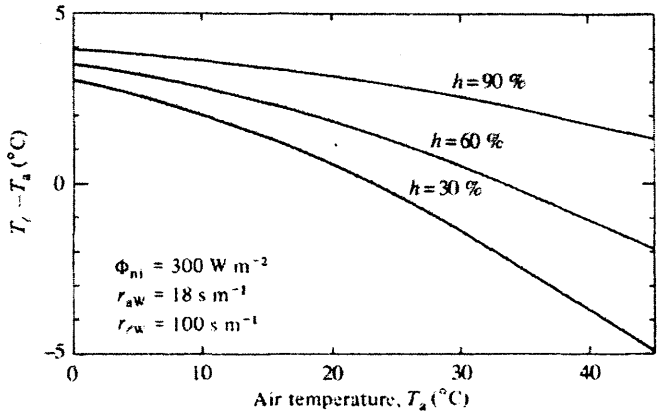

Figure 143. Effect of air humidity and air temperature on leaf-air temperature difference (Jones, 1992)

The stomata of some species also respond to changes in atmospheric humidity by opening as humidity increases and closing as it decreases (Willmer, 1983) (Figure 143). The magnitude of the response depends on species, growing conditions, and particularly on plant water status (Jones, 1992). It is not clear though whether these responses to humidity are due to direct or indirect effects on stomata neither are the effects of plant water balance and atmospheric humidity on stomatal movements completely understood.

4.6.2.5 Other Factors

Stomatal aperture is also affected by many gaseous pollutants such as ozone (O_3), sulphur dioxide (SO_2), and nitrogen oxides (NO_x) (Jones, 1992). Many of these responses are probably related to the toxic effects of these substances on membrane integrity. Stomatal aperture also depends on many other factors such as leaf age, nutrition and disease, which are beyond the scope of this study.

4.6.3 Steady-State Energy Balance

The steady state energy balance on a plant leaf (or canopy) is given by the conservation of energy fluxes into and out of the system (First Law of

Thermodynamics). All energy fluxes must therefore be equal to the rate of storage, thus:

$$\Phi_n - C - \lambda E = M + S \qquad \text{Eq. 40}$$

Where:

Φ_n: net heat gain from radiation (shortwave and longwave) (W/m^2)

C: net sensible heat loss (W/m^2)

λE: net latent heat loss (W/m^2)

M: net heat stored in biochemical reactions (W/m^2)

S: net physical storage (W/m^2)

The net heat stored in biochemical reactions (M) and the net physical storage of the plant (S) are usually negligible compared to the other fluxes at the plant canopies, so they can be omitted from the heat balance equation without major errors (Gates, 1980; Jones, 1992; Monteith and Unsworth, 1990). The rest of the factors are analysed in the following paragraphs.

4.6.3.1 Radiation Distributions within a Canopy Layer

A leaf absorbs a certain fraction of the incident radiation and partitions this energy into three outgoing streams; reradiation, convective heat exchange with the air and transpiration. More than 70% of the solar radiation absorbed by plants is converted into heat and used as energy for transpiration and for convective heat exchange with its surrounding air. A component of the absorbed radiation, up to 28% is used in photosynthesis and stored chemically in high-energy organic compounds (Ross, 1975). Absorbed radiation also plays an important role as a regulator and a controller in processes of growth and development of plants, known as the photomorphogenetic effects. These interactions are not yet totally understood (ibid.), but the active radiation begins in the ultraviolet, extends over the whole visible spectrum and ends in the near infra-red, near 750 nm.

Ross (1975) has summarised the significance of different radiation wavebands for plant life (Table 4). Solar (short wave) radiation is the most important source of energy for the life of a plant. Long wave radiation is insignificant for photosynthetic and photomorphogenic activities. However, it should not be excluded from the

thermal balance of a plant, as it is important for the thermal exchanges of the plant, as for all solids (Table 4, line 5, column 4).

Table 4. Radiation wavebands and their significance for plant life (Ross, 1975)

Type of radiation	Spectral region (μm)	Percent of solar radiant energy	Effect of radiation on plant life		
			Thermal	Photosynthetic	Photomorpho -genetic
Ultraviolet	0.29-0.38	0-4	insignificant	insignificant	moderate
Photosynthetically active radiation (PAR)[35]	0.38-0.71	21-46	significant	significant	significant
Near infra-red radiation (NIR)	0.71-4.00	50-79	significant	insignificant	significant
Long-wave radiation	3.00-100.0	-	significant	insignificant	insignificant

The interaction of radiation with plant leaves is an extremely complex phenomenon. Figure 144 illustrates the absorption, reflection and transmission spectra for typical plant leaves. Details of these properties vary with the species of leaves, according to thickness, age, water content, surface morphology and orientation. The main characteristics are the high absorptance in most of the PAR except the green (hence the green colour of leaves) and the low absorptance in the near-IR. Absorptance is strongly dependent on water content and pubescence, largely as a result of their effects on reflection. Leaves are good absorbers in the far-IR, that is why they behave as black bodies in the longwave, with their emissivity being between 0.94 and 0.99 for most species (Jones, 1992). Plants albedo is usually close to 0.30, with relatively little variation between species (Gates, 1980). It can become higher for white pubescent leaves, waxy leaves or for leaves with low moisture content.

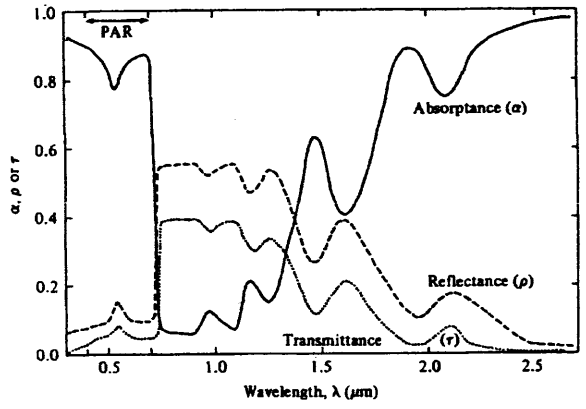

Figure 144. Absorption, transmission and reflection spectra for 'typical' leaves (Jones, 1992)

[35] Photosynthetically Active Radiation (PAR) is the radiation in the particular waveband which excites chlorophyll molecules and thus initiates the flow of energy required in photosynthesis. It is shown (Papaioannou et al., 1996) that the photon flux in the band of 400-700 nm is the best measure of PAR for both natural and artificial light sources.

In terms of the energy absorbed by the whole plant community, and not only by individual leaves, the most important component of the solar radiation is the direct solar radiation received by the leaves. The large variability and inhomogeneity of the architecture of plants makes the expression of radiation transfer within the foliage a complicated problem. The plant community architecture is basically described by its height (h) and its Leaf Area Index (LAI). The Leaf Area Index (LAI) is the leaf area (upper side only) per unit area of soil below it (dimensionless quality). It varies within wide limits and changes seasonally (Figure 145), reaching a maximum before flowering (Ross, 1975; Allen et al., 1998). By its definition, LAI is given by the relationship:

$$LAI = \int_{z}^{h} a(z)dz \qquad \textbf{Eq. 41}$$

Where a(z) (in m^{-1}) is the distribution of foliage with height, z is the reference height and h is the plant height. In natural stands all height, Leaf Area Index and the distribution of the foliage vary considerably. In order to generalise and express these quantities for groups of plants, Ross (1975) introduced a normalised foliage density function ($\tilde{a}(\bar{z})$), given by:

$$\tilde{a}(\bar{z}) = \frac{h \cdot a(z)}{LAI} \qquad \textbf{Eq. 42}$$

Where $\bar{z}$ is the relative height of the foliage ($\bar{z} = z/h$).

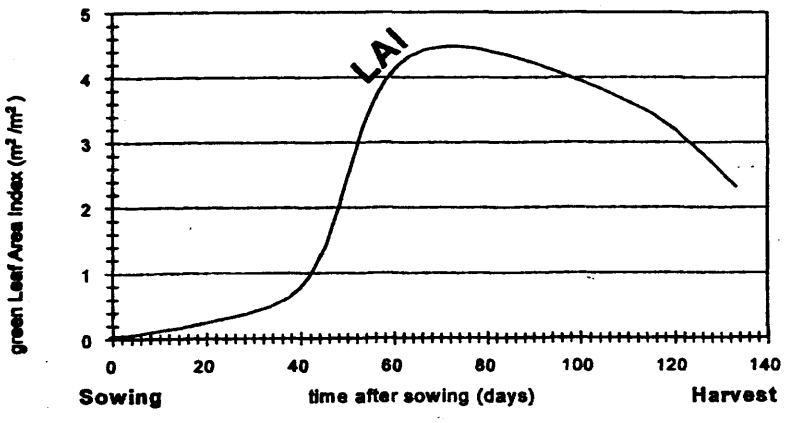

Figure 145. Typical variation of the active Leaf Area Index over the growing season for a maize crop (Allen et al., 1998)

According to Tournebize et al.'s (1996) measurements, the Leaf Area Indexes of grass and shrubs vary from 2.5 to 4.1. For clipped grass, a general equation for LAI is (Allen et al., 1998):

$$LAI = 24h \qquad \textbf{Eq. 43}$$

Where h is the crop height (m).

The active LAI is the index of the leaf area that actively contributes to the surface heat and vapour transfer. It is generally the upper, sunlit portion of a dense canopy. A general equation for LAI_{active} is:

$$LAI_{active} = 0.5LAI \qquad \textbf{Eq. 44}$$

The penetration fraction of direct solar radiation at depth z, ($\tau_s(z)$), is used to describe the fractional area of sun rays entering the plant into depth. Similarly, for diffuse solar radiation, the penetration fraction of diffuse solar radiation at depth z, ($\tau_d(z)$), is defined. Due to the complication of the geometric phenomenon of penetration, both penetration fractions can be summarised by the extinction coefficient, k_o, which is an empirical value, for approximating the transmission and scattering of radiation within the canopy (Ross, 1975). k_o varies from 0.3 to 1.5 (Jones, 1992; Ross, 1975), depending on species, stand type and geometric distribution of leaves. Values less than 1.0 are obtained for non-horizontal leaves or clumped-leaf distributions. Values greater than 1.0 occur with horizontal leaves or more regular arrangement in space (Jones, 1992). k_o can also be expressed as a function of the leaf inclination (θ_l), which is the angle between the vertical and the normal to the upper side of the leaf and the solar elevation (β). If all these parameters are known, the extinction coefficient can be expressed as (Ross, 1975):

$$k_o = \begin{cases} \cos\theta_l & \text{for } \theta_l \le \beta \\ \cos\theta_l \left[1 + \frac{2}{\pi}(\tan\phi_o - \phi_o)\right] & \text{for } \theta_l > \beta \end{cases}$$

Where $\cos\phi_o = \tan\beta \cdot \cot\theta_l$

According to Ross's formula, for horizontal leaves k_o=1 and for vertical leaves $k_o = (1/2)\cot\beta$. It is obvious from this formula, that when the leaf orientation is constant, the extinction coefficient changes with solar elevation.

As the expression of the extinction coefficient might become quite complicated, the penetration fraction of both direct and diffuse solar radiation can be given as an exponential relationship of the empirical, constant extinction coefficient and the leaf area index:

$$\tau = \exp[-k_o LAI] \qquad \text{Eq. 45}$$

This expression of the distribution of the total solar radiation within the plant community throughout the whole day has been applied in this model, as is the common practice in low and medium height vegetation models (Lhomme, 1981; Perrier, 1976; Jones, 1992).

Regarding long wave radiation, which is important for the energy balance of the plant, two components can be distinguished for a leaf area index LAI, on the upper surface of a horizontal plane; the long-wave radiation of the atmosphere which has penetrated the upper layers of a stand without interception and the long-wave radiation of the upper leaves at a given leaf temperature according to the Stefan-Boltzmann law (their sum symbolised as $L_d(LAI)$). On the lower surface, the total long wave radiation ($L_u(LAI)$) consists of the radiation from the ground surface and the radiation of the lower leaves. The net long wave radiation is ($L_n(LAI)$) (Ross, 1975):

$$\begin{aligned} L_n(LAI) &= L_d(LAI) - L_u(LAI) = \\ &= -\left[\varepsilon_l \sigma T_l^4 - L_d(0)\right]\tau_{d1}(LAI) - \left[L_g - \varepsilon_l \sigma T_l^4\right]\tau_{d2}(LAI) \end{aligned} \qquad \text{Eq. 46}$$

Where $L_d(0)$ is the long wave radiation from the atmosphere and L_g the long wave radiation from the ground (σT_g^4). $\tau_{d1}(LAI)$ is the penetration fraction for downward diffuse radiation and $\tau_{d2}(LAI)$ is the penetration fraction of upward long-wave radiation. $\tau_{d1}(LAI)$ is given by the relationship (Ross, 1975; Lhomme, 1981):

$$\tau_{d1}(LAI) = 2\int_0^{\pi/2} \exp\left[\frac{G(\theta)}{\cos\theta}\right]\cos\theta \sin\theta d\theta \qquad \text{Eq. 47}$$

Where θ is the inclination of the solar beam and $G(\theta)$ is the G-function, representing the mean projection of a unit foliage area in the direction determined by the inclination and the azimuth. Empirically, $G(\theta)$ can be given as a function of solar elevation (β) (Ross, 1975; Perrier, 1976):

$$G(\theta) = a + b\sin^2\beta \qquad \text{Eq. 48}$$

Where a and b are empirical coefficients. $\tau_{d2}(LAI)$ is expressed by the relationship (Ross, 1975):

$$\tau_{d2}(LAI) = 2\int_0^{\pi/2} \exp[-k_o(LAI_o - LAI)]\cos\theta \sin\theta d\theta \qquad \text{Eq. 49}$$

In reality, these complicated relations are neither practical, nor can approximate in full detail the complexity of canopies (Jones, 1992). The empirically determined extinction coefficient, k_o, is a means of describing the geometry of canopies in a convenient and practical way (Jones, 1992; Gates, 1980). Another general relationship for the distribution of net radiation within the canopy, which correlates well with observations is the following one (Ross, 1975; Perrier, 1976):

$$\Phi_n(LAI) = \Phi_n \exp\left[-a_o LAI + \beta_o LAI^2\right] \qquad \textbf{Eq. 50}$$

Where α_o and β_o are coefficients of the magnitude of 0.622 and 0.055 respectively. Thus, the net radiation within and above stands has a diurnal course, being positive in daytime and negative in night-time.

In Table 5 a summary is presented of the expressions of the distribution of short wave and long wave radiation within a plant canopy, as suggested by various researchers.

Table 5. Expressions of total net radiation distribution within the canopy layer from different researchers (Jones, 1992; Palomo Del Barrio, 1998; Ross, 1975; Perrier, 1976; Lhomme, 1981; Monteith and Unsworth, 1990)

Source	Expression
Jones (1992)	$\Phi_n = (I_s + I_s\alpha_{soil})(1-\alpha_{s(leaf)}) + I_{Ld} + \sigma T_{lawn}^4 - 2\sigma T_{leaf}^4$
Palomo Del Barrio (1998)	$\Phi_{n,sw} = [1-\tau_s-(1-\tau_s)\rho_\infty](1+\tau_s\rho_g)I_s$ $\Phi_{n,lw} = (1-\tau_l)[\sigma T_{sky}^4 + \sigma T_{ground}^4 - 2\sigma T_{leaf}^4]$
Ross (1975)	$\Phi_n(LAI) = \Phi_n \exp[-a_o LAI + \beta_o LAI^2]$
Perrier (1976)	$\Phi_n(LAI) = \Phi_n \exp[-a_o LAI + \beta_o LAI^2]$
Lhomme (1981)	$\Phi_n = (1-a_{s(leaf)})I_s + \varepsilon_{leaf}(I_{Ld} - \sigma T_{leaf}^4)$
Monteith and Unsworth (1990)	For short grass lawn: $\Phi_n = (1-a_{s(leaf)})I_s + I_{Ld} - \sigma T_{leaf}^4$ For horizontal leaf: $\Phi_n = \{(1-a_{s(leaf)})(1-a_{soil})I_s + I_{Ld} + \sigma T_{soil}^4 - 2\sigma T_{leaf}^4\}/2$

In this model, the relationship suggested by Jones (1992), multiplied by the penetration fraction is used to describe short wave and long wave radiation in the canopy.

$$\Phi_n = [(I_s + I_s\alpha_{soil})(1-\alpha_{s(leaf)}) + I_{Ld} + \sigma T_{lawn}^4 - 2\sigma T_{leaf}^4]\exp[-k_o LAI] \qquad \textbf{Eq. 51}$$

4.6.3.2 Convective Exchanges

The convective sensible heat loss can be expressed as (Jones, 1992):

$$C = \frac{\rho_a c_p}{r_{aH}}(T_a - T_\ell) \qquad \text{Eq. 52}$$

Where:

ρ_a: air density (kg/m^3)

c_p: air specific heat capacity (J/kgK)

T_a: air temperature (K)

T_ℓ: leaf surface temperature (K)

r_{aH}: convective heat resistance (s/m)

The determination of the convective heat resistance, r_{aH}, is discussed in paragraph 4.6.4.1.

4.6.3.3 Evapotranspiration

Evaporation from a wet surface to the air is proportional to the concentration difference of water vapour between the air and the surface. Raschke related evaporation from a leaf to the difference between the vapour pressure inside the leaf and the air well outside. He assumed that the vapour inside the leaf was saturated, while the vapour in the air was not (Waggoner, 1975). The net latent heat flux from a crop can thus be given by the equation:

$$\lambda E = \frac{\rho_a c_p}{\gamma(r_a + r_s)}(e_s(T_\ell) - e_a) \qquad \text{Eq. 53}$$

Where:

γ: psychrometric constant (Pa/K)

r_a: aerodynamic resistance (s/m)

r_s: bulk surface resistance (s/m)

$e_s(T_\ell)$ saturation water vapour pressure at leaf temperature (Pa)

e_a: water vapour pressure in the bulk air (Pa)

The difference between the saturation water vapour pressure at leaf temperature and the water vapour pressure in the bulk air can be given by (Jones, 1992):

$$e_a - e_s(T_l) = (e_s(T_a) - e_a) - s(T_a - T_l) \qquad \textbf{Eq. 54}$$

Where s is the slope of saturation vapour pressure curve (Pa/K). The slope of saturation vapour pressure curve s can be given by the equation (Monteith and Unsworth, 1990):

$$s = \frac{\lambda M_w e_s(T_a)}{RT_a^2} \qquad \textbf{Eq. 55}$$

Where:

λ: latent heat of evaporation of water (J/kg)

M_w: molecular weight of water ($18 \cdot 10^{-3}$kg/mol)

R: Universal gas constant (8.31J/molK)

$e_s(T_a)$: saturation vapour pressure (Pa)

The saturation vapour pressure can be derived from the Clausius-Clapeyron equation, which approximates the temperature variation of the saturation vapour pressure of water over a liquid surface as:

$$\frac{de_s(T_a)}{dT_a} = \frac{\rho_{a,s}}{T_a}\lambda \qquad \textbf{Eq. 56}$$

It is proven (Jacobson, 1999) that the saturation vapour pressure of water over a liquid surface is:

$$e_s(T_a) = 611.2\exp\left[6816\left(\frac{1}{273.15} - T_a\right) + 5.1309\ln\left(\frac{273.15}{T_a}\right)\right] \qquad \textbf{Eq. 57}$$

Where T_a is expressed in Kelvin and $e_s(T_a)$ in Pascal.

More simplified expressions for $e_s(T_a)$ have been given by Bolton (Jacobson, 1999):

$$e_s(T_a) = 611.2\exp\left[\frac{17.67T_a}{T_a + 243.3}\right] \qquad \textbf{Eq. 58}$$

A variation of Bolton's formula (with different factors) has been suggested by Tatan (Lhomme, 1981; Tournebize et al., 1996):

$$e_s(T_a) = 611\exp\left[\frac{17.25T_a}{T_a + 237.3}\right] \qquad \text{Eq. 59}$$

In both Tatan and Bolton expressions $e_s(T_a)$ is in Pascal and T_a in Celsius degrees and they are valid for a band of $-35^oC < T_a < 35^oC$.

Vapour pressure can be given as a function of relative humidity and saturation vapour pressure:

$$e_a = e_s(T_a) \cdot \frac{RH_a}{100} \qquad \text{Eq. 60}$$

4.6.4 *Plants Resistances*

In plant physiology it is common practice instead of conductance constants to use their reciprocal, the resistance, mentioned in paragraphs 4.6.3.2-4.6.3.3. Resistances express the difficulty of a flux (heat or diffusion) across a certain path with a given driving force. For the heat and vapour exchanges of a surface of a leaf, and generally, of a canopy, with the atmosphere, its exchanges are described by three resistances; the convective heat resistance, r_{aH}, describing the difficulty of exchange of heat between the leaf surface and its surrounding air, the aerodynamic resistance, r_a, which describes the surface resistance to water vapour loss, and the stomatal resistance, r_s, which describes the resistance to water losses from within the leaf. These resistances are summarised in Figure 146 and analysed in the following paragraphs.

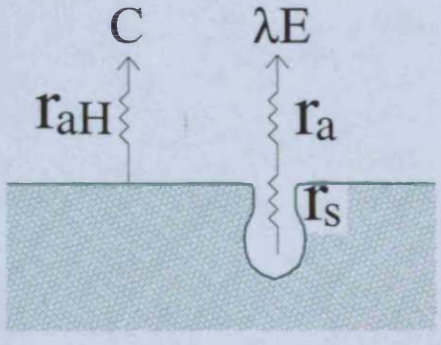

Figure 146. Convective heat resistance, r_{aH}, aerodynamic resistance, r_a, and stomatal resistance, r_s, at a leaf's thermal and vapour exchanges with its surrounding air

4.6.4.1 Convective Heat Resistance

The convective heat resistance, r_{aH}, which expresses the resistance to sensible heat loss from the leaf to the air surrounding it, is given (in s/mm) by the relationship (Jones, 1992):

$$r_{aH} = \left[6.62 \left(\frac{w}{d} \right)^{0.5} \right]^{-1} \qquad \textbf{Eq. 61}$$

Where:

w: wind velocity (m/s)

d: the characteristic dimension or distance to leading edge (m)

For cylinders with their long axis normal to the flow:

$$r_{aH} = \left[4.03 \frac{w^{0.6}}{d^{0.4}} \right]^{-1} \qquad \textbf{Eq. 62}$$

And for spheres:

$$r_{aH} = \left[5.71 \frac{w^{0.6}}{d^{0.4}} \right]^{-1} \qquad \textbf{Eq. 63}$$

4.6.4.2 Aerodynamic Resistance

The aerodynamic resistance, r_a, describes the resistance of the canopy surface to water vapour loss from the vegetation surface upwards. It involves friction from the air flow over the vegetated surfaces. Allen et al. (1998) express it as:

$$r_a = \frac{\ln\left[\frac{z_m - d}{z_{om}} \right] \ln\left[\frac{z_h - d}{z_{oh}} \right]}{k^2 w_z} \qquad \textbf{Eq. 64}$$

Where:

z_m: height of wind measurements (m)

z_h: height of humidity measurements (m)

d: zero plane displacement height (m)

z_{om}: roughness length governing momentum transfer (m)

z_{oh}: roughness length governing transfer of heat and vapour (m)

k: von Karman's constant (0.41, in this formula)

w_z: wind speed at height z (m/s)

These parameters are given as a relation to the crop height (h) by the following equations:

$$d = \frac{2}{3}h \qquad \textbf{Eq. 65}$$

$$z_{om} = 0.123h \qquad \textbf{Eq. 66}$$

$$z_{oh} = 0.1z_{om} \qquad \textbf{Eq. 67}$$

For still air and relatively low wind speeds, r_a can be expressed as (Jones, 1992):

$$r_a = \frac{r_{aH}}{1.12} \qquad \textbf{Eq. 68}$$

Generally r_a is of the magnitude of 10 to 100 s/m for a single leaf (Jones, 1992). Obviously for a whole canopy, this value is larger; for grassland Jones (1992) suggests 50-200 s/m per unit ground area.

4.6.4.3 Stomatal Resistance

From the research on stomatal behaviour (presented in paragraph 4.6.1) it is clear that a total understanding of the stomatal function has not been achieved. Various researchers have proposed several relationships of expressing stomatal resistance, as a function of stomata opening and closing, in relation to environmental characteristics. Pielke (2002) suggests the following formula for calculating the diurnal stomatal resistance of a leaf in s/m:

$$r_{si} = r_c\left[\frac{I_{max}}{0.03I_{max} + I} + P + \left(\frac{\eta_{wilt}}{\eta_{root}}\right)^2\right] \qquad \textbf{Eq. 69}$$

Where:

I_{max}: the noon incoming solar radiation under a cloudless, clear sky (W/m^2)

P: function of time of year (P=0 during the growing season and P>>0 at other times) (dimensionless)

η_{wilt}: the level of soil moisture below which permanent wilting of the plant occurs (m^3/m^3)

η_{root}: the minimum value of soil moisture occurring in the root zone of the plant (m^3/m^3) (equal to the minimum value of ω_g of the model).

r_c: bulk stomatal resistance (s/m)

The bulk stomatal resistance, r_c, expresses the plant type and measures the biological (surface) resistance of a canopy to losses of water. It is the average resistance to loosing water vapour and gases such as carbon dioxide from an individual leaf. This resistance is crop specific and varies among crop varieties and different crop management styles. It usually increases as the crop ages and begins to ripen (Allen et al., 1998). It is influenced by climate and water availability. However these influences may affect different kinds of crops in different ways. For a single leaf of reference grass, r_c can be assumed to be 100s/m.

Tournebize et al. (1996) have implemented the empirical model developed by Jarvis, according to which, stomatal resistance of a leaf is given by:

$$r_{si,x} = \frac{a_1 + PAR}{a_2 \cdot PAR} \qquad \textbf{Eq. 70}$$

Where the suffix x refers to one of the sides of the leaf (upper or lower, depending on where the stomata are), a_1 and a_2 are parameters depending on the plant species and the soil water availability and PAR is the photosynthetically active radiation.

Jacobson (1999) suggests the following formula to express the stomatal resistance of a single leaf:

$$r_{si,q} = r_{\min}\left[1+\left(\frac{200}{I+0.1}\right)^2\right]\frac{400}{T_{a,c}\left(40-T_{a,c}\right)}\frac{D_v}{D_q} \qquad \textbf{Eq. 71}$$

Where r_{min} is the minimum bulk stomata resistance for water vapour, I is the surface solar irradiance (W/m^2), $T_{a,c}$ is the surface air temperature (°C) and D_v/D_q is the ratio of the molecular diffusion of water vapour to that of gas q. In the case where the gas q is water, $D_v/D_q=1$.

The total stomatal resistance of the canopy, r_s, is expressed as (Allen et al., 1998):

$$r_s = \frac{r_{si}}{LAI_{active}} \qquad \text{Eq. 72}$$

It is noted that in most expressions of stomatal resistance, the resistance is inversely proportional to the incoming solar radiation. The higher the solar radiation is the more stomata tend to open to photosynthesise and to transpire, and reduce their temperatures to the desired levels of survival. Thus, their resistance to opening lowers as solar radiation increases and it reaches a maximum during night time.

As will be explained in paragraph 4.11.1.6, the formula suggested by Pielke (2002) is chosen to describe stomatal resistance in this model, as it manages to combine the major environmental factors which affect the stomatal function; the amount of irradiation and water potential. In this way stomatal resistance is quite high at night (stomata close at night) and much smaller during daytime (when stomata are open).

4.6.5 Dynamic Heat and Mass Transfer Equations in Plants

There have been models of vegetation which have considered the canopy layer as a uniform material with combined properties of air and foliage (e.g. Lhomme, 1981; Perrier, 1976). This approach has been adopted by many models of green roofs as a simpler one (e.g. Takakura et al., 2000). Such an approach had been followed at the beginning of the construction of this model (Alexandri and Jones, 2003). An even simpler one which has been adopted is to assume a certain thermal resistance of the layers of the green roof (soil, plants) and add them up to calculate the total U-value of the roof (Bumorfopoulou and Aravantinos, 1998) and thus estimate its thermal benefits to the interior of the building. However, models which consider a single canopy layer of combined leaf-air characteristics have been criticised for having a questionable accuracy (Waggoner, 1975). As leaves are solid bodies and the air among them is gas, it is not easy to combine them into a solid body, without jeopardising the accuracy of the model. Although a quite detailed model could be produced, taking into consideration the turbulent exchanges within the air of the foliage and inserting them as parameters of the combined material, as with the dynamic model developed by Lhomme (1981), it was considered more appropriate to develop a model which distinguishes the heat and mass exchanges between leaves and air in the canopy layer.

Based on models which take into account the heat exchanges between the leaves of the canopy and the air among them (Waggoner, 1975; Zhang et al., 1997; Palomo Del Barrio, 1998), a model of plant-air canopy layer, described in Figure 147, is developed. The assumptions of this model are the following:

- Horizontal homogeneity is sufficient and vertical fluxes are much greater than horizontal flux divergence that the latter can be ignored and a model can be constructed in the vertical direction alone.
- Vertical transfer of vapour and sensible heat in the air is proportional to vertical differences in humidity and temperature.
- Air beneath stomata is saturated with water (Waggoner, 1975; Monteith and Unsworth, 1990).
- Energy gain produced by the biochemical reactions of the plant are considered to be negligible (Jones, 1992; Gates, 1980; Tournebize et al., 1996; Monteith and Unsworth, 1990).
- The conductive heat transfer within the leaf itself and between the leaf and the plant (by its petiole) are too small to be taken into consideration (Monteith and Unsworth, 1990; Jones, 1992; Gates, 1980).
- Neither a rainfall case nor excessive water from irrigation is taken into consideration. Water distribution within the canopy is homogenous.
- Plants are considered to be healthy, free from parasites that might alter their functions and evapotranspirational rate, adequately irrigated, and actively growing in their full-grown stage (mid season) (Allen et al., 1998; Lhomme, 1981).
- The plant - soil layer is free from mulch. Although plant-residue does occur between the plants and the soil, this is not taken into consideration in the model, as the low vegetation of extensive green roofs cannot produce large amounts of mulch. In addition, little is known about mulch properties (Enrique et al., 1999), making it more difficult to model, without the essential experimental and theoretical background.

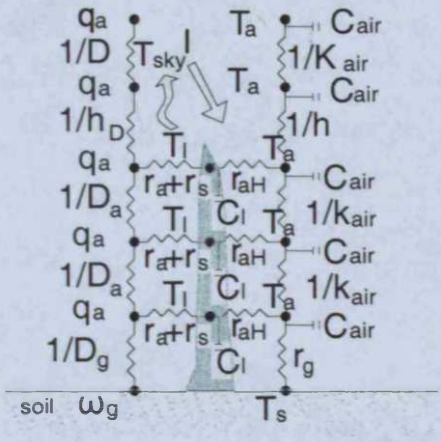

Figure 147. Heat and mass transfer in the canopy layer, for distinguished leaf and air nodes within the canopy layer

The leaf temperature is thus given by combining equations 52 (for convection), 53 (for latent heat) and 51 (radiation):

$$\rho_\ell c_{p\ell} \Delta x \frac{dT_\ell}{dt} = \frac{\rho_a c_{pa}}{r_{aH}}(T_a - T_\ell) - \frac{\rho_a c_{pa}}{\gamma} \frac{e_s(T_\ell) - e_a}{r_a + r_s} +$$

$$+ \left[I(1+\alpha_s)(1-\alpha_\ell) + I_{Ld} + \sigma\varepsilon_s T_s^4 - 2\sigma\varepsilon_\ell T_\ell^4 \right] \exp[-k_o LAI] \qquad \textbf{Eq. 73}$$

Where:

ρ_ℓ: density of the leaf tissue (kg/m^3)

$c_{p\ell}$: specific heat capacity of the leaf tissue (J/kgK)

T_ℓ: leaf surface temperature (K)

T_a: air temperature (K)

a_ℓ: leaf surface albedo

a_s: soil surface albedo

ε_ℓ: leaf surface emissivity

ε_s: soil surface emissivity

The air temperature within the canopy layer is expressed by the relationship, discussed in paragraph 4.4:

$$\frac{dT}{dt} = a_a \frac{d^2T}{dz^2} + \frac{1}{r_{aH}}(T_\ell - T_a) - \frac{c_1 - c_2}{c_{pa}} D_a \frac{\partial q}{\partial z} \frac{\partial T}{\partial z}\bigg|_a \qquad \textbf{Eq. 74}$$

Similarly, vapour diffusion in the air is given by:

$$\frac{dq}{dt} = D_a \frac{d^2q}{dz^2} + \frac{1}{r_a + r_s}(e_s(T_\ell) - e_a) \qquad \textbf{Eq. 75}$$

The solution of the surface temperature of leaves (equation 73) is given with two methods in appendix 2: an analytical method and a method of linearisation of the radiative heat transfer term. The method selected for the model is discussed in paragraph 4.11.1.6.

4.7 Solution with Finite Differences

The system of equations described in paragraphs 4.3 to 4.6 represents a simultaneous set of nonlinear partial differential equations. They are "simultaneous" because each conservation relation must be satisfied at any given time and involve partial derivatives. This is because in their more general, three-dimensional expression they involve four independent variables, three for space (x, y, z) and one for time (t). The non linear character of the equations occurs because products of the dependent variables are included in the relationships.

Mathematical techniques have evolved over the last several hundred years which permit the exact solutions of a range of algebraic and differential equations. However, with the exception of a few simplified and idealised situations, no method exists to solve general sets of nonlinear equations. In order to solve these nonlinear equations, the differential operators must be approximated for use in a numerical model. In this case, the finite-difference approximation is used.

A finite-difference approximation involves the replacement of each continuous differential operator (d) with a discrete difference analogue (Δ). This analog is an approximation written in terms of a finite number of values of the variable being operated on at each temporal or spatial node. The physical properties of each node are considered to be uniform. The molecular structure and molecular motions of the material may be ignored in the scale examined. A node is then the smallest possible element whose macroscopic properties are not influenced by individual molecules (Versteeg and Malalasekera, 1995).

Finite-difference approximations can derive from a Taylor series expansion. Development of the Taylor series for u(x+Δx,y) about (x,y) gives:

$$u(x+\Delta x, y) = u(x, y) + \Delta x \frac{\partial u}{\partial x}(x, y) + \frac{(\Delta x)^2}{2!}\frac{\partial^2 u}{\partial x^2}(x, y) + \frac{(\Delta x)^3}{3!}\frac{\partial^3 u}{\partial x^3}(x, y) + O\left[(\Delta x)^4\right] \quad \textbf{Eq. 76}$$

Which, upon division by Δx results to the relation:

$$\frac{\partial u}{\partial x}(x,y)=\frac{u(x+\Delta x,y)-u(x,y)}{\Delta x}+O(\Delta x) \qquad \text{Eq. 77}$$

The forward-difference of equation 77 provides the simplest first order approximation. The quantity O(Δx) represents the asymptotic notation for the truncation error of this approximation (Ames, 1977). If O(Δx) is considered to be a very small quantity, then:

$$\frac{\partial u}{\partial x}\approx\frac{u(x+\Delta x,y)-u(x,y)}{\Delta x} \qquad \text{Eq. 78}$$

which is known as the first order forward approximation. Similarly, development of the Taylor series for u(x-Δx,y) about (x,y) gives:

$$u(x-\Delta x,y)=u(x,y)-\Delta x\frac{\partial u}{\partial x}(x,y)+\frac{(\Delta x)^2}{2!}\frac{\partial^2 u}{\partial x^2}(x,y)-\frac{(\Delta x)^3}{3!}\frac{\partial^3 u}{\partial x^3}(x,y)+O\left[(\Delta x)^4\right] \qquad \text{Eq. 79}$$

By adding u(x+Δx,y) and u(x-Δx,y):

$$\frac{\partial^2 u}{\partial x^2}(x,y)=\frac{u(x+\Delta x,y)-2u(x,y)+u(x-\Delta x,y)}{(\Delta x)^2}+O\left[(\Delta x)^4\right] \qquad \text{Eq. 80}$$

If the truncation error is very small:

$$\frac{\partial^2 u}{\partial x^2}(x,y)\approx\frac{u(x+\Delta x,y)-2u(x,y)+u(x-\Delta x,y)}{(\Delta x)^2} \qquad \text{Eq. 81}$$

which is a second-order central difference approximation of $\partial^2 u/\partial x^2$, also known as Forward Euler Scheme (explicit method, Figure 199, Chapter 5). For expressing the second-order parts of the heat and mass transfer equations, this second-order central, explicit method is applied. For expressing the first part of the heat and mass transfer equations (changes in time), the first order forward approximation (equation 78) is used. Thus, equation 21 becomes:

$$\frac{q_i^{t+1}-q_i^t}{\Delta t}=a_m\frac{q_{i+1}^t-2q_i^t+q_{i-1}^t}{\Delta z^2} \qquad \text{Eq. 82}$$

Where t is the current time point, t+1 the following time point, i the current point in space, i+1 the following point in space, i-1 the previous point in space. By solving it:

$$q_i^{t+1}=\left(1-2\Delta t\frac{a_m}{\Delta z^2}\right)q_i^t+\Delta t\frac{a_m}{\rho_c c_c}\frac{q_{i+1}^t+q_{i-1}^t}{\Delta z^2} \qquad \text{Eq. 83}$$

For the stability of the method, the factor of q_i^t must be positive, thus:

$$\Delta t \leq \frac{2\Delta z^2 \rho_c c_c}{K_m} \qquad \textbf{Eq. 84}$$

This choice of time step is applied to all factors of q_i^t and T_i^t as well as in their boundary layer expressions, discussed in paragraph 4.8.

For expressing thermal diffusion in the heat transfer equation, the second order central approximation is used:

$$\frac{\partial u}{\partial x} \approx \frac{u(x+\Delta x, y) - u(x-\Delta x, y)}{2\Delta x} \qquad \textbf{Eq. 85}$$

4.7.1 Solution for a Non-Uniform Grid

When grid spacing and diffusion coefficients vary in space, the second-order discretisation of the conduction/eddy diffusion term is (Jacobson, 1999):

$$\frac{\partial}{\partial x}\left(K\frac{\partial N}{\partial x}\right) = \frac{\dfrac{K_{i+1/2}(N_{i+1}-N_i)}{x_{i+1}-x_i} - \dfrac{K_{i-1/2}(N_i-N_{i-1})}{x_i-x_{i-1}}}{x_{i+1/2}-x_{i-1/2}} \qquad \textbf{Eq. 86}$$

Where:

$$K_{i+1/2} = \frac{K_i + K_{i+1}}{2} \qquad \textbf{Eq. 87}$$

$$K_{i-1/2} = \frac{K_{i-1} + K_i}{2} \qquad \textbf{Eq. 88}$$

$$x_{i+1/2} = \frac{x_i + x_{i+1}}{2} \qquad \textbf{Eq. 89}$$

$$x_{i-1/2} = \frac{x_{i-1} + x_i}{2} \qquad \textbf{Eq. 90}$$

4.7.2 Errors

According to Scraton (1968) the errors which arise from these arithmetic methods can be classified into three types; rounding errors, truncation errors and blunders or arithmetical errors.

Rounding errors are caused by rounding numbers to a finite number of decimal places. Their effect can be reduced by keeping an extra decimal place in the working. Truncation errors are caused by using only a finite number of terms of an infinite series. In practice, the truncation error can be found as the first neglected term in the Taylor series (equation 80). To make sure that the truncation error remains negligible, it is usual to ensure that the magnitude of any term neglected is less than half a unit of the last decimal place. Blunders or arithmetical errors can only be avoided by suitable checking.

It is proved (Ames, 1977; Forsythe and Wasow, 1960) that the difference between the value from the analytical solution of the differential equation and the value from the finite differences solution, which is the error of the finite differences solution, tends to zero, as time step and space step tend to zero. Thus, the smaller the time step and the space steps are, the more accurate the finite difference approximation is.

It is not easy to quantify the total error of a finite difference; the differentials which compose the truncation error might be too difficult to estimate, making its calculation impossible. Also, due to its nature, the error which could be calculated from this procedure could only be a local one (Forsythe and Wasow, 1960). As a result, a maximum value is defined, determining the upper boundary of the absolute value of the finite difference error. The total error of the finite difference solution is the difference between the solution of the differential equation and the solution of the finite difference equation. If the first one at the point i,t is symbolised with $u_{i,t}$ and the second one at the same point with $U_{i,t}$ and their difference with $z_{i,t}$, the total error will be:

$$z_{i,t} = u_{i,t} - U_{i,t} \qquad \textbf{Eq. 91}$$

It is proved (Ames, 1977) that for explicit methods:

$$\max\left|z_{i,t}\right| \le AT\left[\Delta t + (\Delta x)^2\right] \qquad \textbf{Eq. 92}$$

where T is the upper boundary of time and A depends upon upper bounds for $\partial^2 u/\partial t^2$.

As is obvious from this relationship, the solution of the finite difference analogue converges to the solution of the differential equation as Δx and Δt tend to zero. In addition, Δt should be smaller than a specific value, equal to the factor of the T_i^t and q_i^t component, so that stability and convergence are achieved, as discussed in paragraph 4.7.

In order to minimise errors in the model, time step and space steps are chosen cautiously (paragraph 5.7, chapter 5) and so is the amount of decimal points in the variables entering the algorithm and the amount of decimals in its outputs. In C++, where the model is programmed, all numbers, apart from integrals, are declared as doubles, instead of floats; it has been preferred that each variable occupies more space in the computer memory rather than jeopardise the accuracy of the model. Thus, the rounding error is considered to be negligible. For Δt equal to 10sec and Δx 0.10m, the total error, as derived from Ames (1977), should be less than 0.3K for temperature and less than 0.003kg/kg for specific humidity (leading to a maximum error of 3.5% for relative humidity).

4.8 Boundary Conditions

The algorithms presented above are capable of describing heat and mass fluxes in a plain roof and in a green roof. Figure 148 represents the different layers of a plain and a green roof. The heat and mass transfer equations of a capillary porous body, as have been described in paragraph 4.3, are applied in the roof nodes (symbolised with "c"). Soil nodes, whose fluxes are described in paragraph 4.5, are symbolised with "s". Vegetated canopy is symbolised as "gr", described by the algorithms of paragraph 4.6, and heat and mass transfer in the air (symbolised as "air") has been presented in paragraph 4.4. At the boundaries of the model, the air node inside the building is named "internal node" and the node with the climatic characteristics of the city under examination is called "urban node". Temperature and relative humidity at the internal node are kept constant, at 20°C and 50%, respectively (Pignolet-Tardan et al., 1997). In the urban node, the climatic characteristics (air temperature, relative humidity and

wind speed) are input, derived from hourly data of meteorological stations. At the boundary layers, where a change of material occurs (nodes c,in, c,s, s,out, gr-in, gr-out, a1), the principle of continuity is applied, as presented below.

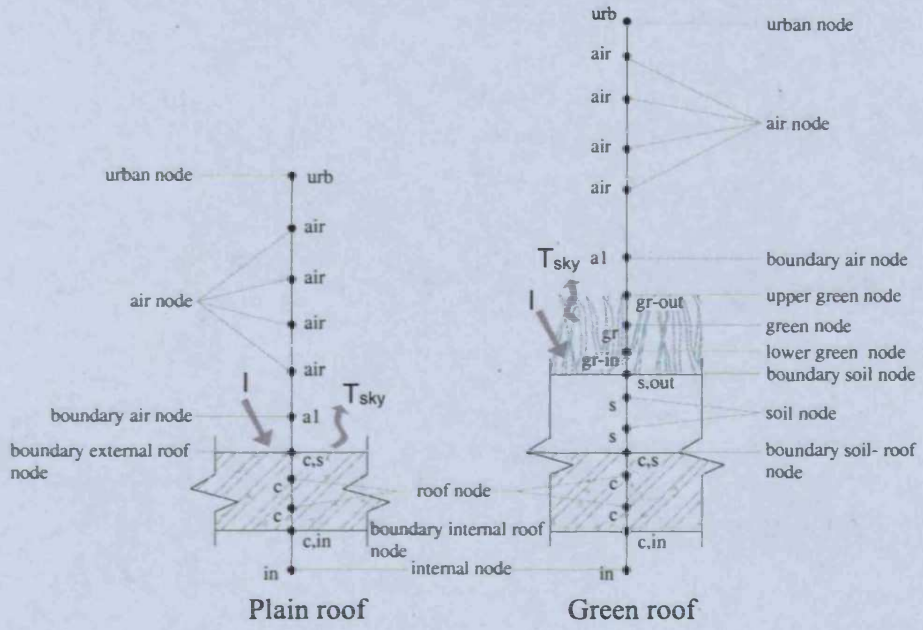

Figure 148. One dimensional model for plain and green roof

4.8.1 Boundary Roof Nodes

For the roof material two boundary nodes can be distinguished; its internal surface (c,in) and its external one (c,s). Its internal surface can be bound with the air inside the building with the boundary equations:

$$\frac{dT}{dt} = a_c \frac{\partial^2 T}{\partial z^2}\bigg|_{s,in} + \frac{h_{in}}{\rho_c c_c} \frac{\partial T}{\partial z}\bigg|_{s,in} + \frac{\varepsilon\lambda}{c_c} \frac{\partial q}{\partial t}\bigg|_{s,in} \qquad \textbf{Eq. 93}$$

$$\frac{dq}{dt} = a_m \frac{\partial^2 q}{\partial z^2}\bigg|_{s,in} + h_{D,in} \frac{\partial q}{\partial z}\bigg|_{s,in} \qquad \textbf{Eq. 94}$$

Where ρ_c is the density of the material (kg/m^3) and h_{in} is the internal convection heat transfer coefficient (W/m^{2}K). The internal heat convection is a simplified 5W/m^{2}K one. $h_{D,in}$ is the internal convective diffusion coefficient (m/s), defined in paragraph 4.8.10.

For the external surface of the roof, the factors of the incoming solar radiation at the roof's plane and the longwave exchanges with its surroundings are taken into

consideration at the heat transfer relationship. Thus, heat and mass transfer at the external boundary node of the roof can be expressed as:

$$\frac{dT}{dt} = a_c \frac{\partial^2 T}{\partial z^2}\bigg|_s + \frac{h_{out}}{\rho_c c_c}\frac{\partial T}{\partial z}\bigg|_s + \frac{\varepsilon\lambda}{c_c}\frac{\partial q}{\partial t}\bigg|_s + \frac{\partial}{\partial z}\left(\frac{1}{\rho_c c_c}\left[(1-\alpha_c)I + \sigma\varepsilon_c\left(T_{sky}^4 - T_s^4\right)\right]\right) \quad \textbf{Eq. 95}$$

$$\frac{dq}{dt} = a_m \frac{\partial^2 q}{\partial z^2}\bigg|_s + h_D \frac{\partial q}{\partial z}\bigg|_s \quad \textbf{Eq. 96}$$

Where:

h_{out}: external convective heat transfer coefficient (W/m^2K)

a_c: albedo of the surface material

I: solar radiation on the surface (W/m^2)

σ: Stefan-Boltzmann constant ($5.67 \cdot 10^{-8} W/m^2K^4$)

ε_c: emissivity of the surface material

T_{sky}: sky temperature (K)

h_D: external convective diffusion coefficient (m/s)

The expression of sky temperature (T_{sky}) is discussed in paragraph 4.8.7. The determination of the external convective heat transfer coefficient is discussed in paragraph 4.8.9 and the expression of the external convective diffusion coefficient is presented in paragraph 4.8.10.

4.8.2 Boundary Air Node

As will be discussed more thoroughly in paragraph 4.8.8, in the boundary air layer close to a heated surface, local plumes are created. This can be expressed by the convection heat transfer coefficient. Thus, heat and mass transfer in the boundary air node (a1) to the roof become:

$$\frac{dT}{dt} = a_a \frac{\partial^2 T}{\partial z^2}\bigg|_a + \frac{h_{out}}{\rho_a c_{pa}}\frac{\partial T}{\partial z}\bigg|_a - \frac{c_1 - c_2}{c_{pa}} D \frac{\partial q}{\partial z}\frac{\partial T}{\partial z}\bigg|_a \quad \textbf{Eq. 97}$$

$$\frac{dq}{dt} = D\frac{\partial^2 q}{\partial z^2}\bigg|_a + h_D \frac{\partial q}{\partial z}\bigg|_a \quad \textbf{Eq. 98}$$

4.8.3 Boundary Roof – Soil Node

In this node, where the change from the building material to soil occurs, the principle of continuity of the state variables and flux intensity is applied. The specific thermal capacity of both materials is ignored, but this does not lead to crucial errors (Holman, 2002). Before proceeding to the expression of heat and mass transfer at the boundary roof-soil node, a relation should be established between q and ω_g.

This relation derives from their definitions; q is the ratio of the water mass (m_w) to the mass of the dry body (m_s) (m_w/m_s). Therefore it is moisture content expressed as kg of water/kg of dry body. On the other hand ω_g is expressed as volumetric water content of soil, which means the ratio of the volume of water to the volume of the total soil-water-air mixture (V_w/V_{tot}) (m^3 of water /m^3 of soil-water-air mixture). The ratio of the density of solid to the density of water gives us:

$$\frac{\rho_s}{\rho_w} = \frac{\frac{m_s}{V_{tot}}}{\frac{m_w}{V_w}} = \frac{m_s}{m_w}\frac{V_w}{V_{tot}} = \frac{1}{q}\omega_g \qquad \textbf{Eq. 99}$$

Therefore:

$$\omega_g = q\frac{\rho_s}{\rho_w} \qquad \textbf{Eq. 100}$$

And

$$q = \omega_g\frac{\rho_w}{\rho_s} \qquad \textbf{Eq. 101}$$

Thus, the continuity of heat and mass flux at the boundary building material-soil is given by:

$$K_s\frac{\partial T}{\partial z}\bigg|_s = K_c\frac{\partial T}{\partial z}\bigg|_c + \frac{\varepsilon\lambda}{c_c}\frac{\partial q}{\partial t}\bigg|_c \qquad \textbf{Eq. 102}$$

$$\left(D_g\frac{\partial \omega_g}{\partial z} + K_g\right)\bigg|_s = \frac{\rho_w}{\rho_s}\frac{\partial \omega_g}{\partial z}\bigg|_c \qquad \textbf{Eq. 103}$$

4.8.4 Boundary Canopy – External Air Node

The boundary canopy nodes towards the open air (gr-out) is the same as the canopy nodes (gr) only that the convection heat transfer and the convective diffusion terms are added at the heat and mass transfer relationships, respectively:

$$\frac{dT}{dt} = a_a \frac{d^2T}{dz^2} + \frac{1}{r_{aH}}(T_\ell - T_a) + \frac{h_{out}}{\rho_a c_{pa}} \frac{\partial T}{\partial z}\bigg|_a - \frac{c_1 - c_2}{c_{pa}} D_a \frac{\partial q}{\partial z}\frac{\partial T}{\partial z}\bigg|_a \qquad \textbf{Eq. 104}$$

$$\frac{dq}{dt} = D\frac{d^2q}{dz^2} + \frac{1}{r_a + r_s}(e_s(T_\ell) - e_a) + h_D \frac{\partial q}{\partial z}\bigg|_a \qquad \textbf{Eq. 105}$$

Leaf temperature's expression remains the same, as in paragraph 4.6.5.

4.8.5 Boundary Canopy –Soil Node

In most agricultural applications the heat transfer from the ground is usually assumed to be a proportion of the income irradiation, of the magnitude of 30% (Monteith and Unsworth, 1990; Jones, 1992; Lhomme, 1981; Perrier, 1976). However, in the case of green roofs, such an assumption could lead to errors, as it would break the continuity of heat transfer. Thus, the approach of "binding" the heat exchanges between the soil and the canopy layer with the air above the soil has been used. The aerodynamic resistance for the transport of heat from the air just above the soil surface to the air in the canopy layer has been used for that (Figure 147), as has been practiced by several researchers (Zhang et al., 1997; Palomo Del Barrio, 1998). Thus, the heat flux between the soil and the air within the canopy layer is given by:

$$H_s = \frac{\rho_a c_{pa}}{r_g}(T_s - T_a) \qquad \textbf{Eq. 106}$$

An empirical relationship for the aerodynamic resistance of heat transfer between soil and air in the foliage is given by Tournebize et al. (1996):

$$r_g = 200\left(\frac{\omega_g}{\omega_{g,s}}\right)^{-1.6} \qquad \textbf{Eq. 107}$$

Where ω_g and $\omega_{g,s}$ have been defined in paragraph 4.5.

The governing equations for the air layer of the boundary canopy node, gr-in, are:

$$\frac{dT}{dt} = a_a \frac{d^2T}{dz^2} + \frac{1}{r_{aH}}(T_\ell - T_a) + \frac{\rho_a c_{pa}}{r_g}(T_s - T_a) - \frac{c_1 - c_2}{c_{pa}} D_a \frac{\partial q}{\partial z}\frac{\partial T}{\partial z}\bigg|_a \quad \textbf{Eq. 108}$$

$$\frac{dq}{dt} = D\frac{d^2q}{dz^2} + \frac{1}{r_a + r_s}\left(e_s(T_\ell) - e_s(T_a)\frac{\rho_a q_a}{\rho_{s,a}(1-q_a)}\right) + \frac{1}{r_g}(e_s - e_a) \quad \textbf{Eq. 109}$$

Where $h_{D,g}$ is defined in paragraph 4.8.10. Leaf temperature's expression remains the same, as in paragraph 4.6.5.

4.8.6 Boundary Soil Node

At the boundary soil node, the short and long wave radiation reaching the soil are taken into consideration, as well as the heat flux between the soil and the air within the canopy layer.

$$\frac{dT_s}{dt} = \frac{1}{\rho_g c_G}\frac{\partial}{\partial z}\left(K_s \frac{\partial T_s}{\partial z}\right) + \frac{\rho_a c_{pa}}{r_g}(T_a - T_s) + \left[I(1-\alpha_s) + \sigma\varepsilon_s\left(T_{sky}^4 - T_s^4\right)\right]\exp[-k_o LAI] \quad \textbf{Eq. 110}$$

$$\frac{d\omega_g}{dt} = \frac{\partial}{\partial z}\left(K_g\left(\frac{\partial \psi_p}{\partial z} + 1\right)\right) + \frac{\rho_w}{\rho_s}\frac{1}{r_g}\left((e_s(T_a) - e_s(T_s))\frac{\rho_a q_a}{\rho_{s,a}(1-q_a)}\right) \quad \textbf{Eq. 111}$$

4.8.7 Sky Temperature

Sky temperature (T_{sky}) is a fictitious temperature, introduced to model the long wave radiation exchanges with the sky (Adelard et al., 1998). It is defined as the equivalent black-body temperature of the sky vault based on sky radiance covering the entire infrared spectrum (Nowak, 1989). Generally, sky temperature has been expressed as a function of air temperature for thermal modelling at the ground.

Swinbank, having examined observed data and the formulations of Ångström and Brunt, expressed the thermal downward radiation of a clear sky as the following function of the air temperature near the ground (Gates, 1980):

$$\Phi_L = 1.22\sigma T_a^4 - 171 \quad \textbf{Eq. 112}$$

where T_a is expressed in Kelvin.

He went on to state that the radiation from the sky temperature is not necessarily a power of 4. From observations, he changed the power to 6, due to the water vapour influence, thus:

$$\Phi_L = 53.1 \cdot 10^{-14} T_a^6 \qquad \textbf{Eq. 113}$$

Where T_a is expressed in Kelvin.

For clear night-time sky conditions and for horizontal surfaces Swinbank expressed the sky temperature from the following formula (Nowak, 1989):

$$T_{sky} = 0.0553 \cdot T_a^{1.5} \qquad \textbf{Eq. 114}$$

Where T_a is expressed in Kelvin.

Measurements by Brown and Nowak showed that the sky temperature calculated by Swinback's nocturnal formula was 10°C lower, on average, than that which was measured. This difference was attributed to the presence of atmospheric pollutants (Nowak, 1989).

Dreyfus has suggested a simpler approach; that sky temperature could be treated as equal to the air temperature ($T_{sky} = T_a$), while Daguenet suggested the following relationship (Adelard et al., 1998):

$$T_{sky}^4 = T_a^4 \left(1 - 0.261 \exp\left(-7.77 \cdot 10^{-4} \right)(T_a - 273)^2\right) \qquad \textbf{Eq. 115}$$

Where T_a is expressed in °C.

Although it is possible to express theoretically the atmospheric (sky) radiation, the derivation is extremely complex and difficult mathematically (Gates, 1980). Thus sky radiation and its fictitious temperature have been mostly expressed in empirical forms. Most researchers have expressed sky temperature only as a relationship of the air temperature near the ground. Empirical results have shown that the sky behaves approximately as a black body with its temperature being approximately 20K below the measured air temperature, for a clear sky (Jones, 1992).

$$T_{sky} = T_a - 20 \qquad \textbf{Eq. 116}$$

This relationship also derives from the linearisation of Swinbank's relationship. For clear sky conditions it is shown that (Gates, 1980):

$$T_{sky} = T_a - 20.4 + 0.22 T_a \qquad \textbf{Eq. 117}$$

The downward flux of longwave radiation under clear skies is thus given by:

$$\Phi_{Ld}\downarrow \approx \sigma(T_a - 20)^4 \qquad \textbf{Eq. 118}$$

where T_a is expressed in Kelvin.

If the surface in question has an emissivity ε_s and a surface temperature T_s, the total longwave radiation on it is:

$$\Phi_L = \Phi_{Ld}\downarrow - \Phi_{Lu}\uparrow \qquad \textbf{Eq. 119}$$

$$\Phi_L = \sigma T_{sky}^4 - \sigma \varepsilon_s T_s^4 \qquad \textbf{Eq. 120}$$

All temperatures are expressed in Kelvin.

The sky atmosphere has also been assimilated as a grey body by a number of researchers. In this case, the long wave radiation emitted from the sky can be expressed as a function of air temperature at soil height and a sky emissivity.

$$\Phi_{Ld}\downarrow = \varepsilon_{sky}(0)\cdot\sigma\cdot T_a^4 \qquad \textbf{Eq. 121}$$

where "0" represents the cloudless sky conditions.

The sky's emissivity strongly depends on the water content of the atmosphere, expressing the long wave radiation absorbed by water vapour. As colder air contains less water vapour, it has a smaller emissivity than warmer air (Table 6, last line). Various researchers have given different expressions for $\varepsilon_{sky}(0)$. Some of them are summarised in Table 6.

Table 6. Different expressions of sky emissivity (Noilhan, 1979; Monteith and Unsworth, 1990; Gates, 1980).

Source	Expression
Ångström	$\varepsilon_{sky}(0) = 0.82 - 0.25\cdot 10^{-0.07e}$
Brunt	$\varepsilon_{sky}(0) = 0.56 - 0.08\cdot\sqrt{e}$
Lennqvist	$\varepsilon_{sky}(0) = 0.54 - 0.05\cdot\sqrt{u_{H_2O}}$
Unworth & Monteith	$\varepsilon_{sky}(0) = c + d\sigma T_a^4$
Gates	0.91 for T_a=40°C, 0.81 for T_a=20°C, 0.69 for T_a=0°C

Where e is the water tension on the soil and u_{H_2O} is a quantity expressed in mm. u_{H_2O} is given by the relationship:

$$\ln u_{H_2O} = 0.295\sqrt{e} - 0.803 \qquad \textbf{Eq. 122}$$

The factors d and c in Unworth and Monteith's formula (second line from the bottom in Table 6) are summarised in Table 7, as they have been estimated by different researchers:

Table 7. Factors in Unworth and Monteith's formula (Noilhan, 1979; Monteith and Unsworth, 1990)

Source / Factor	Unworth and Monteith (measurements in the English Midlands for a temperature range from -6 to 26°C)	Swinbank (measurements in Australia)	Dines
c	-119±16 [W/m^2]	-171	-131
d	1.06±0.04	1.20	1.05

For a clear sky, and at an air temperature above a base of 283K the Unsworth and Monteith formula gives the following expression for the downward longwave radiation:

$$\Phi_{Ld} \downarrow = 5.5 \cdot T_a + 213 \qquad \textbf{Eq. 123}$$

Where $\Phi_{Ld} \downarrow$ is in W/m^2 and T_a is in °C.

For an overcast sky Unworth and Monteith (1990) propose the following formula:

$$\frac{1-\varepsilon_{sky}(1)}{1-\varepsilon_{sky}(0)} = 4\frac{\Delta T}{T_a} \qquad \textbf{Eq. 124}$$

Where $\varepsilon_{sky}(1)$ is the overcast sky emissivity and ΔT is the temperature difference between the temperature at the base of the cloud and the temperature at the ground, T_a. From an analysis of a series of measurements near Oxford, Unsworth and Monteith found an annual mean of ΔT=11K with a seasonal variation of ±2K. Assuming T_a equal to 283K, the emissivity of an overcast sky can be expressed as (Monteith and Unsworth, 1990):

$$\varepsilon_{sky}(1) = 0.84 + 0.16\varepsilon_{sky}(0) \qquad \textbf{Eq. 125}$$

For a sky covered with a fraction c of cloud, the emissivity $\varepsilon_{sky}(c)$ is given by:

$$\varepsilon_{sky}(c) = (1-0.84c)\varepsilon_{sky}(0) + 0.84c \qquad \textbf{Eq. 126}$$

The main limitation to this formula lies in the choice of the appropriate values for cloud and for ΔT, which depend on base height and cloud type (Monteith and Unsworth, 1990).

Berger has proposed two relations for the determination of sky emissivity, using the dew point temperature (Adelard et al., 1998):

$$\varepsilon_{sky} = 0.77 + 0.0038 T_{dp} \quad \text{for daytime} \quad \textbf{Eq. 127}$$

$$\varepsilon_{sky} = 0.752 + 0.0048 T_{dp} \quad \text{for night-time} \quad \textbf{Eq. 128}$$

The model developed here, focuses on clear sky conditions. For reasons of simplification, sky temperature is expressed only in relationship to air temperature, deriving from the expression suggested by Jones (1992) (equation 118).

4.8.8 Plumes at the Boundary Air Layer

When a surface which is hotter than its environment emits heat, it warms the surrounding air and produces a local density deficiency relative to the ambient air. The density gradients in turn produce a weight deficiency and a pressure gradient which accelerates the heated fluid vertically, in a convective process (Figure 149). For a heat source H the rate of production of weight deficiency depends on the volumetric coefficient of thermal expansion of the fluid. In many fluids, for limited temperature ranges the volumetric coefficient of thermal expansion is constant. In this case, the rate of production of weight deficiency, which is called the specific buoyancy flux, is given by the relationship:

$$B = \frac{g\beta H}{\rho_a c_{pa}} \quad \textbf{Eq. 129}$$

Where:

B: specific buoyancy flux (m^4/s^3)

g: acceleration due to gravity (9.81 m/s^2)

β: volumetric thermal expansion coefficient (1/K)

H: heat source (W)

ρ_a: fluid density (kg/m^3)

c_{pa}: fluid specific heat at constant pressure (J/kgK)

For a steady source of buoyancy flux the mean velocity of the fluid of the axis of the plume depends on the specific buoyancy flux (B), the vertical distance above the source (z), the fluid kinematic viscosity (ν_a), and the fluid thermal diffusivity (a_a).

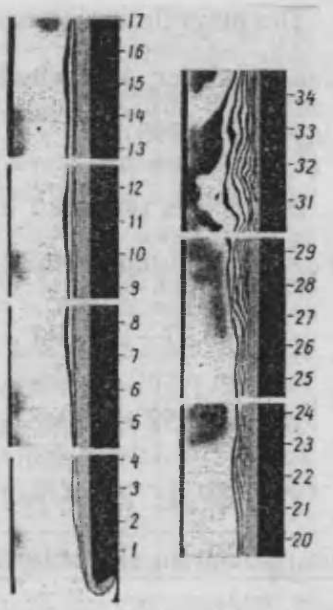

Figure 149. Boundary layer of a vertical heated plate under free convection (Luikov, 1961)

For round plumes the mean velocity is given by the relationship:

$$U_m = k_R \left(\frac{B}{z} \right)^{1/3} \qquad \textbf{Eq. 130}$$

And for plane plumes:

$$U_m = k_P B^{1/3} \qquad \textbf{Eq. 131}$$

Where k_R and k_P are dimensionless constants for the round and plane plume respectively (List, 1982). For plane plumes B is defines as the specific buoyancy flux per unit length of the plume and is therefore expressed in m^3/s^3. The values of k_R and k_P have been discussed by many researchers. The results, mostly derived from experimental data, are summarised in Table 8.

Table 8. Values of k_R and k_P, as have been suggested by various researchers (adapted from List, 1982)

Source	k_R	k_P
Chen and Rodi, 1980	3.5	1.9
Kotsovinos, 1975	-	1.66
Rouse, Yih and Humphreys, 1952	4.7[36]	-
George et al, 1977; Nakagome and Hirata, 1976; Beuther, 1980	3.4 - 3.9	-

[36] According to List (1982) this result is dubious, as the turbulent transport was ignored in the experiment.

The effect of this boundary air velocity in the heat transfer mechanism between the layer of the fluid near a surface and the surface is expressed by the convection heat transfer coefficient.

4.8.9 Convection Heat Transfer Coefficient

The convection heat transfer coefficient summarises the heat transfer mechanism between the layer of the fluid near a surface and the exterior of the surface. It depends on the form of the surface (flat or curved) and its roughness. It also depends on the fluid characteristics (density, viscosity, specific heat and heat conductivity) and on the wind speed.

From Newton's Law of Cooling between a wall and a fluid flowing next to it, the heat transfer between the surface and the fluid is:

$$q = h(T_w - T_\infty) \qquad \textbf{Eq. 132}$$

Where T_∞ is air temperature well away from the boundary air layer. From the conductive heat transfer within the wall heat transfer is:

$$q = -k\frac{\partial T}{\partial z}\bigg|_{wall} \qquad \textbf{Eq. 133}$$

By combining these two equations, the convection heat transfer coefficient can be expressed as:

$$h = -\frac{k}{T_w - T_\infty}\left(\frac{\partial T}{\partial z}\right)_{wall} \qquad \textbf{Eq. 134}$$

The value of the convection heat transfer coefficient depends on the type of flow of the fluid near the surface. Two types of diverse fluid movements are distinct; free and forced, both of them divided into laminar and turbulent flow.

4.8.9.1 Free Convection

Free or natural convection occurs when the movement of the fluid is not forced by a factor (e.g. wind) but because of differences in its density and the action of gravity (paragraph 4.8.8). Heat transfer coefficients for natural convection are generally much

lower than for forced convection, but they should not be ignored, as the free convection transfer might be of the same magnitude as radiative heat transfer (ASHRAE, 1985). When cold air flows next to a hot surface, the fluid in immediate contact with the surface is heated by conduction, becomes lighter and rises because of its difference in density to the adjacent fluid. The motion is resisted by the viscosity of the fluid. Thus, the heat transfer in free convection is influenced by the gravitational force due to thermal expansion, the viscous drag and the thermal diffusion of the fluid. These variables can be expressed by the dimensionless numbers of Prandtl (Pr) and Grashof (Gr).

In general, for free convection, the Nusselt number is given by the relationship:

$$Nu = c(Gr \cdot \Pr)^n \qquad \textbf{Eq. 135}$$

Where c is a constant and n an exponent.

For both horizontal and vertical planes the Nusselt number is given by (ASHRAE, 1985):

For laminar range $(10^4<(\mathrm{Gr}\cdot\mathrm{Pr})<10^8)$:

$$Nu = 0.56(Gr \cdot \Pr)^{0.25} \qquad \textbf{Eq. 136}$$

For turbulent range $(10^8<(\mathrm{Gr}\cdot\mathrm{Pr})<10^{12})$:

$$Nu = 0.13(Gr \cdot \Pr)^{0.33} \qquad \textbf{Eq. 137}$$

Where:

$$Gr = \frac{L^3 \rho_a^2 \beta g(\Delta T)}{\mu^2} \qquad \textbf{Eq. 138}$$

$$\Pr = \frac{\mu c_{pa}}{k_a} \qquad \textbf{Eq. 139}$$

Where L is the length (in m) for the horizontal plates and the height for the vertical ones and μ is the dynamic viscosity of air (in kg/ms).

4.8.9.2 Forced convection with Laminar Flow

For forced convection with laminar flow, h can be expressed as:

$$h = 0.331k \frac{\Pr^{1/3}}{\sqrt[3]{1-\left(\frac{x_o}{x}\right)^{3/4}}} \sqrt{\frac{w_a}{\nu x}} \qquad \text{Eq. 140}$$

Where x_o is the length of the plate which is not heated, but over which laminar flow occurs. The same relationship holds for both a horizontal and a vertical plane (Holman, 2002).

It is proved (Luikov, 1961; Eckert and Drake, 1959) that for forced convection with laminar flow, for vertical planes in forced flow and the plate being heated over its entire length, as is the case in the model's walls and roofs, the following relationship holds true:

$$h = 0.331k \Pr^{1/3} \sqrt{\frac{w_a}{\nu x}} \qquad \text{Eq. 141}$$

For calculations of heat exchanges the average value of the heat transfer coefficient is important, instead of the local one. For a plate heated over its entire length, this value is given by:

$$\bar{h} = \frac{1}{x} \int_0^x h dx \qquad \text{Eq. 142}$$

It is proved (Eckert and Drake, 1959; Holman, 2002) that the average heat transfer coefficient in forced convection with laminar flow is the double of the local heat transfer coefficient.

$$\bar{h} = 2h \qquad \text{Eq. 143}$$

4.8.9.3 Forced Convection with Turbulent Flow

For vertical planes in forced convection with turbulent flow, the convection heat transfer coefficient can be expressed by the following relationship:

$$h = \frac{p_s \frac{c_p}{w_a}}{1 + \frac{w_b}{w_a}(\Pr - 1)} \qquad \text{Eq. 144}$$

A laminar boundary layer exists in the neighbourhood of the leading edge with w_a being its velocity. p_s is the shear stress at the surface of the plate. It can be expressed as:

$$p_s = \mu \frac{\partial u}{\partial y} \qquad \textbf{Eq. 145}$$

The shear stress at the surface of the plate can be determined by Blasius's formula, which is valid for smooth surfaces and for a not too large Reynolds number ($Re<10^7$) (Luikov, 1961; Eckert and Drake, 1959).

$$p_s = 0.0228 \rho_a w_a^2 \left(\frac{\nu}{w_a \delta} \right)^{1/4} \qquad \textbf{Eq. 146}$$

The shear stress at the surface of the plate can also be expressed by (Holman, 2002):

$$p_s = \frac{3}{2} \frac{\mu w_a}{4.64} \left(\frac{w_a}{\nu x} \right)^{1/2} \qquad \textbf{Eq. 147}$$

According to Holman (2002) the Colburn analogy between fluid friction and heat transfer yields results which are in agreement with experiment and is easier to apply and of a simpler form. It is proved (ibid.), that the average Nusselt number, for both horizontal and vertical plates, is given by:

$$\overline{Nu}_L = \mathrm{Pr}^{1/3} \left(0.037 \, \mathrm{Re}_L^{0.8} - 871 \right) \qquad \text{for } 5 \cdot 10^5 < \mathrm{Re_L} < 10^7 \qquad \textbf{Eq. 148}$$

$$\overline{Nu}_L = \mathrm{Pr}^{1/3} \left(0.037 \, \mathrm{Re}_L \left(\log \mathrm{Re}_L \right)^{-2.584} - 871 \right) \qquad \text{for } 10^7 < \mathrm{Re_L} < 10^9 \qquad \textbf{Eq. 149}$$

Where:

$$\mathrm{Re}_L = \frac{\rho w_a L}{\mu} \qquad \textbf{Eq. 150}$$

And the average convection heat transfer coefficient is given by:

$$\bar{h} = Nu_L \frac{k}{L} \qquad \textbf{Eq. 151}$$

For a constant heat flux on the plate in turbulent flow, it is proved (Holman, 2002) that the local Nusselt number is only by about 4% higher than for the isothermal surface:

$$Nu_x = 1.04 Nu_x|_{T_w=const} \qquad \text{Eq. 152}$$

4.8.9.4 Empirical Relationships

Empirical relationships for the convection heat transfer coefficient have been proposed by a number of researchers, based on both theory and experiments. A selection of these expressions is summarised in Table 9.

Table 9. Expressions of the convection heat transfer coefficient (ASHRAE, 1985; Noilhan, 1979; Wu, 1996)

Source	Convection heat transfer coefficient (W/m^2K)		
Fisher and Dufton; Nusselt and Jurges	U<5m/s $5.8+4.1U$	5m/s<U<10m/s $7.3U^{0.78}$	
Sturrock	1m/s<U<10m/s $23+5.7U$ *(around cubes)*		
Fanger; Penicaud	U<0.1m/s $2.05(T_s - T_a)^{0.25}$	0.1m/s<U<2.2m/s $10.4U^{0.5}$ *(laminar fl)*	2.2m/s<U<10m/s $8U^{0.5}$ *(turbulent fl)*
Terjung and O'Rourke	$2.84(0.00033U)^{0.8}$		
ASHRAE	U<5 m/s $5.6+18.6U$	5m/s<U<30 m/s $7.2U^{0.78}$	

Where U is wind speed well away from the boundary layer. It is clear from Table 9 that ASHRAE has adopted the expressions of convection heat transfer coefficient which Fisher and Dufton and Nusselt and Jurges developed.

Empirical relationships have also been proposed for the convection and radiation heat transfer coefficient for walls and roofs. Noilhan (1979) has summarised those that are most commonly used (Table 10).

Table 10. Expressions of the combined convection and radiative heat transfer coefficient (Noilhan, 1979)

Source	Combined convection and radiation heat transfer coefficient (W/m^2K)		
IHVE Vertical surface Horizontal surface	U=1m/s 12.50 14.00	U=3m/s 18.00 22.00	U=9m/s 33.50 50.00
MacAdams	$h = \left(a - 0.003\frac{T_s + T_a}{2}\right)\sqrt[3]{T_s - T_a} + 3.5U$ $a = 1.5$ for a horizontal surface $a = 1.4$ for a vertical surface		

The choice of the proper expression of the convection heat transfer coefficient is crucial; different expressions of the coefficient might lead to different values and distributions of both surface and air temperatures. Lü (2002), in the model which he developed for the heat and moisture transfer for the interior of buildings, used the general empirical relationship of the form of $c(\Delta T)^n$ for the convection heat transfer coefficient for the interior sides of the walls[37]. By altering c from 0.2 to 20 (Figure 150) he came to the conclusion that alterations on the expression of the convection heat transfer coefficient can lead to diverse values and distributions of both predicted temperature and relative humidity, as is obvious from Figure 150.

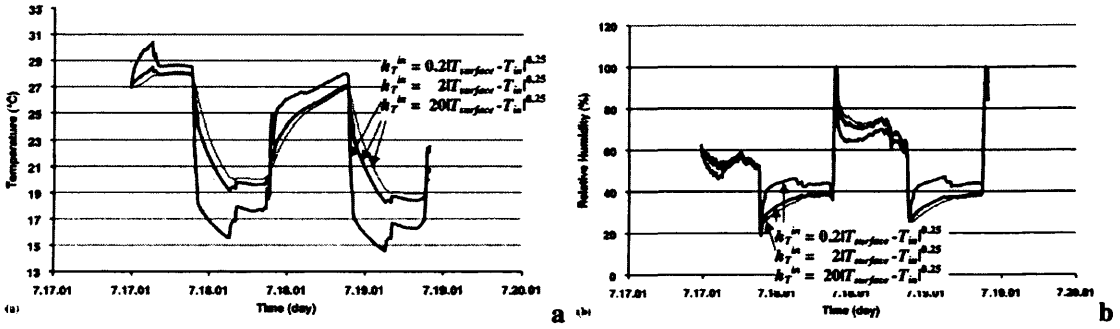

Figure 150. Simulated indoor (a) temperature and (b) relative humidity with different convection heat transfer coefficients (Lü, 2002)

4.8.10 Convective Diffusion Coefficient

The choice of the expression of the convective heat transfer coefficient (h_{out}) affects the expression of the convective diffusion coefficient (h_D), as it is related to it. According to the Lewis relation, for turbulent flow, the convective diffusion coefficient can be given by the convective heat transfer coefficient by the relationship (Holman, 2002; Olioso and Bocquillon, 1992):

$$\frac{h_{out}}{h_D} = c_a \rho_a Le^{2/3} \qquad \text{Eq. 153}$$

Where:

Le: Lewis number.

Lewis number is given by:

---

[37] Where c is a constant, n an exponent and ΔT refers to the temperature difference between the

$$Le = \frac{a_a}{D} \qquad \text{Eq. 154}$$

The convective diffusion coefficient, h_D, is expressed in m/s.

4.9 Expressing Heat and Mass Transfer in Detail; Necessity or Scientific Curiosity?

It might be questioned why there is so much persistence in expressing heat and mass transfer in such detail. The answer is that since the effect of green roofs is examined on the outdoor environment and not the indoor one, simplified assumptions which would take its insulative properties into consideration only, could lead to errors and false predictions for outdoor spaces. As will be justified in paragraph 4.11, only with such a detailed description can the model predict accurate external temperature distributions.

In the instance of Takakura et al. (2000), simplifications which might be useful for predicting interior temperatures, might lead to serious errors, concerning quantities which affect mostly outdoor heat fluxes. Takakura et al. (2000) developed a one-dimensional dynamic model for describing the thermal effects of green roofs on the internal temperatures of buildings. They solved the differential equations with finite difference approximations, considering the plant-air canopy to be a homogenous solid (discussed in paragraph 4.6.5). They verified the results of the model with an experiment, measuring temperatures on a green roof covered with grass and ivy and a bare concrete one. The results of the comparison between the measurement and the simulation show that the simulated soil surface temperatures are higher than the measured ones during daytime and lower at night time (Figure 151). The authors justified this temperature discrepancy due to the very rough estimation of the evapotranspiration of plants and soil (ibid.). For estimating indoor conditions this rough estimation may be acceptable, but for predicting the effect of evapotranspiration on outdoor thermal conditions, such a discrepancy may lead to crucial errors.

---

wall surface temperature and the air temperature.

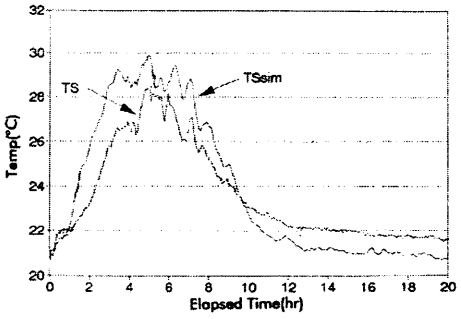

Figure 151. Takakura et al.'s results of measured (TS) and simulated (TSsim) soil surface temperature for a green roof (adapted from Takakura et al., 2000)

4.10 Presentation of the One-Dimensional Model

The one-dimensional heat and mass transfer model for both vegetated building surfaces and plain building elements has been described by the equations presented and developed in paragraphs 4.2 to 4.8.10 and is illustrated in Figure 148. In Figure 152 and Figure 153 a flow diagram of the model is presented, showing the inputs, outputs, and the equations used for each type of node for both the plain and the concrete roof.

For both types of roofs two sets of input nodes are needed; the "urban" node, where the climatic characteristics of air temperature, relative humidity and wind speed (Turb, RHurb and V, respectively) are input and the "internal" node, where constant temperature and relative humidity are input (Tin, RHin), as discussed in paragraph 4.8. Temperature and relative humidity[38] for the nodes between the two input nodes are calculated simultaneously with the use of equations 27 to 111, as described in Figure 152 and Figure 153, solved with finite differences, as presented in paragraphs 4.7-4.7.1. For both types of roofs, the temperature and relative humidity in the air nodes well above the roof are calculated with the use of equations 27 and 28 (page 155), while for the boundary air temperature and relative humidity, equations 97 and 98 (page 187) are used for both green and plain roofs. In order to describe temperature and specific humidity fluctuations on the internal surface of the construction material of the roof, equations 93 and 94 (page 186) are used for both plain and green roofs.

[38] Relative humidity of aerial nodes is related to the specific humidity (calculated from the mass transfer equations) with equation 30 (page 155).

For heat and mass transfer within the building material, equations 19 and 21 are implemented (pages 151 and 152) in both plain and green roof changes.

Differentiation between the two types of roof occurs at the external surface node of the structural part of the roof; for the plain roof equations 95 and 96 (page 187) are used. Solar radiation on the roof's plane (I) and sky temperature (Tsky) are input in equation 95, while for the green roof equations 102 and 103 (page 188) are used to predict temperature and volumetric water content of the soil at its boundary with the construction layer. For the green roof, temperature and volumetric water content within the soil are described by equations 32 and 36, respectively (pages 156 and 158), while for the boundary soil node with the plants, equations 110 and 111 (page 190) are used. In the heat transfer equation of the latter (equation 110) solar radiation and sky temperature are input. For the canopy (green) nodes, the outputs are three; air temperature (T), leaf temperature (T_ℓ) and relative humidity (RH), while solar radiation and sky temperature are input in all canopy nodes. The equation used to calculate leaf temperature is the same for all the three distinct green nodes, equation 73 (page 180), whose solution is presented in Appendix 2. For the lower green node equations 108 and 109 (page 190) are used to describe air temperature and relative humidity, respectively, for the canopy layer close to the soil. For the nodes within the canopy layer (green nodes) equations 74 and 75 (page 180) are used to calculate air temperature and relative humidity, while for the boundary canopy layer (upper green node) equations 104 and 105 (page 189) are used.

Scheme	Type of Node / Equation	Input	Output
urb	urban node	Turb, RHurb, V	-
air air air air	air node (Eq. 27, 28)	-	T, RH air layer
I, Tsky a1	boundary air node (Eq. 97, 98)	-	T, RH boudary air layer
c,s	boundary external roof node (Eq. 95, 96)	I, Tsky	T, q external roof surface
c c	roof node (Eq. 19, 21)	-	T, q roof (inside the material)
c,in	boundary internal roof node (Eq. 93, 94)	-	T, q internal roof surface
in	internal node	Tin, RHin	-

Figure 152. One dimensional model; plain roof

Scheme	Type of Node / Equation	Input	Output
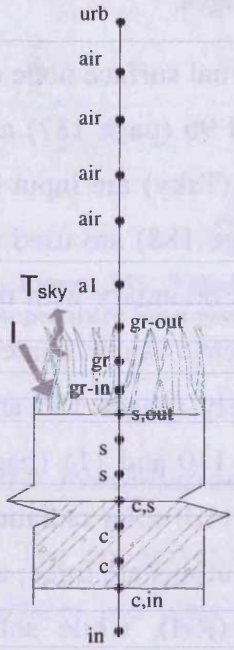	urban node	Turb, RHurb, V	-
	air node (Eq. 27, 28)	-	T, RH air layer
	boundary air node (Eq. 97, 98)	-	T, RH boudary air layer
	upper green node (Eq. 104, 73, 105)	I, Tsky	T, T_f, RH plant, boundary with air
	green node (Eq. 74, 73, 75)	I, Tsky	T, T_f, RH plant (inside)
	lower green node (Eq. 108, 73, 109)	I, Tsky	T, T_f, RH plant, boundary with soil
	boundary soil node (Eq. 110, 111)	I, Tsky	T, ω_g soil, boundary with plant
	soil node (Eq. 32, 36)	-	T, ω_g soil (inside)
	boundary soil-roof node (Eq. 102, 103)	-	T, ω_g soil, boundary with roof
	roof node (Eq. 19, 21)	-	T, q roof (inside the material)
	boundary internal roof node (Eq. 93, 94)	-	T, q internal roof surface
	internal node	Tin, RHin	-

Figure 153. One dimensional model; green roof

4.11 Validation of the Model - Experiment

For validating the accuracy of the model, an experiment has been conducted on the roof of the Welsh School of Architecture (Bute Building, Cardiff) for five days in August 2004 (2nd August until 6th August, 2004). Two test cells have been constructed; one which carries plain pavement grey slabs, the "concrete test cell", and another one, the "green test cell" where a vegetated medium (grass and soil) has been placed on top of the pavement slabs.

The test cells have a simple construction; as the intention is to measure the "outdoor" temperatures, there is no need to create an enclosed environment. In fact, this has been considered to be an obstacle to the needs of the experiment, as the stored heat within the cell (especially from the bare slabs) would raise their temperature significantly. A timber frame is constructed for each cell (Figure 154), made out of timber beams of 0.10m×0.05m, on top of which the slabs are placed (Figure 155). The frame is not shielded, so that the concrete slabs do not store important amounts of heat underneath them.

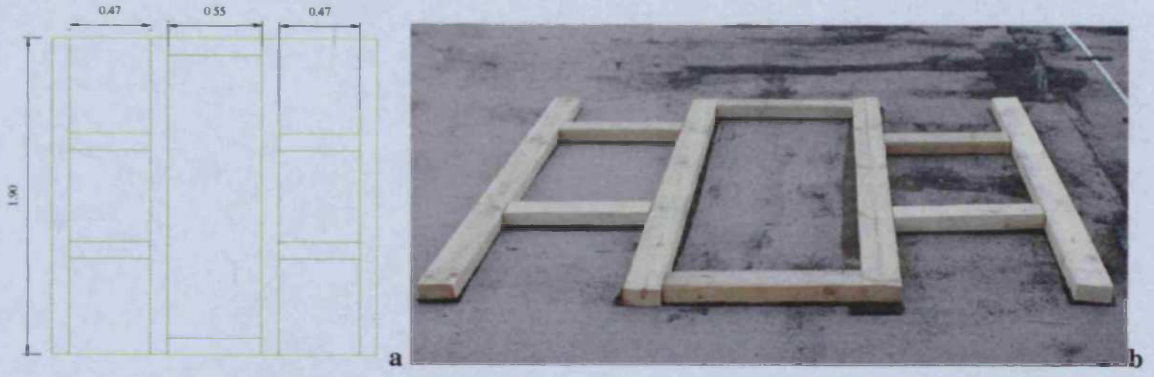

Figure 154. Timber frame (b) and its dimensions in meters (a)

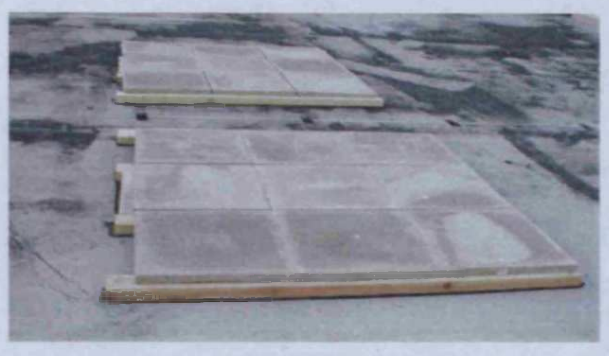

Figure 155. Slabs on the top of timber frames for both "concrete" and "green" test cells

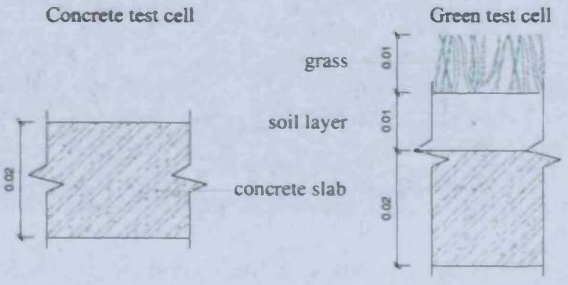

Figure 156. Layers and dimensions (in m) of concrete and green test cells

The layers of each test cell are illustrated in Figure 156. The concrete slabs are 2cm thick, the soil layer is 1cm thick, and the vegetated surface has a height of 1cm. Sensors are placed in the middle of each test cell, to monitor the heat and mass transfer phenomena described by the one-dimension model, developed in this study. The uniformity of the two test cells, covering an area of 3.61m^2 each, is sufficient so that thermal and mass transfer in the middle of the component is adequately described by a one-dimensional model.

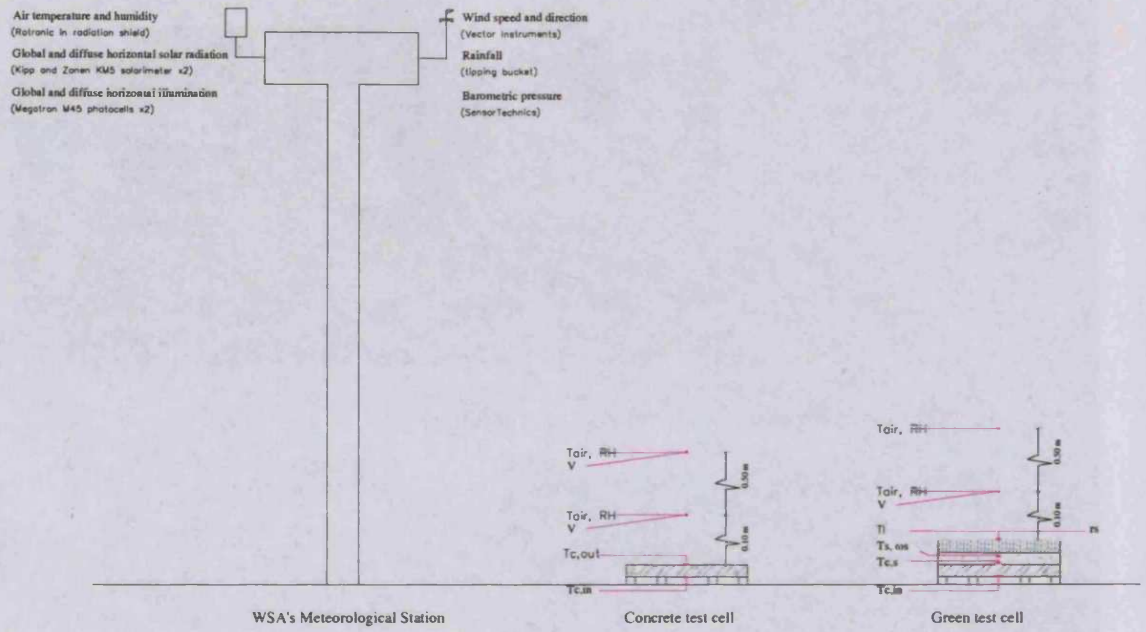

Figure 157. Sensors on each test cell

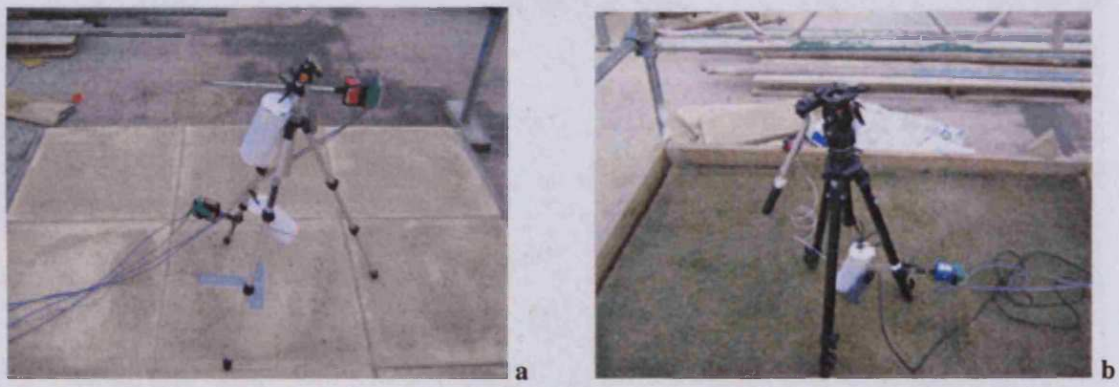

Figure 158. Partial view of (a) concrete and (b) green test cell with their sensors

The sensors placed on the test cells are illustrated in Figure 157 and can be seen in Figure 158. For the plain concrete test cell, a surface temperature sensor is placed on the bottom of the slab, measuring the "interior" surface concrete temperature ($T_{c,in}$). Another surface temperature sensor is placed at the top of the slab, measuring the "external" surface temperature ($T_{c,out}$). The sensor is covered with insulating white tape and is kept shaded, so that its measurements are those of the surface temperature of the material and not the sensor's own raised temperature. Two air temperature and humidity sensors and two hot wire anemometers are placed over the slab, at 10 and 60 cm distance from the upper part of the concrete layer (named a1 and air nodes, respectively). The air temperature sensors are sheltered within cylinders made out of thick white paper to the exterior and black to the interior (Figure 159). The white colour to the outside is chosen so that any radiant temperature towards the sensor is reflected. Black is placed in the interior so that any incoming radiant temperature will

be absorbed by the cylinder and not reflected to the sensor. The cylinders have small, frequently scattered holes, so that the air is able to enter and its actual temperature can be measured.

Figure 159. Shield of air temperature sensors

For the vegetated component, two surface temperature sensors are placed on each side of the concrete slab (lower and upper, $T_{c,in}$ and $T_{s,c}$, respectively). A soil temperature sensor and a soil moisture sensor are placed in the middle of the soil layer. The surface temperature of the grass is measured with an infra-red thermometer and its resistance with a porometer. Again, two air temperature and humidity sensors are placed at 10 and 60 cm distance from the upper part of the green layer. A hot wire anemometer is placed 10 cm above the grass.

Air temperature and humidity well above the ground (symbolised as "urban"), the wind speed and direction, the solar irradiance (total and diffuse), cloud cover, rainfall and barometric pressure are measured at the School's meteorological station, which is situated on the same roof.

The measurements are taken at 5 minutes intervals, synchronised to the meteorological station's 5 minute interval reads. The four surface temperature sensors, the soil humidity sensor and the three hot wire anemometers are connected to a 1000 Series Squirrel data logger (details of the connections are given in figure 1, appendix 3). The squirrel is programmed to take readings every 10 seconds and it averages them in 5 minutes intervals. The four air temperature and humidity sensors and the soil temperature sensor are wireless Gemini sensors, with their own data logger each. The infrared sensor measuring the surface temperature of grass could not be connected to a data logger, thus these measurements are taken manually with a 5 minutes interval. The aerodynamic stomatal resistance of leaves is measured with a porometer, again manually. As the University regulations allow for people to be on the roof only during the opening times of the building (9am to 5pm), the manual measurements only take place during this period of the day and only a few hours of

night-time measurements have been exceptionally allowed on the 5th/8/2004, under clear sky conditions.

The characteristics of each sensor, the quantity that has been measuring and the data logger to which it has been connected are summarised in Table 11.

Table 11. List of sensors with their characteristics

Sensor	Range	Accuracy	Quantity	Data Logger
Tinytags TGU-1500	-30°C to +50°C 0 to 95%	± 0.2°C For 0°C-50°C ±3%	Air temperature / Relative Humidity	-
Thermocouple	-30°C to +100°C	± 0.3°C	Surface temperature	Squirrel
Tinytalk II	-10°C to +50°C	± 0.2°C	Soil temperature	-
Infratrace 801	-40°C to +150°C	± 2.0°C	Leaf surface temperature	-
Soil Moisture Probe type ML2x	0.0 to 0.6 m^3/m^3	± 0.02m^3/m^3	Soil humidity content	Squirrel
Porometer AP4	-	Up to 10%	Stomatal resistance	-
Model 8450 (Hot wire anemometer)	0-10 m/s	± 0.1m/s	Wind speed near the ground	Squirrel

The estimated accuracy of the sensor might be lower than that suggested by its manual. The age of the sensor, its storing conditions, its connections with the data logger, the conditions of the data logger's ports and electronics and many imponderables, determining the sensor's – logger's behaviour, are factors which might affect the true accuracy of the measurement. Sensors were tested in the laboratory, before the start of the experiment, yet there is always a factor of uncertainty when measuring. To express this factor, the accuracy suggested by the sensor's manual has been increased by 10%.

The climatic conditions of the period of the measurements are summarised in Figure 160-Figure 162. As the model under examination considers clear sky conditions, the 5th August is chosen as the clearest day during the experiment's period. The measured temperature and relative humidity distributions at the test cells are summarised in Figure 163 and Figure 164, respectively.

The validation of the model is focused on temperature and relative humidity fluctuations of the nodes whose temperatures have been measured. The nodes and their names, of both the concrete and the green cell are shown in Figure 165.

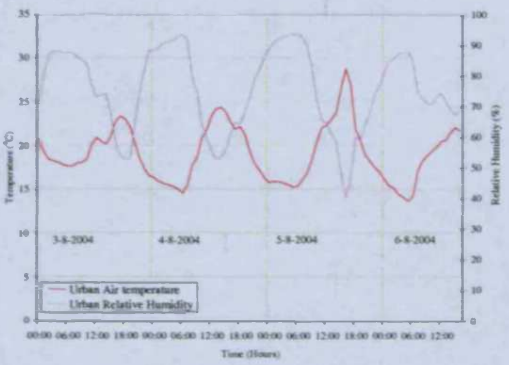

Figure 160. "Urban" air temperature and relative humidity, as measured by the meteorological station of the WSA in Cardiff, from 3-8-2004 to 6-8-2004

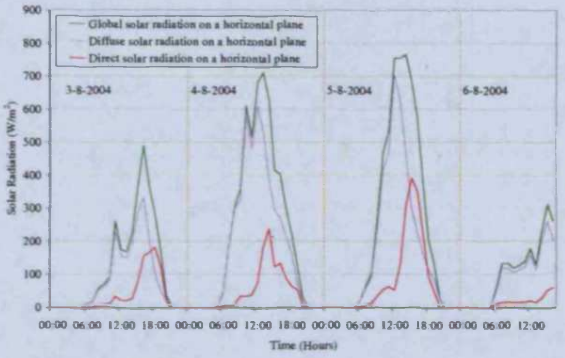

Figure 161. Solar radiation on a horizontal plane, as measured by the meteorological station of the WSA in Cardiff, from 3-8-2004 to 6-8-2004

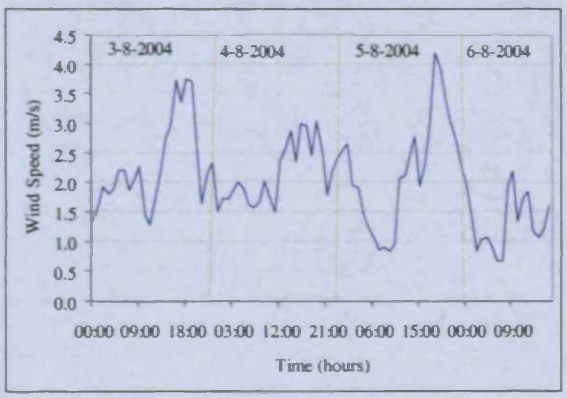

Figure 162. Wind speed as measured by the meteorological station of the WSA in Cardiff, from 3-8-2004 to 6-8-2004

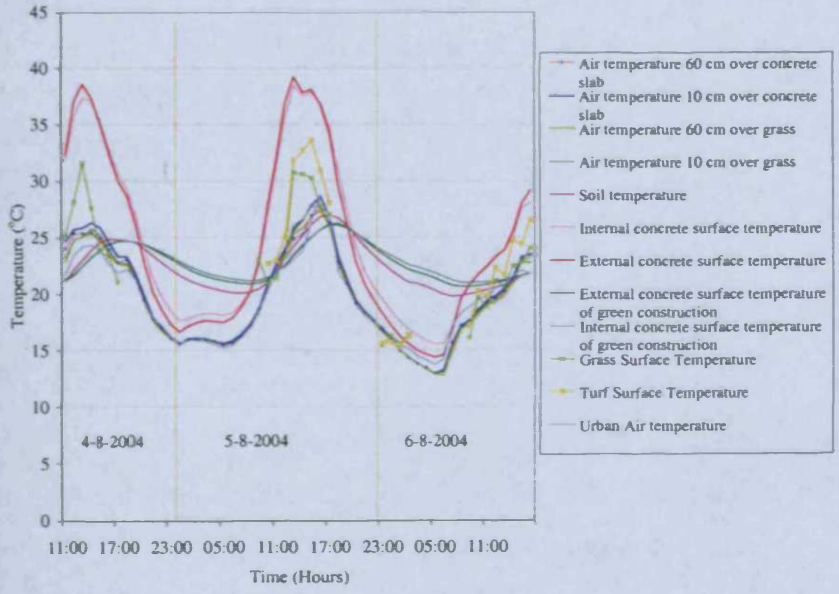

Figure 163. Temperature measurements at the concrete and the grass test cells, from 4-8-2004 to 6-8-2004

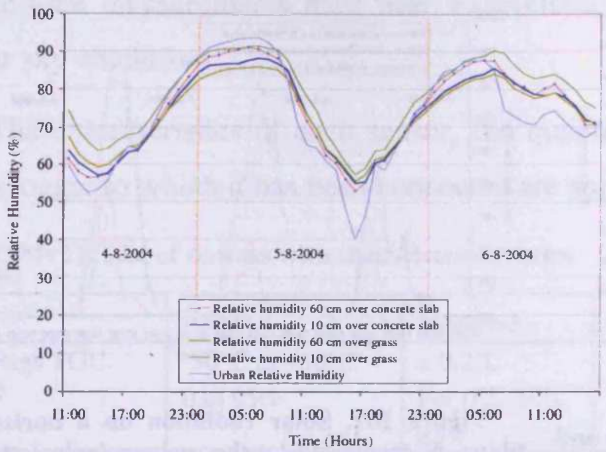

Figure 164. Relative humidity measurements at the concrete and the grass test cells, from 4-8-2004 to 6-8-2004

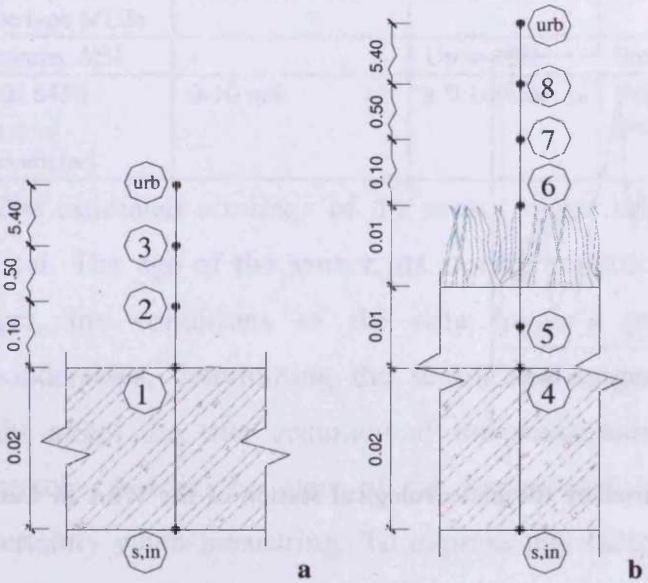

Figure 165. Nodes examined and their distances (in m) for calculated and measured quantities (a) at the concrete cell and (b) at the green cell

4.11.1 Comparison between Measured and Calculated Temperatures

In this section the comparison between measured and calculated temperatures is presented. In all diagrams the calculated temperature or humidity (symbolised as "Calculated") is given by a red line, and the measured one (symbolised as "Measured") is given by a blue line. The difference between the measured and the calculated temperature or relative humidity is the error (symbolised by DT for temperatures and DRH for relative humidity). It is a brown line, which is graphed on a secondary axis, on which the "Temperature Difference" or "Relative Humidity

Difference" is graphed. A yellow box covers the band where the values of DT and DRH are acceptable, determined by the accuracy of the sensors and the error of the finite differences approximation.

In paragraphs 4.11.1.1 to 4.11.1.3 the nodes of the bare concrete test cell are examined, while in paragraphs 4.11.1.4 to 4.11.1.8 the nodes of the green test cell are discussed.

4.11.1.1 Node 1: External Concrete Surface of Concrete Test Cell

Where the external surface temperature of the concrete test cell is concerned, the distribution of measured and calculated temperatures is given in Figure 166. Generally, the difference between the two distributions is within the error band, with an average error of 0.7K, 0.1K above the acceptable error band. A few points are out of the band, during the midday, at sun dawn and sunset, reaching a maximum difference of the order of 1.8K during daytime and of the magnitude of 1.3K during dawn and sunset. Due to this symmetry, suspicion rises that these discrepancies might be related to the amount of irradiation on the sensor and/or surface albedo. This could be due to the steel frame that was placed[39] tightly around the two test cells by builders, as construction works were taking place during the experiment. Although the sensor was shielded, it could be possible that it could have been receiving some additional reflected radiation from the steel frame during the morning (reflections from the eastern frame), at noon (reflections from the southern frame) and the evening (reflections from the western frame). It may also be the case, that the steel frame is completely irrelevant to these errors and that the assumption that concrete slab's albedo is constant throughout the day has caused these elevated errors. Optical properties are not as constant as have been assumed, but depend on the incident angle of direct radiation. Nonetheless, the points with the elevated error are few and their discrepancy is not considerably large. In the distribution given in Figure 166, the convection heat transfer coefficient in the expression of the surface concrete temperature, is calculated with the analytical method, which is investigated in the following paragraph.

[39] I had tried to remove it, but its joints were too tight and heavy for me to remove.

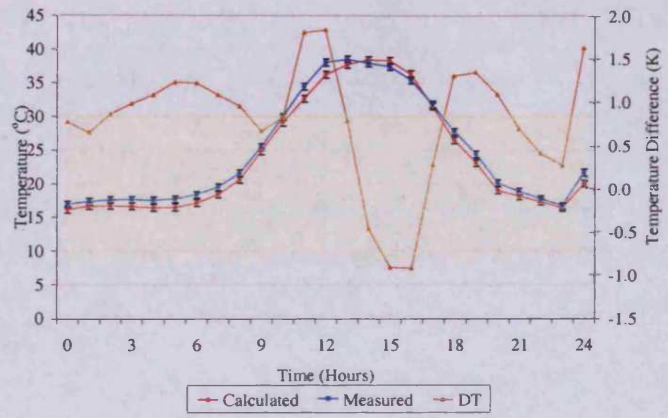

Figure 166. Node 1: Comparison between calculated and measured external concrete surface temperature

4.11.1.2 Node 2: Boundary Air Layer above the Concrete Test Cell (10 cm away from the External Surface of the Concrete Slab)

A comparison is made between the temperature measured when using an analytical method for defining the convective heat transfer coefficient (h) and when using a simplified one. The method of calculating the convective heat transfer coefficient between a solid surface and a fluid around it has been discussed thoroughly in paragraph 4.8.9. In this paragraph, the analytical determination of the convective heat transfer coefficient, described in paragraphs 4.8.9.1-4.8.9.3 and the simplified one, suggested by ASHRAE (Table 9, last line, paragraph 4.8.9.4) are examined.

As is obvious from Figure 167, the results from the calculations with the use of the analytical h are much closer to measurements than the results from the simplified formula. Especially for day-time, the calculated temperature with the simplified convection heat transfer coefficient can exceed the measured temperature by 2.4K, with an average of 1.0K, while the total acceptable error band is 0.6K. For the analytical method, maximum error only reaches 1.3K, with an average of 0.3K. For the simplified convection heat transfer coefficient most of the day-time values are not within the band of the acceptable error, while the night-time temperature distribution is closer to the measured temperatures. In all, the simplified method has 14 values outside the error band, while for the analytical method this number becomes only 3. As has been discussed by many researchers and was mentioned in paragraph 4.8.9.4, the choice of the expression of h affects crucially the distribution of predicted temperatures. It is therefore essential to choose an expression which will not forfeit the accuracy of the model. As the analytical method is the one that offers the fewest

discrepancies between the measured and calculated temperatures, it is the one chosen to calculate the convective heat transfer coefficient in the model.

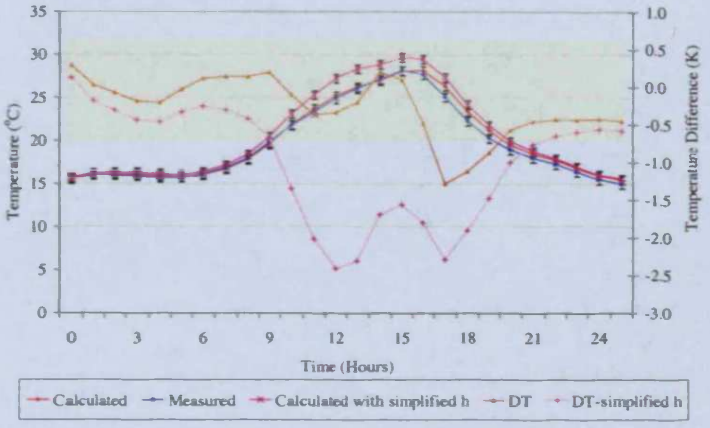

Figure 167. Node 2: Comparison between measured and calculated air temperature with different convective heat transfer coefficients 10 cm above the concrete slab

4.11.1.3 Node 3: Air node well away from the Boundary Layer of the Concrete Test Cell (60 cm away from the External Concrete Surface)

The calculated distribution of the air temperature 60cm above the concrete surface does not take into consideration the air velocity in the air nodes; the expression of heat transfer in this figure is the one which ignores air velocity and only takes into account thermal diffusion in the air (equation 27). Although 5/8/2004 was moderately windy in Cardiff (Figure 162) the error between calculation and measurement are not significant (Figure 168); air velocities near the ground are not particularly large. For calculated and measured air temperature, all errors are within the acceptable error band, with only 6 calculated points exceeding the error band and an average error of 0.4K.

Due to the lack of sensors of material moisture content, the node whose calculated humidity content could be compared to the measured one is the air node 60cm above the test cell. As can be seen in Figure 169, the convergence between the measured and calculated relative humidity is very satisfying; all values are within the error band (±6.5%) and the average error is 2.6%, with a maximum of 4.0%.

It is evident in both Figure 167 and Figure 168 that there is a larger convergence between calculated and measured air temperatures during night time. This is due to the fact that less turbulence and plumes are created over the concrete slab at night time. Nonetheless, for the relatively low air velocities near the ground, not taking air

velocities into consideration in the heat and mass transfer equation does not lead to significant errors in either day or night time.

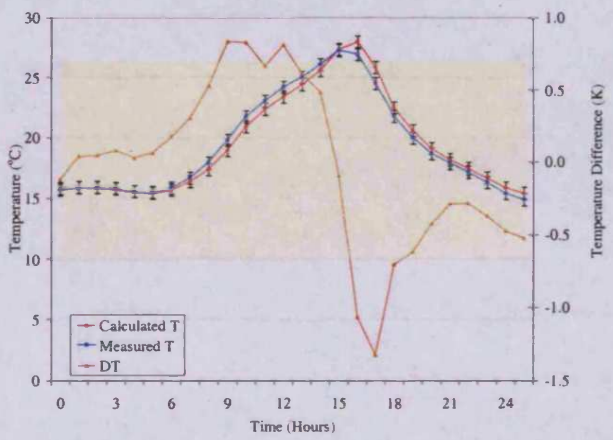

Figure 168. Node 3: Comparison between measured and calculated air temperature 60 cm above the concrete slab

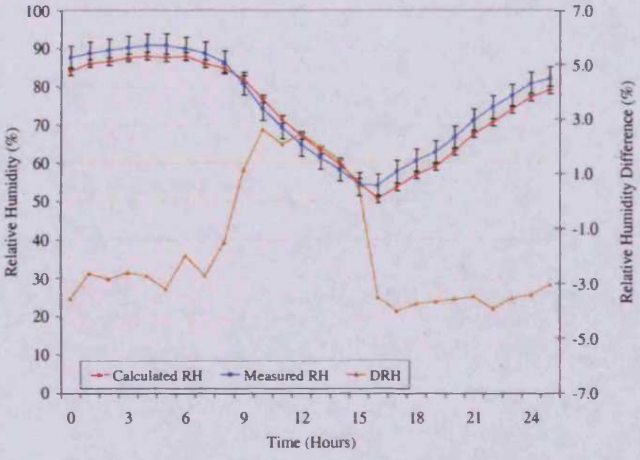

Figure 169. Node 3: Comparison between measured and calculated relative humidity 60 cm above the concrete slab

4.11.1.4 Node 4: Concrete Surface under the Soil Layer of the Green Test Cell

Where the concrete surface temperature under the soil layer of the green test-cell is concerned, there is a very good convergence between the calculated and the measured values (Figure 170). The difference between the two exceeds the error band by only 4 calculated points and the average error is 0.5K. Although at this node, as has been discussed in paragraph 4.8.3, the thermal capacity of the two materials is not taken into consideration and the formula of this node derives from the continuity equation, it is obvious from Figure 170 that this does not forfeit the accuracy of the model. It is clear that the calculated temperatures are slightly lower than the measured

temperatures during night time and slightly higher during day time, due to the lack of the thermal capacity participation in the equation. Since the thermal capacity of materials is taken into consideration in all mathematical expressions of the model, apart from the boundary ones inside the solids, and errors in node 4 are so small, it is confirmed that the omission of the thermal capacity at the boundary nodes between solids does not lead to any unacceptable errors.

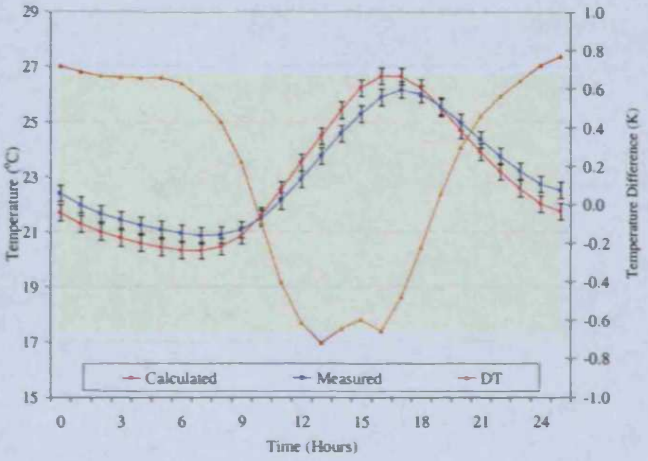

Figure 170. Node 4: Comparison between measured and calculated concrete surface temperature under the soil layer

4.11.1.5 Node 5: Soil Layer of the Green Test Cell

Again, for the soil layer, the difference between the measured and the calculated soil temperature is mostly within the error band, with a 0.5K average error. Although the soil matrix is characterised by high inhomogenity and the parameters which describe its heat and mass transfer performance are quite numerous, an appropriate selection of their values turns out to give results which are very close to the measurements (Figure 171).

Most of the values of the volumetric water content of the soil are also within the acceptable error band, with only three exceeding the expected difference between measured and calculated soil moisture and an average error of $0.008m^3/m^3$ (Figure 172). Nonetheless, there is a quite close relationship between the calculated and measured soil volumetric water content, despite the inhomogenity of the medium.

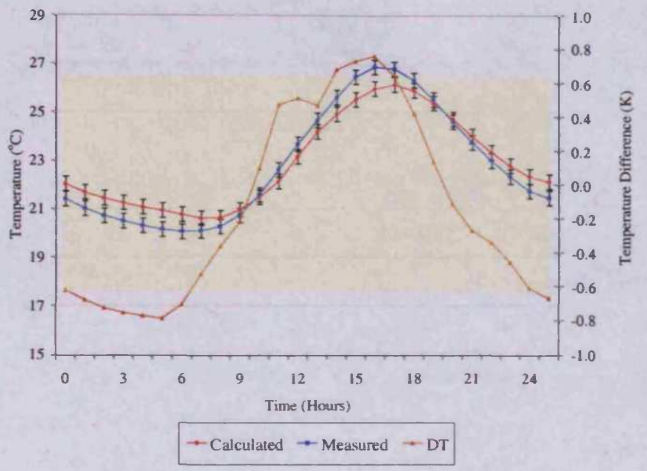

Figure 171. Node 5: Comparison between measured and calculated soil temperature

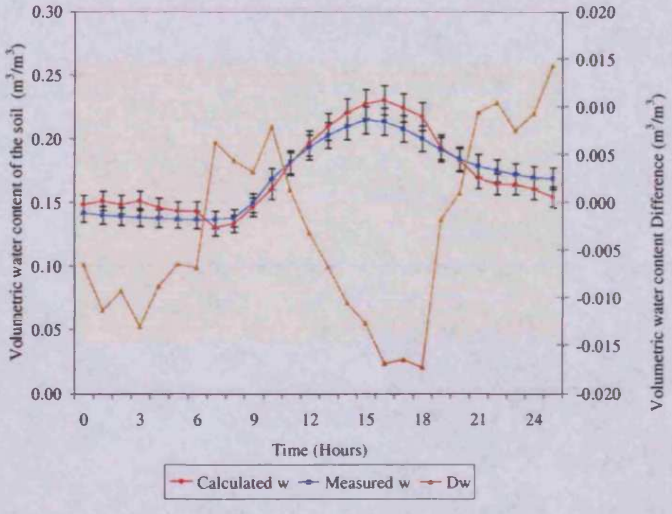

Figure 172. Node 5: Comparison between measured and calculated volumetric water content of the soil

4.11.1.6 Node 6: Grass Surface Temperature in the Green Test Cell

The surface temperature of this node has been calculated with two methods of solution of the heat transfer equation in plants, both presented in appendix 2; the analytical method, described in paragraph 2.1 of the appendix and the method with the linearised radiation term, described in paragraph 2.2. The results of both methods are shown in Figure 174 and Figure 173 respectively. During day-time both methods seem to converge; both have a difference with the measured temperature which exceeds the acceptable error band only at peak time. For the analytical method, the error reaches an average of 1.2°C and a maximum of 2.9°C during day-time. For the linearised method, these numbers become 1.1°C and 2.8°C, respectively (the total

error band being ±2.3°C), with 1 value away from the error band in day-time. This must be due to the fact that the grass temperature has been measured momentarily every five minutes, while the rest of the quantities had been averaged every five minutes; the momentary grass values can have higher maximum and minimum values than the rest of the quantities input in the model. There is a possibility that the instant that the surface grass temperatures were measured momentarily at noon, solar radiation had reached its maximum, which was averaged with the rest of the irradiation readings, thus lowering the stored value. By inputting a lower value of irradiation, air temperature etc in the model, than those which had caused the leaf temperature peak in the experiment, it is obvious that a lower leaf temperature will be predicted by the model. Thus, these peaks of the error (which are few) can be justified by the momentary nature of leaf surface temperature measurements.

In addition, the fact that grass's albedo and relationships to radiation distribution have been input as constant in the model might be responsible for these differences during peak time. As has been discussed in paragraph 4.6.3.1, not only the albedo, but also radiation distributions within the vegetated canopy vary with solar elevation; quite complicated formulas are needed to describe them, which, due to the inhomogeneity of plants, might not lead to particularly accurate predictions. The simplified, constant expressions which are chosen to describe plant albedo and radiation distributions, do not lead to such significant errors, as can be seen in Figure 173. This, and the nature of infra-red measuring surface temperature of leaves (discussed in paragraph 4.11.2), may justify the three points beyond the error band during peak time in the calculation of grass's surface temperature.

During night time it is obvious that the equation with the linearised radiation term (Figure 173) has a better convergence with the measurements, with only 1 out of 4 values exceeding the error band and an average error of 2.2K, which is within the total error band, than the analytical method, whose error is 2.8K, exceeding the error band and so do 3 out of 4 nocturnal values (Figure 174). As explained in paragraph 2.1, appendix 2, the leaf radiation factor has been omitted from the analytical method, due to its much smaller magnitude in comparison with the rest of the factors of the equation. During night time, especially under clear sky conditions, the long wave radiative heat exchanges play a more indispensable role in the overall heat transfer exchanges. Thus it is considered reasonable to use the equation with the linearised radiation term of the leaf temperature in the model.

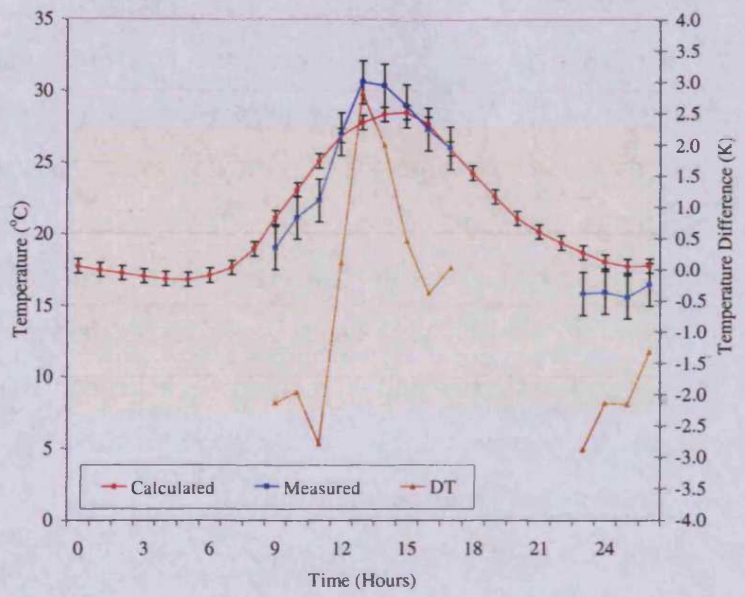

Figure 173. Node 6: Comparison between measured and calculated with linearised radiation term leaf temperature

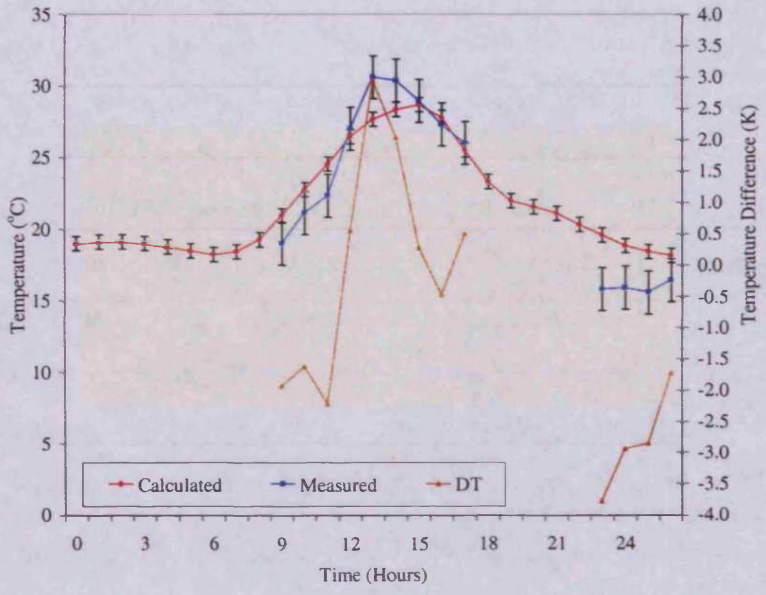

Figure 174. Node 6: Comparison between measured and calculated with analytical method leaf temperature

Stomatal resistance in the model is calculated using the formula suggested by Pielke (equation 69). However, for reasons of comparison, it has also been calculated with the formula suggested by Jacobson (equation 72). Night-time resistances become infinite with the use of the formula suggested by Jacobson, making it difficult to use for computer modelling. The error of both these formulae is unknown.

Stomatal resistances were measured manually, with the ΔT AP4 porometer fitted on the leaves, as shown in Figure 175. Measurements were taken from a number of

leaves, and were averaged over hourly periods. Before taking a stomatal resistance reading, the porometer had to be calibrated and the reading was taken only after a 10% error had been reached[40].

As can be observed in Figure 176, there is a very good convergence between the measured stomatal resistance and the calculated resistance with the equation suggested by Pielke (equation 69), for both day-time and night-time. Their difference is within the 10% porometer's error band (21.1s/m during day-time and 1.7s/m during night-time). The formula suggested by Jacobson does not converge as well with measurements, being much lower than the measured resistances during day-time, with an average day-time error of the magnitude of 211.0s/m.

Apart from its practicality with computer modelling, equation 69, which has been used to express stomatal resistance in the model, shows a very good convergence with the measured stomatal resistance of grass, with the ΔT AP4 Porometer. Equation 72 shows a poor convergence with measurements, while the expression of stomatal resistance through equation 71 has not been considered, due to the impracticality of gathering data of PAR. Since the equation suggested by Pielke reveals such a good convergence with measurements, it is applied in the model under construction with great confidence.

Figure 175. The head unit of the ΔT AP4 Porometer, measuring a leaf stomatal resistance during the experiment

[40] According to the manual, the error should not exceed 10% (Webb, 1999).

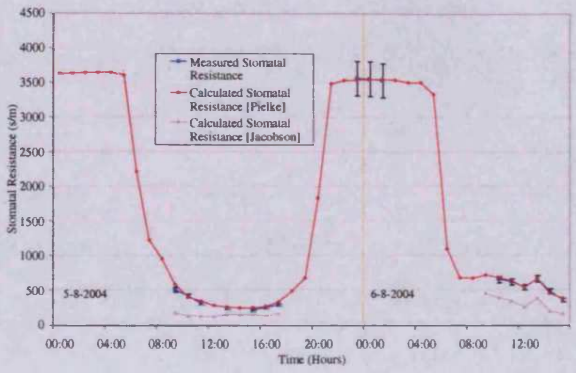

Figure 176. Comparison between measured and calculated stomatal resistance

4.11.1.7 Node 7: Boundary Air Layer above the Grass (10 cm away from the Upper Part of the Grass Layer)

In node 7, as its equivalent node 2 of the concrete layer, the convergence between the calculated and the measured temperature are very satisfying, with an average 0.4K error. The calculated temperature presented in Figure 177 is calculated with the analytical determination of the convective heat transfer coefficient. The convergence between the calculated and measured air temperature is even more satisfying for node 7, as not a single value is outside the expected error band, while there are few in node 2. This is because the grass surface does not raise its temperature as much as the concrete surface, and therefore creates plumes of less significance. The chaotic nature of turbulence has a smaller impact on the air above the vegetated surface, than the layer over the heated concrete surface.

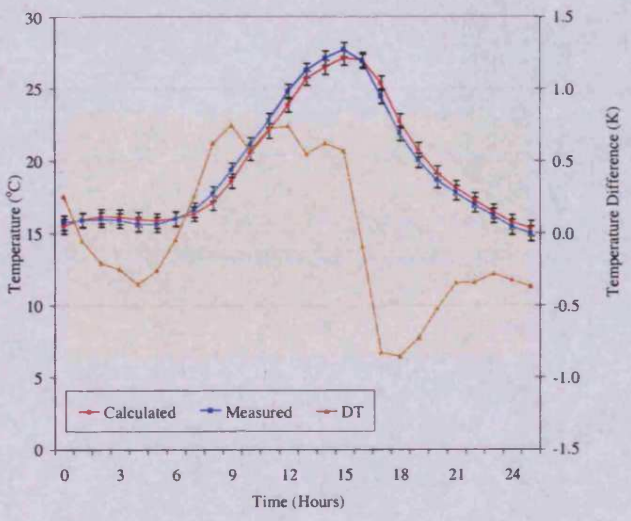

Figure 177. Node 7: Comparison between measured and calculated air temperature 10 cm height the grass layer

4.11.1.8 Node 8: Air Node well away from the Boundary Layer of the Grass Layer (60 cm away from the upper part of the Grass Layer)

Again, node 8 is the equivalent of node 3 of the bare concrete test cell. The difference between measured and calculated air temperature is not high, with a 0.4K average error (Figure 178). Minimum differences also occur during night time when the air velocity above the surfaces reaches its minimum, as explained in paragraph 4.11.1.3.

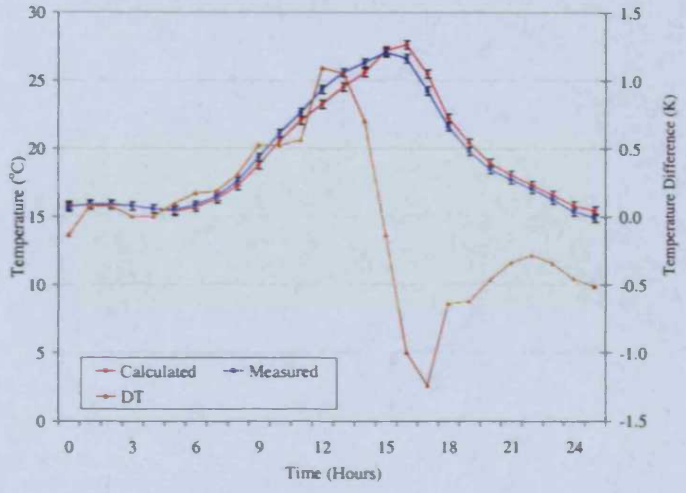

Figure 178. Node 8: Comparison between measured and calculated air temperature at 60 cm height above the grass layer

4.11.1.9 Comparison between Measured and Calculated Air Temperature without Thermal Diffusion

Measured temperatures are also compared with calculated temperatures without the expression of thermal diffusion. The results from this calculation for node 3, the air node 60 cm above the concrete test cell, are given in Figure 179. It is evident, that for all the nodes and solutions examined up to now, this case displays the largest divergence between measured and calculated values. Errors exceed the acceptable error band for up to 15 calculated points. On the other hand, for the heat and mass transfer algorithm, only 6 calculated points exceed the acceptable error band (Figure 168, paragraph 4.11.1.3). By comparing Figure 179 with Figure 168, it is obvious that there is a much larger convergence between measured air temperature and the calculated temperature with the thermal diffusion, than between the measured temperature and temperature calculated taking into consideration only thermal conduction in both solid and air nodes. The error for the heat transfer algorithm reaches a maximum of 1.7K, with 0.7K average. For the heat and mass transfer

relationship, these numbers become 1.3K and 0.4K, respectively. The average error of the heat and mass transfer algorithm is within the 0.6K error band of the numerical and sensors' error, while the mass transfer algorithm's error is not.

It is therefore quite important to express the effect of moisture on temperature in both the air and solid nodes for the full expression of heat transfer. As Gaur and Bansal (2002) conclude: *"moisture transfer should necessarily be considered especially in hygroscopic media in order to have a true assessment of air temperature variations of a building"*.

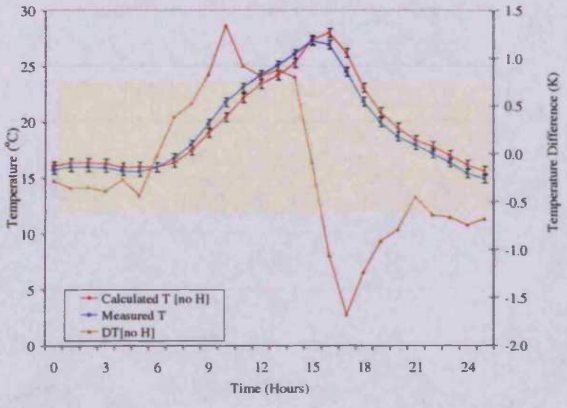

Figure 179. Node 3: Comparison between measured and calculated air temperature 60 cm above the concrete slab, without taking into consideration thermal diffusion in the calculated air temperature

4.11.2 Discussion of Results

It is clear that for the heat transfer within the solid bodies there is a larger correlation between measurements and calculations. This is due to the largest homogeneity of solids, compared to liquids and gases. Less factors of uncertainty exist within the heat and mass transfer in solids than in gases, where the variation of phenomena and their inhomogenity makes them more difficult to express with constant parameters.

It is observed, from the comparison of most measured temperatures and the estimated temperatures from the algorithm developed, that most of them are within the error band of the sensor and the numerical method. However, there are a few values exceeding this band for some of the nodes. There are many possible explanations for this. Firstly, the placement of the sensors could be brought into question and whether the quantities which sensors actually measure are the same as

one presumes they measure. From the general agreement between theory and measurements, it can be assumed that the sensors were placed as carefully as possible, in order to measure the desired quantities. However, natural phenomena, particularly meteorological factors, can be of a chaotic nature. A small, undetectable input in the system may change the system's response for shorter or longer periods. This cannot be described mathematically with the analytical method developed here, but only with statistical and probability methods.

Especially where surface temperatures are concerned, there is a larger discrepancy between measured and predicted temperatures. Although the sensor was glued to the surface, in order to have the best possible contact, the thermal conductivity of the glue could make an additional error to the measurement. Sensors were covered with thick, white tape, in order to insulate them from solar radiation and convection. Care was also given to keep the sensors shaded during the sunshine hours, so that they would actually measure the surface temperature and not their own, increased temperature.

Furthermore, practical factors could also be responsible for the observed, small discrepancy; in the model, material properties, such as thermal conductivity, optical properties of both structure materials and plants are considered to be constant. In reality, as has been discussed in paragraphs 4.3 and 4.6.3.1, some of these properties vary with time and / or in relation to other properties. When they exceed the band of the assumed constant value of the model, a disagreement may be caused between measured and calculated values.

Concerning infra red measurements, the existence of particles, such as water vapour in the air between the sensor and the surface might lead to a measurement error. Although the sensor was placed as close to the surface as possible, in order to minimise the probability of measurement errors, the water vapour transpired by the leaves might have altered the reading. The reading was instantaneous every 5 minutes and not averaged, as was the case of the other sensors' readings. They were more rigid than the rest of the readings, representing momentary quantities, instead of quantities averaged over a period of time. This is why it had been expected that the quantities measured with the infra red sensor may have exceeded the predictions of the model, where their maximum and minimum values were concerned.

In addition, all five minute intervals at the measurements were linearly interpolated to 10 second intervals for reasons of adapting to the time step needs of the model

(explained in paragraph 4.7 and paragraph 5.6, chapter 5). This might lead to an error between the estimated value at the 10 second interval and the real one. To have a 10 second interval for the measurements had been considered unnecessary. The 5 minute interval of the data from the meteorological station was fixed, thus any other interval from the rest of the measurements was not considered to be essential.

Despite all these measurement uncertainties, true for all experimental procedures (Gilliaert et al., 1992), there is a large convergence between measured and calculated temperature, humidity and stomatal resistance, as has been shown in paragraphs 4.11.1.1 to 4.11.1.9. In most cases the differences between calculated and measured quantities are within the expected error band and the few values outside the error band can be physically explained. They are either due to properties considered constant in the model, which are not so constant in nature, or to excessive turbulence phenomena, not fully described by the physical factors implemented.

In order not to jeopardise the accuracy of the model, these physical factors are chosen so that calculated quantities have the largest convergence possible with measurements. The convective heat transfer coefficient is defined with the analytical method, because, as has been discussed in paragraph 4.11.1.2, it shows the best convergence between calculated and measured quantities. Regarding the surface temperature of canopies, the method with the linearised radiation term is used, as it shows the largest convergence, especially for night time temperatures (paragraph 4.11.1.6). Stomatal resistance is calculated with the formula suggested by Pielke (equation 69), as its predicted resistances are the closest to measurements. On the subject of heat transfer and heat and mass transfer calculations, it is shown in paragraph 4.11.1.9, that there is a larger divergence for the plain heat transfer calculations than for those of the heat and mass transfer. Thermal diffusion is quite a significant factor in modelling thermal exchanges in the built environment. The role of thermal diffusion and moisture transfer cannot be underestimated, especially when the effect of moisture release on temperature is determined near the ground.

4.12 One-Dimensional Simulations

After the validation of all these algorithms with the experiment, it can be said, quite positively, that calculated temperature and humidity distributions with this one-

dimensional model should lead to quite accurate predictions. Before proceeding to the two-dimensional model, the results of the one-dimensional model are presented. They concern plain (concrete) and green roofs, examined for either different expressions of heat transfer (paragraph 4.12.1) or for different climates (paragraph 4.12.2) and different albedos of the concrete roof (paragraph 4.12.3). The geometry and names of the nodes of the green and concrete roof one-dimensional models are given in Figure 180. The vegetation examined in this chapter and the following one is grass, which, as explained in chapter 1, does not add up to the static load of the building and could therefore be easily applied on existing urban buildings.

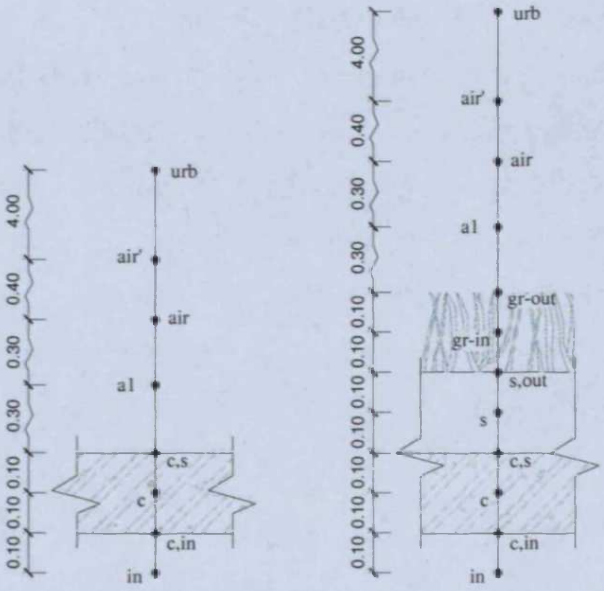

Figure 180. One-dimensional concrete and green roof model and distances between the nodes (in m)

4.12.1 Comparison of Heat and Heat and Mass Transfer Expressions

Using air temperature and solar radiation for a typical day in July for Athens, heat exchanges on a concrete roof have been calculated, using heat and heat and mass transfer equations. For the latter, three sets of relative humidities have been input; the relative humidity of a typical July day of dry –in summertime– Athens, a typical July day of arid Riyadh and a typical May day of humid Mumbai[41]. For the boundary air

[41] The climatic characteristics of each city are given in appendix 6.

node 0.30m above the roof (node a1) the results of all four cases are summarised in Figure 181 for the concrete roof and Figure 182 for the green roof.

As can be observed in Figure 181, even for the building material, neglecting the expression the effects of diffusion on heat flux (line Ta1[no H]) as well as different humidity concentrations (lines Ta1[H Ath], Ta1[H Mumb], and Ta1[H Ry]), result in different outcomes. The differences between the [no H] temperature and the one calculated with the relative humidity of Athens [H Ath] one range from -2.7°C to 1.7°C (3.0°C discrepancy), with an average of absolute differences of the magnitude of 1.5°C. For the different humidity concentrations, differences become slightly smaller. For Mumbai's relative humidity concentration [H Mumb] the calculated temperature differs from that of Athens by an average of absolute values of 0.8°C, with a 2.4°C discrepancy (values ranging from -0.7°C to 1.6°C). For Riyadh's relative humidity [H Ry], the differences with [H Ath] have an average of absolute values of 0.9°C and a range from -2.5°C to 0.2°C (2.7°C discrepancy). When comparing the results of low Riyadh humidity with high Mumbai humidity levels, the differences in predicted temperatures become even larger, reaching a 1.4°C average difference and a range from 0.0°C to 1.9°C (1.9°C discrepancy).

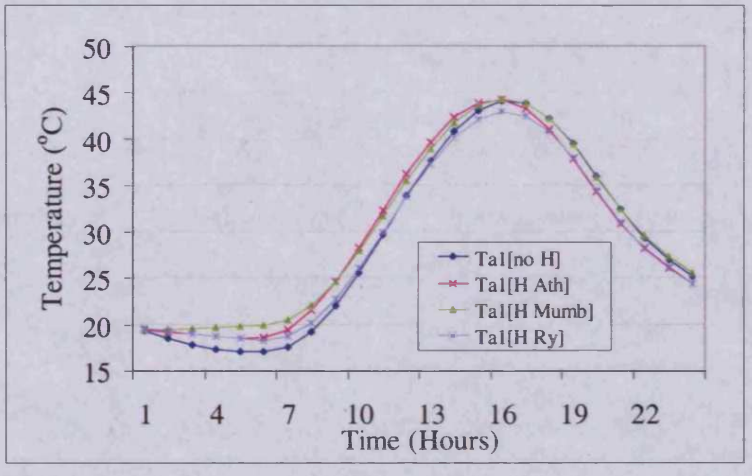

Figure 181. Air temperature above the concrete roof for Athens solar radiation and air temperature, (1) without relative humidity being taken into consideration in the thermal balance [no H], (2) with Athens' relative humidity [H Ath], (3) with Mumbai's relative humidity [H Mumb], and (4) with Riyadh's relative humidity [H Ry]

Regarding the green roof (Figure 182), the differences between the [no H] case and the cases where the role of humidity in temperature distributions has been taken into consideration, become even larger. For the [no H] case the average difference with the [H Ath] boundary air (a1) temperature becomes 5.0°C, with a 4.7°C discrepancy (from -6.6°C to -1.9°C). For the different humidity cases, their average differences with the

Athens base case, remain of the same magnitude as for the concrete roof, but their discrepancy becomes lower; for the [H Mumb] case, the average difference becomes 0.8°C, with a 1.6°C discrepancy (from 0.1°C to 1.7°C). For the drier [H Ry] case, the differences become larger, with a 1.0°C average and 1.8°C discrepancy (values ranging from -1.8°C to 0.0°C). When compared with the humidity of Mumbai, these differences become even larger, reaching an average difference of 1.9°C with a 3.1°C discrepancy (values ranging from -0.2°C to 3.3°C).

As has been discussed in paragraph 4.9 and has been pointed out in paragraph 4.11.1.9 as well, the expression of the effect of humidity diffusion in heat transfer is quite important for the correct expression of temperature distributions. With the one-dimensional model developed here, temperature has been expressed with both only heat and heat and mass transfer equations. Their results show differences of the magnitude of 1.5°C for building materials, to 5.0°C for plants. When thermal diffusion is taken into consideration, different input relative humidity may lead to different temperature predictions. In the cases examined the average of these differences ranged from 0.8°C to 1.4°C; such differences cannot be neglected in modelling the thermal behaviour of the built environment. Especially when the aim is to describe the effects of water vapour release on the air temperature, such an omission may lead to quite large errors.

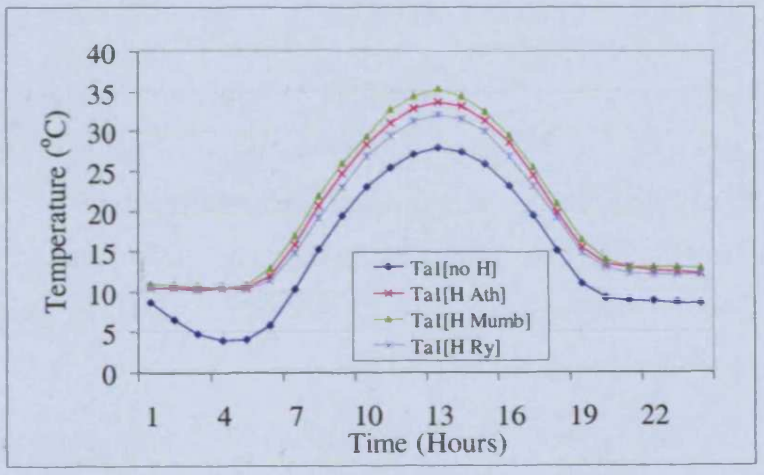

Figure 182. Air temperature above the green roof for Athens solar radiation and air temperature, (1) without relative humidity being taken into consideration in the thermal balance [no H], (2) with Athens' relative humidity [H Ath], (3) with Mumbai's relative humidity [H Mumb], and (4) with Riyadh's relative humidity [H Ry]

4.12.2 Comparison of green and concrete roofs in Athens, Mumbai and Riyadh

For a typical[42] day in Athens and Riyadh in July and a typical day in Mumbai in May, a comparison is made between calculated temperatures for a concrete and a green roof, the thermal properties of which are given in Table 17, chapter 6. In the instance of Athens, concrete roofs (node c,s, Figure 180) reach peak surface temperatures of the magnitude of 54.6°C and an average day-time temperature of 43.1°C (Figure 183a). At the same time, green roofs (node gr-out, Figure 180) reach a peak of only 34.9°C and a day-time average of 26.1°C (Figure 184a). The two roofs reach an average day-time surface temperature difference of the magnitude of 17.0°C. During peak time this difference reaches 26.2°C. Regarding the boundary air temperature (0.30m above the roof, a1 node), its day-time average difference reaches 10.2°C. During peak time this difference goes up to 22.4°C. For the air node 1m above the roof (air' node), these differences become smaller, but still sensible, with a 3.1°C day-time average and a 7.3°C peak.

On the subject of relative humidity, it tends to rise during noon over the green roof, as plants evapotranspire (Figure 184b). For the concrete roof, relative humidity at its proximity fluctuates less than the input "urban" relative humidity, as the surface water content of the roof is relatively constant (Figure 183b). The differences between the relative humidity above a green and a concrete roof are not as striking as for temperatures; a 18.2% is only reached at peak time, with a 10.8% day-time average.

For Mumbai, with its higher amounts of solar radiation and higher air temperature, the differences between the two roofs are even larger (comparison of Figure 185a and Figure 186a); surface temperatures reach a day-time average difference of 17.4°C, with 27.6°C peak. For the boundary air layer, these values become 11.4°C and 23.8°C, respectively, while for the air node 1m away they lower to 3.6°C and 8.0°C, respectively.

For the more saturated air of Mumbai, relative humidity differences between the two roofs are not as high as for Athens, reaching 2.7% day-time average difference and 11.1% maximum, for the boundary air node (comparison of Figure 185b and

[42] The term "typical" implies a day whose hourly values are the averaged hourly values of the examined month.

Figure 186b). For the air node 1m above the roof, these differences become even smoother, with a 0.4% day-time average and 2.9% maximum.

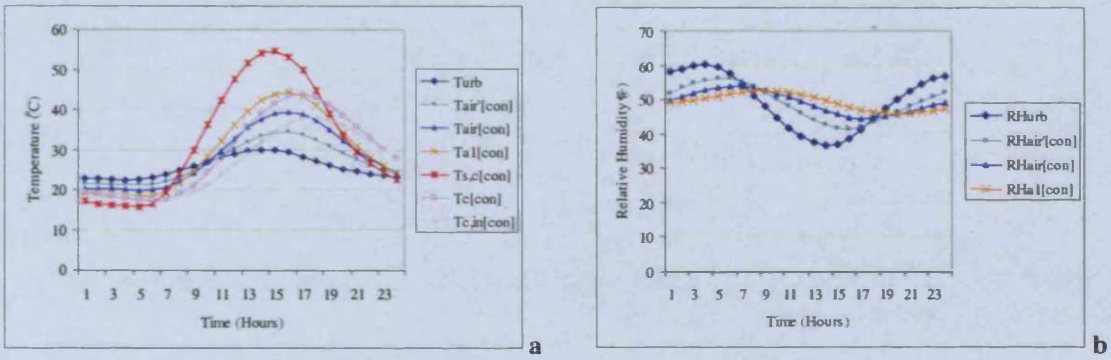

Figure 183. (a) Temperature and (b) relative humidity distributions at a concrete roof for a typical day in Athens, in July

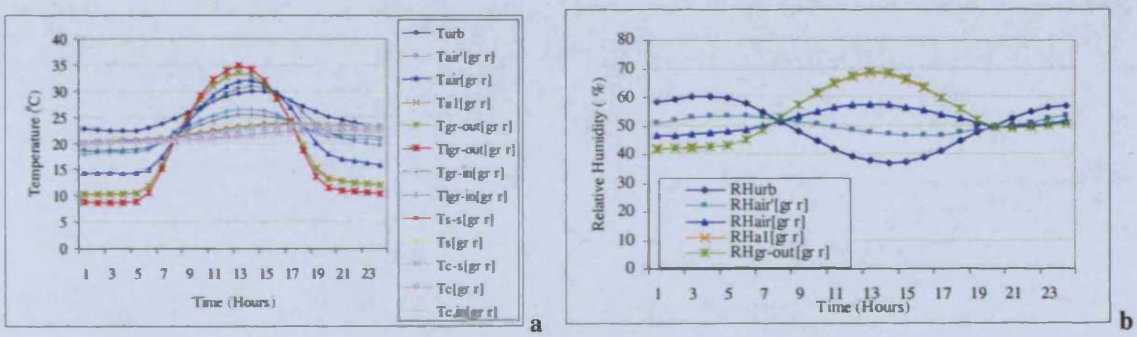

Figure 184. (a) Temperature and (b) relative humidity distributions at a green roof for a typical day in Athens, in July

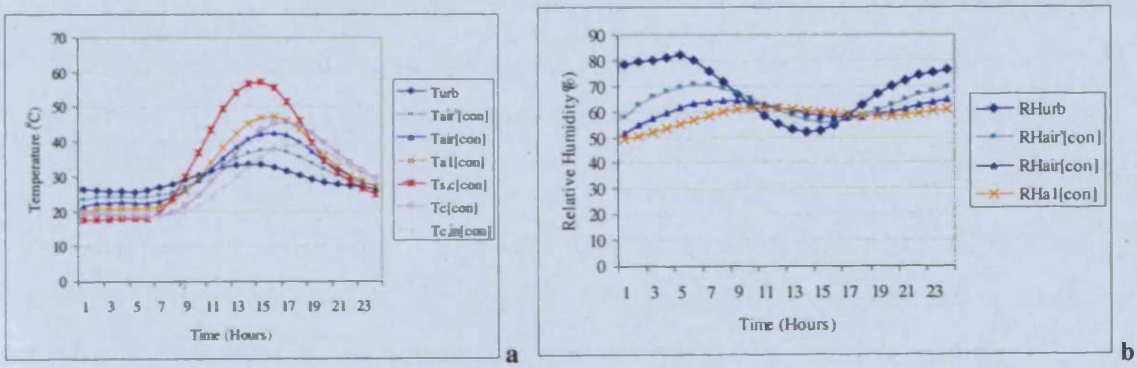

Figure 185. (a) Temperature and (b) relative humidity distributions at a concrete roof for a typical day in Mumbai, in Mai

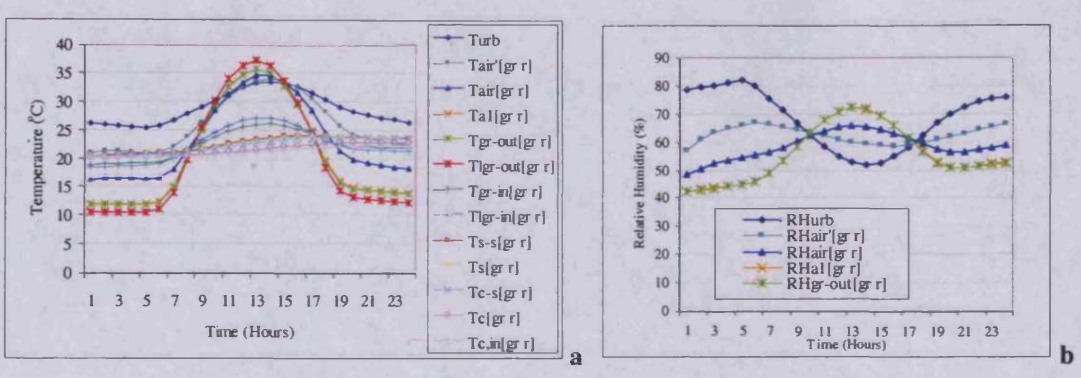

Figure 186. (a) Temperature and (b) relative humidity distributions at a green roof for a typical day in Mumbai, in Mai

The results for arid and hot Riyadh display the largest differences between concrete and green roofs (comparison of Figure 187a and Figure 188a). Surface temperature differences reach a 21.0°C day-time average and 29.5°C maximum. For the boundary air layer, these differences become 16.5°C and 27.1°C, respectively, while the air layer 1m above the roof shows a 5.2°C day-time average and 8.8°C maximum decrease.

As the evapotranspiration of plants increases humidity concentrations locally, in the very dry air of Riyadh, the differences between the relative humidity of the concrete and the green roof at the boundary layer are the largest ones. For the boundary air above the concrete roof, relative humidity reaches a 42.7% day-time average, while for the green-roof this average becomes 52.1% (comparison of Figure 187b and Figure 188b). The differences between the two reach a day-time average of the magnitude of 16.3% and 23.3% maximum, much larger than that of Athens or Mumbai.

In all of the cases examined, it has been shown that in all three dry, humid and arid climates, green roofs are capable of lowering not only surface temperatures, but also air temperatures above them (Table 12). The largest temperature decreases are noted for the arid climate of Riyadh (21.0°C day-time average and 29.5°C maximum, for the surface temperature) and the smallest ones for Athens (17.0°C day-time average and 26.2°C maximum, for the surface temperature). Relative humidity is also altered by the presence of plants; at the boundary layer of arid Riyadh it rises quite significantly (16.2% day-time average and 23.3% maximum), while for humid Mumbai these increases are much smaller (0.4% and 2.9%, respectively).

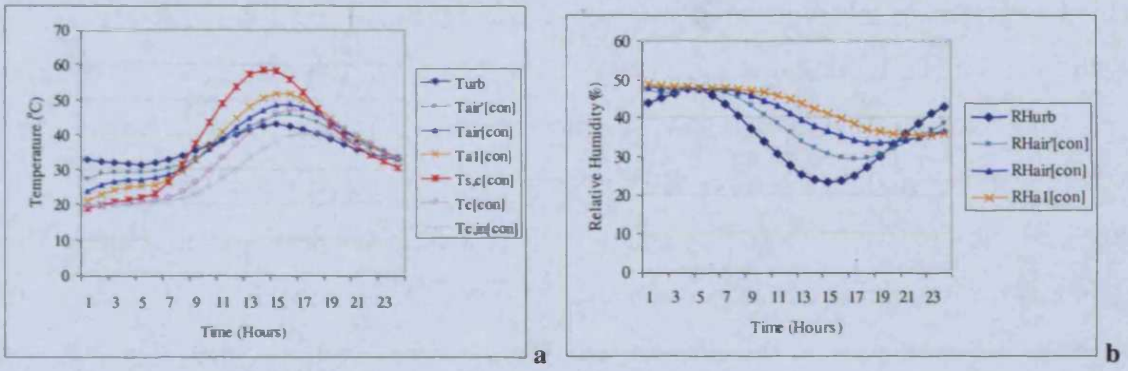

Figure 187. (a) Temperature and (b) relative humidity distributions at a concrete roof for a typical day in Riyadh, in July

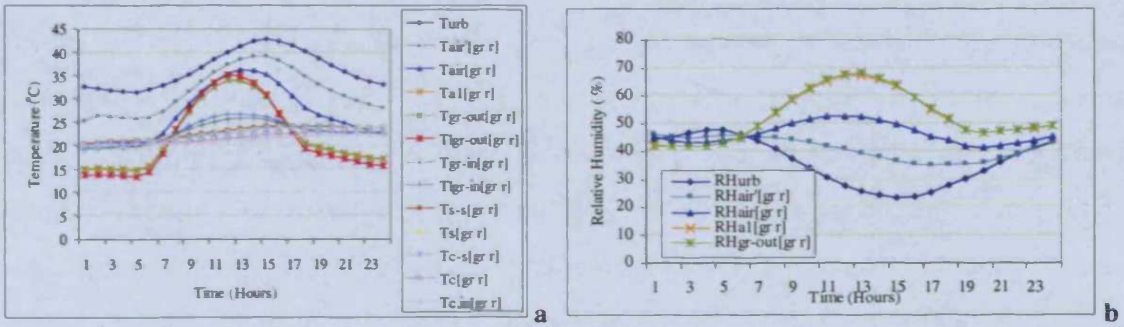

Figure 188. (a) Temperature and (b) relative humidity distributions at a green roof for a typical day in Riyadh, in July

Table 12. Average and maximum differences between temperatures and relative humidities at a concrete and a green roof

City	ΔTs (°C)		ΔTa1 (°C)		ΔRHa1 (%)		ΔTair' (°C)		ΔRHair' (%)	
	max	ave	max	ave	max	ave	max	ave	max	ave
Athens	26.2	17.0	22.4	10.2	18.2	10.8	7.3	3.1	4.7	2.6
Mumbai	27.6	17.4	23.8	11.4	11.1	2.7	8.0	3.6	2.9	0.4
Riyadh	29.5	21.0	27.1	16.5	23.3	16.3	8.8	5.2	5.6	3.8

4.12.3 Green Roofs Versus White Concrete Roofs

Before proceeding to the two-dimensional model it would be interesting to study the differences between a green roof and a white painted, concrete one. High albedo roofs (such as white ones) have been proven to cool down urban temperatures (Akbari et al., 1997; Taha, 1997; Konopacki, 1998). By decreasing surface temperature, with a coating which does not absorb a large part of incoming radiation, air temperature is also lowered. Nonetheless, such coatings need frequent maintenance, as, in most cases they loose 25% or more of their albedo within three years (Unknown, 2003). In this

paragraph, a green roof will be examined, versus a concrete roof without any coating (with a 0.23 albedo), which is the case discussed in paragraph 4.12.2, a concrete roof with white coating (0.70 albedo) and a concrete roof with white coating, 3 years after it has been applied (0.53 albedo). All four cases are examined for the climatic characteristics of Athens and Riyadh in July and Mumbai in May. In Figure 189-Figure 194, surface and air temperatures at the green roof are symbolised as [gr r], for the plain concrete roof as [con], [wh-con] for the white concrete roof and [old-wh-con] for the three-year-old, white-painted concrete roof.

In the case of Athens, as can be observed in Figure 189 and Figure 190, both the surface temperature of the green roof and the air temperature above it are higher than the white concrete's temperatures in the morning, for 7 hours, with a 3.5°C average difference at this time of the day. For the boundary air layer this difference becomes 4.1°C and for the air layer 1m above the roof, it reaches only 1.3°C. Later on during the day, as heat is stored up in the white concrete roof, its surface and air temperatures become higher than those of the green roof's, reaching a much larger average difference of 8.8°C for the surface, 8.1°C for the boundary layer and 2.7°C for the air layer 1m above the roof.

Three years after the coating has been applied ([old-wh-con] case), surface temperature of plants exceed that of the roof's only by a negligible 0.2°C (Figure 189), while the air above it slightly exceeds it by 1.6°C in the boundary layer and by 0.6°C at 1m height above the roof, in the morning (Figure 190). The rest of the day, the green roof shows much lower temperatures, by an average difference of 10.1°C for the surface, 11.2°C for the boundary air layer and 3.2°C for the air layer 1m above the roof.

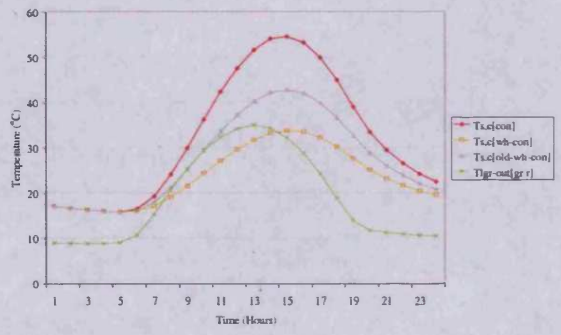

Figure 189. Comparison of surface temperature distributions of a concrete roof, a white concrete roof, a 3-year old white concrete roof and a green roof, for a typical day in Athens, in July

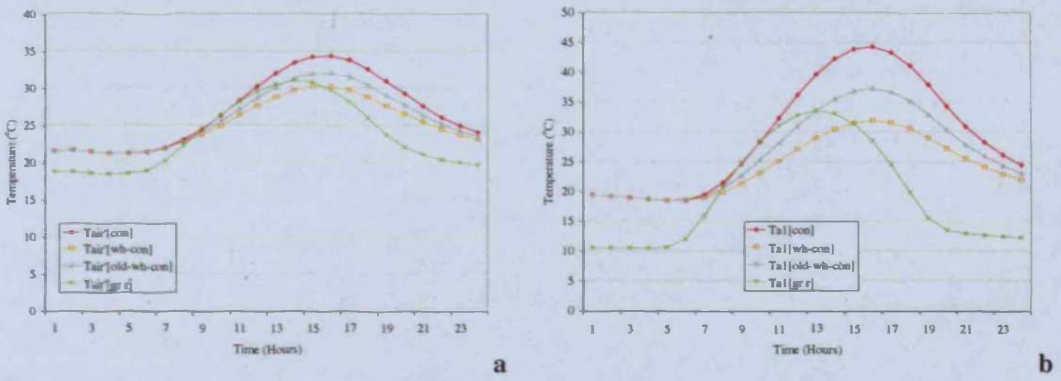

Figure 190. Comparison of air temperature distributions of a concrete roof, a white concrete roof, a 3-year old white concrete roof and a green roof (a) 1.0m above the roof and (b) 0.3m above the roof (boundary layer) for a typical day in Athens, in July

For Mumbai, with its slightly higher irradiation, the morning hours when the green roof has higher surface temperatures than the newly coated white concrete one, are 6, less than that for Athens. During this period, the average difference between the surface temperatures reaches 3.1°C (Figure 191). For the boundary air layer it reaches 3.5°C and for the air layer 1m above the roof 1.1°C (Figure 192), all three are slightly smaller than for Athens. The rest of the day differences between the lowered temperatures above the green roof and the higher white concrete ones are even larger, reaching an average difference of 10.5°C for the surface, 10.2°C for the boundary air layer and 3.4°C for the air layer 1m above the roof.

Three years after the coating has been applied, green roofs in Mumbai have a far cooler behaviour than the old white-coated concrete surface. Green surface temperature is still lower than that of the old white concrete surface, while the air temperature above the green roof exceeds that above the old white concrete roof by an average of 1.6°C for the boundary layer and 0.5°C at 1m height, for only 4 hours. For the rest of the day, temperature at the boundary air layer above the green roof is lower than the one above the old white roof by an average of 11.4°C and at 1m height this difference becomes 3.8°C. Regarding surface temperature, plants have a lower surface temperature than the old white roof throughout the whole day, by a 13.2°C average.

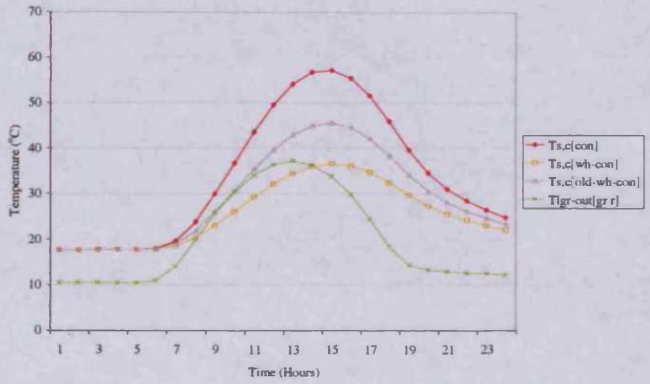

Figure 191. Comparison of surface temperature distributions of a concrete roof, a white concrete roof, a 3-year old white concrete roof and a green roof, for a typical day in Mumbai, in Mai

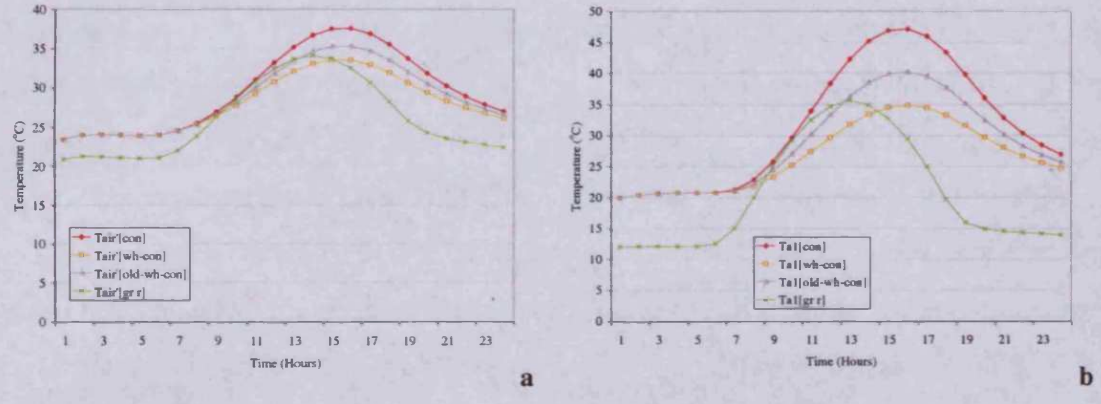

Figure 192. Comparison of air temperature distributions of a concrete roof, a white concrete roof, a 3-year old white concrete roof and a green roof (a) 1.0m above the roof and (b) 0.3m above the roof (boundary layer) for a typical day in Mumbai, in Mai

The optimum conditions for the green roof to cool its surroundings are those of the arid climate of Riyadh, with its high temperatures and insolation in July. Its surface temperature does not exceed the surface temperature of the white concrete roof (Figure 193), nor do air temperatures above it (Figure 194). For the freshly white coated roof, the day-time average difference between its surface temperature and the surface temperature of plants on the concrete roof, reaches 8.8°C. The day-time average temperature difference for the boundary air layer is 9.2°C and 2.8°C for the air layer 1m above the roof.

After three years, when the white paint's albedo has been reduced by 25%, these differences become even larger, with the green roof having a smaller surface temperature by a day-time average of 14.1°C. The difference between the two boundary air layers reaches 11.9°C and at 1m above the roof the day-time average difference is of the magnitude of 3.9°C.

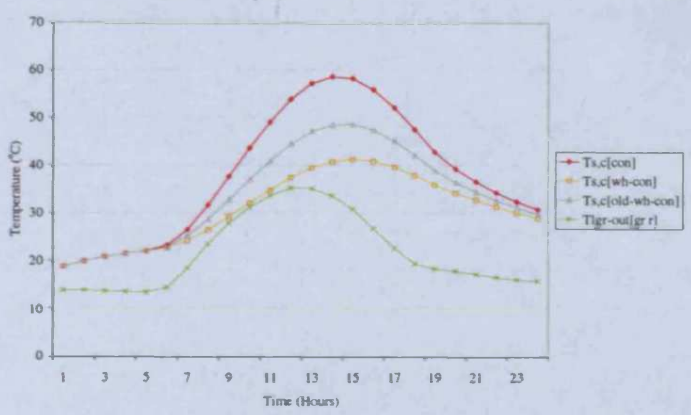

Figure 193. Comparison of surface temperature distributions of a concrete roof, a white concrete roof, a 3-year old white concrete roof and a green roof, for a typical day in Riyadh, in July

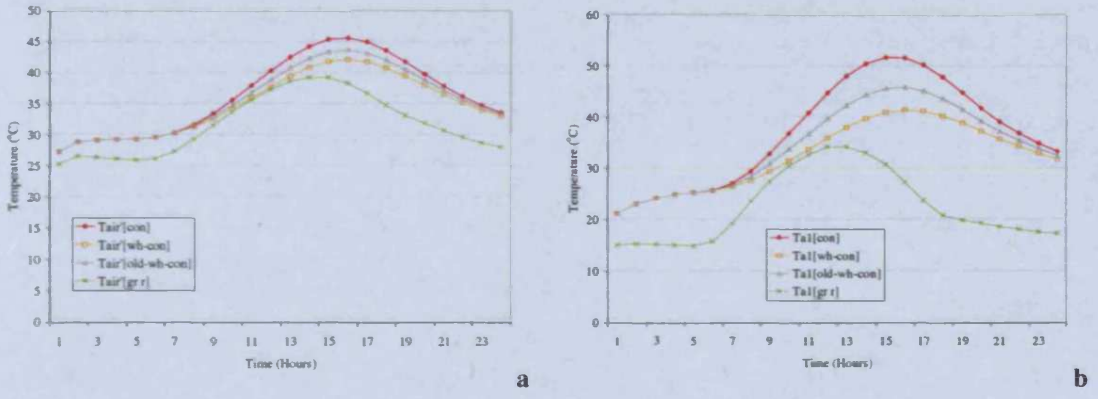

a b

Figure 194. Comparison of air temperature distributions of a concrete roof, a white concrete roof, a 3-year old white concrete roof and a green roof (a) 1.0m above the roof and (b) 0.3m above the roof (boundary layer) for a typical day in Riyadh, in July

The day-time average differences between a newly coated white concrete roof and a green roof are summarised in Table 13. The differences between the three-year-old white concrete roof and the green roof are given in Table 14. A distinction is made between the periods that the green roof has higher temperatures ([gr r]>[wh-con]) and the periods when its temperatures are lower ([gr r]<[wh-con]). In general, arid Riyadh seems to benefit more by green roofs than by white painted concrete ones. The city which benefits most from white painted roofs is Athens. Yet again, the periods when green roofs offer cooler effects than the white painted roofs are longer and of larger intensity, for all three climates. In all cases, the white coating loses its high albedo relatively quickly, and the amplitude of its difference with green roofs becomes even larger for all three cities examined. It could therefore be concluded, that to lower urban temperatures, it would be more effective, from a thermal point of view, to cover roofs with vegetation, than with white paint.

Table 13. Day-time average temperature differences (in °C) between a white coated concrete roof and a green one

City	ΔTs ([grr]>[wh-con])	ΔTs ([grr]<[wh-con])	ΔTal ([grr]>[wh-con])	ΔTal ([grr]<[wh-con])	ΔTair' ([grr]>[wh-con])	ΔTair' ([grr]<[wh-con])
Athens	3.5	8.8	4.1	8.1	1.3	2.7
Mumbai	3.1	10.5	3.5	10.2	1.1	3.4
Riyadh	-	8.8	-	9.2	-	2.8

Table 14. Day-time average temperature differences (in °C) between a three-year-old white coated concrete roof and a green one

City	ΔTs ([grr]>[old-wh-con])	ΔTs ([grr]<[old-wh-con])	ΔTal ([grr]>[old-wh-con])	ΔTal ([grr]<[old-wh-con])	ΔTair' ([grr]>[old-wh-con])	ΔTair' ([grr]<[old-wh-con])
Athens	0.2	10.1	1.6	11.2	0.6	3.2
Mumbai	-	13.2	1.6	11.4	0.5	3.8
Riyadh	-	14.1	-	11.9	-	3.9

4.13 Summary

In this chapter the one dimensional model describing heat and mass transfer at a plain and a green roof and the air layer above them has been presented. Governing heat and mass transfer equations have been solved with finite difference approximations. In order to test the model's validity, these solutions have been compared with an experiment, measuring temperature and humidity at a concrete and a green test cell. The convergence between measurements and calculations has been satisfactory, proving the validity of the model's prognostic outputs. The importance of expressing the thermal diffusion in heat transfer has been pointed out, through experimental and theoretical work.

Using the model, one-dimensional simulations have been carried out, assuming no wind in the air, to compare concrete and green roofs for three different climatic types (hot and dry Athens, hot and humid Mumbai and hot and arid Riyadh). It has been proved that the more solar radiation a roof receives and the drier the air is, the more beneficial it is to cover the roof with vegetation. For Riyadh, the roof's surface temperature decreases by an average of 21.0°C and the air temperature 1m above it by 5.2°C, while for Athens these numbers become 17.0°C and 3.1°C, respectively and for Mumbai 17.4°C and 3.6°C, respectively.

Regarding the comparison between green roofs and white roofs, it has been pointed out that although white roofs might result in lower temperatures during the morning, nonetheless, green roofs result in lower temperatures throughout the afternoon and evening and their effects are of a much larger intensity. In the case of arid Riyadh, green roofs have lower temperatures than white ones, even in the morning (Table 13). As the albedo of white roofs lowers quite quickly, a comparison is also carried out with roofs of lowered reflectivity (Table 14), where differences are even larger and green roofs have lower temperatures than the old white ones, practically the whole day. From this comparison, it can be argued that in order to decrease urban temperatures, it is more effective, from a thermal point of view, to cover roofs with vegetation than with white paint.

4.14 References

1. L. Adelard, F. Pignolet-Tardan, T. Mara, P. Lauret, F. Garde, and H. Boyer (1998) *Sky Temperature Modelisation and Applications in Building Simulation.* Renewable Energy, Vol. 15, pp 418-430.
2. H. Akbari, S. Bretz, D.M. Kurn, and J. Hanford (1997) *Peak Power and Cooling Energy Savings of High-Albedo Roofs.* Energy and Buildings, Vol. 25, pp 117-126.
3. E. Alexandri and P. Jones (2003) *Micro-scale Modelling of the Thermal Effects of Green Roofs.* PLEA 2003, Santiago, Chile.
4. R.G. Allen, L.S. Pereira, D. Raes and M. Smith (1998) *Crop Evapotranspiration - Guidelines for Computing Crop Water Requirements - FAO Irrigation and Drainage Paper 56. FAO* - Food and Agriculture Organization of the United Nations, Rome.
5. W.F. Ames (1977) *Numerical Methods for Partial Differential Equations.* Academic Press, New York, San Francisco.
6. ASHRAE (1985) *ASHRAE Handbook, 1985 Fundamentals, SI Edition.* American Society of Heating, Cooling and Air-Conditioning Engineers, Inc., Atlanta.
7. P.-A. Bois (2002) *Singularités de la Rhéologie de l'Air Humide Saturé et Diffusion Moléculaire dans les Milieux Nuageux.* C. R. Mecanique Vol. 330 (2002), pp 627–632.

8. R.M.L. Coelho and A.S. Telles (2002) *Extended Graetz Problem Accompanied by Dufour and Soret Effects.* International Journal of Heat and Mass Transfer Vol. 45 (2002), pp 3101–3110.
9. G.M. Dusinberre (1961) *Heat-Transfer Calculations by Finite Differences.* International Textbook Company, Scranton.
10. E.R.G. Eckert and R.M. Drake (1959) *Heat and Mass Transfer.* McGraw-Hill Book Company Inc., New York, Toronto, London.
11. G.-s. Enrique, I. Braud, J.-L. Thony, M. Vauclin., P. Bessemoulin and J.-C. Calvet (1999) *Modelling Heat and Water Exchanges of Fallow Land Covered with Plant-Residue Mulch.* Agriculture and Forest Meteorology, Vol. 97, pp 151-169.
12. E. Eumorfopoulou and D. Aravantinos (1998) *The Contribution of a Planted Roof to the Thermal Protection of Buildings in Greece.* Energy and Buildings, Vol. 27, pp 29-36.
13. G.E. Forsythe and W.R. Wasow (1960) *Finite-Difference Methods for Partial Differential Equations.* John Wiley and Sons, Inc., New York, London.
14. D.M. Gates (1980) *Biophysical Ecology.* Springer-Verlag, New York.
15. R.C. Gaur and N.K. Bansal (2002) *Effect of Moisture Transfer across Building Components on Room Temperature.* Building and Environment, Vol. 37, pp 11-17.
16. R. Geiger (1965) *The Climate near the Ground.* Harvard University Press, Cambridge, Massachusetts.
17. D. Gilliaert, A. Landabaso, W.B. Gillett, and P.A. Ruyssevelt (1992) *Guidelines for the Assessment of Active and Passive Solar Technologies.* Institute for Systems Engineering and Informatics, Joint Research Centre, Commission of the European Communities.
18. J.P. Holman (2002) *Heat Transfer.* McGraw Hill, Boston, New York.
19. W. Hort, S.J. Linz and M. Lücke (1992) *Onset of Convection in Binary Gas Mixtures: Role of the Dufour Effect.* Physical Review A, Vol. 45, No. 6, pp 3737-3748.
20. M.Z. Jacobson (1999) *Fundamentals of Atmospheric Modeling.* Cambridge University Press, Cambridge.
21. H.G. Jones (1992) *Plants and Microclimate.* Cambridge University Press, Cambridge.

22. S. Konopacki, L. Gartland, H. Akbari and L. Rainer (1998) *Demonstration of Energy Savings of Cool Roofs.* A Report Prepared for the U.S. Environmental Protection Agency, Heat Island Project, University of California, Berkeley.
23. J.P. Lhomme (1981) *La Fonctionnement de l'Atmosphère au Niveau de son Interface avec une Vegetation: Étude de la Dynamique des Échanges de Masse et d'Énergie Liée aux Fluctuations Climatiques.* Thèse de Docteur-Ingenieur, Paris 6 (Université Pierre et Marie Curie).
24. E.J. List (1982) Mechanics of Turbulent Buoyant Jets and Plumes. *In:* W. Rodi (ed.) *Turbulent Buoyant Jets and Plumes.* Pergamon Press, Oxford, New York, pp 1-68.
25. X. Lü (2002) *Modelling of Heat and Moisture Transfer in Buildings; I. Model Program.* Energy and Buildings, Vol. 34 (2002), pp 1033-1043.
26. A.V. Luikov (1961) *Heat and Mass Transfer in Capillary-Porous Bodies.* Pergamon Press, Oxford, London, New York.
27. J.L. Monteith and M. Unsworth (1990) *Principles of Environmental Physics.* Edward Arnold, London, New York.
28. J. Noilhan (1979) *Les Facteurs Physiques du Microclimat au Voisinage d'un Batiment. Etude bibliographique.* Centre Scientifique et Tecnique du Batiment, Etablissement de Nantes.
29. H. Nowak (1989) *The Sky Temperature in Net Radiant Heat Loss Calculations from Low-Sloped Roofs.* Infrared Physics, Vol. 29, No. 2-4, pp 231-232.
30. T.R. Oke (1987) *Boundary Layer Climates.* Routledge, London.
31. T.R. Oke (1999) *Observing Urban Weather and Climate Using "Standard" Stations.* Available from http://www.meteo.bg/EURASAP/35/paper1.html [Accessed 25th January 2002].
32. A. Olioso and C. Bocquillon (1992) *Simulation des Échanges d'Énergie et de Masse d'un Couvert Vegetal dans le But de Relier la Transpiration et la Photosynthèse aux Mesures de Reflectance et de Temperature de Surface.* Thèse Doctorat, Sciences Biologiques Fondamentales et Appliquées. Montpellier 2.
33. E. Palomo Del Barrio (1998) *Analysis of the Green Roofs Cooling Potential in Buildings.* Energy and Buildings, Vol. 27 (1998), pp 179-193.
34. G. Papaioannou, G. Nikolidakis, D. Asimakopoulos and D. Retalis (1996) *Photosynthetically Active Radiation in Athens.* Agricultural and Forest Meteorology, Vol. 81, pp 287-298.

35. A. Perrier (1976) *Etude et Essai de Modélisation des Echanges de Mass et d'Energie au Niveau des Couverts Végétaux: Profils Microclimatiques, Evapotranspiration et Photosynthèse Nette.* Doctorat d'Etat, Paris 6 (Université Pierre et Marie Curie).
36. R.A. Pielke (2002) *Mesoscale Meteorological Modeling.* Academic Press, San Diego, San Francisco, New York.
37. F. Pignolet-Tardan, P. Depecker, F. Garde, L. Adelard, J.C. Gatina (1997) *Modelling of the Heat Island Generated by an Urban Unit.* Proceedings of International Building Performance Simulation Association 97, Volume 3: pp. 41-48. Available from http://www.ibpsa.org/bs_97.htm [Accessed 3rd December 2001].
38. J. Ross (1975) Radiative Transfer in Plant Communities. *In:* J. L. Monteith (ed) *Vegetation and the Atmosphere. Volume 1, Principles.* Academic Press, London, New York, San Francisco, pp 13-55.
39. A.J. Rutter (1975) The Hydrological Cycle in Vegetation *In:* J. L. Monteith (ed) *Vegetation and the Atmosphere. Volume 1, Principles.* Academic Press, London, New York, San Francisco, pp 111-154.
40. Ch.S. Sachsamanoglou and T.I. Makrogiannis. (1998) *General Meteorology.* Ziti Editions, Thessalonica.
41. R.E. Scraton (1968) *Elementary Numerical Methods.* Heinemann Educational Books Ltd, London.
42. H. Taha (1997) *Urban Climates and Heat Islands: Albedo, Evapotranspiration, and Anthropogenic Heat.* Energy and Buildings, Vol. 25, pp 99-103.
43. T. Takakura, S. Kitade and E. Goto (2000) *Cooling Effect of Green Cover over a Building.* Energy and Buildings, Vol. 31 (2000), pp 1-6.
44. A.S. Thom (1975) Momentum, Mass and Heat Exchange. *In:* J. L. Monteith (ed) *Vegetation and the Atmosphere. Volume 1, Principles.* Academic Press, London, New York, San Francisco, pp 57-109.
45. R. Tournebize, H. Sinoquet and F. Bussière (1996) *Modelling Evapotranspiration Partitioning in a Shrup/Grass Alley Crop.* Agricultural and Forest Meteorology, Vol. 81, pp 255-272.
46. Unknown (2003) *Cool Roof Rating Council Product Listing, As of May 5, 2003.* Available from http://www.coolroofs.org [Accessed 13-5-2003]

47. H.K. Versteeg and W. Malalasekera (1995) *An Introduction to Computational Fluid Dynamics.* Prentice Hall, Harlow, London, New York.

48. P.E. Waggoner (1975) Micrometeorological Models. *In:* J. L. Monteith (ed) *Vegetation and the Atmosphere. Volume 1, Principles.* Academic Press, London, New York, San Francisco, pp 205-228.

49. N. Webb (ed) (1999) *AP4 Porometer User Manual.* Delta-T Devices Ltd, Cambridge.

50. C.M. Willmer (1983) *Stomata.* Longman Inc., New York.

51. L. Wu (1996) *An Itegration of a Surface Energy Balance Climate Model with TIN and GRID in GIS.* Third International Conference Workshop on Integrating GIS and Environmental Modeling, Santa Fe, CD.

52. E. Zeiger, G.D. Farquhar and I.R. Cowan (eds) (1987) *Stomatal Function.* Stanford University Press, Stanford.

53. J.Q. Zhang, X.P. Fang, H.X. Zhang, W.Yang and C.C. Zhu (1997) *A Heat Balance Model for Partially Vegetated Surfaces.* Infrared Physics & Technology, Vol. 38, pp 287-294.

Chapter 5

Two Dimensional Model

5 Two Dimensional Model

In order to fully describe the microclimatic characteristics of an urban canyon and the effect of green roofs in it, the one-dimensional model described in the previous chapter, has to be developed into two or three dimensions. Assuming a canyon with a length long enough to ignore divergence in its axis, phenomena could be described with a two dimensional model. In this chapter, the evolution of the one dimensional model described in chapter 4 to a two dimensional model is presented. A diagnostic estimation of the temperature decrease due to green roofs at a mesoscale level is also carried out.

5.1 Meso-Scale Estimations

Before proceeding to the development of the two-dimensional model, a rough estimation of the thermal effects of green roofs is approximated on a meso-scale. Meso-scale can give an estimation of the temperature decrease at an urban scale, as a local meteorological phenomenon (Oke, 1999a). In this paragraph, a diagnostic estimation is performed for the averaged air temperature above the city.

In order to study the phenomenon in meso scale, the energy balance is used:

Energy input = energy output + energy storage

Which can lead to a diagnostic estimation of the air temperature decrease, due to green roofs, without describing the phenomena of heat and mass transfer in detail, but only through the balance of measured or estimated heat fluxes. Generally, when there is water evaporation or condensation in the atmosphere the energy released or absorbed (latent heat of vaporisation/condensation) is of the magnitude of $2.49 \cdot 10^6 J/kgrH_2O$. If an urban module is considered, the energy balance of a building-air volume is given by the relation (Oke, 1987):

$$Q^* + Q_F = Q_H + Q_E + \Delta Q_S + \Delta Q_A \qquad \text{Eq. 155}$$

Where:

Q^*: net all-wave radiation (W/m^2)

Q_F: heat due to anthropogenic heat release (W/m^2)

Q_H: sensible heat (W/m^2)

Q_E: latent heat (W/m^2)

ΔQ_S: net rate of physical heat storage by the urban texture (W/m^2)

ΔQ_A: net energy gain or loss through advection, due to horizontal sensible and latent heat transport (W/m^2)

If water is evaporated in an air mass whose temperature is T, then the temperature change is (Sachsamanoglou and Makrogiannis, 1998):

$$dT = -\frac{Q_E}{c_{pa}} \cdot dr_s \qquad \textbf{Eq. 156}$$

Where:

c_{pa}: isobaric specific heat capacity of dry air (1005J/kgrK)

dr_s: difference of the mixing ratio (ratio of the mass of water vapour to the mass of dry air with which they make up humid air)

By solving this differential relationship, air temperature due to the evaporation of water in the atmosphere is given by the relationship:

$$T_w = T - \frac{[r(T) - r_s(T_w)] \cdot Q_E}{c_{pa}} \qquad \textbf{Eq. 157}$$

By adding vegetation in an existing urban environment, its heat flux due to evaporation (Q_E) is increased. The evapotranspiration rate of a specific crop (ET_c) is given by the relationship:

$$ET_c = K_c ET_o \qquad \textbf{Eq. 158}$$

Where ET_o is the reference crop evapotranspiration [mm/day] and K_c is a crop factor, which takes into consideration the crop type, its variety and development stage, its height, roughness, reflection, resistance to transpiration, its rooting characteristics and the ground cover.

The reference crop evapotranspiration (ET_o), according to the FAO Penman-Monteith method is defined as (Allen et al., 1998):

$$ET_o = \frac{0.408\Delta(R_n - G) + \gamma \frac{900}{T + 273} u_2 (e_s - e_a)}{\Delta + \gamma(1 + 0.34u_2)} \qquad \textbf{Eq. 159}$$

Where:

R_n: net radiation at the crop surface (MJ/m^{2}day)

G: soil heat flux density (MJ/m^{2}day)

T: mean daily air temperature at 2m height (^{o}C)

u_2: wind speed at 2m height (m/s)

e_s: saturation vapour pressure (kPa)[43]

e_a: actual vapour pressure (kPa)

$e_s - e_a$: saturation vapour pressure deficit (kPa)

Δ: slope vapour pressure curve (kPa/^{o}C)

γ: psychrometric constant (kPa/^{o}C)

In order to estimate the meso-scale effect of green roofs, existing measurements have been used. The estimation is based on measurements of Mexico City, Mexico (Oke, 1999b) and Vancouver, Canada (Oke, 1987). The methodology followed is that all measured heat fluxes, described in equation 155 remain constant (net all-wave radiation and net rate of physical heat storage in the urban texture), while latent heat changes, according to the amount of vegetation that is inputted. Sensible heat is altered, due to the latent heat changes, causing a temperature change. This temperature change is estimated from equation 157. The results for the urban temperature, for different percentages of covering of the city roofs with vegetation (grass) (10% of the city's roofs, 20%, 50%, 70% and 100%) are summarised in the following figures:

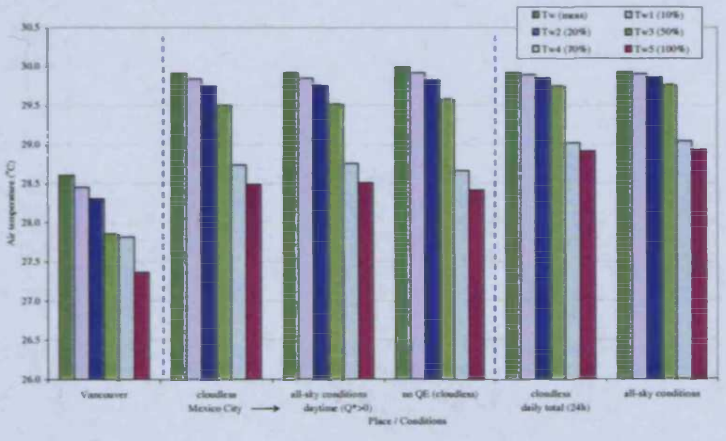

Figure 195. Urban temperature in Vancouver and Mexico city, without any green roofs [Tw(meas)] and with 10%, 20%, 50%, 70% and 100% of the city's roofs covered with grass plants (Tw1, Tw2, Tw3, Tw4, and Tw5, respectively)

[43] Pressure is expressed in kPa in this formula, instead of Pa in which it was expressed in chapter 4, for reasons of consistency of the units used in the model presented in chapter 4 and the units used for equation 159.

Table 227. Comparison of temperature decreases (in °C) of the canyon walls for green-roofs, green-walls and green-all, for H5W10, N-S orientation, wind flow parallel to the canyon, Riyadh

	ΔTw1,d, surf		ΔTw1,d, air		ΔTw2,d, surf		ΔTw2,d, air		ΔTw1,a, surf		ΔTw2,a, surf	
	Max	Ave	Max	Ave	Max	Ave	Max	Ave	Max	Ave	Max	Ave
Green roofs	0.4	0.3	0.2	0.0	0.4	0.2	0.3	0.2	0.4	0.2	0.2	0.1
Green walls	19.4	14.6	17.5	11.8	20.0	12.7	11.7	6.0	18.8	14.0	12.5	5.6
Green all	19.4	14.6	17.6	11.8	20.0	12.7	11.9	6.2	18.8	14.0	12.5	5.6

Table 228. Comparison of temperature decreases (in °C) above the roofs, for green-roofs, green-walls and green-all, for H5W10, N-S orientation, wind flow parallel to the canyon, Riyadh

	ΔTrf, surf		ΔTrf, air		ΔTrf,f		ΔTrf,g		ΔTrf,h	
	Max	Ave	Max	Ave	Max	Ave	Max	Ave	Max	Ave
Green roofs	30.9	16.5	31.3	15.1	26.4	12.6	21.4	10.2	13.4	6.4
Green walls	0.0	0.0	0.0	0.0	0.1	0.0	0.1	0.0	0.0	0.0
Green all	30.6	16.3	31.0	14.9	26.3	12.6	21.3	10.1	13.3	6.4

Table 229. Comparison of temperature decreases (in °C) above the canyon, for green-roofs, green-walls and green-all, for H5W10, N-S orientation, wind flow parallel to the canyon, Riyadh

	ΔTf,VIII		ΔTg,VIII		ΔTh,VIII		ΔTf,XI		ΔTg,XI		ΔTh,XI	
	Max	Ave	Max	Ave	Max	Ave	Max	Ave	Max	Ave	Max	Ave
Green roofs	1.5	0.8	2.0	1.2	1.1	0.6	2.1	0.9	3.2	1.3	1.7	0.7
Green walls	9.1	6.0	7.1	4.7	4.2	2.8	2.0	1.3	1.6	1.1	0.9	0.6
Green all	11.2	7.8	8.8	6.2	5.2	3.6	7.2	5.0	5.7	3.9	3.3	2.3

6.2.15.5 Riyadh, H5W15, East-West Orientation, Wind Flow Perpendicular to the Canyon

Concerning different geometries in arid Riyadh, the effect of vegetation is stronger on narrower H5W10 canyon, than on the wider H5W15 canyon. Yet, the differences between the temperature decreases of the two geometries are not as large as for more humid Mumbai and Athens. The differences between the air temperature decrease of the two geometries inside the canyon reach an average of 1.9°C, for the green-all case, while this difference is 1.5°C for more humid Athens and 1.4°C for much more humid Mumbai. For the green-walls case the difference between the two geometries becomes

more evident, with an average difference of 3.7°C (this value being 2.2°C for Athens and 2.1°C for Mumbai). In general, the E-W-oriented H5W15 canyon reaches air temperature decreases of maxima from 8.4°C to 11.3°C and daytime averages from 5.0°C to 9.1°C for the green-all case (Table 230). The effect is weaker for the green-walls case, with maxima from 1.2°C to 3.2°C and daytime averages from 0.4°C to 0.8°C, while it is unnoticeable for the green-roofs case. Asphalt surface temperature decreases reach a maximum of 1.3°C and daytime average of 0.8°C, while these values were 2.0°C and 1.2°C, respectively, for the H5W10 canyon. Regarding wall surface temperature decreases (Table 231), north-oriented wall reaches averaged maximum of 13.9°C and daytime average of 10.3°C, while these values become 12.3°C and 8.7°C, respectively, for the south-oriented wall.

Table 230. Comparison of temperature decreases (in °C) inside the canyon for green-roofs, green-walls and green-all, for H5W15, E-W orientation, wind flow perpendicular to the canyon, Riyadh

	ΔTasph, surf		ΔTasph, air		ΔTa,VIII		ΔTa,XI		ΔTd,VIII		ΔTd,XI	
	Max	Ave	Max	Ave	Max	Ave	Max	Ave	Max	Ave	Max	Ave
Green roofs	0.0	0.0	0.0	0.0	0.2	0.0	0.2	0.1	0.1	0.1	0.4	0.1
Green walls	1.3	0.8	1.3	0.8	1.8	0.8	1.2	0.5	3.2	0.5	2.1	0.4
Green all	1.3	0.8	12.3	9.7	11.3	9.1	11.0	8.5	9.3	6.2	8.4	5.0

Table 231. Comparison of temperature decreases (in °C) of the canyon walls for green-roofs, green-walls and green-all, for H5W15, E-W orientation, wind flow perpendicular to the canyon, Riyadh

	ΔTw1,d, surf		ΔTw1,d, air		ΔTw2,d, surf		ΔTw2,d, air		ΔTw1,a, surf		ΔTw2,a, surf	
	Max	Ave	Max	Ave	Max	Ave	Max	Ave	Max	Ave	Max	Ave
Green roofs	0.0	0.0	0.5	0.0	0.0	0.0	0.0	0.0	0.0	0.0	0.0	0.0
Green walls	20.0	15.1	17.6	10.8	7.7	5.4	4.1	2.4	19.4	14.5	5.1	2.9
Green all	20.0	15.1	17.7	11.0	7.7	5.4	4.3	2.4	19.4	14.5	5.1	2.9

Regarding temperature decreases above the roof, they are of the same magnitude as those of the H5W10 canyon. The canyon geometry does not affect temperature decreases at roof level. As can be observed in Table 232, the largest decreases are noted on the roof's surface (30.1-30.3°C maximum, 15.9-16.2°C daytime average) to the lowest, but still significant ones, 6m above the roof (12.7-12.8°C maximum and 5.9-6.0°C daytime average). Concerning temperature decreases above the canyon (Table 233) they are much lower than for the H5W10 geometry. The average

differences between the decreases of the two geometries reach 1.1°C for the green-all case, 2.2°C for the green-walls cases and even larger (4.3°C) for the green-roofs case. Temperature decreases for the E-W-oriented H5W15 canyon range from 4.1°C averaged for green-all, 1.0°C for green-walls and 0.3°C for green-roofs. It is noted that the green-roofs case has the weakest effect at the air layer above the canyon, than for any of the other geometries examined. The wider the canyon becomes, the weaker the effect of green roofs on the air layer above the canyon.

Table 232. Comparison of temperature decreases (in °C) above the roofs, for green-roofs, green-walls and green-all, for H5W15, E-W orientation, wind flow perpendicular to the canyon, Riyadh

	ΔTrf, surf		ΔTrf, air		ΔTrf,f		ΔTrf,g		ΔTrf,h	
	Max	Ave	Max	Ave	Max	Ave	Max	Ave	Max	Ave
Green roofs	30.1	15.9	30.3	14.4	25.3	11.8	20.5	9.6	12.8	6.0
Green walls	0.0	0.0	0.0	0.0	0.0	0.0	0.0	0.0	0.0	0.0
Green all	30.3	16.2	30.6	14.7	25.2	11.8	20.4	9.4	12.7	5.9

Table 233. Comparison of temperature decreases (in °C) above the canyon, for green-roofs, green-walls and green-all, for H5W15, E-W orientation, wind flow perpendicular to the canyon, Riyadh

	ΔTf,VIII		ΔTg,VIII		ΔTh,VIII		ΔTf,XI		ΔTg,XI		ΔTh,XI	
	Max	Ave	Max	Ave	Max	Ave	Max	Ave	Max	Ave	Max	Ave
Green roofs	0.9	0.2	0.8	0.7	0.8	0.5	1.2	0.1	0.9	0.4	0.3	0.1
Green walls	2.5	0.7	2.0	1.0	2.1	1.4	2.3	0.4	2.2	0.9	2.0	1.6
Green all	6.6	4.8	5.6	4.2	4.7	3.4	7.3	4.6	6.0	4.2	4.1	3.5

6.2.15.6 Riyadh, H5W15, North-South Orientation, Wind Flow Perpendicular to the Canyon

As was the case in the previous climates and geometries examined, the N-S-oriented H5W15 canyon has very similar, but slightly lower decreases than the E-W-oriented canyon. For the air layer inside the canyon, the differences between the E-W- and the N-S-oriented H5W15 canyons reach an average of 0.1°C for both the green-walls and green-all cases. When compared to the N-S-oriented H5W10 canyon, the differences become larger, reaching an average of 1.8°C for the green-all case and 2.7°C for the green-walls case. Temperature decreases inside the canyon for the

H5W15 geometry are summarised in Table 234-Table 235. Maximum decreases from 8.4°C to 13.4°C are reached for the green-all case with daytime average from 4.7°C to 9.1°C. For the green-walls case maximum decreases range from 1.0°C to 2.1°C and daytime averages from 1.1°C to 0.5°C and they are almost negligible for the green-roofs case. Surface temperatures decrease by a daytime average of 2.1-3.9°C and a maximum of 4.2-8.4°C for the west-oriented wall and 15.7-18.2°C and 9.6-13.5°C, respectively, for the east-oriented wall.

Table 234. Comparison of temperature decreases (in °C) inside the canyon for green-roofs, green-walls and green-all, for H5W15, N-S orientation, wind flow perpendicular to the canyon, Riyadh

	ΔTasph, surf		ΔTasph, air		ΔTa,VIII		ΔTa,XI		ΔTd,VIII		ΔTd,XI	
	Max	Ave	Max	Ave	Max	Ave	Max	Ave	Max	Ave	Max	Ave
Green roofs	0.0	0.0	0.0	0.0	0.2	0.1	0.2	0.1	0.5	0.4	0.4	0.2
Green walls	1.2	0.7	1.2	0.7	1.4	0.6	1.0	0.3	2.1	0.5	1.6	1.1
Green all	1.2	0.7	13.4	9.8	12.5	9.1	12.0	8.9	8.5	5.8	8.4	4.7

Table 235. Comparison of temperature decreases (in °C) of the canyon walls for green-roofs, green-walls and green-all, for H5W15, N-S orientation, wind flow perpendicular to the canyon, Riyadh

	ΔTw1,d, surf		ΔTw1,d, air		ΔTw2,d, surf		ΔTw2,d, air		ΔTw1,a, surf		ΔTw2,a, surf	
	Max	Ave	Max	Ave	Max	Ave	Max	Ave	Max	Ave	Max	Ave
Green roofs	0.0	0.0	0.1	0.0	0.0	0.0	0.0	0.0	0.1	0.0	0.0	0.0
Green walls	18.8	14.2	15.7	9.6	8.4	3.9	3.3	2.0	18.2	13.5	4.2	2.1
Green all	18.8	14.2	15.9	9.8	8.4	3.9	3.3	2.1	18.2	13.5	4.2	2.1

Regarding temperature decreases above the roof, they are summarised in Table 236. They are of the same magnitude as for the E-W-oriented canyon (paragraph 6.2.15.5). Temperature decreases above the canyon are of very similar magnitude as the E-W-oriented H5W15 decreases, with average differences between the two orientation of 0.1°C for the green-all case and 0.2°C for both the green-walls and green-roofs cases. The differences between the temperature decreases of the two geometries of the same orientation (N-S-oriented H5W10 and H5W15) reach averages of 0.8°C for the green-all case, 1.9°C for the green-walls case and 0.4°C for the green-roofs cases, with decreases being larger for the H5W10 geometry. For the N-S-oriented H5W15 canyon, temperature decreases reach averaged values of 4.0°C

for the green-all case, 0.8°C for the green-walls case and 0.5°C for the green-roofs cases (Table 237).

Table 236. Comparison of temperature decreases (in °C) above the roofs, for green-roofs, green-walls and green-all, for H5W15, N-S orientation, wind flow perpendicular to the canyon, Riyadh

	ΔTrf, surf		ΔTrf, air		ΔTrf,f		ΔTrf,g		ΔTrf,h	
	Max	Ave	Max	Ave	Max	Ave	Max	Ave	Max	Ave
Green roofs	30.1	15.9	30.3	14.4	25.3	11.8	20.5	9.6	12.8	6.0
Green walls	0.0	0.0	0.0	0.0	0.0	0.0	0.0	0.0	0.0	0.0
Green all	30.3	16.2	30.6	14.7	25.2	11.8	20.4	9.4	12.7	5.9

Table 237. Comparison of temperature decreases (in °C) above the canyon, for green-roofs, green-walls and green-all, for H5W15, N-S orientation, wind flow perpendicular to the canyon, Riyadh

	ΔTf,VIII		ΔTg,VIII		ΔTh,VIII		ΔTf,XI		ΔTg,XI		ΔTh,XI	
	Max	Ave	Max	Ave	Max	Ave	Max	Ave	Max	Ave	Max	Ave
Green roofs	0.9	0.5	0.8	0.4	0.8	0.5	1.0	0.6	0.9	0.9	0.4	0.1
Green walls	1.7	0.4	1.5	0.8	2.0	1.4	1.9	0.1	2.0	0.6	2.0	1.6
Green all	6.5	4.5	5.9	4.1	5.0	3.4	7.3	4.4	6.1	4.1	4.4	3.6

6.2.15.7 Riyadh, H5W15, East-West Orientation, Wind Flow Parallel to the Canyon

Regarding temperature decreases for the parallel to the canyon axis wind flow, they are of the same magnitude as for the perpendicular wind flow, though their differences are slightly higher than for the other examined geometries. For the E-W-oriented H5W15 canyon the averaged differences for the air inside the canyon between the perpendicular and the parallel flow reach 0.5°C for the green-all case and 0.3°C for the green-walls case (while being 0.0°C and 0.2°C, respectively, for the E-W-oriented H5W10 canyon). Larger air velocities evolve in the wider H5W15 canyon, thus wind direction becomes more a more important factor for the magnitude and direction of these velocities, affecting temperature distributions and thus temperature decreases inside the canyon. Temperature decreases inside the E-W-oriented H5W15 canyon with parallel wind flow are summarised in Table 238-Table 239. For the air inside the canyon averaged decreases range from 6.7°C for the green-

all case to 0.6°C for the green-walls case. Surface temperature decreases are of the same magnitude as for the perpendicular flow (discussed in paragraph 6.2.15.5).

Temperature decreases above the roof are summarised in Table 239 and are of the same magnitude as for the perpendicular flow. Regarding temperature decreases above the canyon (Table 240), they reach an average difference with the perpendicular flow's decreases of the magnitude of 0.3°C for both the green-walls and green-all cases and 0.1°C for the green-roofs case. Temperature decreases at this level reach a daytime average of 3.8°C for the green-all case, 0.7°C for the green-walls case and 0.4°C for the green-roofs cases.

Table 238. Comparison of temperature decreases (in °C) inside the canyon for green-roofs, green-walls and green-all, for H5W15, E-W orientation, wind flow parallel to the canyon, Riyadh

	ΔTasph, surf		ΔTasph, air		ΔTa,VIII		ΔTa,XI		ΔTd,VIII		ΔTd,XI	
	Max	Ave	Max	Ave	Max	Ave	Max	Ave	Max	Ave	Max	Ave
Green roofs	0.0	0.0	0.0	0.0	0.2	0.1	0.2	0.1	0.9	0.5	0.5	0.4
Green walls	1.3	0.8	1.3	0.8	1.5	0.6	1.1	0.5	1.5	0.8	1.9	0.6
Green all	1.3	0.8	12.2	9.6	11.0	8.8	11.0	8.4	8.0	5.1	7.9	4.6

Table 239. Comparison of temperature decreases (in °C) of the canyon walls for green-roofs, green-walls and green-all, for H5W15, E-W orientation, wind flow parallel to the canyon, Riyadh

	ΔTw1,d, surf		ΔTw1,d, air		ΔTw2,d, surf		ΔTw2,d, air		ΔTw1,a, surf		ΔTw2,a, surf	
	Max	Ave	Max	Ave	Max	Ave	Max	Ave	Max	Ave	Max	Ave
Green roofs	0.0	0.0	0.7	0.1	0.0	0.0	0.5	0.0	0.1	0.0	0.0	0.0
Green walls	20.0	15.1	18.0	11.1	7.7	5.4	4.2	2.4	19.4	14.5	5.1	2.9
Green all	20.0	15.1	18.2	11.3	7.7	5.4	4.3	2.4	19.4	14.5	5.1	2.9

Table 240. Comparison of temperature decreases (in °C) above the roofs, for green-roofs, green-walls and green-all, for H5W15, E-W orientation, wind flow parallel to the canyon, Riyadh

	ΔTrf, surf		ΔTrf, air		ΔTrf,f		ΔTrf,g		ΔTrf,h	
	Max	Ave	Max	Ave	Max	Ave	Max	Ave	Max	Ave
Green roofs	30.8	16.6	31.2	15.2	26.2	12.6	21.3	10.2	13.3	6.4
Green walls	0.0	0.0	0.0	0.0	0.2	0.1	0.1	0.1	0.1	0.1
Green all	31.8	17.2	32.4	15.9	26.2	12.6	21.3	10.2	13.3	6.4

Table 241. Comparison of temperature decreases (in °C) above the canyon, for green-roofs, green-walls and green-all, for H5W15, E-W orientation, wind flow parallel to the canyon, Riyadh

	ΔTf,VIII		ΔTg,VIII		ΔTh,VIII		ΔTf,XI		ΔTg,XI		ΔTh,XI	
	Max	Ave	Max	Ave	Max	Ave	Max	Ave	Max	Ave	Max	Ave
Green roofs	0.9	0.5	1.0	0.4	0.5	0.4	1.0	0.4	0.9	0.5	0.5	0.3
Green walls	1.5	0.1	1.4	0.4	1.4	1.2	2.1	0.2	2.0	0.7	1.7	1.4
Green all	6.4	4.4	5.2	4.0	3.9	3.3	6.6	4.1	5.5	3.8	3.8	3.3

6.2.15.8 Riyadh, H5W15, North-South Orientation, Wind Flow Parallel to the Canyon

On the subject of temperature decreases for the N-S-oriented H5W15 canyon, with parallel to the canyon's axis wind flow, the results are very similar as for the E-W orientation (discussed in paragraph 6.2.15.7). The average differences between the two flows for the air inside the N-S-oriented canyon reach 0.4°C for the green-all case and 0.3°C for the green-walls case. The average temperature decreases for the parallel flow are 6.7°C for the green-all case and 0.8°C for the green-walls case (Table 242). Regarding surface temperature decreases inside the canyon (Table 243) and temperature decreases above the roof (Table 244) they are of the same magnitude as for the perpendicular flow (paragraph 6.2.15.6). Concerning temperature decreases above the canyon (Table 245), average differences of 0.3°C for the green-all case and 0.2°C for the green-walls and green-roofs cases are reached between the two flows, with the perpendicular flow resulting in slightly higher decreases.

Table 242. Comparison of temperature decreases (in °C) inside the canyon for green-roofs, green-walls and green-all, for H5W15, N-S orientation, wind flow parallel to the canyon, Riyadh

	ΔTasph, surf		ΔTasph, air		ΔTa,VIII		ΔTa,XI		ΔTd,VIII		ΔTd,XI	
	Max	Ave	Max	Ave	Max	Ave	Max	Ave	Max	Ave	Max	Ave
Green roofs	0.0	0.0	0.0	0.0	0.3	0.1	0.2	0.1	0.9	0.4	0.8	0.2
Green walls	1.2	0.7	1.2	0.7	1.1	0.4	0.9	0.3	0.5	1.3	1.3	1.3
Green all	1.2	0.7	13.2	9.7	12.2	8.8	11.9	8.8	7.2	4.8	7.9	4.3

Table 243. Comparison of temperature decreases (in °C) of the canyon walls for green-roofs, green-walls and green-all, for H5W15, N-S orientation, wind flow parallel to the canyon, Riyadh

	ΔTw1,d, surf		ΔTw1,d, air		ΔTw2,d, surf		ΔTw2,d, air		ΔTw1,a, surf		ΔTw2,a, surf	
	Max	Ave	Max	Ave	Max	Ave	Max	Ave	Max	Ave	Max	Ave
Green roofs	0.0	0.0	0.1	0.0	0.0	0.0	0.0	0.0	0.1	0.0	0.0	0.0
Green walls	18.8	14.2	16.1	9.9	8.4	3.9	3.3	0.0	18.2	13.5	4.2	0.1
Green all	18.8	14.2	16.3	10.1	8.4	3.9	3.3	0.1	18.2	13.5	4.2	0.1

Table 244. Comparison of temperature decreases (in °C) above the roofs, for green-roofs, green-walls and green-all, for H5W15, N-S orientation, wind flow parallel to the canyon, Riyadh

	ΔTrf, surf		ΔTrf, air		ΔTrf,f		ΔTrf,g		ΔTrf,h	
	Max	Ave	Max	Ave	Max	Ave	Max	Ave	Max	Ave
Green roofs	30.8	16.6	31.2	15.2	26.2	12.6	21.3	10.2	13.3	6.4
Green walls	0.0	0.0	0.0	0.0	0.2	0.1	0.1	0.1	0.1	0.1
Green all	30.8	17.2	32.4	15.9	26.2	12.6	21.3	10.2	13.3	6.4

Table 245. Comparison of temperature decreases (in °C) above the canyon, for green-roofs, green-walls and green-all, for H5W15, N-S orientation, wind flow parallel to the canyon, Riyadh

	ΔTf,VIII		ΔTg,VIII		ΔTh,VIII		ΔTf,XI		ΔTg,XI		ΔTh,XI	
	Max	Ave	Max	Ave	Max	Ave	Max	Ave	Max	Ave	Max	Ave
Green roofs	0.9	0.8	0.8	0.7	0.5	0.4	1.0	0.8	0.9	0.9	0.6	0.3
Green walls	0.8	0.4	0.9	0.2	1.4	1.2	1.7	0.3	1.7	0.4	1.8	1.4
Green all	5.9	4.1	4.9	3.9	4.2	3.3	6.7	3.9	5.6	3.7	4.0	3.4

6.2.15.9 Riyadh, H10W5, East-West Orientation, Wind Flow Perpendicular to the Canyon

Temperature decreases inside the narrower and more vegetated H10W5 canyon are higher than for all the other geometries in Riyadh, as was also the case in Athens and Mumbai. Asphalt surface temperature decreases reach 2.4°C maximum and 1.3°C daytime average, being larger than in the H5W10 canyon's asphalt decreases by 0.4°C for the maximum and 0.1°C for the daytime average. Air temperature decreases inside the canyon reach maxima from 12.2°C to14.5°C for the green-all case and daytime averages from 8.3°C to 10.0°C for the green-all case (Table 246). They become

smaller for the green-walls case (from 4.3°C to 13.8°C and from 2.8°C to 9.5°C, respectively) and almost negligible for the green-roofs case. The green-walls case has a stronger effect in the H10W5 canyon than for any of the previous geometries examined. Its averaged difference with the H5W10, green-walls case is 1.7°C. Differences are smaller between the green-all cases of the perpendicular and parallel flow, of an average of 0.8°C.

Table 246. Comparison of temperature decreases (in °C) inside the canyon for green-roofs, green-walls and green-all, for H5W15, E-W orientation, wind flow perpendicular to the canyon, Riyadh

	ΔTasph, surf		ΔTasph, air		ΔTa,VIII		ΔTa,XI		ΔTd,VIII		ΔTd,XI	
	Max	Ave	Max	Ave	Max	Ave	Max	Ave	Max	Ave	Max	Ave
Green roofs	0.0	0.0	0.0	0.0	0.1	0.1	0.3	0.2	0.1	0.0	0.1	0.1
Green walls	2.4	1.3	2.5	1.3	9.6	5.7	4.3	2.8	13.8	9.5	8.8	5.8
Green all	2.4	1.3	9.2	7.6	13.0	8.7	12.2	8.3	14.5	10.0	13.1	8.9

Table 247. Comparison of temperature decreases (in °C) of the canyon walls for green-roofs, green-walls and green-all, for H5W15, E-W orientation, wind flow perpendicular to the canyon, Riyadh

	ΔTw1,d, surf		ΔTw1,d, air		ΔTw2,d, surf		ΔTw2,d, air		ΔTw1,a, surf		ΔTw2,a, surf	
	Max	Ave	Max	Ave	Max	Ave	Max	Ave	Max	Ave	Max	Ave
Green roofs	0.0	0.0	0.0	0.0	0.0	0.0	0.0	0.0	0.1	0.1	0.0	0.0
Green walls	15.9	11.3	15.6	10.4	14.3	9.6	13.9	8.9	15.3	10.7	17.2	10.0
Green all	15.9	11.3	15.6	10.4	14.3	9.6	14.1	8.9	15.3	10.7	17.2	10.0

Concerning temperature decreases above the roof (Table 247) they are of the same magnitude as those of the roofs of the H5W10 canyon. Maximum decreases are noticed on the surface temperatures, with 31.2°C maximum and 16.7°C daytime average decreases. Air temperature decreases range from 26.6°C maximum and 12.8°C daytime average 1m above the roof to 13.5°C and 6.5°C, respectively, 6m above the roof for both the green-roofs and green-all cases. Regarding temperature decreases at the air layer above the canyon H10W5 has a more significant effect than the H5W10 canyon. The average difference between the decreases of the two geometries is 1.5°C for the green-walls case and 0.7°C for the green-all case. The green-roofs case for the H10W5 canyon reaches maximum decreases from 0.6°C (nodes h,VIII and h,XI) to 2.0°C (node f,XI) and daytime average from 0.4°C (nodes h,VIII and h,XI) to 0.9°C (node g,XI). Green-walls and green-all cases show

decreases of the same magnitude as those of the H5W10 geometry, with maxima ranging from 4.3°C (node h,XI) to 10.7°C (node f,VIII) and daytime averages from 3.6°C (node h,XI) to 8.7°C (node f,VIII). For the green-walls case, these decreases range from 2.5°C (node h,XI) to 10.4°C (node f,VIII) and from 2.1°C (node h,XI) to 8.5°C (node f,VIII), respectively.

Table 248. Comparison of temperature decreases (in °C) above the roofs, for green-roofs, green-walls and green-all, for H5W15, E-W orientation, wind flow perpendicular to the canyon, Riyadh

	ΔTrf, surf		ΔTrf, air		ΔTrf,f		ΔTrf,g		ΔTrf,h	
	Max	Ave	Max	Ave	Max	Ave	Max	Ave	Max	Ave
Green roofs	31.1	16.6	31.5	15.2	26.6	12.8	21.5	10.3	13.5	6.5
Green walls	0.0	0.0	0.0	0.0	0.2	0.0	0.2	0.1	0.1	0.1
Green all	31.2	16.7	31.6	15.3	26.6	12.8	21.6	10.3	13.5	6.5

Table 249. Comparison of temperature decreases (in °C) above the canyon, for green-roofs, green-walls and green-all, for H5W15, E-W orientation, wind flow perpendicular to the canyon, Riyadh

	ΔTf,VIII		ΔTg,VIII		ΔTh,VIII		ΔTf,XI		ΔTg,XI		ΔTh,XI	
	Max	Ave	Max	Ave	Max	Ave	Max	Ave	Max	Ave	Max	Ave
Green roofs	1.8	0.5	1.9	0.8	0.6	0.4	2.0	0.4	1.8	0.9	0.6	0.4
Green walls	10.4	8.5	7.6	6.3	4.8	4.1	5.5	4.2	3.9	3.1	2.5	2.1
Green all	10.7	8.7	7.7	6.4	4.9	4.2	9.5	7.4	6.8	5.5	4.3	3.6

6.2.15.10 Riyadh, H10W5, North-South Orientation, Wind Flow Perpendicular to the Canyon

Regarding the N-S-oriented H10W5 canyon, the same is observed as in the previous cases; its decreases are of the same magnitude, though slightly smaller than for the E-W-oriented H10W5 canyon. The average difference between the two temperature decreases inside the canyon is of a magnitude of 0.5°C for the green-walls case and 1.1°C for the green-all case. Air temperature decrease inside the canyon shows an average maximum of 12.2°C for the green-all and 9.0°C for the green-walls cases. The averaged daytime average air temperature decrease inside the canyon reaches 7.8°C for the green-all case and 5.5°C for the green-walls cases (Table 250). When compared with the N-S-oriented H5W10 canyon, the differences between

the two geometries reach an average of 0.9°C for the green-all case and 2.3°C for the green-walls case, with the evapotranspirational effect being larger in the skimming flow canyon. Regarding wall surface temperature decreases (Table 251), the differences between the two geometries reach an average of 4.5°C for the east-oriented wall and 1.8°C for the west-oriented one. Again, the most exposed to solar radiation surfaces benefit mostly when covered with vegetation.

Temperatures above the roof (Table 252) show the same decreases as the ones discussed in paragraph 6.2.15.9. Regarding temperature decreases above the canyon (Table 253), they are slightly lower than the E-W-oriented canyon decreases. The average differences between the two orientations are 0.7°C for the green-all case, 0.4°C for the green-walls case and 0.1°C for the green-roofs case. The average differences between the N-S-oriented H10W5 canyon and the N-S skimming flow H5W10 canyon reach 0.4°C for the green-all case, 1.7°C for the green-walls case and 0.5°C for the green-roofs case, with the H10W5 canyon temperature decreases being higher than the H5W10 decreases.

Table 250. Comparison of temperature decreases (in °C) inside the canyon for green-roofs, green-walls and green-all, for H5W15, N-S orientation, wind flow perpendicular to the canyon, Riyadh

	ΔTasph, surf		ΔTasph, air		ΔTa,VIII		ΔTa,XI		ΔTd,VIII		ΔTd,XI	
	Max	Ave	Max	Ave	Max	Ave	Max	Ave	Max	Ave	Max	Ave
Green roofs	0.0	0.0	0.0	0.0	0.1	0.0	0.3	0.1	0.1	0.0	0.1	0.1
Green walls	2.1	1.1	2.2	1.1	8.0	4.7	5.4	3.3	12.9	8.6	9.6	5.4
Green all	2.1	1.1	11.1	8.2	11.9	7.8	11.5	7.3	13.4	9.0	12.0	7.2

Table 251. Comparison of temperature decreases (in °C) of the canyon walls for green-roofs, green-walls and green-all, for H5W15, N-S orientation, wind flow perpendicular to the canyon, Riyadh

	ΔTw1,d, surf		ΔTw1,d, air		ΔTw2,d, surf		ΔTw2,d, air		ΔTw1,a, surf		ΔTw2,a, surf	
	Max	Ave	Max	Ave	Max	Ave	Max	Ave	Max	Ave	Max	Ave
Green roofs	0.0	0.0	0.0	0.0	0.0	0.0	0.0	0.0	0.1	0.0	0.0	0.0
Green walls	14.6	10.2	14.2	9.3	14.4	7.7	13.9	6.9	14.0	9.4	13.6	7.1
Green all	14.6	10.2	14.3	9.4	14.4	7.7	14.0	6.9	14.0	9.4	13.6	7.1

Table 252. Comparison of temperature decreases (in °C) above the roofs, for green-roofs, green-walls and green-all, for H5W15, N-S orientation, wind flow perpendicular to the canyon, Riyadh

	ΔTrf, surf		ΔTrf, air		ΔTrf,f		ΔTrf,g		ΔTrf,h	
	Max	Ave	Max	Ave	Max	Ave	Max	Ave	Max	Ave
Green roofs	31.1	16.6	31.5	15.2	26.6	12.8	21.5	10.3	13.5	6.5
Green walls	0.1	0.0	0.1	0.1	0.2	0.1	0.2	0.1	0.1	0.1
Green all	31.2	16.7	31.6	15.3	26.6	12.8	21.6	10.3	13.5	6.5

Table 253. Comparison of temperature decreases (in °C) above the canyon, for green-roofs, green-walls and green-all, for H5W15, N-S orientation, wind flow perpendicular to the canyon, Riyadh

	ΔTf,VIII		ΔTg,VIII		ΔTh,VIII		ΔTf,XI		ΔTg,XI		ΔTh,XI	
	Max	Ave	Max	Ave	Max	Ave	Max	Ave	Max	Ave	Max	Ave
Green roofs	1.7	0.1	1.9	0.8	0.4	0.1	1.9	0.3	1.8	1.0	0.4	0.0
Green walls	10.3	8.0	7.5	5.9	4.8	3.9	4.9	3.6	3.5	2.7	2.1	1.8
Green all	10.4	8.1	7.5	5.9	4.8	3.9	7.3	6.0	5.2	4.5	3.2	3.0

6.2.15.11 Riyadh, H10W5, East-West Orientation, Wind Flow Perpendicular to the Canyon

Regarding differences between the temperature decreases of the skimming flow canyon with different wind directions, they are very small, compared to other geometries. For the much narrower canyon, the direction of wind flow is not as significant for the direction and magnitude of air velocities developed inside it, which remain small. The averaged differences between the air temperature decreases inside the canyon for the two wind directions are 0.0°C for both the green-all and green-wall cases. For the air layer above the canyon these differences become more significant, with an averaged value of 0.4°C for the green-all case, 0.2°C for the green-walls case and 0.7°C for the green-roofs case. Temperature decreases for the parallel wind flow in the E-W-oriented H10W5 canyon in Riyadh are summarised in Table 254-Table 257.

Table 254. Comparison of temperature decreases (in °C) inside the canyon for green-roofs, green-walls and green-all, for H5W15, E-W orientation, wind flow parallel to the canyon, Riyadh

	ΔTasph, surf		ΔTasph, air		ΔTa,VIII		ΔTa,XI		ΔTd,VIII		ΔTd,XI	
	Max	Ave	Max	Ave	Max	Ave	Max	Ave	Max	Ave	Max	Ave
Green roofs	0.0	0.0	0.0	0.0	0.1	0.1	0.3	0.2	0.1	0.1	0.2	0.1
Green walls	2.4	1.3	2.5	1.3	9.6	5.7	4.3	2.8	13.8	9.5	8.9	5.9
Green all	2.4	1.3	9.2	7.6	13.0	8.7	12.2	8.3	14.4	10.0	13.2	9.0

Table 255. Comparison of temperature decreases (in °C) of the canyon walls for green-roofs, green-walls and green-all, for H5W15, E-W orientation, wind flow parallel to the canyon, Riyadh

	ΔTw1,d, surf		ΔTw1,d, air		ΔTw2,d, surf		ΔTw2,d, air		ΔTw1,a, surf		ΔTw2,a, surf	
	Max	Ave	Max	Ave	Max	Ave	Max	Ave	Max	Ave	Max	Ave
Green roofs	0.0	0.0	0.0	0.0	0.0	0.0	0.0	0.0	0.1	0.1	0.0	0.0
Green walls	15.9	11.3	15.6	10.4	14.3	9.6	14.0	8.9	15.3	10.7	17.2	10.0
Green all	15.9	11.3	15.6	10.4	14.3	9.6	14.1	9.0	15.3	10.7	17.2	10.0

Table 256. Comparison of temperature decreases (in °C) above the roofs, for green-roofs, green-walls and green-all, for H5W15, E-W orientation, wind flow parallel to the canyon, Riyadh

	ΔTrf, surf		ΔTrf, air		ΔTrf,f		ΔTrf,g		ΔTrf,h	
	Max	Ave	Max	Ave	Max	Ave	Max	Ave	Max	Ave
Green roofs	31.0	16.6	31.4	15.2	26.4	12.7	21.4	10.2	13.4	6.4
Green walls	0.2	0.0	0.2	0.0	0.4	0.0	0.4	0.1	0.2	0.0
Green all	31.2	17.0	31.6	15.6	26.5	12.8	21.5	10.4	13.5	6.5

Table 257. Comparison of temperature decreases (in °C) above the canyon, for green-roofs, green-walls and green-all, for H5W15, E-W orientation, wind flow parallel to the canyon, Riyadh

	ΔTf,VIII		ΔTg,VIII		ΔTh,VIII		ΔTf,XI		ΔTg,XI		ΔTh,XI	
	Max	Ave	Max	Ave	Max	Ave	Max	Ave	Max	Ave	Max	Ave
Green roofs	2.3	1.5	2.3	1.9	0.4	0.4	2.0	1.3	2.1	1.7	0.4	0.3
Green walls	10.1	8.2	7.5	6.2	4.9	4.2	5.4	4.3	4.1	3.6	3.1	2.7
Green all	10.8	8.9	7.9	6.6	5.2	4.4	10.0	7.9	7.4	6.0	4.9	4.1

6.2.15.12 Riyadh, H10W5, North-South Orientation, Wind Flow Perpendicular to the Canyon

The temperature decreases of the N-S-oriented H10W5 canyon with parallel wind flow are summarised in Table 258-Table 261. As was discussed in paragraph6.2.15.11, the difference of temperature decreases inside the canyon between the parallel and the perpendicular wind flow are null for the skimming flow canyon, despite its orientation. Air and surface temperature decreases inside the N-S-oriented canyon and at roof level are as the ones discussed in paragraph 6.2.15.10. Differences between the two flows become noticeable at the air layer above the canyon, with an averaged difference between the temperature decreases of 0.3°C for both the green-all and green-walls cases and 0.8°C for the green-roofs case.

Table 258. Comparison of temperature decreases (in °C) inside the canyon for green-roofs, green-walls and green-all, for H5W15, N-S orientation, wind flow parallel to the canyon, Riyadh

	ΔTasph, surf		ΔTasph, air		ΔTa,VIII		ΔTa,XI		ΔTd,VIII		ΔTd,XI	
	Max	Ave	Max	Ave	Max	Ave	Max	Ave	Max	Ave	Max	Ave
Green roofs	0.0	0.0	0.0	0.0	0.1	0.0	0.2	0.1	0.1	0.0	0.2	0.1
Green walls	2.1	1.1	2.2	1.1	8.0	4.7	5.3	3.2	12.8	8.6	9.5	5.3
Green all	2.1	1.1	11.1	8.2	11.9	7.8	11.5	7.3	13.3	8.9	12.1	7.3

Table 259. Comparison of temperature decreases (in °C) of the canyon walls for green-roofs, green-walls and green-all, for H5W15, N-S orientation, wind flow parallel to the canyon, Riyadh

	ΔTw1,d, surf		ΔTw1,d, air		ΔTw2,d, surf		ΔTw2,d, air		ΔTw1,a, surf		ΔTw2,a, surf	
	Max	Ave	Max	Ave	Max	Ave	Max	Ave	Max	Ave	Max	Ave
Green roofs	0.0	0.0	0.0	0.0	0.0	0.0	0.1	0.0	0.1	0.0	0.0	0.0
Green walls	14.6	10.2	14.3	9.3	14.4	7.7	14.0	6.9	14.0	9.4	13.6	7.1
Green all	14.6	10.2	14.3	9.4	14.4	7.7	14.0	6.9	14.0	9.4	13.6	7.1

Table 260. Comparison of temperature decreases (in °C) above the roofs, for green-roofs, green-walls and green-all, for H5W15, N-S orientation, wind flow parallel to the canyon, Riyadh

	ΔTrf, surf		ΔTrf, air		ΔTrf,f		ΔTrf,g		ΔTrf,h	
	Max	Ave	Max	Ave	Max	Ave	Max	Ave	Max	Ave
Green roofs	31.0	16.6	31.4	15.2	26.4	12.7	21.4	10.2	13.4	6.4
Green walls	0.1	0.1	0.1	0.1	0.2	0.1	0.2	0.2	0.1	0.1
Green all	31.2	17.0	31.6	15.6	26.5	12.8	21.5	10.4	13.5	6.5

Table 261. Comparison of temperature decreases (in °C) above the canyon, for green-roofs, green-walls and green-all, for H5W15, N-S orientation, wind flow parallel to the canyon, Riyadh

	ΔTf,VIII		ΔTg,VIII		ΔTh,VIII		ΔTf,XI		ΔTg,XI		ΔTh,XI	
	Max	Ave	Max	Ave	Max	Ave	Max	Ave	Max	Ave	Max	Ave
Green roofs	2.2	1.4	2.3	1.8	0.4	0.4	2.0	1.4	2.1	1.8	0.4	0.3
Green walls	10.2	7.9	7.6	6.0	5.0	4.1	5.3	4.0	4.0	3.2	2.7	2.4
Green all	10.5	8.2	7.7	6.2	5.1	4.2	7.8	6.5	5.8	5.0	3.8	3.4

6.2.15.13 Riyadh, Summary for Different Geometries

Concerning temperature decrease caused by different geometries in Riyadh, it is obvious from Figure 268 that regarding air temperature decrease inside the canyon, the green-all, H5W10 case benefits the most. For the green-all case, temperature decrease reaches a daytime average of 34.0%, with 40.1% maximum and 29.3% minimum daytime decrease. For the more shaded H10W5 canyon decreases of the green-all case reach 27.0% average, 32.5% maximum and 23.4% minimum. The wider and more exposed to the sun H5W15 canyon shows lower daytime average, maximum and minimum than the narrower H5W10 canyon (28.7%, 34.2%, and 25.1%, respectively). For arid Riyadh, the additional cooling from green roofs is essential for enhancing temperature decreases inside the canyon. As can be observed in Figure 268, not only does the green-walls case produce smaller temperature decreases, but also the magnitude of its effect on each geometry is completely different from the effect of the green-all case. For the green-walls case, the largest decreases are noticed in the H10W5 canyon, with its larger area of walls, with 19.1% average temperature decrease, 24.2% maximum and 16.2% minimum. Decreases become slightly smaller for the H5W10 geometry (19.1%, 24.2%, and 16.2%, respectively). For the wider H5W15 canyon the lowest decrease in the air inside the canyon is observed (6.7%) with the largest discrepancy (25.5% maximum and 1.0% minimum).

Air temperature decreases above the roof follow a different pattern to air temperature decreases inside the canyon (Figure 269); they are relatively low in the morning, but raise significantly in the afternoon and evening, since plants do not absorb and store the amounts of solar radiation building materials do. 1m above the roof, the average air temperature decrease is of the same magnitude as for the air

inside the canyon (27.8%), but with a much larger discrepancy (53.6% maximum and 2.4% minimum).

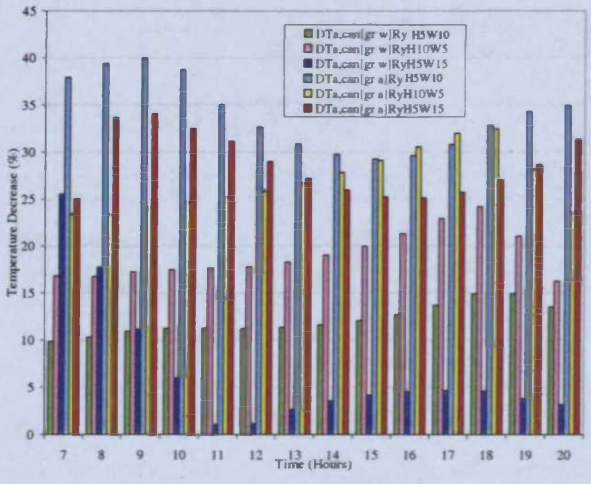

Figure 268. Air temperature decrease (%) inside the canyon for the green-all and green-walls cases, for the different canyon geometries examined for Riyadh

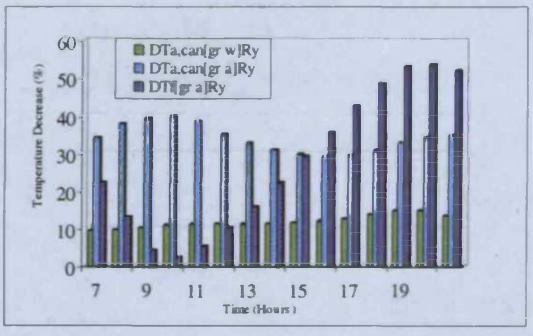

Figure 269. Comparison of air temperature decrease (%) 1m above the roof (ΔTf[gr a]) for the green-roofs and green-all cases with the air temperature decrease inside the canyon for the green-walls and green-all cases, for the H5W10 canyon, Riyadh

Regarding relative humidity increases, they are higher for the H10W5 geometry, with its larger walls, for both the green-all and green walls cases (Figure 270). For the H10W5 green-all case in arid Riyadh, relative humidity increases inside the canyon reach 56.5% average, with 85.1% maximum and 19.8% minimum. These values become smaller for H5W10 (42.3%, 72.4%, and 7.5%, respectively) and even smaller, with smaller discrepancy for wider H5W15 (12.7%, 19.3%, and 4.6%, respectively). The green-walls case shows smaller relative humidity increases, for all three geometries. The largest increases can be observed in H10W5, with 36.6% average, 53.6% maximum and 15.2% minimum. For the H5W10 canyon relative humidity increases are lower, with 12.6% average and discrepancy from 19.3% maximum to 4.5% minimum. For the H5W15 canyon, with its wide 15m street, these increases become even smaller, with 1.7% average, 4.3% maximum and 0.1% minimum.

Relative humidity increases at the air layer 1m above the roof are not so great as for inside the green-all canyons, reaching a peak increase during afternoon hours (Figure 271). Relative humidity increase above the roof reaches an average of 25.8%, with a discrepancy of 43.7% maximum to 2.1% minimum.

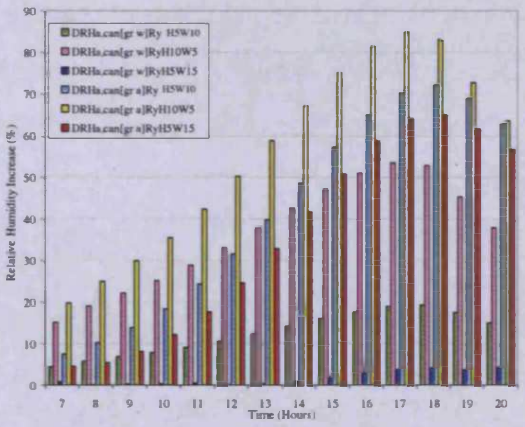

Figure 270. Relative humidity increase (%) inside the canyon for the green-all and green-walls cases, for the different canyon geometries examined for Riyadh

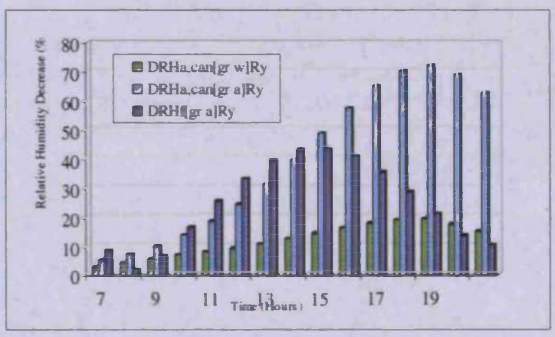

Figure 271. Comparison of relative humidity increase (%) 1m above the roof (ΔRHf[gr a]) for the green-roofs and green-all cases with relative humidity increase inside the canyon for the green-walls and green-all cases, for the H5W10 canyon, Riyadh

6.3 Thermal Comfort in Urban Spaces

It is quite useful to examine the impact of those calculated surface and air temperatures on outdoor thermal comfort, in order to estimate their impact on the thermal sensation of people. According to ASHRAE (1985), comfort is defined as *"a condition of mind in which satisfaction is expressed with the environment"*. The factors which affect human comfort can be either physical or psychological. Thermal comfort, apart from psychological factors, is very much influenced by physical factors such as temperature (air and global), wind speed and solar radiation, factors which are dominant in a system's energy balance. Indeed, from a physical point of view, thermal

comfort can be determined as the situation in which the human body makes the least effort to maintain its energy balance with its surroundings.

If the system surroundings - human body is considered, according to the Law of Conservation of Energy, the body exchanges heat with its surroundings in order to achieve energy equilibrium. The body exchanges heat with its surroundings through radiation, convection, conduction and evaporation, on a dynamic basis, depending on the changes of the parameters influencing the phenomenon. Olgyay (1973) has summarised this energy balance schematically:

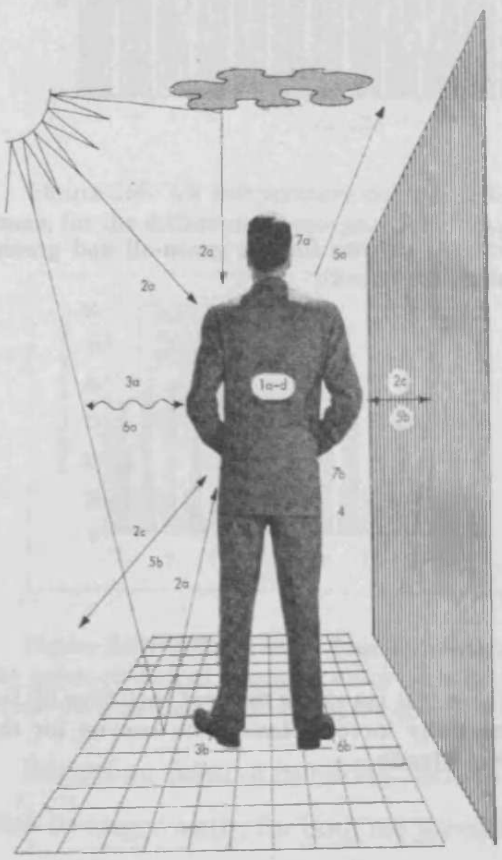

GAINS:

1. Heat produced by:
   a) Basic processes
   b) Activity
   c) Digestive, etc. processes
   d) Muscle tensing and shivering in response to cold
2. Absorption of radiant energy:
   a) From sun directly or reflected
   b) From glowing radiators
   c) From non-glowing hot objects
3. Heat conduction / convection toward the body:
   a) Convection from air above skin temperature
   b) Conduction by contact with hotter objects
4. Condensation of atmospheric moisture (occasional)

LOSSES:

5. Outward radiation:
   a) To "sky"
   b) To colder surroundings
6. Heat conduction / convection away from the body:
   a) Convection to air temperature below skin temperature
   b) Conduction by contact with colder objects
7. Evaporation:
   a) From respiratory tract
   b) From skin

Figure 272. Heat exchange between man and surroundings (Olgyay, 1973)

Chernko expressed mathematically this energy balance between the system surroundings - human body as (cited in Nikolopoulou, 1998):

$$M - W = E + R + C + S \qquad \textbf{Eq. 234}$$

Where:

M: Metabolic rate

W: Rate at which this energy balance is expended in external mechanical work

E: Rate of heat loss by evaporation

R: Rate of heat loss by radiation

C: Rate of heat loss by conduction

S: Rate at which heat is stored within the body.

Bedford, when investigating the comfort of factory workers in England, came to the conclusion that the parameters influencing thermal comfort were the ones upon which individual heat exchange mechanisms depend; air temperature, mean radiant temperature, relative humidity and air movement. He combined these factors with indoors thermal comfort in the following equation (cited in Nikolopoulou, 1998):

$$N = 11.16 - 0.0556t_a - 0.0538t_w - 0.0372f - 0.00144\sqrt{v(100 - t_a)} \qquad \text{Eq. 235}$$

Where:

N: Numerical value assigned to the sensation of warmth ("comfortable=4")

t_a: Air temperature [°F]

t_w: Mean radiant temperature [°F]

f: Partial pressure of water vapour present in the air [mmHg]

v: Air velocity [ft/min]

It can be observed from Bedford's equation that air temperature and mean radiant temperature have coefficients of the same order of magnitude (0.0556 and 0.0538, respectively), indicating that the two temperatures are equally important for indoor thermal comfort.

Nikolopoulou, carrying out outdoor thermal comfort measurements in Cambridge, concluded that both *"air and globe temperatures have the biggest impact on the Actual Thermal Sensation Vote"* when both these temperatures, wind speed and solar radiation are *"the most important parameters of comfort outdoors"* (Nikolopoulou, 1998). For assessing thermal comfort models for open urban spaces in the RUROS project Nikolopolou (2004)[54] pointed out that for a microclimatic comfort index, shading conditions, radiative heat and vegetation distribution are the most important factors. Scudo et al. (2004) confirmed the importance of the mean radiant temperature

[54] I would like to express my gratitude to Lydia-Chara Pavlopoulou for sending me a copy of the RUROS project report.

for outdoor thermal comfort, especially inside urban canyons. The lower the W/H (street width/building height) ratio is, the more significant the effect of wall temperatures and the choice of surface materials are on the canyon's microclimate. Radiant temperature is the most important factor among the meteorological parameters for human thermal comfort, especially during summer months (Mantzarakis et al., 2002).

In the detailed microclimatic thermal comfort mapping of open spaces in Kassel, undertaken for the RUROS project (Katzschner et al., 2004), the importance of thermal radiation - as well as the existence of vegetation - was demonstrated and used, in conjunction with air velocities. It was found out that for the same open space thermal comfort mapping may vary from "cool comfortable" to "very warm", depending on the distance from buildings and the thermal and short wave radiation distribution. In conclusion, for the estimation of outdoor thermal comfort, thermal radiation (depending on geometry and surface materials) is an important factor, in combination with air temperature and humidity, solar radiation distribution and wind flow pattern.

The temperature of a surface is therefore quite important, influencing thermal comfort quite significantly, for both indoor and outdoor spaces. For outdoor spaces, where the fabric raises its temperature to more extreme levels than indoors, radiative heat exchanges between the human body and its surrounding surfaces become more crucial to thermal comfort.

A quite useful tool for expressing the effect of radiant and air temperature on thermal comfort for outdoor spaces is the Physiological Equivalent Temperature (PET). PET is defined as the air temperature at which, in a typical indoor setting (without any wind and solar radiation), the heat budget of the human body is balanced with the same core and skin temperature as under the complex outdoor conditions to be assessed (Nikolopoulou, 2004). In this way a comparison is available between the integral effects of complex thermal conditions and indoor, less complicated, thermal conditions (Jendritzky et al., 2001). PET can be related to the Predicted Mean Vote, PMV (Kuttler, 2004), as shown in Table 262. It can be expressed as a linear relationship with urban characteristics such as air temperature, mean radiant temperature (MRT), wind speed, vapour pressure, short and long wave radiation from the upper and lower hemisphere. For the parameters in which this study is interested -

air and radiant temperature - PET has been derived from experiments during sunny, summer days in Freiburg, Germany (Matzarakis et al., 2002), as:

$$PET(Ta) = 1.354Ta - 5.0 \qquad \text{Eq. 236}$$

$$PET(Tmrt) = 0.519Tmrt + 6.8 \qquad \text{Eq. 237}$$

Where T_{mrt} is the mean radiant temperature, the uniform temperature of a surrounding surface emitting as a black body, which results in the same radiation gain of a human body as the prevailing radiation fluxes, which usually vary significantly in open spaces (Matzarakis, 2001; Nikolopoulou, 2004). In other words, MRT is the averaged value of surface temperatures around the body. It can be calculated by the relationship (Matzarakis, 2001):

$$T_{mrt} = \left[\frac{1}{\sigma}\left(\sum_{i=1}^{n}\left(\sigma\varepsilon_i T_i^4 + (1-a_i)\frac{D}{\varepsilon_h}\right) + f_p(1-a_i)\frac{I^*}{\varepsilon_h}\right)\right]^{0.25} \qquad \text{Eq. 238}$$

where σ is the Stephan-Boltzmann constant, ε_i is the emissivity of the i^{th} surface, α_i its albedo, T_i its temperature and F_i is the view factor between the surface and the human body. ε_h is the human body's emissivity (with a 0.97 standard value), D the sum of diffuse solar radiation and diffusely reflected global radiation on the i^{th} surface. I^* is the radiation intensity of the sun on a surface perpendicular to the incident radiation direction and f_p is the surface projection factor, which is a function of the incident radiation direction and the body posture. It ranges for 0.308 for 0° solar altitude to 0.082 for 90°.

Table 262. Relationships of PMV, PET and thermal sensation (adapted from Kuttler, 2004)

PMV	PET (°C)	Thermal Sensation
-3.5	4	Very Cold
-2.5	8	Cold
-1.5	13	Cool
-0.5	18	Slightly cool
0.0	20	Comfortable
0.5	23	Slightly Warm
1.5	29	Warm
2.5	35	Hot
3.5	41	Very Hot

By calculating the mean radiant temperature, and thus PET, one is able to evaluate the direct effects of covering building surfaces with plants on thermal comfort in urban spaces. The human body is considered to be standing, thus it can be treated as an infinitesimal element, when compared to urban surfaces, the latter being treated as plates, quite large for their distance from the body (Figure 273). The view factor between an infinitesimal element and a plate parallel to it is 1 (Paspalas, 1993); when an angle, α, is formed between the element and the plate, the view factor is given by (ibid.):

$$F = \frac{1}{2}(1+\cos\alpha) \qquad \textbf{Eq. 239}$$

A human body standing in an urban canyon can be considered parallel to walls ($F_2=F_4=1$) and perpendicular to the street and the sky ($F_1=F_3=1/2$). A human body standing on the rooftop can be considered perpendicular to both the roof and the sky ($F_5=F_3=1/2$).

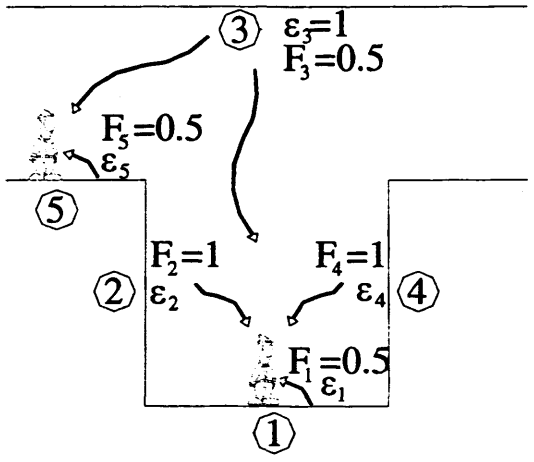

Figure 273. Radiative heat exchanges and view factors between the human body and the surfaces in the urban canyon and on the roof[55]

For all climates examined, the results for averaged PET, calculated from air temperature and mean radiant temperature, are given in Figure 274 to Figure 276. As can be observed from these figures, the largest PET is for the more exposed to direct solar radiation roof, than for the canyon, with more uncomfortable conditions occurring at roof level. In all hot climates (Athens, Beijing, Hong Kong, Mumbai and Riyadh), PET for the bare, concrete roof reaches the "very hot" zone in the afternoon. For Brasília and Montréal, the "hot" zone is reached in the afternoon, while cooler

[55] The sketch of the man is taken from Arkas's comic *Life After* (2000, Grammata Editions, Athens).

London and Moscow reach only the "warm" zone in the afternoon (line "PET,rf[no gr]", in all cases in Figure 274-Figure 276). When the roof is covered with vegetation (line "PET,rf[gr a]"), PET is reduced to more comfortable levels, reaching only "warm" for Athens, Beijing, Brasília, Hong Kong, Montréal, Mumbai and Riyadh and "slightly warm" for London and Moscow. In the late evening hours, PET for green roofs reduces to "comfortable", "slightly cool" or "cool" levels, while PETs for all concrete roofs, due to the heat stored inside the concrete, do not fall below the "slightly warm" zone.

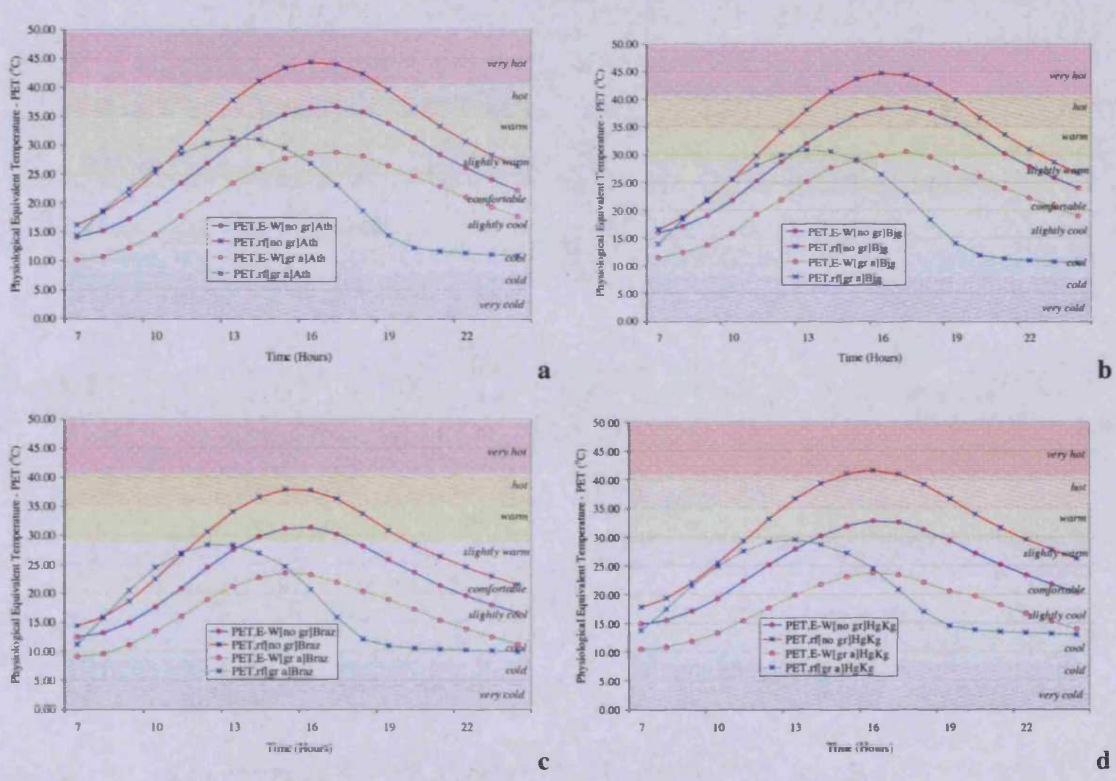

Figure 274. PET for the E-W-oriented H5W10 canyon, for the no-green [no gr] and green-all [gr-a] cases, in (a) Athens, (b) Beijing, (c) Brasília, and (d) Hong Kong

Regarding conditions in the less exposed to direct radiation no-green canyon, they are, in general, more comfortable than at the no-green roof. The "very hot" zone is not reached inside the canyon by any of the climates examined. Athens, Beijing, Mumbai and Riyadh reach the "hot" level in the afternoon, Brasília, Hong Kong and Montréal reach the "warm" zone, while London and Moscow reach only the "slightly warm" zone (line "PET,E-W[no gr]"). When the canyon walls are covered with vegetation, Athens, Beijing, Mumbai and Riyadh reach the "warm" zone in the afternoon, Brasília, Hong Kong, Montréal the "slightly warm" and Moscow the "comfortable" or "slightly cool" one, while London remains in the "slightly cool" zone throughout the whole day (line "PET,E-W[gr a]").

When the roof is covered with green, cooler levels are reached much faster after sunset than when the canyon walls are covered with green. This is due to the fact that inside the canyon the street surface is not covered with vegetation, but remains covered with asphalt, which reaches high temperatures and stores heat. In addition, the canyon is less exposed to the sky than the roof, allowing for lower long wave radiation exchanges between the body and the clear sky during late evening hours, than on the roof top.

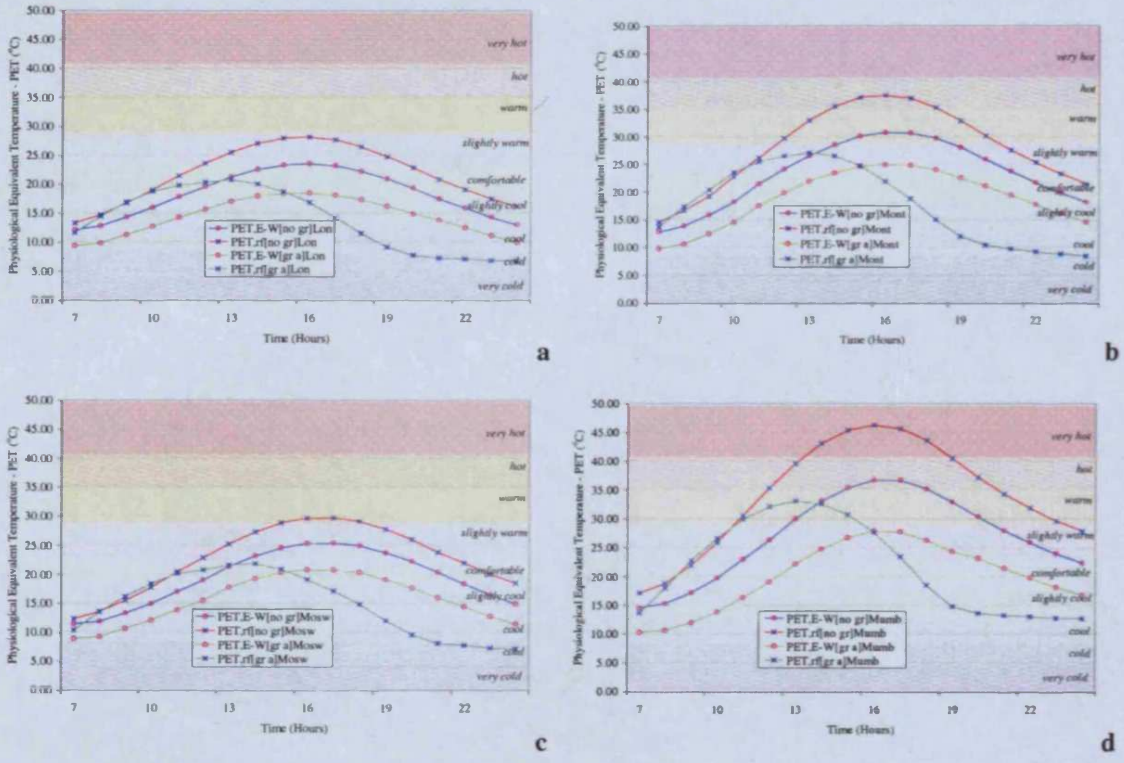

Figure 275. PET for the E-W-oriented H5W10 canyon, for the no-green [no gr] and green-all [gr-a] cases, in (a) London, (b) Montréal, (c) Moscow, and (d) Mumbai

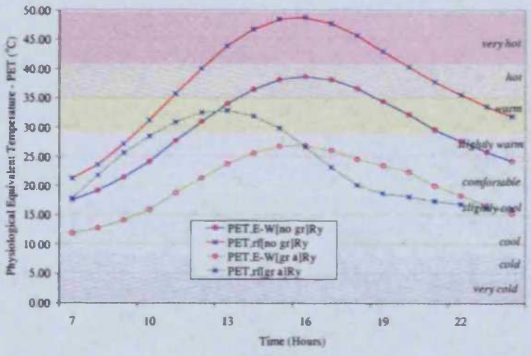

Figure 276. PET for the E-W-oriented H5W10 canyon, for the no-green [no gr] and green-all [gr-a] cases, in Riyadh

Regarding thermal comfort inside wider or narrower canyons, it can be observed in Figure 277 that the latter reach more uncomfortable and hotter conditions much faster.

For the no-green case, it can be observed, by comparing the line "PET,E-W[no gr]Ry H5W15" for the wider H5W15 canyon (Figure 277b) with the "PET,E-W[no gr]Ry H10W5" for the narrower H10W5 (Figure 277a), that despite the fact that both of them are in the "hot" zone during the afternoon, the H10W5, reaches higher peaks, almost close to the "very hot" zone (with a maximum PET of 39.3°C, while the maximum PET for the H5W15 canyon is 37.3°C). The H5W15 canyon reaches PETs that are in the "hot" zone for only 5 hours, while the H10W5 canyon PET is in the "hot" area for 7 hours, never falling to the "slightly warm" level, which is reached in the H5W15 canyon at the end of the day. When the two canyons are covered with vegetation (line "PET,E-W[gr a]Ry H5W15" for H5W15 and "PET,E-W[gr a]Ry H10W5" for H10W5), thermal conditions are improved, with both green canyons reaching only the "slightly warm" sensation zone. Again, the sensation lasts for longer in the H10W5 canyon (13 hours) than in the H5W15 canyon, where the green-all case is in the "slightly warm" zone for 7 hours, 5 hours in the "comfortable" zone and 4 hours in the "slightly cool" one. The green H10W5 canyon reaches the "comfortable" zone only in the early morning and not in the evening hours as does the wider H5W15 canyon.

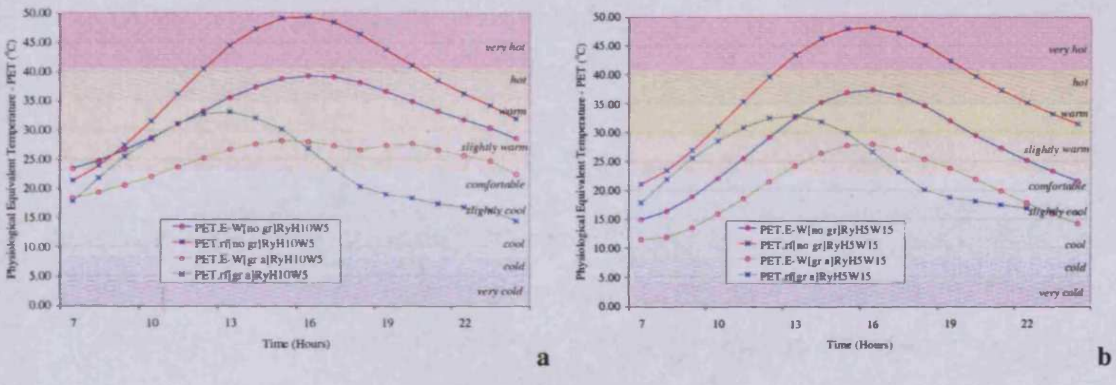

Figure 277. PET for the E-W-oriented (a) H10W5 and (b) H5W15 canyon, for the no-green [no gr] and green-all [gr-a] cases, in Riyadh

Using the Physiological Equivalent Temperature, PET, it has been shown in this section that thermal comfort in urban spaces in summer can improve quite significantly when walls and roofs are covered with vegetation. For the unshaded roof level the results are more dramatic, reaching even "comfortable" levels in extremely hot climates, such as Mumbai or Riyadh. Even for the less exposed canyon, the situation improves notably when walls are covered with vegetation, lowering from "hot" to "warm" and from "warm" to "slightly warm" conditions. For colder climates, such as London and Moscow, the "comfortable" or "slightly cool" level can be

maintained for the larger part of the day, both inside the canyon and on the roof top, when building surfaces are covered with green.

6.4 Energy Savings from Green Walls and Roofs

Apart from creating outdoor conditions which are more "human-friendly", from a thermal point of view, especially in hot climates, green roofs and green walls can also prove beneficial for indoor thermal conditions. In addition to the fact that they add a further insulation layer to the building's fabric (as discussed in chapter 3), due to their microclimatic modifications, they can decrease cooling load demands inside the building quite significantly.

In a simplified steady-state analysis, without taking into consideration internal thermal gains, heat gains/losses (q) from the building's fabric with an average U-value U, an indoors temperature T_{in} and an outdoors temperature T_{out} are given by the relationship:

$$q = U(T_{out} - T_{in}) \qquad \textbf{Eq. 240}$$

For the no-green base case [no gr], the cooling load for the non-vegetated canyon is given by the relationship:

$$q_{[nogr]} = U(T_{[nogr]} - T_{in}) \qquad \textbf{Eq. 241}$$

Where $T_{[no\ gr]}$ is the averaged air temperature inside the canyon when no vegetation is placed either on walls or on roofs. For the green-all case, with an average air temperature inside the canyon $T_{[gr\ a]}$, heat gains are[56]:

$$q_{[gra]} = U(T_{[gra]} - T_{in}) \qquad \textbf{Eq. 242}$$

Thus, the decrease in the cooling load, when both walls and roofs are covered with green is given by:

$$\Delta q_{[gra]} = \frac{q_{[nogr]} - q_{[gra]}}{q_{[nogr]}} \quad \Rightarrow$$

[56] Despite the fact that the U-value is altered, when vegetation is placed on the building's fabric, leading to further cooling load decreases, this is not taken into consideration here, as the aim is to directly compare between the effects of the microclimatic alterations on the buildings' cooling load, without it being affected by alterations to the fabric.

$$\Delta q_{[gra]} = \frac{T_{[nogr]} - T_{[gra]}}{T_{[nogr]} - T_{in}} \qquad \text{Eq. 243}$$

For $T_{[no\ gr]} \neq T_{in}$, $T_{[no\ gr]} > T_{in}$ and $T_{[gr\ a]} > T_{in}$.

Similarly, for the green-walls case, if T[gr w] is the average air temperature inside the canyon with the green walls, the cooling load decrease becomes:

$$\Delta q_{[grw]} = \frac{T_{[nogr]} - T_{[grw]}}{T_{[nogr]} - T_{in}} \qquad \text{Eq. 244}$$

For $T_{[no\ gr]} \neq T_{in}$, $T_{[no\ gr]} > T_{in}$ and $T_{[gr\ w]} > T_{in}$.

Considering an indoor limit temperature for cooling of 23°C for all climates studied, cooling load decreases due to green-all and green-walls cases are given as an average in Figure 278 and at an hourly basis in Figure 279.

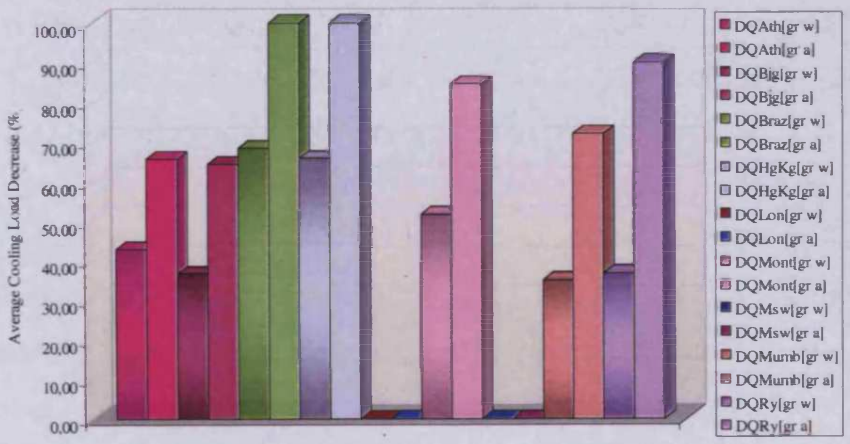

Figure 278. Average cooling load decreases (%), with a 23°C indoors temperature, for the green-walls and the green-all cases of all the climates examined

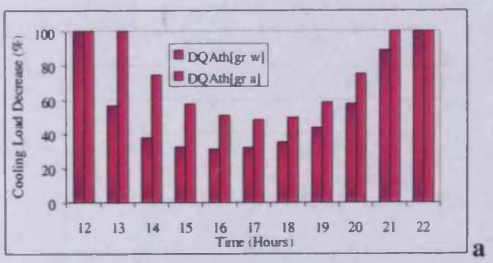

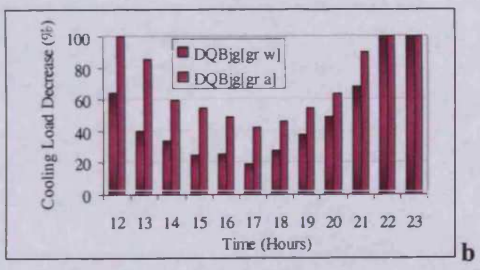

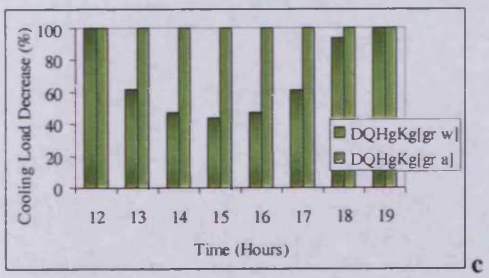

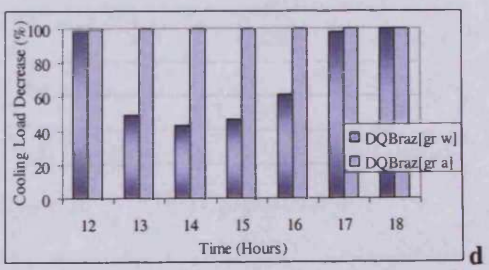

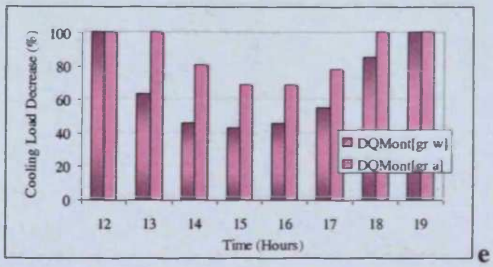

e

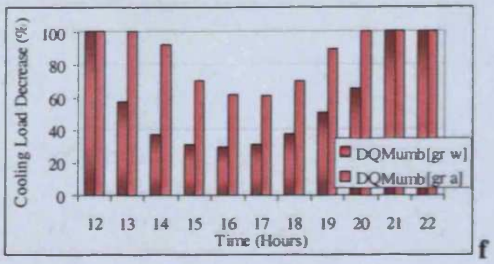

f

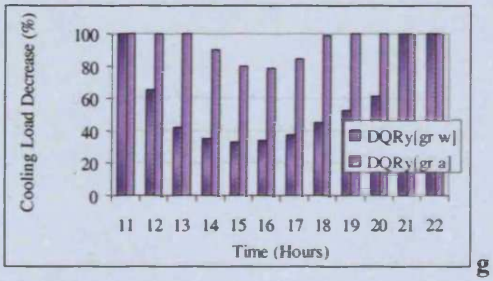

g

Figure 279. Cooling load decreases (%) for (a) Athens, (b) Beijing, (c) Hong Kong, (d) Brasília, (e) Montréal, (f) Mumbai and (g) Riyadh for green-all and green-walls cases

As can be observed from Figure 278, the largest cooling load decreases in all climates examined, occur for the green-all case. For the geometries examined for Brasília and Hong Kong, cooling load decreases for the green-all case reaches 100%; no cooling load is needed after covering roofs and walls with green, while in both cities cooling is needed in the afternoon and early evening for the no-green case (Figure 279c and d). London and Moscow are not affected at all, regarding cooling loads, as no cooling load was needed for the typical day examined, even before vegetation was placed around the canyon. Riyadh experiences a quite high cooling load decrease, of the magnitude of 90%, as does Montréal (85%) for the green-all case, lowering their total hours of cooling demand from 12 to 5 and from 8 to 4, respectively (Figure 279e and g). For the green-all case, Mumbai reaches a 72% decrease, lowering its cooling energy demand from 11 hours to 6 (Figure 279f), while for Athens and Beijing the decrease is 66% and 64%, respectively, lowering their energy demand by 4 and 3 hours, respectively (Figure 279a and b).

For the green-walls cases, cooling load decreases are less dramatic. The largest one is noted in Brasília (68%), with 6 hours decrease in cooling demand (Figure 279d). It is followed by a 66% and two hours decrease for Hong Kong (Figure 279e), 52% and 2 hours for Montréal (Figure 279e), 43% and 2 hours for Athens (Figure 279a), 37% and 2 hours for Beijing (Figure 279b), 37% and 3 hours for Riyadh (Figure 279g) and 35% and 3 hours for Mumbai (Figure 279f). It can be noted that the differences between the green-all and green-walls cooling loads are smaller for humid climates

(of the magnitude of 32-37%) and greater for arid climates (53% for Riyadh), due to the different humidity concentrations in the two climatic groups and their significance on outdoor temperature decrease.

In general, green roofs and green walls cool the microclimate around them, which can lead to quite important energy savings from cooling, depending on the climatic type, the amount and position of vegetation on the building. In cases where little cooling load is needed, cooling demand can be reduced to zero by covering building surfaces with vegetation. In other cases, energy savings can also be significant, varying from 90% to 35%[57]. In addition to the energy savings themselves, this could lead to successful applications of further passive cooling techniques, especially ones employing ventilation, which are not easy to implement in the extremely hot urban conditions.

6.5 Summary

Through this two-dimensional model, it has been proved theoretically that when plants are placed on the building fabric (roofs and walls), they can cool the microclimate around buildings quite significantly in summer. Plants do not raise their surface temperature as much as building materials do, leading to quite significant air temperature reductions. In addition, through evapotranspiration, they lower air temperatures quite significantly. For the nine climatic types examined, it can be concluded that the drier and hotter a climate is, the more significant the effect of vegetation is on creating an oasis in the built environment. Hot and humid climates benefit from the combination of green walls and green roofs more than expected, since impermeable asphalt lowers humidity concentrations inside the canyon, allowing for further humidity concentration increase and thus further air temperature decrease in the vicinity of buildings. Colder climates, with milder summers, benefit from the existence of vegetation on their urban environment but not to the extent that hot climates do.

[57] These percentages can become even greater, when a higher than 23°C limit temperature for cooling is considered. In general, inhabitants of hot climates are accustomed to higher temperatures (in the instance of Greek regulations, the limit temperature for cooling is set to 26°C).

In all climates, the most beneficial case for the air inside the canyon is the case where both roofs and walls are covered with vegetation; the cooled air masses from the green roof enter the canyon, allowing for further cooling from the green walls inside the canyon. More humid climates lower their air temperature more when both roofs and walls are covered with green, than when only the walls are covered with green. In all climates, the upper parts of the canyon, being further away from the asphalt's thermal effect and also more exposed to solar gains, benefit more from green walls than do lower parts, allowing for larger temperature decreases. The air layer above the canyon also benefits most, when both roofs and walls are covered with green; cooled air masses exist in both the horizontal and vertical axis at this level, leading to larger decreases than when only the walls or only the roofs are covered with vegetation.

When only the walls are covered with green (green-walls case), their effect can be noticed only inside the canyon and at the air layer above it, but not at the roof level. When only roofs are covered with green (green-roofs case), temperatures lower significantly at the air layer above the roof and their effect can be sensed at the air layer above the canyon, but not as much as for the green-all and green-walls cases. For the air layer inside the canyon, the effect of green roofs can be sensed only at its upper levels and is of a much lower magnitude than for the green-walls case. The thermal effect of green-roofs is null at the lower parts of the canyon.

As can be observed by comparing Figure 280a and Figure 280b, for all the nine climatic cases examined an average decrease of the air temperature inside the canyon of the magnitude of 25.8% occurs for the green-all case, while for the green-walls case it reaches only 10.6%. The maximum decrease observed for all nine climates examined is for the green-all case of hot and arid Riyadh (with 40.1% maximum and 34.0% daytime average decrease). The lowest decreases for the green-all case are observed for London and Montréal, the first reaching the lowest maximum (27.7%) and the second reaching the lowest daytime average decrease (19.4%). For the green-walls case the discrepancy between the maximum and the average decreases of all nine climates becomes smaller, ranging for the maximum from 12.5% (Montréal) to 15.1% (London) and for the average from 8.2% (Brasília) to 12.1% (Riyadh).

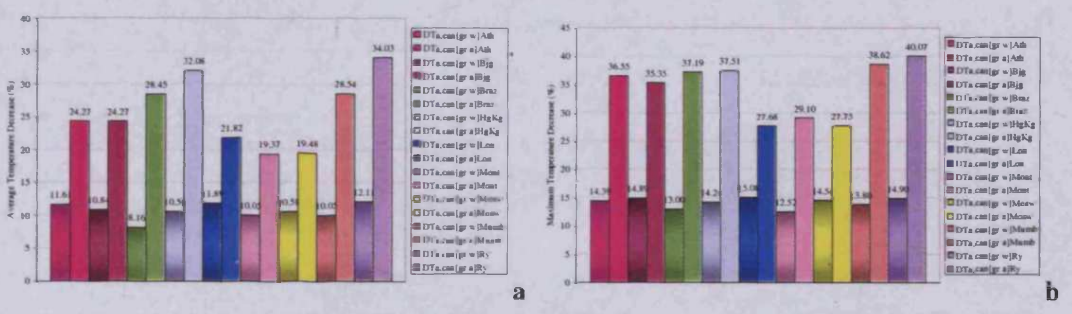

Figure 280. (a) Average and (b) maximum daytime temperature decreases (%) for the air layer inside the canyon, for green-wall and green-all cases for the E-W-oriented H5W10 canyon, for all nine cities

Regarding the air layer above the roofs, it is not affected by temperature distributions inside the canyon. Green walls do not have any impact at roof level. Green roofs have the same effect as when combined with green walls, allowing for high maximum and average temperature decreases. These decreases are mainly due to surface temperature alterations, which are lowered significantly when roofs are covered with plants. Due to the peaks reached by concrete roofs in summer, the maximum decreases for all climates examined range from 53.6% for Riyadh to 63.1% for Athens (Figure 281). Daytime average decreases at the air layer 1m above the roof range in magnitude from 23.0% for Moscow to 28.6% for Brasília. Decreases at roof level start being significant only after 12:00 at noon, when the concrete surface of the bare roof starts raising its temperature significantly, while the green roof keeps it at much lower levels.

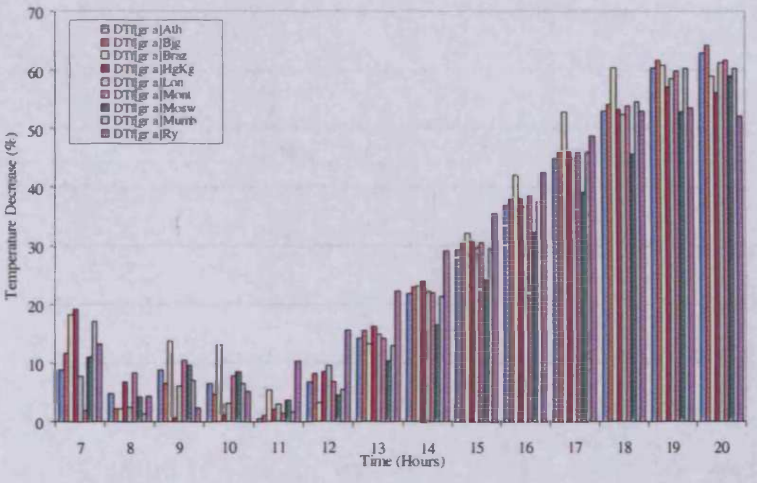

Figure 281. Daytime temperature decreases (%) for the air layer 1m above the roof (level f), when roofs are covered with green (green-all and green-roofs cases) for the E-W-oriented H5W10 canyon, for all nine cities

For all the nine cities examined a summary of the maximum, minimum and average temperature decreases inside the canyon and at roof level are summarised in

Table 263, as a percentage of the temperature which existed in the canyon before the implementation of vegetation on roofs and walls.

Table 263. Air temperature decrease (%) for all cities examined, for the E-W H5W10 canyon with perpendicular flow, for the averaged air temperature inside the canyon for the green-all and the green-walls cases and for the averaged air temperature 1m above the roof (level f) for the green-all case

City		Canyon, green-all	Canyon, green-walls	Roof, level f
Athens	max	36.6	14.4	63.1
	min	17.5	10.0	0.5
	ave	24.3	11.6	25.7
Beijing	max	35.3	14.9	64.4
	min	17.2	7.9	1.1
	ave	24.3	10.8	26.3
Brasília	max	37.2	13.0	60.9
	min	23.5	3.4	2.3
	ave	28.5	8.2	28.6
Hong Kong	max	37.5	14.2	57.1
	min	27.1	8.2	0.7
	ave	32.1	10.6	25.8
London	max	27.7	15.1	61.4
	min	18.9	9.9	2.6
	ave	21.8	11.9	25.3
Montréal	max	29.1	12.5	61.7
	min	15.1	8.1	1.5
	ave	19.4	10.0	26.0
Moscow	max	27.8	14.5	59.0
	min	14.3	8.0	3.7
	ave	19.5	10.6	23.0
Mumbai	max	38.6	13.8	60.4
	min	22.0	7.4	1.4
	ave	28.5	10.1	25.9
Riyadh	max	40.1	14.9	53.6
	min	29.3	9.8	2.4
	ave	34.0	12.1	27.8

Regarding canyon orientation, it has been observed in those nine climates examined for the E-W and N-S orientation, that the more exposed a canyon is to direct solar radiation, the most significant the effect of vegetation is on its temperature decreases. Surfaces exposed to larger amounts of irradiation benefit the most from being covered with vegetation. Yet these decreases are not significantly different for the two orientations, reaching differences from 0.1°C up to 1.2°C for the air layer inside the canyon. The difference between the decreases is strongly affected by the latitude, which determines shading distributions inside the canyon and the amount of solar radiation received on each plane. No general guideline can be drawn, as higher latitudes are more exposed to solar radiation in summer months, but receive smaller

amounts of irradiation than lower latitudes. In general, both orientations benefit from the presence of vegetation: the E-W canyon by lowering surface temperatures of its exposed south- and north-oriented walls, and the N-S canyon by lowering the peaks of its west-oriented wall. In both cases, even the temperature of the asphalt surface is lowered when walls are covered with green, by a 0.8°C average for all climates, due to its radiative exchanges with surfaces of lowered temperatures.

Regarding different flow directions (perpendicular and parallel to the canyon axis), insignificant differences have been observed between the two flows for all climates. In general, the perpendicular flow shows slightly higher decreases than the parallel flow. Nonetheless, this is not a universal rule: in the instance of the skimming flow H10W5 canyon, where the surface of green walls increases, the parallel flow causes slightly higher decreases than perpendicular one; in the example of Athens, the parallel flow results in higher decreases by 0.2°C at the air layer above the canyon, but no difference between the two flows can be traced for the extremely low wind velocities inside the skimming flow canyon itself.

The strongest effect of different flows is observed at the air layer above the canyon. In general, the perpendicular flow seems to make the role of green roofs stronger (green-roofs and green-all cases), while the parallel flow gains greatest benefit from the existence of green walls (green-walls and green-all cases). In humid climates, where the differences between air temperature decreases inside the canyon for the green-walls and the green-all cases are quite significant, the two flows may cause different results for each case. In the instance of Hong Kong, the green-all case benefits more from the perpendicular flow, while the green-walls case shows higher increases for the parallel wind flow. Nonetheless, differences between the two decreases are not significant, reaching only a 0.1°C difference.

Regarding different geometries, their effect is more significant on temperature decreases than is the wind flow direction. As they determine both the wind flow pattern inside and around the canyon and the amount of direct solar radiation that surfaces receive, their temperature decreases may be quite different. In the instance of Athens (Figure 282a), the temperature decrease for the green-all case is by an average 3.6% higher in the H5W10 canyon than in the H10W5 one and by a 7.2% higher than in the H5W15 canyon. For the green-all case of Mumbai (Figure 282b) these values become 7.2% and 7.7%, respectively, and for Riyadh 7.1% and 5.3%. Nonetheless,

for the green-walls case these values become completely different; the difference between the H5W10 and H10W5 canyon is 4.6% (the latter showing the highest decreases) and between the H5W10 and H5W15 canyon the average difference is of the magnitude of 3.8%. For Mumbai, these differences become 3.2% and 1.0%, respectively, and for Riyadh, 6.9% and 5.4%, respectively. In general, the wider a canyon is, the less significant the effect of green roofs and green walls on its air temperature; asphalt, being the most dominant factor in the formation of air temperatures inside the canyon, becomes a more predominant factor, when the canyon width, thus its surface, increases, making the thermal effect from walls and roofs even smaller. For a narrower canyon (H10W5), the effect of covering its walls with green is more significant than in wider canyons. Yet, as it is more shaded, the decreases themselves might seem higher for a wider canyon (as in the green-all case, when it is compared with the H5W10 canyon). In general, the effect of the green-all case in the H10W5 is not significantly greater than the green-walls case, in all three climates this study has examined. The proportion of the wall in the canyon geometry makes its thermal effect stronger, when covered with vegetation.

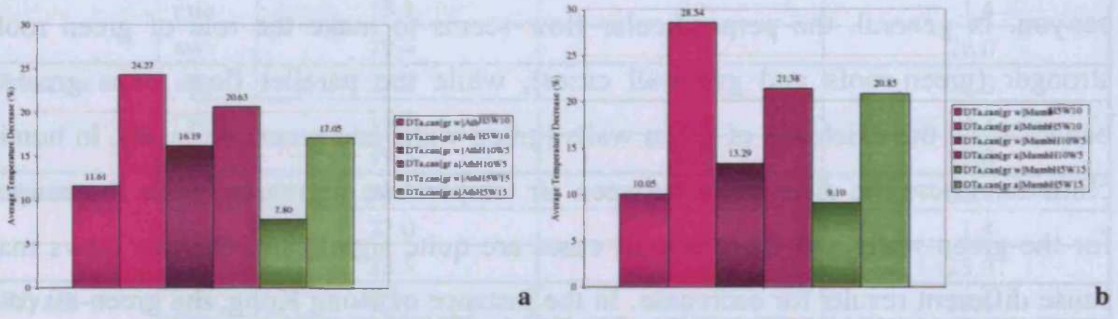

Figure 282. Average temperature decreases (%) for H5W10, H10W5 and H5W15 geometries for (a) Athens and (b) Mumbai

In conclusion, for the geometries examined, green roofs and green walls are capable of lowering air temperatures in the microclimate of buildings from 34.0% (daytime average decrease for Riyadh) to 8.2% (daytime average decrease for Brasília). The hotter and more arid the climate is, the stronger the effect of vegetation is on its built microclimate.

The most important factor in this temperature reduction is the amount and the geometry of vegetation. In all climates examined, the most beneficial case for the canyon's microclimate is that where both roofs and walls are covered with vegetation. The more exposed that surfaces are to direct solar radiation, the greater the effect of green walls and green roofs on lowering microclimatic temperatures. Wind direction

is not important for temperature decreases. For canyon geometries where the canyon width is the predominant factor, the effect of green roofs and green walls is smaller than in other geometries. Temperatures at roof level are not affected by the canyon's orientation or geometry.

On the question of the geometry and amount of vegetation, it has been clear that the more surfaces are covered with vegetation, the greater the temperature decreases. From the cases examined, the case where both roofs and walls are covered with vegetation shows the largest temperature decreases at roof level, inside and above the canyon, leading to greater energy savings and more comfortable thermal conditions in outdoor spaces. Green walls can only be beneficial in creating a microclimate inside the canyon. At roof level their effect is unnoticeable. Green roofs, on the other hand, mitigate the high temperatures at roof level, being able to influence the air masses above the roofs thus urban temperature, but have insignificant effect inside the canyon. If there has to be a choice between the two options (green walls or green roofs), the question which has to be answered is whether the effect should be only local, inside the canyon, or whether there could be a larger scale effect on the whole city, but not be sensed inside the canyon. If the desired effect is better microclimatic conditions inside the canyon, then green walls should be preferred. If the interest is not focused inside the canyon but on improving thermal conditions at the rooftop or the urban scale, then green roofs should be implemented.

6.6 References

1. E. Alexandri and P. Jones (2004) *The Thermal Effects of Green Roofs and Green Façades on an Urban Canyon.* PLEA2004, Eindhoven.
2. ASHRAE (1985) *Fundamentals, SI Edition.* American Society of Heating, Refrigerating and Air-Conditioning Engineers Inc, Atlanda.
3. H.J. Critchfield (1974) *General Climatology.* Prentice-Hall International Inc., London.
4. R. Doernach (1988) *Biotecture I: Living Houses.* The Rainforest Information Centre Good Wood Guide. Available from: http://www.rainforestinfo.org.au [Accessed 25th October 2004].

5. EDSL (1992) *TAS (Thermal Analysis Software) 3D Modelling, Version 7.6.* Environmental Design Solutions Limited, Milton Keynes.
6. D.M. Gates (1980) *Biophysical Ecology.* Springer-Verlag, New York.
7. R. Geiger (1967) *The Climate Near the Ground.* Harvard University Press, Cambridge Massachusetts.
8. G. Jendritzky, A. Maarouf, and H. Stainger (2001) *Looking for a Universal Thermal Climate Index UTCI for Outdoor Applications.* Conference on Thermal Standards, Windsor, pp 1-17.
9. H.G. Jones (1992) *Plants and Microclimate.* Cambridge University Press, Cambridge.
10. L. Katzschner, U. Bosch, and M. Roettgen (2004) Thermal Comfort Mapping and Zoning. *In:* M. Nikolopoulou (ed) *Designing Open Spaces in the Urban Environment: A Bioclimatic Approach.* RUROS project, Centre of Renewable Energy Sources, Athens, pp 22-26.
11. W. Kuttler (2004) Stadklima, Teil 2: Phänomene und Wirkungen. *In:* D. Möller (2004) *Beitragsserie Klimaänderung und Klimaschutz.* Available from: http://www.uni-essen.de/klimatologie [Accessed 3rd April 2005].
12. A. Marsh (2003) *Ecotect, Version 5.20(b).* Square One Research PTY LTD.
13. A. Matzarakis (2001) *Estimation and Calculation of the Mean Radiant Temperature within Urban Structures.* Available from: http://www.mif.uni-freiburg.de/rayman.description.htm [Accessed 3rd April 2005].
14. A. Matzarakis, H. Mayer, and F. Rutz (2002) *Radiation and Thermal Comfort.* 6th Hellenic Conference in Meteorology, Climatology and Atmospheric Physics, Ioannina, Vol. 2, pp739-744.
15. M. Nikolopoulou (1998) *Thermal Comfort in Outdoor Urban Spaces.* Ph.D. Dissertation, Department of Architecture, University of Cambridge.
16. M. Nikolopoulou (ed) (2004) *Designing Open Spaces in the Urban Environment: A Bioclimatic Approach.* RUROS project, Centre of Renewable Energy Sources, Athens.
17. T.R. Oke (1988) *Street Design and Urban Canopy Layer Climate.* Energy and Buildings, 1988, Vol. 11, pp 103-113.

18. V. Olgyay (1973) *Design with Climate. Bioclimatic Approach to Architectural Regionalism.* Princeton University Press, New Jersey.

19. K. Paspalas (1993) *Heat Transfer.* Salonikidis Editions, Thessalonica.

20. J. Remund, R. Lang, and S. Kunz (1997) *Meteonorm, Version 3.0.* Meteotest, Bern.

21. M. Santamouris (ed) (2001) *Energy and Climate in the Urban Built Environment.* James & James, London.

22. G. Scudo, V. Dessi and A. Rogora (2004) Evaluation of Radiant Conditions in Urban Spaces. *In:* M. Nikolopoulou (ed) *Designing Open Spaces in the Urban Environment: A Bioclimatic Approach.* RUROS project, Centre of Renewable Energy Sources, Athens, pp 12-16.

23. *The Times* (1999) *The Times Comprehensive Atlas of the World.* 2000 Times Books, London.

24. *Philip's* (1998) *Philip's Atlas of the World, Comprehensive Edition.* George Philip Limited, Octopus Publishing Group Ltd, London.

25. Welsh School of Architecture, Cardiff University (2003) *WinAir4.* Cardiff.

26. C. Yavuzturk and K. Ksaibati (2002) *Assessment of Temperature Fluctuations in Asphalt Pavements Due to Thermal Environmental Conditions Using a Two-Dimensional, Transient Finite Difference Approach.* Department of Civil and Architectural Engineering, University of Wyoming. Available from www.ndsu.nodac.edu [Accessed 6-4-2004].

Chapter 7

Conclusions

7 Conclusions

7.1 Literature Review

The alterations of the urban climate, discussed in chapter 2 can lead to uncomfortably raised temperatures for both cold and hot climates. Especially during the hot season, the heat island intensity may reach more than 10°C, depending mostly on the number of the population. For hot climates, this temperature rise leads to much higher temperatures and more uncomfortable conditions than in moderate climates. These raised temperatures have a direct effect on energy consumption for cooling and the morbidity and mortality risks of urban population, for not only hot, but also moderate climates. Although the heat island effect had been considered to be beneficial for colder climates (Givoni, 1998; Cantat, 1989), the combination of global warming and the heat island effect and the tendency of urban population to grow (Nash and De Souza, 2002) might lead to undesirable energy demand and morbidity and mortality risks in colder climates, too (Clarke et al., 2002). The death rate due to the heat wave experienced in summer 2003 in Europe cost excessive deaths of 16% for England and Wales and of a similar proportion (15%) for hotter Italy (Koppe et al., 2004). With morbidity and mortality threatening to increase due to the expected raised temperatures, it has been considered necessary to assess the potential of mitigating raised urban temperatures by covering buildings with vegetation in the places where the highest temperatures occur and the majority of the global population inhabits: cities.

It has been pointed out in chapter 3 that vegetation on the building envelope is not just a vision or a trend of the 21st century. Throughout hot and cold climates it has been used either for protecting the fabric from excessive heat and mitigating raised temperatures or for insulating the structure from extreme cold. For diverse societies and eras it has been used either as an elitist expression of power and wealth or as a mere available construction material. Vegetation close to the building and on the building itself has been perceived as a solution to the problems of the city by utopians, especially the 20th century ones, mostly from the point of view of the well-being of man. With environmental awareness in the 1970ies, vegetation on walls and roofs has been perceived as an element able to solve environmental issues in cities, such as raised temperatures, air pollution, and lack of oxygen. This thesis has shown

theoretically up to what extend green roofs and green walls can act as climatic modifiers and lower raised urban temperatures in hot periods, regarding the climate, the urban geometry and its characteristics.

7.2 Heat and Mass Transfer Model

7.2.1 One-Dimensional Model Development

In order to describe in detail the effect of vegetation on temperature decreases, it has been considered necessary to use a heat and mass transfer model. As most existing models describing heat transfer in the micro and local scale do not take into consideration vapour diffusion in molecular heat transfer, a model has been developed which takes this phenomenon into account. In this way, the thermal effect of vegetation for similar temperatures but different humidity concentrations can be described in detail. It is pointed out in chapter 4 that differences of the magnitude of 1.5°C for building materials to 5.0°C for plants can be observed between the predictions of the combined heat and mass transfer and the predictions of heat transfer. For the heat and mass transfer algorithm, with the same input temperature, but different input humidity concentrations, the predicted temperatures differ by up to 1.0°C.

Heat and mass transfer differential equations have been solved with finite differences methods. The forward Euler scheme, the first order forward approximation and second order central approximation are used for the purposes of this study. All three methods are unconditionally stable and with the right choice of time and space step, of a minor error. Nonetheless, these numerical methods have their limitations; in the instance of the choice of the time step, it is directly affected by the choice of the space step. In general, the smallest these steps are, the greatest the accuracy of the method. However, it has been pointed out in chapter 5 that for boundary air nodes, where many different parameters are added, the choice of a very small time step could lead to false predictions, as factors of important significance could be underrated. The preferable choice of time step, is the one close to its upper limit, as defined in paragraph 4.7, chapter 4. For the time and space steps used in this

model (time step 10sec and space step 0.10m) the error of these numerical solutions does not exceed ±0.3°C.

7.2.2 *One-Dimensional Model Validation*

The heat and mass transfer one-dimensional model has been validated with an experiment, presented in chapter 4, with a very good correlation between model and measurements. The experiment has determined the expression of parameters such as convection heat transfer coefficient, stomatal resistance and the method of solving the differential equation expressing the leaf temperature. The differences between the measurements and the predictions of the model have, in most cases, not exceeded the acceptable error band of the sensors (±0.3°C for most of the sensors used) and the finite differences approximations (±0.3°C, for time step 10sec and space step 0.10m), with most averaged errors being of the magnitude of 0.3-0.4°C. For only heat transfer calculations the differences between the measured and predicted temperatures are larger than for the heat and mass transfer algorithms used in the model, reaching errors of more than 1.6°C, with a 0.7°C average error. The measured stomatal resistance has a strong correlation with the predicted resistance, using equation 69. The difference between the measured and the calculated resistances is within the porometer's 10% error band. Nonetheless, these measurements took place in the mild summer of Cardiff. For more raised ambient temperatures, leaves might not evapotranspire as suggested by this formula, with ambient temperatures above 40°C making stomata close for many species (Gates, 1980). This might lead to slightly overestimated temperature decreases for extremely hot climates. Yet again, this is a question of the species of plants used in practice. Some species, when kept well watered continue to open their stomata even in extremely high temperatures (Willmer, 1983).

7.2.3 *Two-Dimensional Model Development*

The two-dimensional model describing the heat and mass exchanges in an urban canyon consists of one-dimensional models of the solid parts of the canyon and a two-

dimensional air mesh, where air velocity is input. The Monin-Obukhov similarity theory has been used to evaluate the eddy diffusion coefficients of energy and water vapour. Although the two-dimensional model has not been validated with an experiment as the one-dimensional model, as it consists of validated one-dimensional models and its two-dimensional part is based on method suggested by many researchers (Jacobson, 1999; Pielke, 2002; Noilhan, 1979), it is considered to be accurate, with its experimental validation being valuable future research.

In order to solve the two-dimensional advection-diffusion equation, the fourth order in space solution has been implemented. The fourth order in space solution, for the two-dimensional advection-diffusion equation has proven to be stable, especially when the eddy diffusion coefficient is not close to zero. From all numerical methods examined in this study, it has been the most unconditionally stable method, whose outputs are validated to be close to the expected ones. However, it is a quite complicated calculative method, which also needs two nodes on each side of the node whose thermal characteristics are calculated. The complication of the numerical solutions increases with the linear interpolation of input data; in order to solve heat and mass transfer inside the capillary porous body, without jeopardising the stability of the model, urban temperature, humidity and solar radiation data have been linearly interpolated, adding up to the complexity of calculations. Nonetheless, despite their complexity, these numerical solutions have proven to be unconditionally stable within reasonable limitations and accurately predicting heat and mass transfer in the complex built-vegetated environment, with an only $\pm 0.3^{\circ}C$ upper limit error.

7.3 Model Application; Assessing the Potential of Cooling Cities through Green Roofs and Green Walls

7.3.1 Green Roofs versus Cool Roofs

In general, it has been shown in this study that there is a significant potential of cooling urban spaces by covering building surfaces with vegetation. The thermal performance of vegetated roofs has been compared with that of high-albedo coated and high thermal capacity roofs (generally classified as "cool" urban materials). In general, green roofs show a much cooler performance than cool structural materials.

Although in the more humid cases examined, green roofs may have higher surface temperatures than white-coated roofs of the magnitude of 3.1-3.5°C in the morning, from the afternoon onwards, green roofs have much lower temperatures, of the magnitude of 8.8-10.5°C. In hot and arid cases, green roofs have lower temperatures than white-coated roofs throughout the day, of the magnitude of 8.8°C. It is also pointed out that three years after the white-coating application, as its albedo decreases, these differences become even larger, reaching 14.1°C for hot and arid climates, with the green roof always having lower temperatures than the white-coated roof.

7.3.2 Meso-Scale Temperature Decreases

From the simplified meso-scale model, presented in chapter 5, it has been pointed out that for the city scale up to 1.0-1.6°C lowered temperatures can be expected when the majority of roofs are covered with green. This mitigation strongly depends on the amount of roofs covered with vegetation and the amount of solar radiation reaching the roofs. When only a few number of roofs are covered with vegetation, this does not have a measurable effect on the urban temperature.

7.3.3 Micro-Scale Temperature Decreases

From the more detailed micro scale model, whose results have been discussed in chapter 6, more detailed conclusions have been drawn about the thermal performance of green roofs and green walls. From the cases examined it has been found that green walls can mitigate raised temperatures within the canyon, but they have no effect at roof level. On the other hand, green roofs can mitigate raised temperatures above the canyon but their thermal effect is insignificant inside the canyon; small temperature decreases can be observed only at the upper levels of the canyon, reaching up to 1.3°C maximum and 0.8°C day-time average, in the instance of the E-W-oriented H10W5 in Brasília. Thus, if the effect needs to be mitigated only at a micro or local scale, green walls should be considered, while for a meso scale mitigation, vegetation should be placed on the roofs.

However, the largest temperature decreases inside the canyon occur when both green roofs and green walls are implemented ("green-all" case). Air masses enter the canyon cooled by the green roofs, instead of warmed by the plain concrete ones. For all climates examined, the averaged maximum temperature decrease inside the canyon for the green-all case reaches 34.3%, with a 25.8% day-time average. For the green-walls case these numbers lower to 14.2% and 10.7%, respectively. Nonetheless, the largest temperature decreases occur at roof level for both green-roofs and green-all cases; the roof is the horizontal element of the canyon which is more exposed to direct solar radiation; not storing excessive gains in its fabric is extremely beneficial, from a thermal point of view. One meter above the roof, the averaged air temperature decrease for all climates reaches a 60.2% maximum, with a 26.0% day-time average. For surface temperature decreases, these numbers become even larger, reaching 69.9% and 32.9%, respectively.

7.3.3.1 The Effect of Wind Flow

Although wind flow direction and canyon orientation play an important role in temperature distributions in and above the canyon, the primary factors which affect temperature decrease are mainly the amount and geometry of vegetation, the climatic characteristics, as well as the geometry of the canyon. Wind direction does not affect temperature decreases so much, as air velocities inside urban canyons are generally, relatively low; the differences between the average temperature decreases of the air inside the canyon for different wind directions reach only 0.1-0.3°C.

7.3.3.2 The Effect of Canyon Orientation

Regarding the canyon orientation, its effect on temperature decreases is not so great for two reasons. First, due to the fact that it is the vertical component of the thermal gradient which plays the most important role in temperatures in the atmosphere near the ground, as has been discussed in chapter 5, making the effect of walls weaker. Second, due to the fact that the cases have been examined for the summer months, when the largest solar radiation reaches the horizontal plane; this makes the thermal effect of vertical planes even weaker. The effect of orientation strongly depends on the latitude, which affects the amounts of insolation on each

orientation. Depending on the latitude, the amount of vegetation, the difference between the averaged temperature decreases inside the canyon for different geometries varies from 0.2°C to 0.7°C.

7.3.3.3 The Effect of Canyon Geometry

The canyon geometry plays a more important role than orientation, as it determines the amount of direct solar radiation reaching vertical and especially horizontal surfaces inside the canyon. In general, it has been shown that the wider a canyon is, the more its temperatures are dominated by the proportionally larger street surface. Thus, green roofs and green walls have the smallest effect on it. In the instance of the three geometries examined for Mumbai, the average air canyon decrease for the narrower H10W5 canyon is of the magnitude of 13.3% (3.7°C). For the wider H5W10, this decrease reaches 10.1% (2.7°C) and for the even wider H5W15 canyon, it is only 9.1% (1.9°C).

7.3.3.4 The Effect of Climatic Characteristics

Regarding which climates are more benefited by green roofs and walls, it can be said with certainty, that the hotter and drier a climate is, the larger its temperature decrease when roofs and walls are covered with vegetation. In the instance of hot and arid Riyadh the average air temperature decrease inside the canyon is of the magnitude of 9.1°C, reaching 11.3°C maximum, for the green-all case. Yet again, for humid climates, due to the relative humidity decreases in the built environment, the effect of vegetation is even stronger than expected, as have been the cases of Mumbai, Hong Kong and Brasília. In the instance of the latter, the temperature decrease for the air inside the canyon, reaches a day-time average of 5.6°C, with 7.6°C maximum for the green-all case. For the green-walls case, this decrease is much lower, with 1.9°C day-time average and 3.5°C maximum. Colder climates, such as London's, Moscow's and Montréal's benefit less from green roofs and walls; in the instance of London, air temperature decreases inside the canyon reach 3.4°C day-time average, and 4.1°C maximum, for the green-all case, much smaller than for hot and arid Riyadh. Nevertheless, even these smaller decreases of colder climates may result in more comfortable and cooler from a thermal point of view, outdoor conditions.

7.3.4 *Outdoor Thermal Comfort*

In general, for all climates examined, outdoor thermal comfort in summer can improve drastically both at roof level and inside the canyon with the use of green roofs and green walls. Especially for the hot climates of Athens, Beijing, Brasília, Hong Kong, Mumbai and Riyadh outdoor conditions can improve from the "very hot" area to the "slightly warm" and "comfortable" zones. For the colder climates of London and Moscow, the predicted canyon and roof physiological equivalent temperatures (PET) are already within the more comfortable band; green walls and green roofs shift them to slightly cooler "comfortable" bands, which might be more pleasant for populations adapted to colder climates. For the warmer summer of Montréal, outdoor thermal comfort conditions are significantly improved, from "hot" and "warm" to "slightly warm" and "comfortable" zones.

7.3.5 *Energy Savings*

These lowered temperatures can also lead to significant energy savings for cooling, up to 100% for the green-all case of Brasília and Hong Kong. For London and Moscow, for a 23°C indoors limit temperature, there is no need for cooling, thus the greening of walls and roofs does not affect energy consumption for cooling for the typical summer day examined for these climates. For the rest of the cities, the much lower temperatures of the green-all case lead to larger energy savings than the green-walls case. In the instance of Athens, the green-all case can lead to 65.7% cooling savings, while for the green-walls case it reaches only 42.8%.

It can thus be concluded that green roofs are beneficial not only at roof level, but also inside the canyon, in conjunction with green walls. Green walls are beneficial only inside the canyon, leading to much smaller temperature decreases for all climates, if not combined with green roofs. Green roofs can lead to significant temperature decreases at roof level and thus in the urban "plume" layer (Figure 27, chapter 2), when the majority of urban roofs are covered with plants. The combination of both green roofs and green walls can improve the thermal conditions of cities in tropical and hot climates drastically, both inside and above the urban canyon.

7.4 Further Research

A detailed study of sustainable irrigation techniques of green roofs and green walls for different climatic conditions and urban characteristics could be very advantageous for the sustainable operation of such a project. Also, assessing the potential of greening walls and roofs from an implementation point of view would be useful; studies on the static load of buildings in existing urban structures, implementation policies of green roofs and green walls in conjunction with water conservation strategies could prove extremely constructive if such an idea is to be implemented for mitigating the heat island effect.

Although this study has focused on ground covering plants, it can be perceived quite easily that different types of vegetation will produce different thermal effects, depending on their resistances. More evapotranspiring plants will lead to further temperature decreases, while less evapotranspiring ones may lead to smaller temperature decreases. A more analytical study, regarding the types of vegetation which can be used, could prove very advantageous in providing guidelines for the different types of vegetation which could be used for different climates, depending on the desired thermal effect as well. Also the combination of ground covering plants, bushes and trees on a roof could be advantageous from a thermal point of view, a thermal description of which would acquire a further development of this model to describe heat and mass transfer in trees.

To this, a classification of thermal and biological properties of various plants, bushes and trees, in libraries, equivalent to those of thermal properties of materials – e.g. like the Food and Agriculture Organization's (FAO) for the evapotranspiration rate (Allen et al., 1998) – could be useful. By applying the factors developed by FAO in species' resistances and not evapotranspiration rate, mathematical models similar to the one developed for the purposes of this study could fully describe temperature and humidity distributions, taking into consideration the special characteristics of each species.

Concerning the model developed in this study, it could evolve from two-dimensional to three-dimensional. In this way the description of advection would be more comprehensive. The thermal effects of green roofs and walls could then be examined in more detail for various urban blocks and geometries. The model could then be used as a local scale, as well. A more detailed description of the sky

temperature expression, as the ones discussed in chapter 4 could be useful, in order to take into consideration other sky conditions apart from the clear sky one, which was studied in this thesis. The study of green walls and green roofs on the canyon's microclimate for other seasons (winter, spring etc), as well as throughout the year, could lead to a more holistic assessment of their climatic behaviour. Also, a more detailed description of the building envelope could lead to more detailed predictions. For instance, if window areas on the façade are modelled and parts of the walls and the roof which are not covered with vegetation are taken into consideration, this could lead to a more detailed parametric study.

Also an investigation on the amount of time (in days) which should precede a run in a microclimatic model should be done. In this way, the resulting temperature distributions and heat exchanges will be fully taking into consideration the heat capacity of materials in the built microclimate.

Parameters such as the heat load from cooling buildings could be added up in the canyon's thermal balances before and after the implementation of vegetation. Thus a more in depth description of the microclimatic temperature decreases could be assessed, taking into consideration the effect of anthropogenic heat release from air conditioning (discussed in paragraph 2.3.8, chapter 2). Quantifying up to what extend the anthropogenic heat release is lowered due to vegetation could also be an interesting study.

It might be advantageous to make a further mathematical investigation into more numerical techniques for solving the differentials of this model, which would be equally stable but less complex (e.g. not demanding linear interpolation of input data). Also, in this model, the differentials have been solved, assuming that the air's density is constant. By solving them with the air density considered unstable and changing with temperature, a more detailed description of the air's movement and thus thermal behaviour could be achieved.

Combination of micro scale models with meso scale models could lead to more comprehensive studies, so as to derive more detailed conclusions about the effect of green roofs and green walls on the climate of the city as a whole. Detailed urban geometry, type and amount of vegetation could be made in a micro scale model, which could be input in the meso scale one, to assess the potential and to find the

optimum vegetation combinations for mitigating the heat island effect for the specific characteristics of each city.

Experimental studies on green walls and green roofs in the urban context could prove extremely fruitful. The impact of urban thermal characteristics on vegetation for different climates and microclimates could be examined, verifying theoretical results. Conclusions could be drawn about which types of vegetation should be used for the less sunny and less windy urban canyon conditions, which could effectively lower canyon temperatures.

Also exploring other issues of green roofs and green walls could be advantageous. For instance, studies on the psychological and social effects of green buildings, for different social and age groups, health issues which might improve (e.g. related to raised temperatures and pollution) or arise (e.g. related to allergies), interplanting for avoiding specific insects (e.g. mosquitoes) could be useful for a holistic approach in the implementation of green roofs and green walls.

In 1902, Ebenezer Howard was envisaging that "town and country *must be married* and out of this joyous union will spring a new hope, a new life, a new civilization" (Howard, 1970). In our times it is quite clear that social reforms cannot occur only through city planning. Garden cities, either in their vertical or horizontal form, naked from their beautiful social visions, have failed to succeed in marrying town and country in most modern cities. Nonetheless, the attempt of improving urban dwellers' everyday life and trying to transform cities into viable and sustainable spaces is not abandoned. If the structure of the city stays as is, but its buildings are covered with vegetation, as this study proposes, a new type of marriage of town-city could evolve (Figure 283a and b). With living building envelopes, not only by the presence of human beings, but also by their vegetated fabric, new relationships between city and nature could be born, new relationships of urban dwellers with nature and their habitat could evolve, in a healthier, more sustainable, cooler and maybe more human-friendly environment. This could be carried on to an urban scale, with green roofs being transformed into superterrestrial urban parks, by linking them with footbridges (Figure 283c), which might be a very challenging urban planning project. In this way the so much desired separation of pedestrian from the automobile (e.g. Le Corbusier, 1948) could be achieved; urban dwellers could be experiencing the city from above,

having the view to the sky that all day-light creatures deserve, while vehicles would be left to move at the bottom of urban canyons.

Figure 283. Partial view of the roofs of Athens in the city centre[58] (a) as are now, (b) covered with ground covering plants, without any particular design and (c) with foot bridges linking them

7.5 References

1. R.G. Allen, L.S. Pereira, D. Raes and M. Smith (1998) *Crop Evapotranspiration - Guidelines for Computing Crop Water Requirements - FAO Irrigation and Drainage Paper 56. FAO* - Food and Agriculture Organization of the United Nations, Rome.
2. O. Cantat (1989) *Contribution à l'Étude des Variations du Bilan d'Énergie en Région Parisienne*. Ph.D. Dissertation, Université Paris-Sorbonne.
3. S. Clarke, J. Kersey, E. Trevorrow, R. Wilby, S. Shackley, J. Turnpenny, A. Wright, A. Hunt and D. Crichton (2002) *A Climate Change Impacts in London Evaluation Study, Final Report.* London Climate Change Partnership.
4. D.M. Gates (1980) *Biophysical Ecology.* Springer-Verlag, New York.
5. B. Givoni (1989) *Urban Design in Different Climates.* University of California, Los Angeles, World Climate Programme Applications.
6. E. Howard (1970) *Garden Cities of To-morrow.* Faber and Faber Ltd, London.
7. M.Z. Jacobson (1999) *Fundamentals of Atmospheric Modeling.* Cambridge University Press, Cambridge.

[58] The picture was taken in spring, under overcast sky. The colours of the green roofs were taken from ground covering vegetation of the area, under the same light conditions.

8. C. Koppe, S. Kovats, G. Jendritzky and B. Menne (2004) *Health and Global Environmental Change; Heat-Waves: Risks and Responses.* Series No. 2, Energy, Environment and Sustainable Development, World Health Organization, Copenhagen.
9. Le Corbusier (1948) *Concerning Town Planning.* The Architectural Press, London.
10. J.G. Nash and R.-M. De Souza (2002) *Making the Link: Population, Health, Environment.* Measure Communication, Population Reference Bureau. Available from http://www.prb.org [Accessed 5th December 2004].
11. J. Noilhan (1979) *Les Facteurs Physiques du Microclimat au Voisinage d'un Batiment. Etude bibliographique.* Centre Scientifique et Tecnique du Batiment, Etablissement de Nantes.
12. R.A. Pielke (2002) *Mesoscale Meteorological Modeling.* Academic Press, San Diego, San Francisco, New York.
13. C.M. Willmer (1983) *Stomata.* Longman Inc., New York.

Appendices

Appendices' Table of Contents

1. Appendix 1: Further Thoughts – Sustainable Irrigation Techniques

When creating any form of garden, especially in dry and arid areas, one should be conscious about the environmental impacts of irrigating them. The first step is to use local vegetation, which has already adapted to the climatic characteristics of the area. Irrational imitation on a large scale of gardens of other climates, might lead to draining out the water resources of the city's greater vicinity to levels which might be irreversible. In the instance of arid Las Vegas, the persistence of its inhabitants in maintaining green lawns and lush vegetation, a stark contrast to the native desert one, is responsible for 39% of the total water consumption of Las Vegas, causing major water issues in this arid area (Stave, 2003).

Apart from choosing local, dry-tolerant and drought-adapted vegetation, one should be conscious of not causing new environmental issues by generating a necessity for further water consumption. In general, cities consume a significant amount of the resources their surrounding environment and one of these is water. In the instance of Athens, water travels from such distances as 188.5km (EYDAP, 2003) in order to supply the city. Quite significant ecological problems might be caused, by augmenting the water demand, not only in the city itself, but also in rural areas which provide the city with its necessary commodities. That is why emphasis is placed on the fact that urban "hanging gardens" could be irrigated with water that the city already consumes, without major surcharge of the water demands of the city.

Following the rationale *"reduce-reuse-recycle"* three solutions of a sustainable nature can be suggested for the irrigation of green roofs and green façades; reduce the amount of water needed for irrigation, reuse rainwater[1] and recycle water which is already used by urban dwellers. Choosing which solution to use and to which extend they are going to be combined, depends on the specific climatic and geometric characteristics of the city in question as well as the culture of its inhabitants.

[1] The solution of using the groundwater of cities is not suggested here as a general guideline here. Cautious study should be done before using the underground water of a city for irrigating large areas of vegetation, without harming the underground water levels and the city above them as well.

1.1. Reduce the Amount of Water Needed for Irrigation

In general, crops on green roofs need to consume less amount of water than crops on the ground. They are contained within the roof structure and water is trapped within it, while a large amount of water irrigating crops on the ground escapes to lower ground layers. Nevertheless, there are several techniques of reducing the amount of water needed for irrigating green roofs. These could include cautious design of the crop geometry and interplanting, as well as deep cultivation. Appropriate irrigation methods could also be applied, such as drip or trickle piped irrigation which deliver water straight to the roots of the crops, or the use of a layer near or under the roots of plants, which would trap water and prevent it from evaporating as easily.

Proper shading of plants can create lower surface temperatures and impose less heat stress on the crops. In general, most plants need a minimum of 6 hours of direct irradiation, especially morning irradiation, which is more beneficial and does not add to its heat stress as the afternoon irradiation (Harper et al., 1994). By interplanting diverse crops, water conservation can be achieved, through shading and wind sheltering for both plants and soil. Drought-adapted plants can shelter and humidify smaller and more delicate ones. Crops with the same water needs should be grouped together and closely planted (ibid.) in order not to waste more water than the amount needed for their proper irrigation. Apart from the distribution of plants, the depth at which the root or the seed is placed can be beneficial for water conservation. Deep cultivation, up to 45cm within the soil layer (ibid.) encourages deep-rooting of crops, as the surface layer of soil dries out quickly, while deep-rooted plants survive drought better than shallow-rooted ones. For the swallow soil layer of extensive green roofs, such deep cultivation might not be feasible, but the concept of rooting plants as deeply as possible should be kept in mind.

Permanent piped irrigation schemes on or below the ground reduce the amount of water lost through evaporation, compared to irrigation channels. Especially drip irrigation, above or below the ground, close to the roots can reduce water wasted when irrigating and minimise it to the levels of water needed for evapotransporation. Clay pot and porous capsule irrigation is a water-conserving irrigation system used by the Romans for many centuries (UNEP, 1997). It increases the storage of water within the soil and improves its distribution within the soil matrix. It is consisted of clay pots

and porous capsules interconnected with pipes. A constant-level reservoir is used to maintain a steady hydrostatic pressure. The pots are partially buried in the soil and open at the top. Water is distributed through the pipes, to ensure a fairly uniform permeability and porosity (ibid).

The most commonly used irrigation systems in watering green roofs are drip irrigation and spray irrigation (Osmundson, 1999), the latter not being a water conserving technique. However, when shrubs and trees are planted, cautious use of spray irrigation could prove beneficial for their well-being. Several techniques have been developed for drip irrigation of green roofs, such as Optima system and ZinCo system. With the Optima system, a layer of water is kept on the roof at all times; it rises through the planting medium with capillary action. Water rises through layers of expanded shale pellets to the soil and plant's roots (Figure 1). The depth of the water layer is kept uniform by overflow pipes, connected to the building's drainage system. In case water levels drop, a float valve releases water from the building's water system –or auxiliary water tanks (paragraph 1.2). The ZinCo system is composed of a series of water-retention troughs and air ventilation holes on top of recycled polyethylene panels, to ensure water retention and the necessary soil layer ventilation (Figure 2). Water again rises through capillary action to the planting medium.

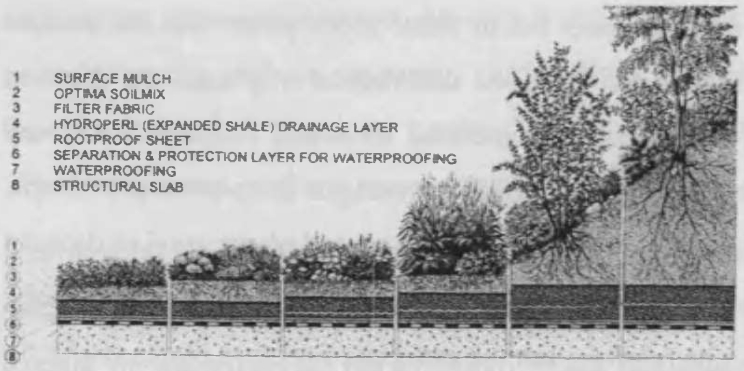

Figure 1. Section of extensive (left) and intensive (right) roof planting watered with Optima system (Osmundson, 1999)

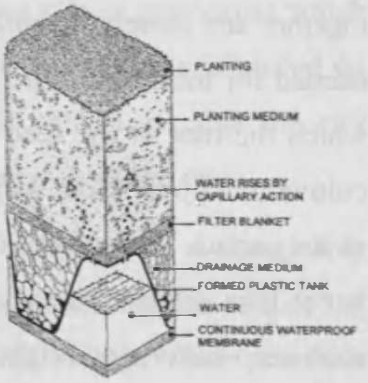

Figure 2. Section of green roof irrigated with ZinCo system (Osmundson, 1999)

Apart from the consciously designed irrigation systems, water reduction can be achieved either by mulching the crops (Ryrie, 2001) or by putting clay linings under lawns (Grant et al., 2000). The numerical and experimental studies of mulch residues show that, in general, a mulch layer tends to lower the soil evaporation and to reduce the soil temperature amplitude (Enrique et al., 1999). Soil temperatures do not reach high peaks and remain relatively constant because of their being shaded by the mulch

layer, which results to reduced heat stress on plants and organisms (Ryrie, 2001). This has been verified by experiments conducted on the effect of mulching on its microclimate, which have shown that due to its insulating properties, during the hot season, mulching can lower temperatures, on both the surface and within the soil (Geiger, 1967). In general, a 2.5cm mulch layer is recommended at the top of green roofs, to prevent excess heating in warm climates and protect plant roots from frost damage in cold climates (Osmundson, 1999). Consequently, roots are protected from extreme temperatures which would lead to increased water demand or death of the plant. It has been estimated (Harper et al., 1994) that mulched soil takes at least 8 times longer than bare soil to evaporate 2.54cm of water[2]. Thus, a mulch layer keeps the soil moist and prevents it from drying out in hot weather.

In general, any kind of humus layer can be extremely beneficial for retaining water; it increases infiltration and water-retentiveness, thus preventing rain and added water from draining away quickly and helping plant roots to extract as much water as possible (Harper et al., 1994). Apart from mulch, a clay lining under the crops can lead to water savings. In general, clay can trap water and retain it within its texture because of its high moisture potential[3] for the saturated soil (which is of the magnitude of -40.5 to -63.0cm compared to sand soil whose moisture potential for saturation is of the magnitude of -12.1cm)[4]. For crops which work well with clay soils (such as peas, potatoes, strawberries, elder etc) (Ryrie, 2001) clay soils could be extremely advantageous. Although clay soil holds nutrients well, it tends to waterlog, causing lack of aeration and thus stresses the plants and soil life (ibid.). It does not allow air and water to penetrate easily; therefore careful design should be done before the clay layer is applied.

Concerning the reduction of water needed for irrigating plants used on green roofs and green walls for mitigating the heat island effect, one should be careful to provide plants with the adequate amount of water needed for proper evapotranspiration without wasting larger amounts than that. In this case the highest priority, apart from the fact that the lives of plants should not be jeopardised, should be that plants are adequately provided with water, so that their evapotranspirational rate is capable of

[2] In the original text, 1 inch of water.

[3] It is reminded here that the moisture potential of soil is the potential energy required to extract water from capillary and adhesive forces in the soil (discussed in chapter 4).

producing the desired reduced urban temperatures. Techniques which retain water within the soil might reduce the evaporational rate from the soil, but if applied properly, not the evapotranspirational rate from the plants themselves. Although the use of excessive water for irrigation and spraying the air might be beneficial for reducing urban temperatures, especially for dry and arid climates, one should be careful about not causing other environmental problems, such as the reduction of the sources of available water. Rainwater reuse and grey water recycle could be advantageous for irrigating green roofs and green façades, with or without taking into consideration water conservation techniques.

1.2. Rainwater Harvesting

The term "rainwater harvesting" describes the collection of rainwater, at a local scale, for reuse[5], either for drinking, domestic use, or irrigation. Depending on its use, rain water is filtered in a different way. When used for irrigating purposes, and not for drinking, it does not need as much further processing and is mostly recommended for this use (Harper et al., 1994; Thornton, 2004; Grant et al., 2000), provided there is sufficient rainfall for making such a project feasible. Rainwater harvesting has been a traditional technique for irrigation and domestic water use in rural areas around the globe (Rose, 1999). Recently, interest in rainwater harvesting has been shown in ecological regeneration projects in urban areas, such as Hanover's Rehblockstrasse, which was built in 1989 and rain water has been used since for toilet-flushing (Kennedy, 1997). Rainwater harvesting has also been applied for the same purposes in Hong Kong buildings, such as the Kadoorie Farm and Botanic Garden (Yang et al., 2002).

Apart from the rain itself, two main features are needed for harvesting rainwater; a catchment area and a storage space. Pipes and gutters are also needed to lead water from the catchment area to the storage space, filters to filter solids may be needed and pumps could also be necessary. The catchment area is the area from which rainwater

[4] Figures as suggested by Jacobson (1999).

[5] There are some objections about the term *"reuse"* instead of *"use"* in rainwater harvesting. Because of the nature of the circle of water and the fact that water keeps being "reused" since the formation of the planet, the term *"reuse"* is employed here.

is collected. It could be either the roofs, or the ground. The first case is more preferable when the ratio of roof area to occupancy is high; in the instance of commercial settings, buildings with high daytime use might offer such conditions (Thornton, 2004; Yang et al., 2002), but this again depends on the architectural characteristics of the city. In the second case water needs more filtering process, as hydrocarbons (oil, petrol, diesel), animal faeces and dirt in general might mix up with the rainwater (Thornton, 2004). Reed beds can be used for treating water in this case (paragraph 1.3). The amount of water which can be harvested from a specific area depends on the rainfall levels of the area, the plan area of the catchment surface (its footprint on the horizontal plane), the tilt and the type of material of the catchment surface. In general, the steeper and smoother the catchment surface is, the more rainwater is harvested.

Rainwater reservoirs can vary from utilitarian underground cisterns to highly ornamental ponds. They can be open, such as a pond (Figure 3b), or closed (Figure 3a), such as a tank. In the case of an open reservoir, the water needs no additional filtering. Shading should be provided to the open reservoir in order to minimise water evaporation (Harper et al., 1994). It should be regularly inspected, especially after conditions of extreme rainfall and excessive flooding (Stern, 1988). Also, it should be provided with a spillway, leading to the storm water main system. Although in an urban space it is not easy to find open spaces to create ponds, they could be implemented as water features in intensive green roofs. It would not be advisable to place open reservoirs at urban ground level –unless within parks– as traffic pollution might deface the water.

Figure 3. Rainwater reservoirs in the Centre for Alternative Technologies; (a) closed tank with filter and (b) pond (open reservoir) with aquatic ornamental plants (author)

Wherever possible, closed reservoirs, such as tanks or cisterns, are preferable for places that suffer from a lack of space. Water should be filtered before entering the tank from solids (Figure 3a), in order to protect the tank from dirt and the development of bacteria and microorganisms on the solids (Thornton, 2004). In cities with high pollution concentrations and long, dry periods, it would be more advisable not to collect the first rainwater from roofs, as a significant amount of pollutants could have been deposited on the roof surface and high concentrations of pollutants could enter the tank (Yaziz et al., 1989). When the first rainwater has cleaned urban roofs from pollutants, rainwater could start being collected in tanks. Tanks should be kept indoors (Figure 4) or underground (Figure 5) in order to avoid direct exposure to irradiation and in a cool place. High temperatures can cause the growth of algae and bacteria within the tank (Thornton, 2004), which contaminate water and might jeopardise public health. Buildings' basements could be ideal for holding such tanks. Water falls into these tanks with the force of gravity, but a pump is needed to lift water up to roof level. A spillway should be placed at the top of the tank, again leading the excessive water to the storm water main system.

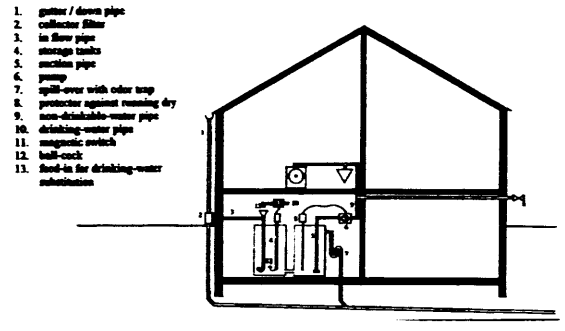

Figure 4. Rain water storage inside a building (Kennedy, 1997)

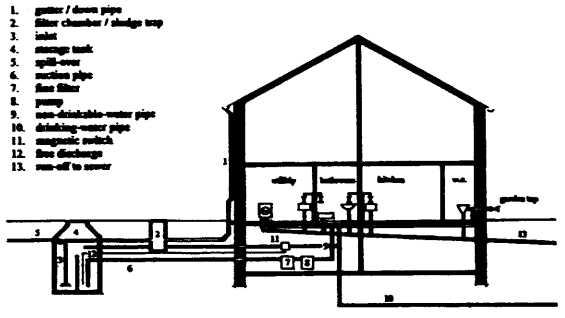

Figure 5. Rain water storage outside the building (Kennedy, 1997)

There is a simple formula for calculating the necessary volume (V) of the tank/reservoir; it is proportional to the annual rainfall (R), the catchment area's footprint on the horizontal plane (A_h), a catchment area factor (η_a) which depends on

the surface material of the catchment area, its tilt and the climatic characteristics[6] as well as from a filter factor (η_f), which depends on the type of filtering process.

$$V = \eta_a \eta_f A_h R \qquad \text{Eq. 1}$$

Collecting rain water from a green roof, especially one on which water conservation techniques have been applied might not be the most efficient way of rainwater harvesting[7]. Nevertheless, in cases of extreme rainfall and flooding, such as the monsoon periods in the rain forest and savana climates, it might prove to be sufficient for irrigation for a sufficient time of the dry period and might be beneficial for the central drainage system in case of floods.

1.3. Grey Water Recycling

Water used in urban buildings could be reused for irrigating purposes. Especially in dry and arid areas this might prove to be very beneficial. Two terms are used to describe water waste from household and office buildings, depending on the degree of contamination of water; "grey water" and "black water". The term "grey water" is used to describe water which has been used for cleaning procedures within the building, such as in showers, hand basins, washing machines, kitchen sinks and dishwashers. The term "black water" describes wastewater from toilet flushings. Both types of domestic wastewater, especially the latter might cause diseases either due to chemical substances (such as heavy metals, toxins in mismanaged industrial effluent) or due to biological agents (pathogens), if not treated properly (Rose, 1999).

Grey water does not need as much treatment as black water and with the appropriate cleansing procedure it could be recycled and stored easily for irrigation purposes at a community scale level. Furthermore, there is a distinction between "dark" and "light" grey water. Dark grey water origins from kitchen sinks and dishwashers (water containing fats) while light grey water comes from showers, baths, basins and washing machines. In general, grey water, both light and dark, is a considerable percentage of total water consumption in the building sector. In the UK

---

[6] This factor is expressed by the ratio of the runoff volume to the precipitation volume.

[7] Its catchment area factor (η_a) ranges from 0.20 to 0.25, while for concrete roofs it ranges from 0.70 to 0.75.

it occupies up to 46% of domestic water usage, out of which 37% (of the total water consumption) is light grey. Concerning office water use grey water is 28% of the total water consumption and all of it is light grey (Thornton, 2004).

Dark grey water is more difficult to clean and store, as it contains fats, which are more difficult to be removed. Straw filters, which should be regularly replaced, could be used to remove food wastes and fats (Harper et al., 1994). Once fats are removed its filtering procedure is the same as that of the light grey water. The cleaning procedure of light grey water includes the removal or neutralisation of sodium salts from soaps and detergents, which can build up in the soil and destroy its structure (Grant et al., 2000), as well as the removal of by-products of cleansing procedures (skin cells etc) (Thornton, 2004).

Both grey water and rainwater –especially the one harvested from ground surfaces– have to be cleansed of any solids (which could be home for dangerous bacteria), microbiological organisms, chemicals, organics and anything which might be contained in water and could be hazardous for public health, the quality of soil and the life of plants. If grey water is stored without any treatment, it should not be stored for longer than 48 hours as aerobic and anaerobic degradation of organic matter occurs. However, it has been found (Dixon et al., 1999) that a 24 hour storage could be beneficial for the settlement of chemicals and the inclination of pH, without any significant increase of coliform concentrations. Solids can be filtered through settlements, flocculation or filtration. A well established technology for the purification of grey water in the UK is reedbeds, both horizontal and vertical ones. Apart from treating water, they also offer a natural habitat, by the flora existing on them. Pond systems, such as solar ponds, settlement ponds and lagoons are also a well-established technique, especially in warm climates, but due to their requirements of large areas for the treatment, they might not be adequate for applications within the urban texture.

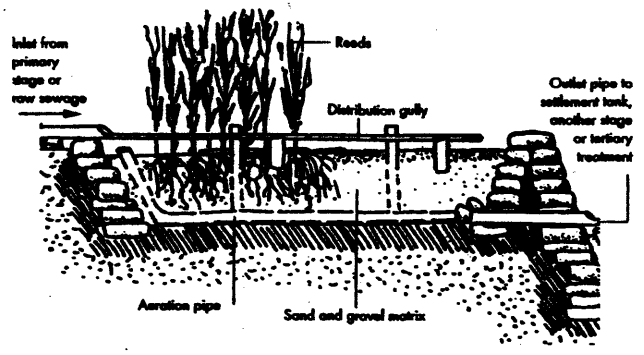

Figure 6. Section of vertical flow reed bed (Grant et al., 2000)

Reed beds are aquatic plant treatment systems of domestic wastewater. In fact, the treatment of wastewater with the use of aquatic plants such as water hyacinth is an age old technique utilised over 1,000 years ago in the Sudan (Rose, 1999). Horizontal flow reed beds or a combination of both vertical and horizontal reed beds if necessary can be used as treatment plans for both grey water and rain water collected from ground level. Vertical flow reed beds consist of a sand-gravel matrix, where aquatic plants, such as common reeds, iris, water mint etc are planted (Figure 6). Water flows vertically, from top to bottom and solids are filtered in the sand-gravel matrix, where they are filtered physically and broken down by micro-organisms. Although it is the sand-gravel matrix which actually performs the treatment, plants are placed there in order to improve the bed's aeration, the hydraulic flow along their roots and insulate the filtering system (Thornton, 2004). Horizontal flow reed beds consist of a swallow gravel layer (up to 60cm deep) with aquatic plants (Figure 7). Water hyacinth, duckweed and water lettuce have shown high performance potential. Especially the first two ones both function in the removal of nutrients, the suppression of algae and sequestering trace organics (Rose, 1999). Water flows horizontally through the bed, leaving less amounts of oxygen at the lower levels of the bed; in this way ideal conditions for nitrogen removal are created (Grant et al., 2000).

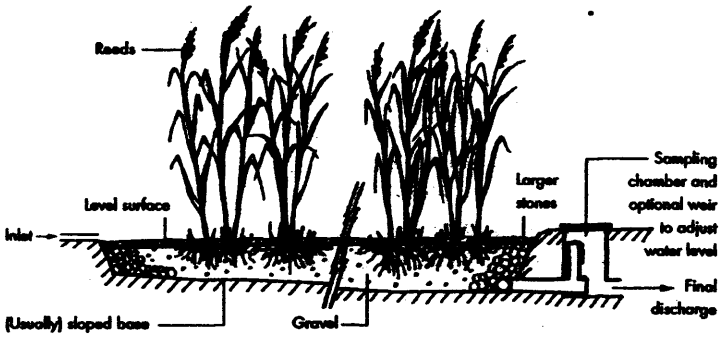

Figure 7. Section of horizontal flow reed bed (Grant et al., 2000)

Where there is insufficient space for the use of both vertical and horizontal reed beds[8], as in the instance of high-density inner city districts, an organic grey water purification installation can be combined with an immersion trickling filter and a vertical reed bed (Figure 8) could be used for purifying grey water for non-drinkable uses. Light grey water is collected centrally to a sedimentation basin. The mechanical pre-purification stage is aided by a second storage tank from where water is led to an immersion trickling filter through a paddle wheel, where it is purified organically. From there it flows to a secondary purification tank, where final lining takes place in a simple sedimentation process. Purification can be augmented by the use of a vertical reed bed. This technology has been tested successively in Berlin-Kreuzberg and in Hanover's Hägewiesen (Kennedy, 1997).

Regarding the health of plants, it should be taken into consideration that grey water, especially when its treatment is less sophisticated than the aquatic systems and trickling filters described above, will almost certainly be alkaline. Its pH should be tested regularly and when it reaches above 7, a way of protecting the soil is by top-dressing it with gypsum (Harper et al., 1994).

Such systems might seem by many as a "waste of space" if perceived only as water purifying areas. Yet, they can be used for planting, both horizontal and vertical flow reed beds, with aquatic the first and soil plants the second. Thus aesthetically attractive habitats are created and urban temperature decreases are achieved, leading to local mitigation of the heat island effect, which has been the subject of this study. Especially horizontal flow reed beds can have other uses apart from purifying water, and embellishing with plants, such as aquaculture. In the instance of extremely sunny California, cautious interplanting of water plants and dilution of nutrients has led to successful integration of aquaculture and grey water treatment (Costa-Pierce, 1998).

[8] About $1m^2$ per person is needed for vertical flow reed beds and $0.5m^2$ per person for horizontal flow ones (Grant et al., 2000).

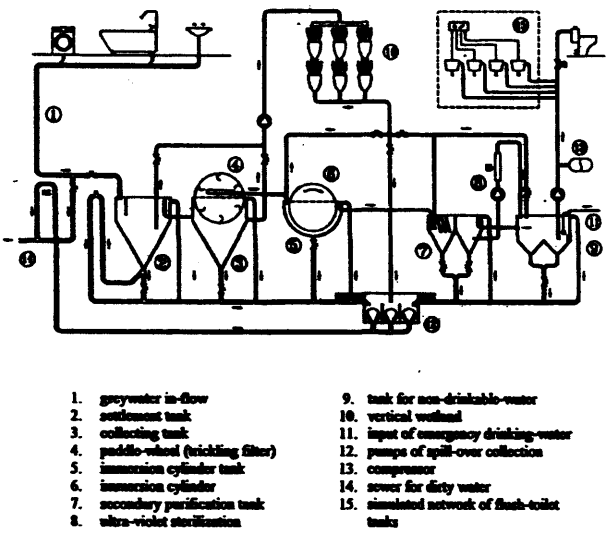

1. greywater in-flow
2. sediment tank
3. collecting tank
4. paddle-wheel (trickling filter)
5. immersion cylinder tank
6. immersion cylinder
7. secondary purification tank
8. ultra-violet sterilisation
9. tank for non-drinkable-water
10. vertical wetland
11. input of emergency drinking-water
12. pumps of spill-over collection
13. compressor
14. sewer for dirty water
15. simulated network of flush-toilet tanks

Figure 8. Organic grey water purification flow diagram (Kennedy, 1997)

1.4. Summary

A brief description of the existing techniques of reducing, reusing and recycling water for irrigation has been presented here. It is obvious that techniques and technology already exist for achieving reduced amounts of water consumed for irrigation in urban areas, in small and larger scales, from high tech to simple solutions, depending on the necessities, needs and aptitudes of each case. The potential for sustainable irrigation of green roofs and green walls does exist in urban settlements, either as reduction of water needed, as rainwater harvesting or as grey water recycling.

When taking into consideration the fact that urban spaces are densely occupied, and diseases could spread easily, public health could not be put at risk with immature installations of water filtering. Rainwater harvesting from roofs could be done individually at each household, without major risks, but the treatment of grey water and rainwater collected from ground level should be carried out properly, through established purification systems, such as reed beds. Due to the cost, space and energy requirements of such installations, it is obvious that it is more appropriate to be implemented in local, community scales or renewal urban projects than in one-family projects. The geometry of most cities would make the second choice extremely difficult. Larger plants not only benefit the environment, but also mean cost savings for the operator (Kennedy, 1997). Although the systems described here for water treatment are those that are less energy-consuming, devices such as pumps may be

needed to lift water from its storage up to the roofs. So as to make the foot-print of the irrigation of green roofs and green walls zero, pumps can be powered by local renewable energy sources, such as photovoltaics, or small wind turbines, depending on the availability of each source in the area.

A quite important factor in small irrigation projects, such as the irrigation of urban green roofs and walls with recycled-reused urban water at a local scale, is the good organisation of the activities amongst the members of the community (Stern, 1988). This could be equally true for the maintenance of green roofs and walls themselves, as well.

1.5. References

1. B.A. Costa-Pierce (1998) *Preliminary Investigation of an Integrated Aquaculture–Wetland Ecosystem Using Tertiary-Treated Municipal Wastewater in Los Angeles County, California.* Ecological Engineering, Vol. 10(1998), pp 341-354.
2. A. Dixon, D. Butler, A. Fewkes and M. Robinson (1999) *Measurement and Modelling of Quality Changes in Stored Untreated Grey Water.* Urban Water, Vol. 1(1999), pp 293-306.
3. EYDAP (2003) *Mornos Aqueduct.* Athens Water Supply and Sewerage Company (EYDAP SA). Available from: http://www.eydap.gr [Accessed 25th March 2005].
4. G.-s. Enrique, I. Braud, J.-L. Thony, M. Vauclin., P. Bessemoulin and J.-C. Calvet (1999) *Modelling Heat and Water Exchanges of Fallow Land Covered with Plant-Residue Mulch.* Agriculture and Forest Meteorology, Vol. 97, pp 151-169.
5. R. Geiger (1967) *The Climate Near the Ground.* Harvard University Press, Cambridge Massachusetts.
6. N. Grant, M. Moodie and C. Weedon (2000) *Sewage Solutions.* CAT Publications, Machynlleth.
7. P. Harper, J. Light and C. Madsen (1994) *The Natural Garden Book.* Gaia Books Limited, London.

8. M.Z. Jacobson (1999) *Fundamentals of Atmospheric Modeling.* Cambridge University Press, Cambridge.
9. M. Kennedy (1997) Water. *In:* M. Kennedy and D. Kennedy (eds) *The Urban Environment in Europe, Designing Ecological Settlements.* Dietrich Reimer Varlag, Berlin, pp 53-82.
10. T. Osmundson (1999) *Roof Gardens: History, Design, and Construction.* W. W. Norton & Company, New York.
11. G.D. Rose (1999) *Community-Based Technologies for Domestic Wastewater Treatment and Reuse: Options for Urban Agriculture.* Cities Feeding People, CFP Repoer Series, Report 27, Rome. Available from: http://www.p2pays.org/ref/03/02008.htm [Accessed 17th August 2004].
12. C. Ryrie (2001) *Soil.* Gaia Books Limited, London.
13. K.A. Stave (2003) *A System Dynamics Model to Facilitate Public Understanding of Water Management Options in Las Vegas, Nevada.* Journal of Environmental Management, Vol. 67(2003), pp 303-313.
14. P.H. Stern (1988) *Operation and Maintenance of Small Irrigation Schemes.* Intermediate Technology Publications Ltd, London.
15. J. Thornton (2004) *The Water Book: Find it, Move it, Store it, Clean it, Use it.* CAT Publications, Machynlleth.
16. UNEP (1997) *Source Book of Alternative Technologies for Fresh Water Augmentation in Latin America and the Caribbean.* International Environmental Technology Centre United Nations Environment Programme. Unit of Sustainable Development and Environmental General Secretariat, Organization of American States, Washington, D. C. Available from: http://www.oas.org/usde/publications/Unit/oea59e/begin.htm#Contents [Accessed 24th November 2004].
17. H.X. Yang, W.H. Chow and J. Burnett (2002) *Water and Energy Conservation of Rainwater Collection Systems on Building Roofs.* Advances in Building Technology, 2002, Hong Kong, Vol. 2, pp 1281–1288.
18. M.I. Yaziz, H. Gunting, N. Sapari and A.W. Ghazali (1989) *Variations in Rainwater Quality from Roof Catchments.* Water Research, Vol. 23 (1989), No. 6, pp 761-765.

2. Appendix 2: Solution of the Equation describing Leaf Surface Temperature

2.1. Analytical Solution

It can be noted that the equation expressing the leaf surface temperature is in the form of Newton's Law of Cooling.

$$\rho_\ell c_{p\ell}\Delta x\frac{dT_\ell}{dt}=\frac{\rho_a c_{pa}}{r_{aH}}(T_a-T_\ell)-\frac{\rho_a c_{pa}}{\gamma}\frac{e_s(T_\ell)-e_a}{r_a+r_s}+$$

$$+\left[I(1+\alpha_s)(1-\alpha_\ell)+\sigma\left(T_{sky}^4+\varepsilon_s T_s^4-2\varepsilon_\ell T_\ell^4\right)\right]\exp[-k_o LAI] \qquad \textbf{Eq. 2}$$

By separating the terms:

$$\frac{\partial T}{\partial t}=-\frac{2\sigma\varepsilon_\ell}{\rho_\ell c_{p\ell}\Delta x_\ell}\exp[-k_o LAI]T^4-\frac{\rho_a c_{pa}}{\rho_\ell c_{p\ell}\Delta x_\ell}\left[\frac{1}{r_{aH}}+\frac{s}{\gamma(r_a+r_s)}\right]T+$$

$$+\frac{\rho_a c_{pa}}{\rho_\ell c_{p\ell}\Delta x_\ell}\left[\frac{1}{r_{aH}}+\frac{s}{\gamma(r_a+r_s)}\right]T_a+\frac{\rho_a c_{pa}}{\rho_\ell c_{p\ell}\Delta x_\ell}\frac{e_s(T_a)\left(r_a\left(\frac{\rho_a u_a}{\rho_{as}(1-u_a)}-1\right)\right)}{\gamma(r_a+r_s)}+$$

$$+\frac{\left[(1+a_s)(1-a_\ell)I+\sigma\left(T_{sky}^4+\varepsilon_s T_s^4\right)\right]}{\rho_\ell c_{p\ell}\Delta x_\ell}\exp[-k_o LAI] \qquad \textbf{Eq. 3}$$

By substituting the factors of T_ℓ with the letters κ, λ, and μ we have:

$$\kappa=\frac{2\sigma\varepsilon_\ell}{\rho_\ell c_{p\ell}\Delta x_\ell}\exp[-k_o LAI] \qquad \textbf{Eq. 4}$$

$$\lambda=\frac{\rho_a c_{pa}}{\rho_\ell c_{p\ell}\Delta x_\ell}\left[\frac{1}{r_{aH}}+\frac{s}{\gamma(r_a+r_s)}\right] \qquad \textbf{Eq. 5}$$

$$\mu=-\frac{\rho_a c_{pa}}{\rho_\ell c_{p\ell}\Delta x_\ell}\left[\frac{1}{r_{aH}}+\frac{s}{\gamma(r_a+r_s)}\right]T_a-\frac{\rho_a c_{pa}}{\rho_\ell c_{p\ell}\Delta x_\ell}\frac{e_s(T_a)\left(\frac{\rho_a u_a}{\rho_{as}(1-u_a)}-1\right)}{\gamma(r_a+r_s)}-$$

$$-\frac{\left[(1+a_s)(1-a_\ell)I+\sigma\left(T_{sky}^4+\varepsilon_s T_s^4\right)\right]}{\rho_\ell c_{p\ell}\Delta x_\ell}\exp[-k_o LAI] \qquad \textbf{Eq. 6}$$

Thus:

$$-\frac{\partial T}{\partial t} = \kappa T^4 + \lambda T + \mu \qquad \textbf{Eq. 7}$$

$$\frac{\partial T}{\kappa T^4 + \lambda T + \mu} = -\partial t \qquad \textbf{Eq. 8}$$

$$\int \frac{\partial T}{\kappa T^4 + \lambda T + \mu} = \int -\partial t \qquad \textbf{Eq. 9}$$

The integral of the form $\int \partial T / (\kappa T^4 + \lambda T + \mu)$ can be solved as an integral of the form $\int \partial x / (Z^m R^n)$. Where:

$Z = \alpha + \beta x$ is a binomial and

$R = \mathrm{a} + bx + cx^2$ is a quadratic trinomial.

Where α, β, a, b and c are constants.

For m=2 and n=1 a fourth degree polynomial is the product of the quadratic trinomial and the binomial. The product Z^2R gives the fourth degree polynomial, as the one which we want to solve:

$$Z^2R = \beta^2 c x^4 + (2\alpha\beta c + \beta^2 b)x^3 + (\alpha^2 c + 2\alpha\beta b + \beta^2 \mathrm{a})x^2 + (\alpha^2 b + 2\alpha\beta \mathrm{a})x + \alpha^2 \mathrm{a} \qquad \textbf{Eq. 10}$$

In our case, (for the polynomial $\kappa T^4 + \lambda T + \mu$) the factors for x^3 and x^2 should equal to zero. Therefore:

$$2\alpha\beta c + \beta^2 b = 0 \quad \Rightarrow \beta = 0 \text{ or } b = -\frac{2\alpha c}{\beta} \qquad \textbf{Eq. 11}$$

β cannot be equal to zero, as it is one of the multipliers of the product of the factor of x^4, which is different to zero. Therefore the second solution is accepted.

$$\alpha^2 c + 2\alpha\beta b + \beta^2 \mathrm{a} = 0 \quad \Rightarrow \quad \mathrm{a} = \frac{3\alpha^2 c}{\beta^2} \qquad \textbf{Eq. 12}$$

The rest of the factors are equal to the factors of the polynomial of the expression of the leaf temperature:

$$\kappa = \beta^2 c \qquad \textbf{Eq. 13}$$

$$\lambda = \alpha^2 c + 2\alpha\beta b + \beta^2 \mathrm{a} \qquad \textbf{Eq. 14}$$

$$\mu = \alpha^2 a \qquad \textbf{Eq. 15}$$

By solving the system of equations we have:

$$\beta = \frac{\mu}{3}\sqrt[3]{\kappa\left(\frac{4}{\lambda}\right)^4} \qquad \textbf{Eq. 16}$$

$$\alpha = \frac{4\mu}{3\lambda} \qquad \textbf{Eq. 17}$$

$$c = \left(\frac{3}{\mu}\right)^2\sqrt[3]{\kappa\left(\frac{\lambda}{4}\right)^8} \qquad \textbf{Eq. 18}$$

$$b = -\frac{3}{2^5}\frac{\lambda^3}{\mu^2} \qquad \textbf{Eq. 19}$$

$$a = \frac{3^3}{\mu^2}\sqrt[3]{\frac{\lambda^{13}}{\kappa}} \qquad \textbf{Eq. 20}$$

According to Gradshteyn and Ryzhik (1965) the solution to this integral is:

$$\int\frac{dx}{Z^m R^n} = -\frac{\beta}{(m-1)A}\frac{1}{Z^{m-1}R^{n-1}} - \frac{(m+n-2)B}{(m-1)A}\int\frac{dx}{Z^{m-1}R^n} - \frac{(m+2n-3)c}{(m-1)A}\int\frac{dx}{Z^{m-2}R^n}$$

Eq. 21

Where:

$$A = a\beta^2 - \alpha b\beta + c\alpha^2 \qquad \textbf{Eq. 22}$$

and

$$B = b\beta - 2c\alpha \qquad \textbf{Eq. 23}$$

For m=2 and n=1 we have:

$$\int\frac{dx}{Z^2 R^1} = -\frac{\beta}{AZ} - \frac{B}{A}\int\frac{dx}{ZR} - \frac{c}{A}\int\frac{dx}{R} \qquad \textbf{Eq. 24}$$

Where (Gradshteyn and Ryzhik, 1965):

$$\int\frac{dx}{ZR} = \frac{\beta}{2AZ}\ln\frac{Z^2}{R} - \frac{B}{2A}\int\frac{dx}{R} \qquad \textbf{Eq. 25}$$

And (ibid.):

$$\int\frac{dx}{R} = \frac{1}{\sqrt{\Delta}}\ln\frac{b+2cx-\sqrt{\Delta}}{b+2cx+\sqrt{\Delta}} \qquad \textbf{Eq. 26}$$

for $\Delta \geq 0$ and where $\Delta = b^2 - 4ac$

Thus:

$$\int \frac{dx}{Z^2 R^1} = -\frac{\beta}{AZ} - \frac{B\beta}{2A^2} \ln \frac{Z^2}{R} + \left[\frac{B^2}{2A^2} - \frac{c}{A} \right] \frac{1}{\sqrt{\Delta}} \ln \frac{b + 2cx - \sqrt{\Delta}}{b + 2cx + \sqrt{\Delta}} \qquad \text{Eq. 27}$$

And:

$$\int \frac{dx}{Z^2 R^1} = \int \frac{\partial T}{\kappa T^4 + \lambda T + \mu} \qquad \text{Eq. 28}$$

Thus:

$$\int \frac{dx}{Z^2 R^1} = -\int dt \qquad \text{Eq. 29}$$

Therefore, by replacing x with T:

$$-\frac{\beta}{AZ} - \frac{B\beta}{2A^2} \ln \frac{Z^2}{R} + \left[\frac{B^2}{2A^2} - \frac{c}{A} \right] \frac{1}{\sqrt{\Delta}} \ln \frac{b + 2cT - \sqrt{\Delta}}{b + 2cT + \sqrt{\Delta}} = -t + const \qquad \text{Eq. 30}$$

For t=0

$$const = -\frac{\beta}{AZ_o} - \frac{B\beta}{2A^2} \ln \frac{Z_o^2}{R_o} + \left[\frac{B^2}{2A^2} - \frac{c}{A} \right] \frac{1}{\sqrt{\Delta}} \ln \frac{b + 2cT_o - \sqrt{\Delta}}{b + 2cT_o + \sqrt{\Delta}} \qquad \text{Eq. 31}$$

It is obvious that this function cannot be solved for T with analytical methods. The Lagrange Interpolation is used for the solution of this function.

According to the theory of the Langragian Interpolation, we can consider a function, f(x), whose values are known in n+1 points of [a, b]. Then there is one polynomial which interpolates this function in these points, thus $P_n(x_i)=f(x_i)$. This polynomial is given by:

$$P_n(x) = \sum_{i=0}^{x} \ell_i(x) f(x_i) \qquad \text{Eq. 32}$$

Where:

$$\ell_i(x) = \frac{(x - x_o)..(x - x_{i-1})(x - x_{i+1})..(x - x_n)}{(x_i - x_o)..(x_i - x_{i-1})(x_i - x_{i+1})..(x_i - x_n)} \qquad \text{Eq. 33}$$

The error of the Lagrange Interpolation is $\xi(x)$ and is given b the relationship (Bakopoulos and Chrisovergis, 1989):

$$f(x)-P_n(x)=\frac{f^{(n+1)}(\xi(x))\prod_{i=0}^{n}(x-x_i)}{(n+1)!} \qquad \textbf{Eq. 34}$$

If three values of the temperature leaf are taken into consideration, equal to the maximum, minimum and average urban temperature, x_1, x_2 and x_3 respectively, then the function takes the values S_1, S_2 and S_3 respectively. Thus a quadratic trinomial will be:

$$P_2(T)=\frac{(T-x_2)(T-x_3)}{(x_1-x_2)(x_1-x_3)}S_1+\frac{(T-x_1)(T-x_3)}{(x_2-x_1)(x_2-x_3)}S_2+\frac{(T-x_1)(T-x_2)}{(x_3-x_1)(x_3-x_2)}S_3 \qquad \textbf{Eq. 35}$$

Which leads to the quadratic trinomial of the form:

$$\Pi T^2-PT+R+\Xi t-const=0 \qquad \textbf{Eq. 36}$$

Where:

$$\Pi=S_1(x_2-x_3)-S_2(x_1-x_3)+S_3(x_1-x_2) \qquad \textbf{Eq. 37}$$

$$P=S_1(x_2^2-x_3^2)-S_2(x_1^2-x_3^2)+S_3(x_1^2-x_2^2) \qquad \textbf{Eq. 38}$$

$$R=S_1x_2x_3(x_2-x_3)-S_2x_1x_3(x_1-x_3)+S_3x_1x_2(x_1-x_2) \qquad \textbf{Eq. 39}$$

$$\Xi=(x_1-x_2)(x_2-x_3)(x_1-x_3) \qquad \textbf{Eq. 40}$$

$$\textbf{for } P^2-4\Pi(R+\Xi t-const)\geq 0 \qquad \textbf{Eq. 41}$$

$$T=\frac{P\pm\sqrt{P^2-4\Pi(R+\Xi t-const)}}{2\Pi} \qquad \textbf{Eq. 42}$$

In the primary form of the equation, $-\partial T/\partial t=\kappa T^4+\lambda T+\mu$, it can be noted that κ, which equals to $2\sigma\varepsilon_\ell \exp[-k_o LAI]/(\rho_\ell c_{p\ell}\Delta x_\ell)$ is much smaller than the other factors of the fourth order polynomial. In general, for plants covering roofs and walls κ is of the magnitude of 10^{-15}, while the other factors, λ and μ are of the magnitude of 10^{-5} and 10^{-3} respectively. T is always of the magnitude of 10^2 (expressed in Kelvin) and thus T^4 of the magnitude of 10^8. Therefore κT^4 is of the magnitude of 10^{-7}, while λT and μ are much bigger, both of the magnitude of 10^{-3}. Therefore it would be a smaller error to omit the factor κT^4, than to solve the function which emerges from the solution of the integral, with the Lagrange Interpolation or any numerical method. Thus:

$$-\frac{\partial T}{\partial t} = \lambda T + \mu \qquad \textbf{Eq. 43}$$

$$\frac{\partial T}{T + \frac{\mu}{\lambda}} = -\frac{\partial t}{\lambda} \qquad \textbf{Eq. 44}$$

$$\ln\left(T + \frac{\mu}{\lambda}\right) = -\frac{t}{\lambda} + const \qquad \textbf{Eq. 45}$$

$$T = -\frac{\mu}{\lambda} + const \exp\left[-\frac{t}{\lambda}\right] \qquad \textbf{Eq. 46}$$

Thus, by replacing μ and λ:

$$T = T_a + \frac{\frac{e_s(T_a)\left(\frac{\rho_a u_a}{\rho_{as}(1-u_a)} - 1\right)}{\gamma(r_a + r_s)} + \frac{\left[(1+a_s)(1-a_l)I + \sigma\left(T_{sky}^4 + \varepsilon_s T_s^4\right)\right]}{\rho_a c_{pa}} \exp[-k_o LAI]}{\left[\frac{1}{r_{aH}} + \frac{s}{\gamma(r_a + r_s)}\right]} +$$

$$+ const \exp\left[-\frac{t}{\frac{\rho_a c_{pa}}{\rho_l c_{pl} \Delta x_l}\left[\frac{1}{r_{aH}} + \frac{s}{\gamma(r_a + r_s)}\right]}\right] \qquad \textbf{Eq. 47}$$

for t=0, $T=T_a=T_o$, thus:

$$const = -\frac{\frac{e_s(T_a)\left(\frac{\rho_a u_a}{\rho_{as}(1-u_a)} - 1\right)}{\gamma(r_a + r_s)} + \frac{\left[(1+a_s)(1-a_l)I + \sigma\left(T_{sky}^4 + \varepsilon_s T_s^4\right)\right]}{\rho_a c_{pa}} \exp[-k_o LAI]}{\left[\frac{1}{r_{aH}} + \frac{s}{\gamma(r_a + r_s)}\right]} \qquad \textbf{Eq. 48}$$

Thus:

$$T = T_a + \frac{\frac{e_s(T_a)\left(\frac{\rho_a u_a}{\rho_{as}(1-u_a)} - 1\right)}{\gamma(r_a + r_s)} + \frac{\left[(1+a_s)(1-a_l)I + \sigma\left(T_{sky}^4 + \varepsilon_s T_s^4\right)\right]}{\rho_a c_{pa}} \exp[-k_o LAI]}{\left[\frac{1}{r_{aH}} + \frac{s}{\gamma(r_a + r_s)}\right]}.$$

$$\cdot\left\{1-\exp\left[-\frac{\rho_\ell c_{p\ell}\Delta x_\ell}{\rho_a c_{pa}}\frac{t}{\left[\frac{1}{r_{aH}}+\frac{s}{\gamma(r_a+r_s)}\right]}\right]\right\} \qquad \textbf{Eq. 49}$$

2.2. Linearised Radiation Term

The dynamic expression of the leaf surface temperature can also be approached by the linearising the radiation term by expanding it about a mean surface temperature ($\overline{T}_\ell$). Thus, the 4th power of leaf surface temperature could be expressed as (Gates, 1980):

$$T_\ell^4 = 4T_\ell\left(\overline{T}_\ell\right)^3 - 4\left(\overline{T}_\ell\right)^4 \qquad \textbf{Eq. 50}$$

And the error of this approximation is:

$$e_\ell = 6\sigma\varepsilon_\ell\left(\overline{T}_\ell\right)^2\left(\overline{T}_\ell - T_\ell\right) \qquad \textbf{Eq. 51}$$

It is obvious that the error is smaller when the difference between the leaf surface temperature ad the mean leaf surface temperature tends to zero and when the mean leaf surface temperature is not very big. According to Jones (1992) instead of the mean leaf surface temperature, the air temperature near the leaf could be used. As the difference between the air temperature near the leaf and the surface temperature of the leaf is not so big, the error due to linearization is expected to be relatively small.

Thus, if we replace the fourth power of leaf surface temperature with its equivalent linear expression, equation 2 becomes:

$$\frac{\partial T}{\partial t} = -\frac{2\sigma\varepsilon_\ell}{\rho_\ell c_{p\ell}\Delta x_\ell}\exp[-k_o LAI]\left(4TT_a^3 - 3T_a^4\right) - \frac{\rho_a c_{pa}}{\rho_\ell c_{p\ell}\Delta x_\ell}\left[\frac{1}{r_{aH}}+\frac{s}{\gamma(r_a+r_s)}\right]T$$

$$+\frac{\rho_a c_{pa}}{\rho_\ell c_{p\ell}\Delta x_\ell}\left[\frac{1}{r_{aH}}+\frac{s}{\gamma(r_a+r_s)}\right]T_a + \frac{\rho_a c_{pa}}{\rho_\ell c_{p\ell}\Delta x_\ell}\frac{e_s(T_a)\left(\frac{\rho_a u_a}{\rho_{as}(1-u_a)}-1\right)}{\gamma(r_a+r_s)} +$$

$$+\frac{\left[(1+a_s)(1-a_\ell)I+\sigma\left(T_{sky}^4+\varepsilon_s T_s^4\right)\right]}{\rho_\ell c_{p\ell}\Delta x_\ell}\exp[-k_o LAI] \qquad \textbf{Eq. 52}$$

Thus, for:

$$\kappa = \frac{2\sigma\varepsilon_\ell}{\rho_\ell c_{p\ell}\Delta x_\ell}\exp[-k_o LAI] \qquad \textbf{Eq. 53}$$

$$\lambda = \frac{\rho_a c_{pa}}{\rho_\ell c_{p\ell}\Delta x_\ell}\left[\frac{1}{r_{aH}} + \frac{s}{\gamma(r_a + r_s)}\right] \qquad \textbf{Eq. 54}$$

$$\mu = \frac{\left[\dfrac{\rho_a c_{pa} e_s(T_a)\left(\dfrac{\rho_a u_a}{\rho_{as}(1-u_a)} - 1\right)}{\gamma(r_a + r_s)} + \left[(1+a_s)(1-a_\ell)I + \sigma\left(T_{sky}^4 + \varepsilon_s T_s^4\right)\right]\exp[-k_o LAI]\right]}{\rho_\ell c_{p\ell}\Delta x_\ell} \qquad \textbf{Eq. 55}$$

$$\frac{\partial T}{\partial t} = -T\left(4\kappa T_a^3 + \lambda\right) + \left(3\kappa T_a^4 + \lambda T_a + \mu\right) \qquad \textbf{Eq. 56}$$

Thus the leaf surface temperature becomes:

$$T = \frac{3\kappa T_a^4 + \lambda T_a + \mu}{4\kappa T_a^3 + \lambda} + \left[T_o\left(1 - \frac{3\kappa T_a^3 + \lambda}{4\kappa T_a^3 + \lambda}\right)\right] + \mu_o \cdot \exp\left[\frac{-t}{4\kappa T_a^3 + \lambda}\right] \qquad \textbf{Eq. 57}$$

2.3. References

19. A. Bakopoulos and I. Chrisovergis (1989) *Introduction to Numeric Analysis.* Symeon Editions, Athens.

20. D.M. Gates (1980) *Biophysical Ecology.* Springer-Verlag, New York.

21. I.S. Gradshteyn and I.M. Ryzhik (1965) *Table of Integrals, Series, and Products.* Academic Press, New York and London.

3. Appendix 3: Measurements

3.1. Squirrel Connections

The connection of the sensors in the Squirrel is given in the following figure.

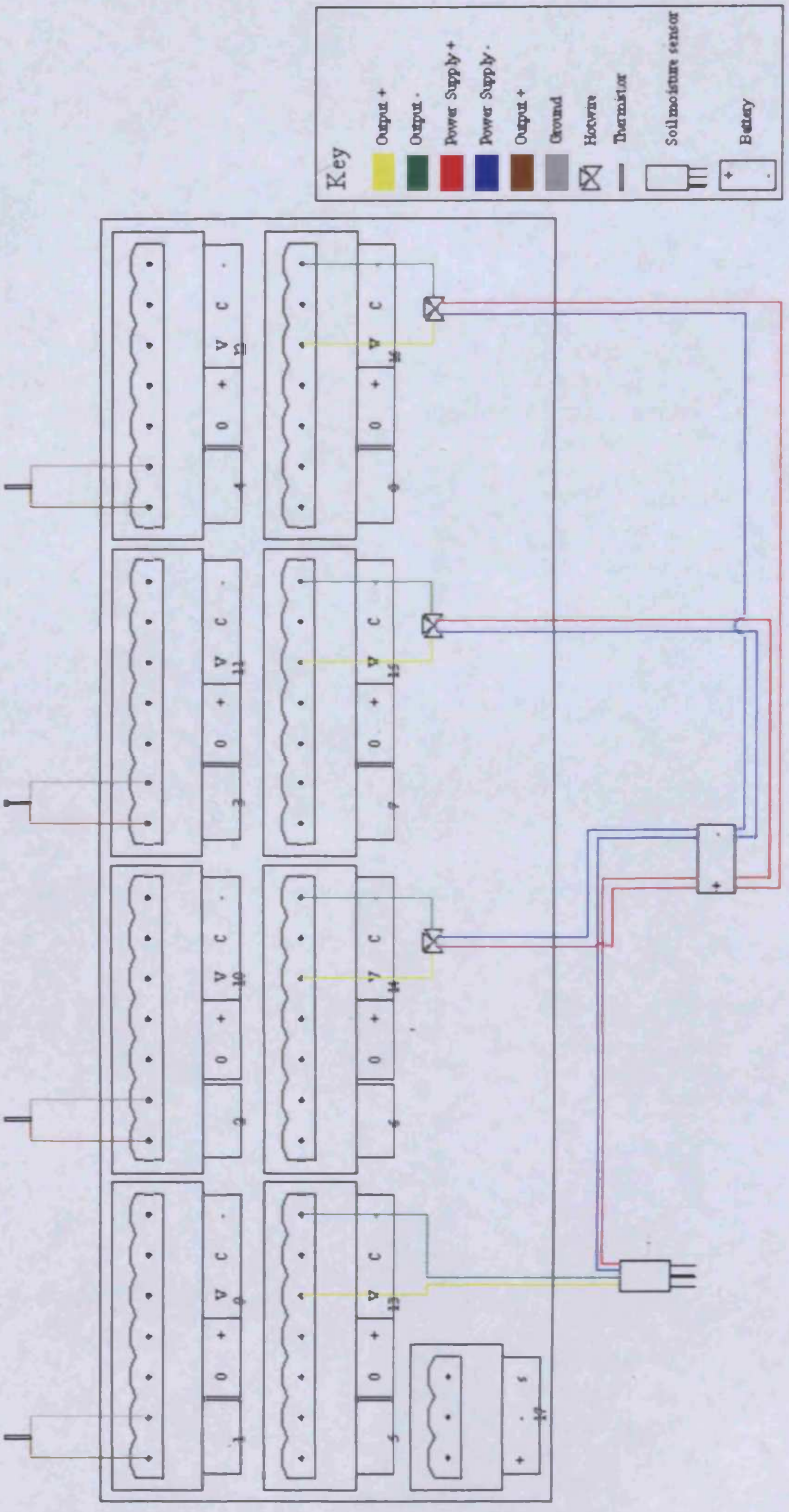

Figure 9. Squirrel connections

3.2. Soil-specific Calibration of ThetaProbe Soil Moisture Sensor, Type ML2x

It has been proved (Delta-T, 1999) that there is a linear relationship between the refractive index (which is equivalent to the square root of the dielectric constant ε of water) and the volumetric content of water in the soil, ω, of the form:

$$\sqrt{\varepsilon} = a_0 + a_1 \cdot \omega \qquad \textbf{Eq. 58}$$

The relationship between the ThetaProbe output (V) in Volts and the square root of ε is given by a 3rd order polynomial (ibid):

$$\sqrt{\varepsilon} = 1.07 + 6.4V - 6.4V^2 + 4.7V^3 \qquad \textbf{Eq. 59}$$

Or by the linear relationship:

$$\sqrt{\varepsilon} = 1.1 + 4.44V \qquad \textbf{Eq. 60}$$

In order to determine the two coefficients α0 and α1, we follow the protocol suggested by Delta-T (1999).

A sample of damp soil is collected. The ThetaProbe is inserted into the sample and the probe output, V_w, is measured.

V_w=0.316 Volts

From equations 59 and 60 $\sqrt{\varepsilon_w}$ can be calculated:

From equation 59: $\sqrt{\varepsilon_w} = 2.601627731$

From equation 60: $\sqrt{\varepsilon_w} = 2.50304$

The damp sample is weighted (its weight being W_w) and its volume is measured (L).

W_w=0.288 kg

L=0.300 lt

The sample is oven-dried, so that all its water content is evaporated (ω≈0). The ThetaProbe is inserted into the dry soil and the probe output, V_0, is measured.

V_0=0.04 Volts

From equations 59 and 60 $\sqrt{\varepsilon_0}$ can be calculated:

From equation 59: $\sqrt{\varepsilon_0}$ =1.3160608

From equation 60: $\sqrt{\varepsilon_0}$ =1.2776

The coefficient α_0 is equal to $\sqrt{\varepsilon_0}$. (The polynomial relationship is used).

α_0=1.32 (α_0 is usually between 1.0 and 2.0).

Or, from the linear relationship: α_0=1.28

The dry sample is weighted (its weight being W_0).

W_0=0.241 kg

The volumetric water content, ω_w, of the original (damp) sample is given by:

$$\omega_w = \frac{W_w - W_0}{L} \qquad \textbf{Eq. 61}$$

Thus:

ω_w=0.157 m^3/m^3

Then, α_1 is given by:

α_1=7.82 (α_1 is usually between 7.6 and 8.6).

Or, for the linear relationship: α_1=7.82

Using the polynomial relationship, the water content determined from a calibrated ThetaProbe is, from equation 1:

$$\omega_w = \frac{\left(1.07 + 6.4V - 6.4V^2 + 4.7V^3\right) - a_0}{a_1} \qquad \textbf{Eq. 62}$$

And from the linear relationship:

$$\omega_w = \frac{\left(1.1 + 4.44V\right) - a_0}{a_1} \qquad \textbf{Eq. 63}$$

3.3. References

22. Delta-T (1999) *ThetaProbe Soil Moisture Sensor, Type ML2x, User Manual.* Delta-T Devices Ltd, Cambridge.

4. Appendix 4: Radiative Heat Transfer in the Canyon

For the system of Figure 10 and, keeping in mind that $\varepsilon_3=1$, we have:

For i=1:

$$\frac{q_1}{\varepsilon_1}-\left[\left(\frac{1}{\varepsilon_2}-1\right)F_{1-2}q_2+\left(\frac{1}{\varepsilon_4}-1\right)F_{1-4}q_4\right]=$$

$$=F_{1-2}(E_{b1}-E_{b2})+F_{1-3}(E_{b1}-E_{b3})+F_{1-4}(E_{b1}-E_{b4}) \qquad \textbf{Eq. 64}$$

For i=2:

$$\frac{q_2}{\varepsilon_2}-\left[\left(\frac{1}{\varepsilon_1}-1\right)F_{2-1}q_1+\left(\frac{1}{\varepsilon_4}-1\right)F_{2-4}q_4\right]=$$

$$=F_{2-1}(E_{b2}-E_{b1})+F_{2-3}(E_{b2}-E_{b3})+F_{2-4}(E_{b2}-E_{b4}) \qquad \textbf{Eq. 65}$$

For i=4:

$$\frac{q_4}{\varepsilon_4}-\left[\left(\frac{1}{\varepsilon_1}-1\right)F_{4-1}q_1+\left(\frac{1}{\varepsilon_2}-1\right)F_{4-2}q_2\right]=$$

$$=F_{4-1}(E_{b4}-E_{b1})+F_{4-2}(E_{b4}-E_{b2})+F_{4-3}(E_{b4}-E_{b3}) \qquad \textbf{Eq. 66}$$

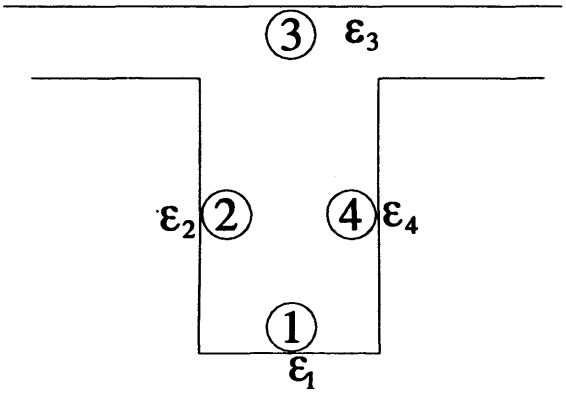

Figure 10. Schematic representation of the radiative model of the canyon

Thanks to the symmetry of the geometry of the canyon and to the law of reciprocity of view factors:

$F_{1-2}=F_{1-4}=a$ $\qquad$ $F_{2-1}=F_{4-1}=c$

$F_{2-3}=F_{4-3}=d$ $\qquad$ $F_{2-4}=F_{4-2}=f$

By replacing the E_{bi}s with their equals (σT_i^4) and by solving the 3×3 system we have:

$$q_1 = \frac{\varepsilon_1\sigma}{q_t}\{T_1^4[f(1-\varepsilon_2)(1-\varepsilon_4)[2a(c+f)+fF_{1-3}]+ac[(1-\varepsilon_2)+(1-\varepsilon_4)]-2aF_{1-3}]+$$
$$+T_2^4[a[-(1-\varepsilon_2)(c+d+f)+1][f(1-\varepsilon_4)+1]]+$$
$$+T_3^4[f(1-\varepsilon_2)(1-\varepsilon_4)[2ad-fF_{1-3}]+ad[(1-\varepsilon_2)+(1-\varepsilon_4)]+F_{1-3}]+$$
$$+T_4^4[a[-(1-\varepsilon_4)(c+d+f)+1][f(1-\varepsilon_2)+1]]\} \quad \textbf{Eq. 67}$$

$$q_2 = \frac{\varepsilon_2\sigma}{q_t}\{T_2^4[ac(1-\varepsilon_1)[(c+d+3f)(1-\varepsilon_4)+1]+f^2(1-\varepsilon_4)-(c+d+f)]+$$
$$+T_1^4[c[-(2a+F_{1-3})(1-\varepsilon_1)+1][f(1-\varepsilon_4)+1]]+$$
$$+T_3^4[[d+cF_{1-3}(1-\varepsilon_1)][f(1-\varepsilon_4)+1]]+$$
$$+T_4^4[[-ac(1-\varepsilon_1)-f[(c+d+f)(1-\varepsilon_4)-1]]\} \quad \textbf{Eq. 68}$$

$$q_4 = \frac{\varepsilon_4\sigma}{q_t}\{T_4^4[ac(1-\varepsilon_1)[(c+d+3f)(1-\varepsilon_2)+1]+f^2(1-\varepsilon_2)-(c+d+f)]+$$
$$+T_2^4[[-ac(1-\varepsilon_1)-f[(c+d+f)(1-\varepsilon_2)-1]]+$$
$$+T_1^4[c[-(2a+F_{1-3})(1-\varepsilon_1)+1][f(1-\varepsilon_2)+1]]+$$
$$+T_3^4[[d+cF_{1-3}(1-\varepsilon_1)][f(1-\varepsilon_2)+1]]\} \quad \textbf{Eq. 69}$$

Where:

$$q_t = \{(1-\varepsilon_4)[ac(1-\varepsilon_1)+f^2(1-\varepsilon_2)]+ac(1-\varepsilon_1)(1-\varepsilon_2)[1+2f(1-\varepsilon_4)]-1\} \quad \textbf{Eq. 70}$$

4.1.1. Calculation of View Factors

As walls are represented as several nodes and so is the street, the view factor of each node (which represents a strip of the surface to which it belongs) is treated as a strip parallel or vertical to a plane. The temperature of the plane is the averaged temperature of all the nodes consisting this plane.

Defining the view factor a $F_{1-2} = F_{1-4} = a$

The view factor between a strip of the street and each of the walls derives as the view factor between a differential strip element to rectangle in plane 90° to the plane of the strip.

According to Modest (1993):

$$X = \frac{h_o}{L} \qquad Y = \frac{x + \Delta x}{L}$$

The view factor between a strip of the street and each of the walls is given by:

$$a = \frac{1}{\pi}\left[\tan^{-1}\frac{1}{Y} + \frac{Y}{2}\ln\frac{Y^2\left(X^2+Y^2+1\right)}{\left(Y^2+1\right)\left(X^2+Y^2\right)} - \frac{Y}{\sqrt{X^2+Y^2}}\tan^{-1}\frac{1}{\sqrt{X^2+Y^2}} \right] \quad \textbf{Eq. 71}$$

Defining the view factor $F_{2-1} = F_{4-1} = c$

The view factor c is defined in the same way as the view factor a, only that:

$$X = \frac{W}{L} \qquad Y = \frac{z + \Delta z}{L}$$

Defining the view factor F_{1-3}

The sky can be considered to be an infinite plane and the canyon surfaces as finite elements parallel or vertical to it. The street is parallel to the sky, therefore its view factor towards the sky is equal to 1 (Paspalas, 1993).

$$F_{1-3} = 1$$

Defining the view factor $F_{2-3} = F_{4-3} = d$

The walls are finite surfaces vertical to the sky. For a finite surface with an angle a towards an infinite plane, the view factor is:

$$F_{ij} = \frac{1}{2}(1 + \cos a)$$

Thus, for a=90°, d becomes:

$$d = F_{2-3} = F_{4-3} = \frac{1}{2}$$

Defining the view factor $F_{2-4} = F_{4-2} = f$

The factor f is defined as the view factor of a stripe parallel to a rectangle with one equal side (in this case the length L of the canyon). Thus (Paspalas, 1993), for:

$$B = \frac{L}{W} \qquad \text{and } C = \frac{h_o}{W}$$

$$f = \frac{1}{\pi}\left[\frac{C}{\sqrt{1+C^2}}\arctan\frac{B}{\sqrt{1+C^2}} + \frac{\sqrt{1+B^2}}{B}\arctan\frac{C}{\sqrt{1+B^2}} - \frac{1}{B}\arctan C\right] \qquad \textbf{Eq. 72}$$

The view factor between the roof and the sky is the same as the one between the street and the sky. It is the view factor of a finite element to an infinite plane, which is equal to 1.

4.2. References

23. M.F. Modest (1993) *Radiative Heat Transfer.* McGraw-Hill International Editions, New York.

24. K. Paspalas (1993) *Heat Transfer.* Salonikidis Editions, Thessalonica.

5. Appendix 5: Model Inputs

5.1. Climatic Data

5.1.1. Athens

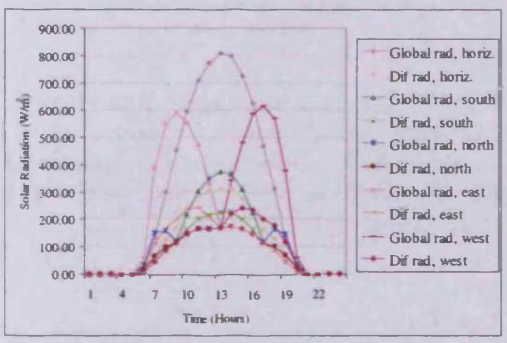

Figure 11. Global and diffuse solar radiation on horizontal plane and on vertical planes with east, west, south and north orientation for a typical day in July, Athens

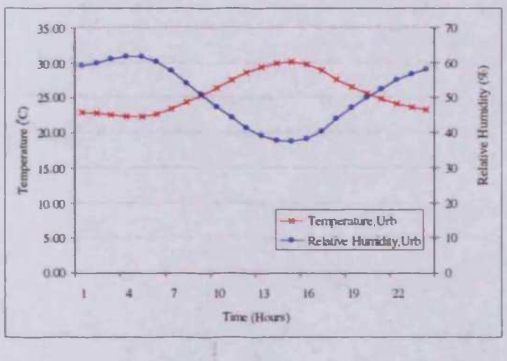

Figure 12. Air temperature and relative humidity for a typical day in July, Athens

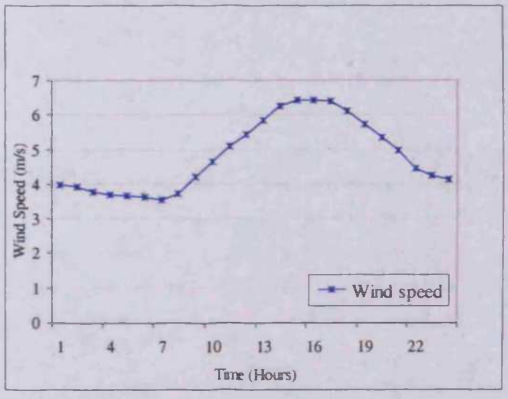

Figure 13. Wind speed for a typical day in July, Athens

5.1.2. Beijing

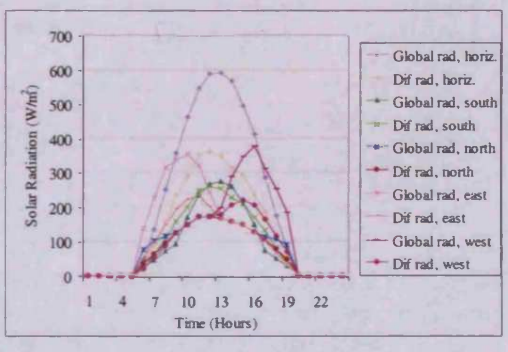

Figure 14. Global and diffuse solar radiation on horizontal plane and on vertical planes with east, west, south and north orientation for a typical day in June, Beijing

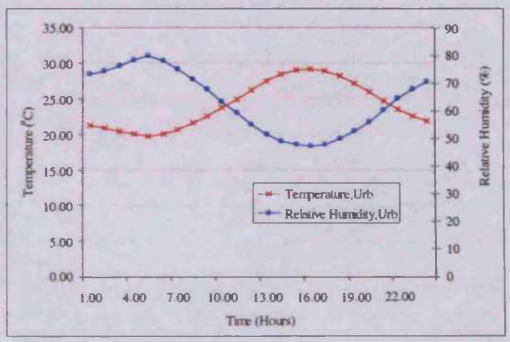

Figure 15. Air temperature and relative humidity for a typical day in June, Beijing

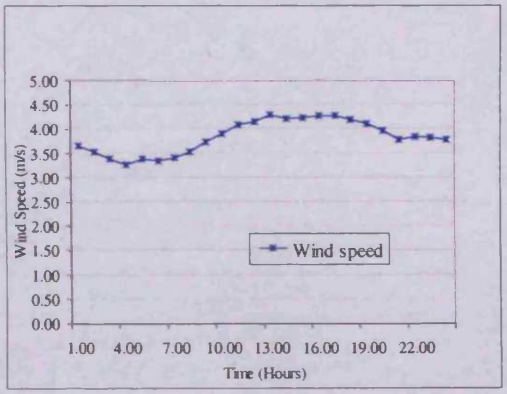

Figure 16. Wind speed for a typical day in June, Beijing

5.1.3. Brasilia

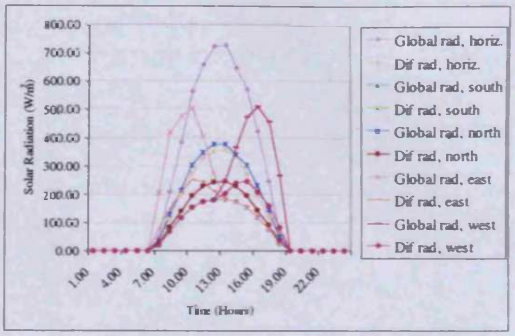

Figure 17. Global and diffuse solar radiation on horizontal plane and on vertical planes with east, west, south and north orientation for a typical day in September, Brasilia

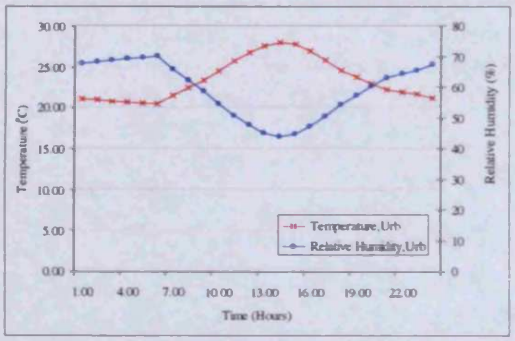

Figure 18. Air temperature and relative humidity for a typical day in September, Brasilia

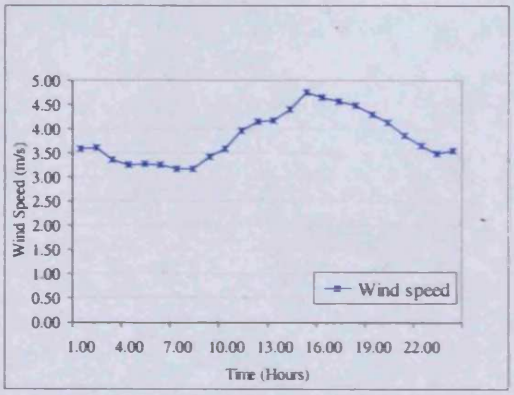

Figure 19. Wind speed for a typical day in September, Brasilia

5.1.4. Hong Kong

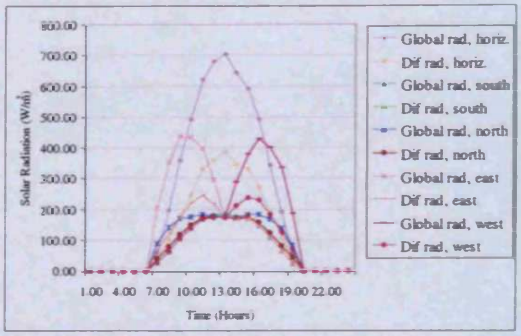

Figure 20. Global and diffuse solar radiation on horizontal plane and on vertical planes with east, west, south and north orientation for a typical day in July, Hong Kong

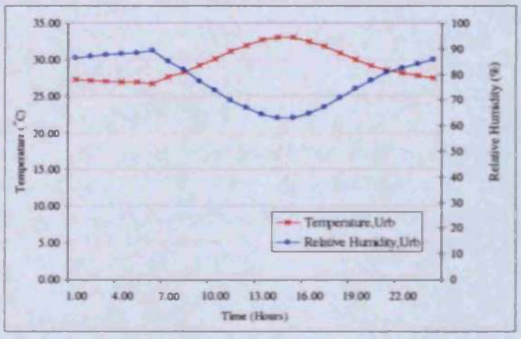

Figure 21. Air temperature and relative humidity for a typical day in July, Hong Kong

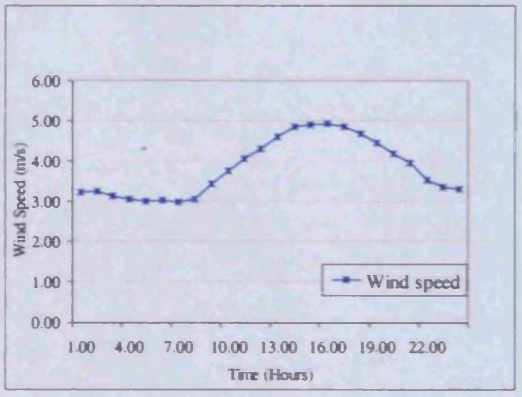

Figure 22. Wind speed for a typical day in July, Hong Kong

5.1.5. London

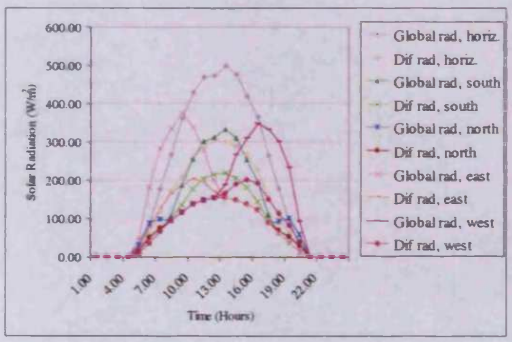

Figure 23. Global and diffuse solar radiation on horizontal plane and on vertical planes with east, west, south and north orientation for a typical day in July, London

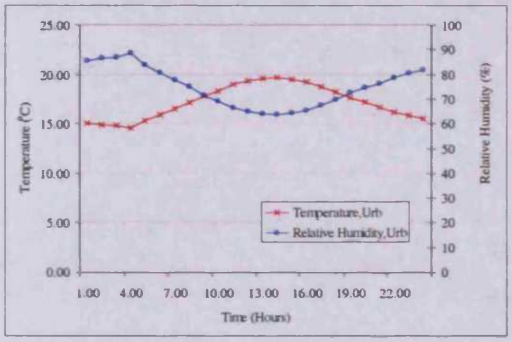

Figure 24. Air temperature and relative humidity for a typical day in July, London

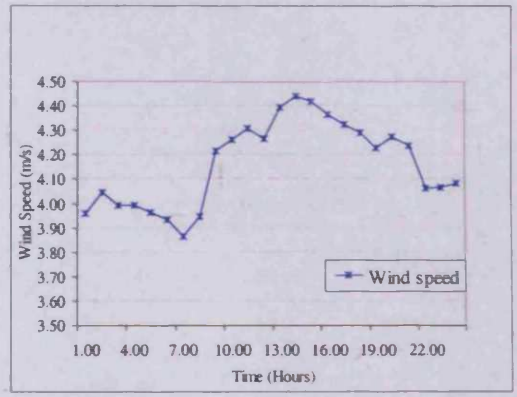

Figure 25. Wind speed for a typical day in July, London

5.1.6. Montreal

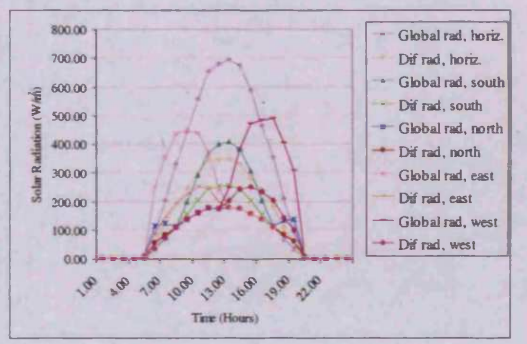

Figure 26. Global and diffuse solar radiation on horizontal plane and on vertical planes with east, west, south and north orientation for a typical day in July, Montreal

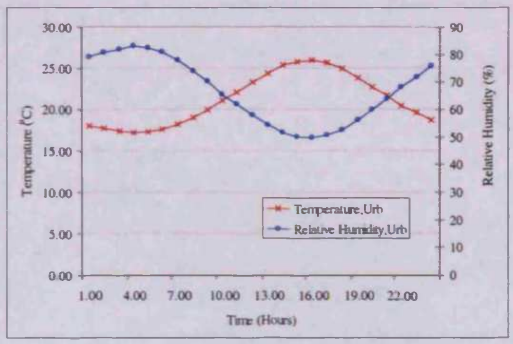

Figure 27. Air temperature and relative humidity for a typical day in July, Montreal

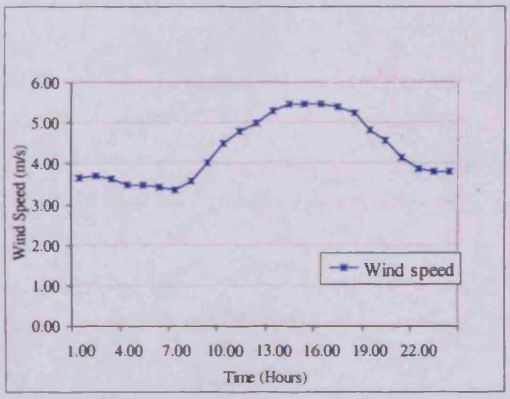

Figure 28. Wind speed for a typical day in July, Montreal

5.1.7. Moscow

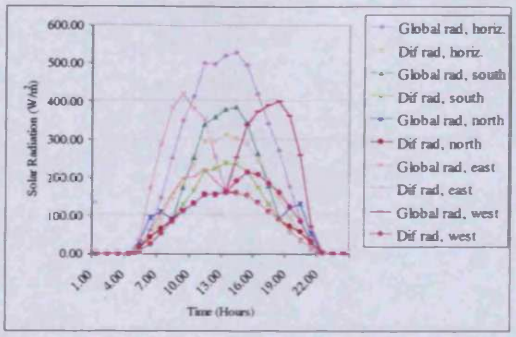

Figure 29. Global and diffuse solar radiation on horizontal plane and on vertical planes with east, west, south and north orientation for a typical day in July, Moscow

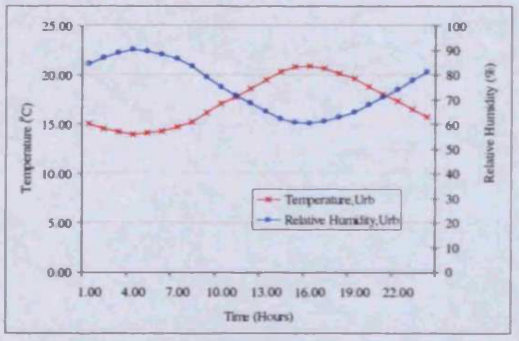

Figure 30. Air temperature and relative humidity for a typical day in July, Moscow

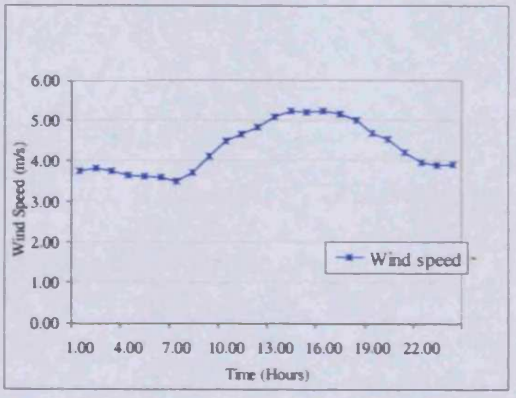

Figure 31. Wind speed for a typical day in July, Moscow

5.1.8. Mumbai

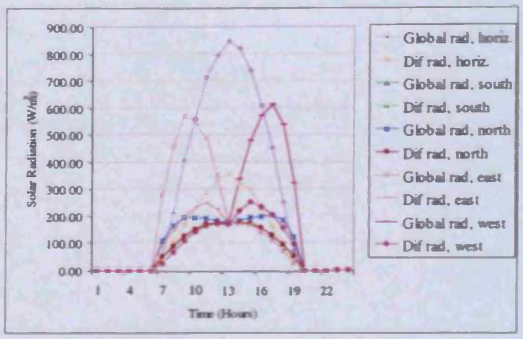

Figure 32. Global and diffuse solar radiation on horizontal plane and on vertical planes with east, west, south and north orientation for a typical day in May, Mumbai

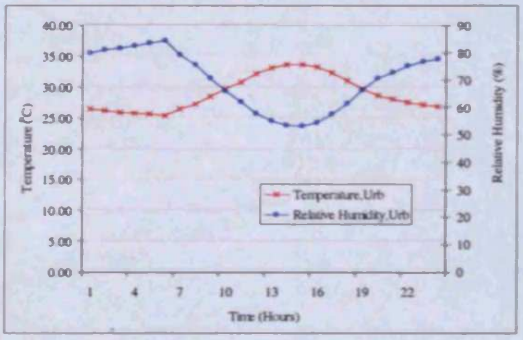

Figure 33. Air temperature and relative humidity for a typical day in May, Mumbai

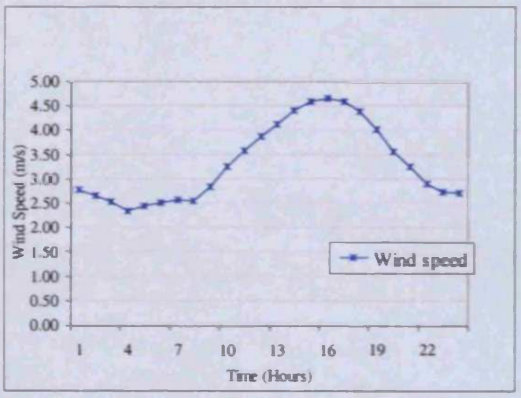

Figure 34. Wind speed for a typical day in May, Mumbai

5.1.9. Riyadh

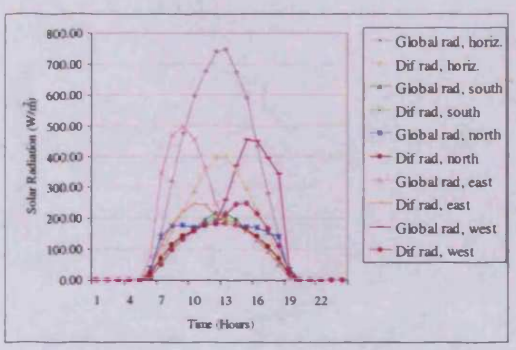

Figure 35. Global and diffuse solar radiation on horizontal plane and on vertical planes with east, west, south and north orientation for a typical day in July, Riyadh

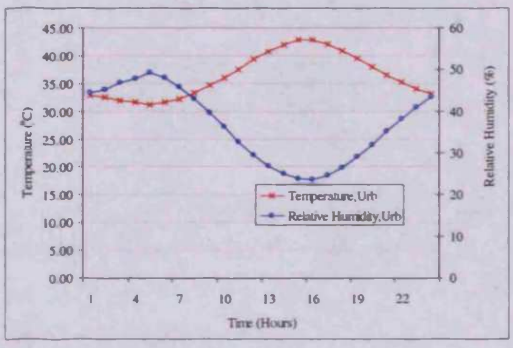

Figure 36. Air temperature and relative humidity for a typical day in July, Riyadh

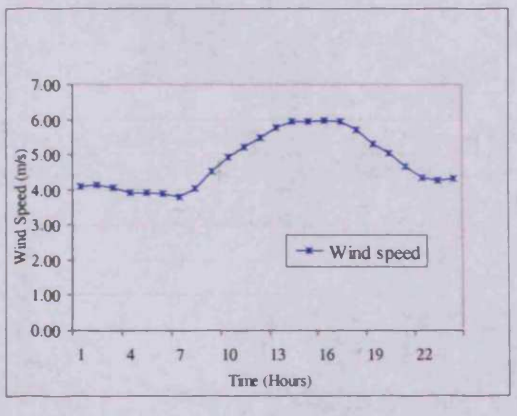

Figure 37. Wind speed for a typical day in July, Riyadh

5.2. Velocity Distributions

5.2.1. H5W10 canyon, Vertical Wind Flow

Figure 38. Air velocities in H5W10 canyon with vertical flow, for 3m/s input wind speed

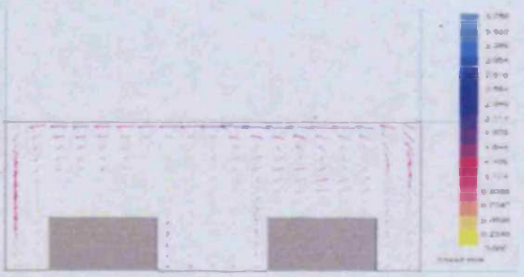

Figure 39. Air velocities in H5W10 canyon with vertical flow, for 4m/s input wind speed

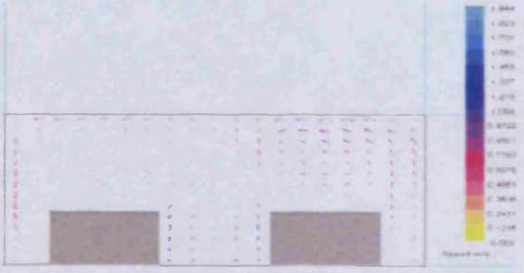

Figure 40. Air velocities in H5W10 canyon with vertical flow, for 5m/s input wind speed

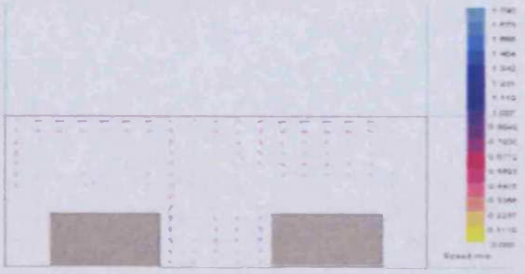

Figure 41. Air velocities in H5W10 canyon with vertical flow, for 6m/s input wind speed

5.2.2. H10W5 canyon, Vertical Wind Flow

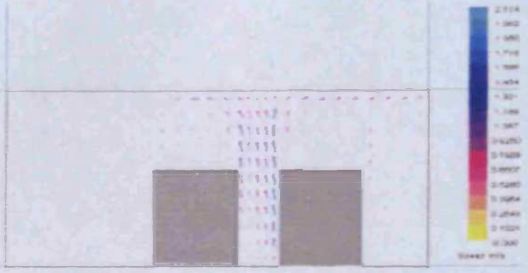

Figure 42. Air velocities in H10W5 canyon with vertical flow, for 3m/s input wind speed

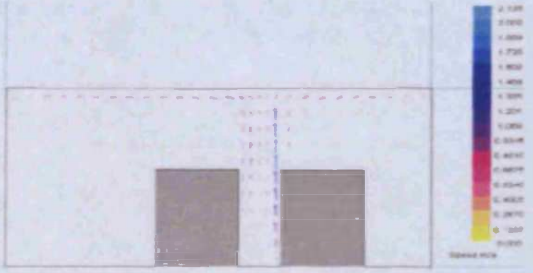

Figure 43. Air velocities in H10W5 canyon with vertical flow, for 4m/s input wind speed

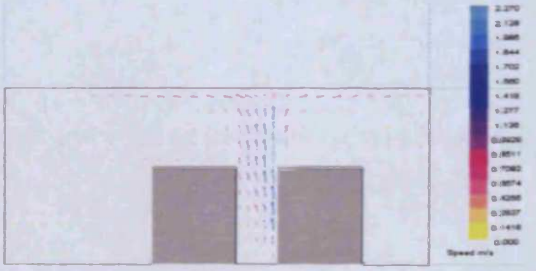

Figure 44. Air velocities in H10W5 canyon with vertical flow, for 5m/s input wind speed

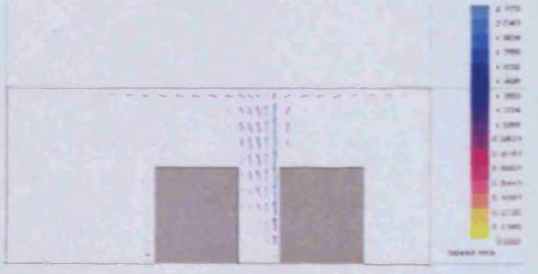

Figure 45. Air velocities in H10W5 canyon with vertical flow, for 6m/s input wind speed

5.2.3. H5W15 canyon,

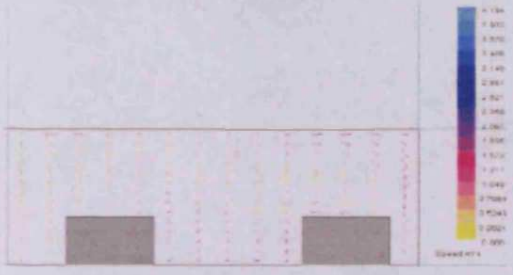

Figure 46. Air velocities in H5W15 canyon with vertical flow, for 3m/s input wind speed

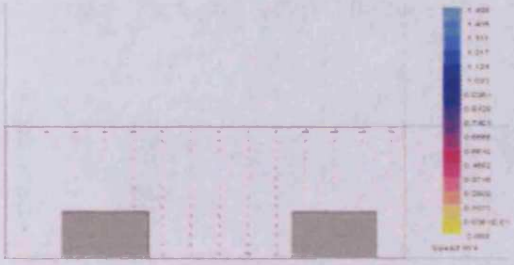

Figure 47. Air velocities in H5W15 canyon with vertical flow, for 4m/s input wind speed

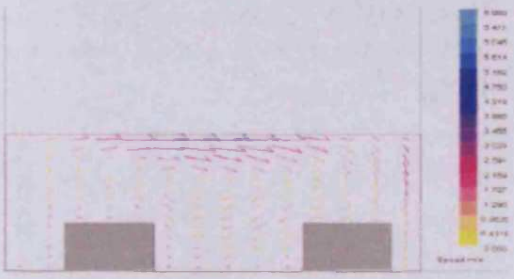

Figure 48. Air velocities in H5W15 canyon with vertical flow, for 5m/s input wind speed

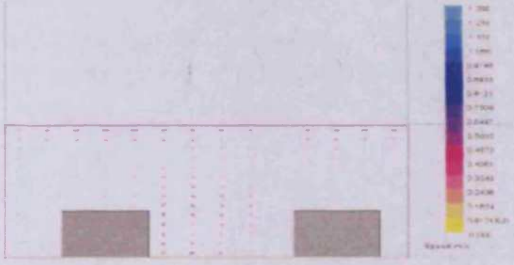

Figure 49. Air velocities in H5W15 canyon with vertical flow, for 6m/s input wind speed

5.2.4. H5W10 canyon, Parallel Wind Flow

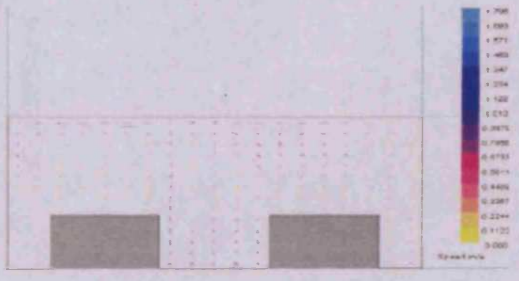

Figure 50. Air velocities in H5W10 canyon with parallel flow, for 3m/s input wind speed

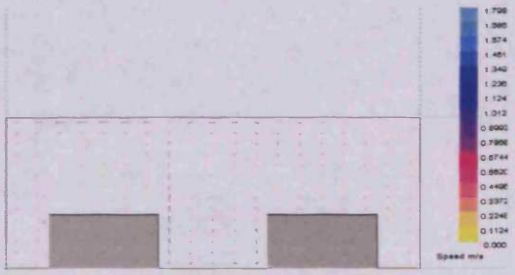

Figure 51. Air velocities in H5W10 canyon with parallel flow, for 4m/s input wind speed

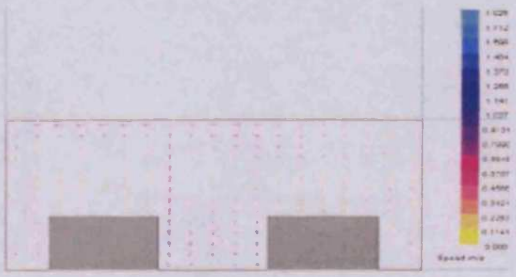

Figure 52. Air velocities in H5W10 canyon with parallel flow, for 5m/s input wind speed

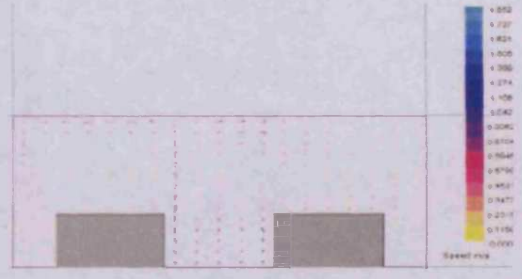

Figure 53. Air velocities in H5W10 canyon with parallel flow, for 6m/s input wind speed

5.2.5. H10W5 canyon, Parallel Wind Flow

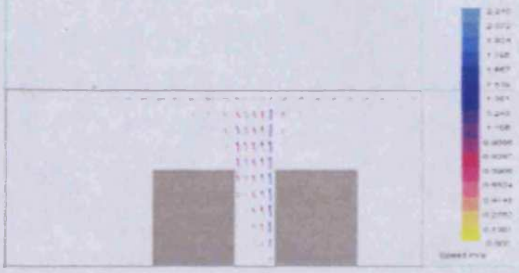

Figure 54. Air velocities in H10W5 canyon with parallel flow, for 3m/s input wind speed

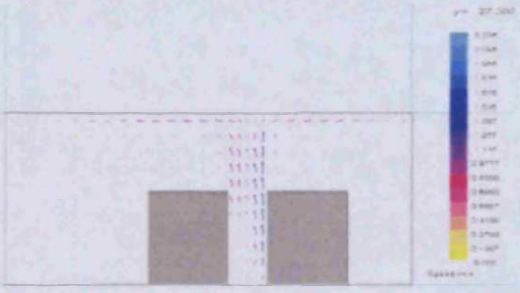

Figure 55. Air velocities in H10W5 canyon with parallel flow, for 4m/s input wind speed

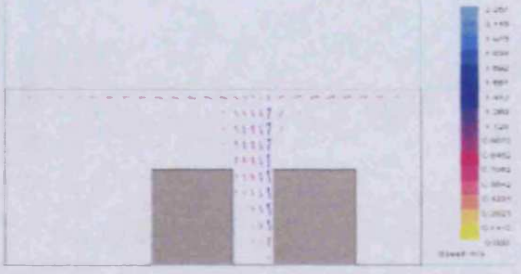

Figure 56. Air velocities in H10W5 canyon with parallel flow, for 5m/s input wind speed

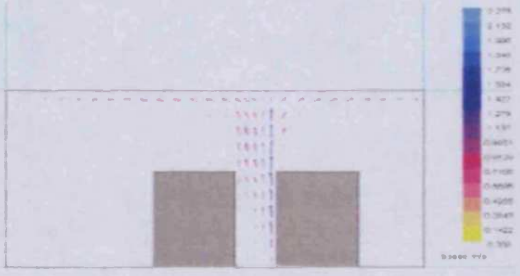

Figure 57. Air velocities in H10W5 canyon with parallel flow, for 6m/s input wind speed

5.2.6. H5W15 canyon, Parallel Wind Flow

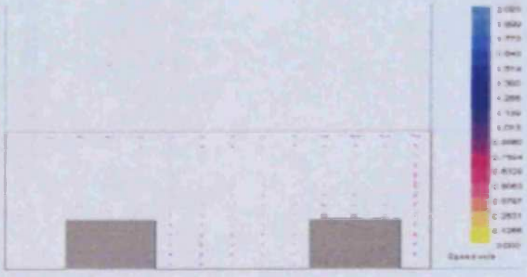

Figure 58. Air velocities in H5W15 canyon with parallel flow, for 3m/s input wind speed

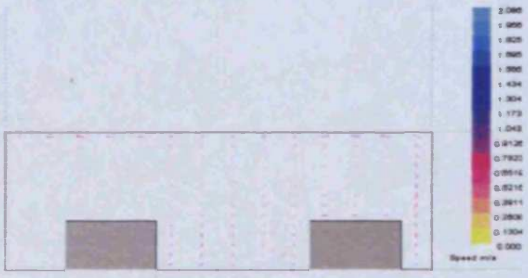

Figure 59. Air velocities in H5W15 canyon with parallel flow, for 4m/s input wind speed

Figure 60. Air velocities in H5W15 canyon with parallel flow, for 5m/s input wind speed

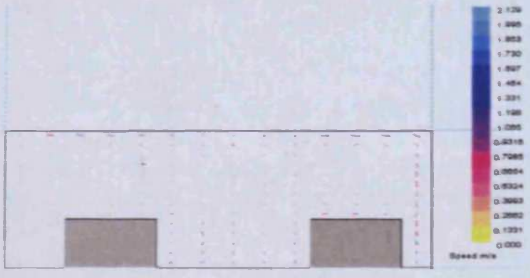

Figure 61. Air velocities in H5W15 canyon with parallel flow, for 6m/s input wind speed

5.3. Solar Geometry

5.3.1. Athens, H5W10 – EW

Asphalt

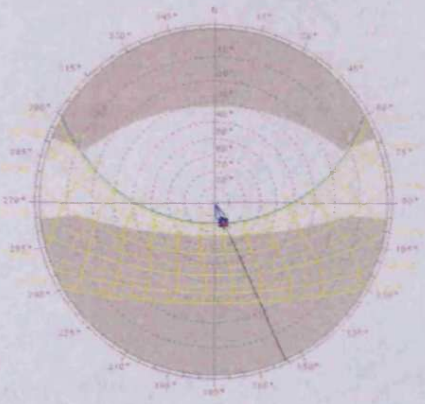

Figure 62. Sun-path diagram and shading for layer VIII on the asphalt of the EW H5W10 canyon, Athens

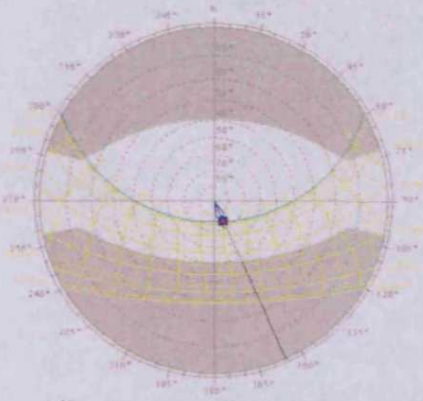

Figure 63. Sun-path diagram and shading for layer IX on the asphalt of the EW H5W10 canyon, Athens

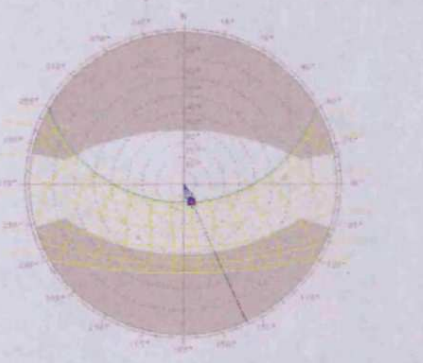

Figure 64. Sun-path diagram and shading for layer X on the asphalt of the EW H5W10 canyon, Athens

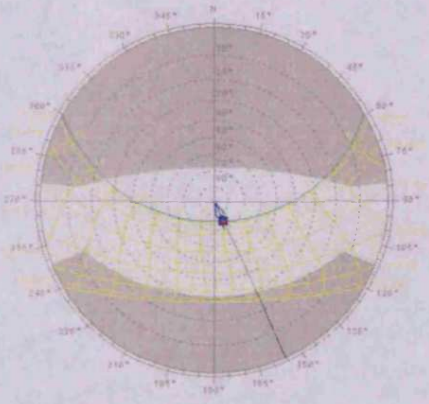

Figure 65. Sun-path diagram and shading for layer XI on the asphalt of the EW H5W10 canyon, Athens

South Wall

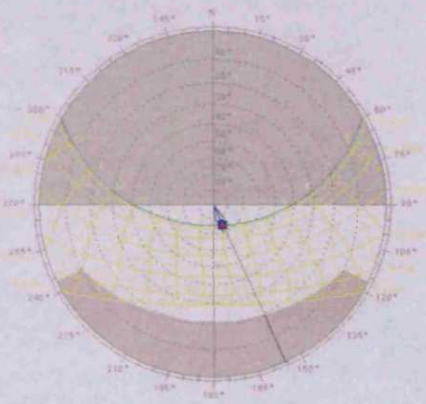

Figure 66. Sun-path diagram and shading for level a on the south wall of the EW H5W10 canyon, Athens

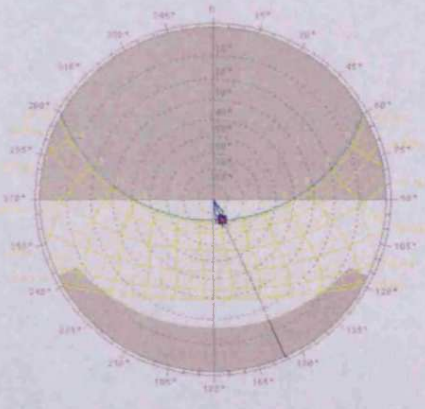

Figure 67. Sun-path diagram and shading for level b on the south wall of the EW H5W10 canyon, Athens

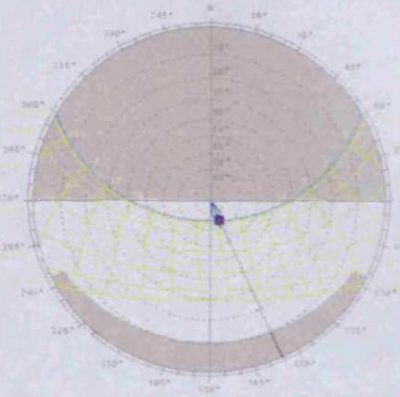

Figure 68. Sun-path diagram and shading for level c on the south wall of the EW H5W10 canyon, Athens

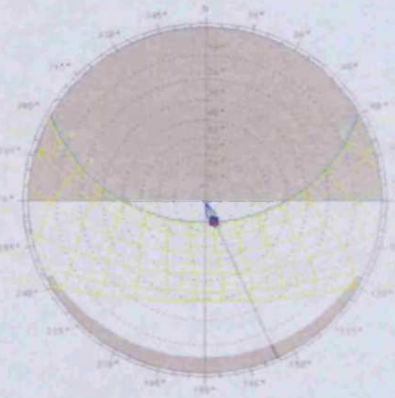

Figure 69. Sun-path diagram and shading for level d on the south wall of the EW H5W10 canyon, Athens

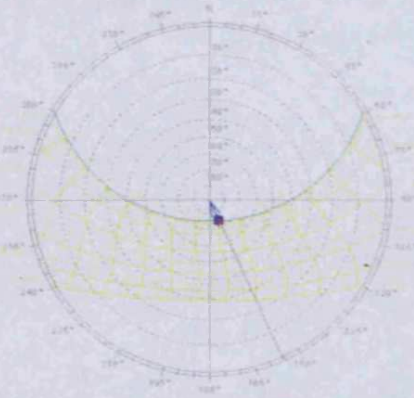

Figure 70. Sun-path diagram and shading for level e on the south wall of the EW H5W10 canyon, Athens

5.3.2. Athens, H5W10 – NS

Asphalt

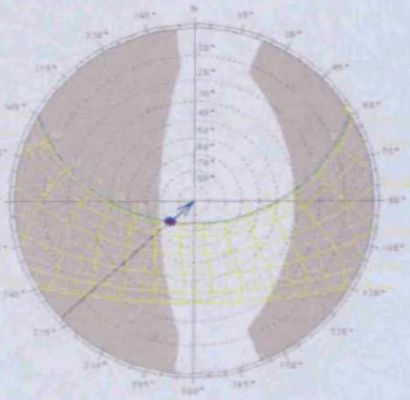

Figure 71. Sun-path diagram and shading for layer VIII on the asphalt of the NS H5W10 canyon, Athens

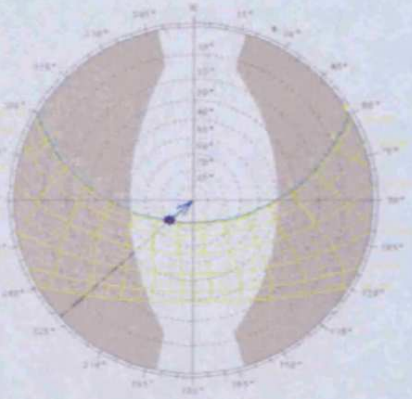

Figure 72. Sun-path diagram and shading for layer IX on the asphalt of the NS H5W10 canyon, Athens

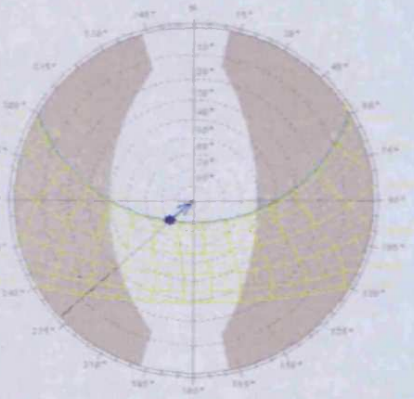

Figure 73. Sun-path diagram and shading for layer X on the asphalt of the NS H5W10 canyon, Athens

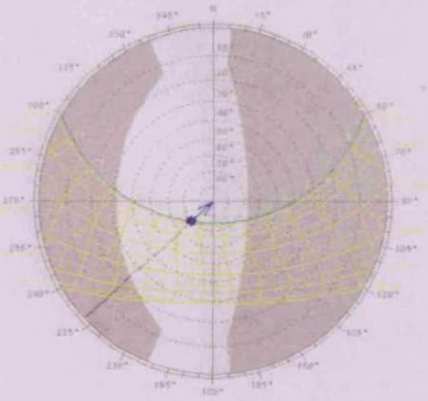

Figure 74. Sun-path diagram and shading for layer XI on the asphalt of the NS H5W10 canyon, Athens

West Wall

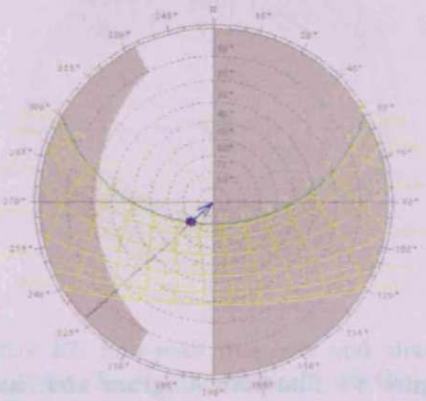

Figure 75. Sun-path diagram and shading for level a on the west wall of the NS H5W10 canyon, Athens

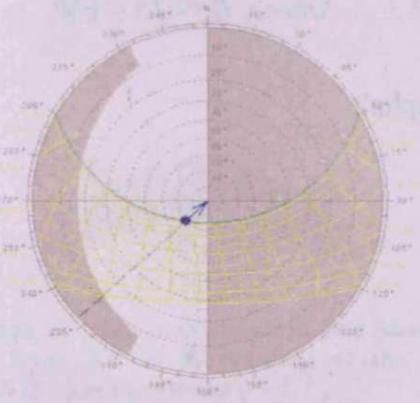

Figure 76. Sun-path diagram and shading for level b on the west wall of the NS H5W10 canyon, Athens

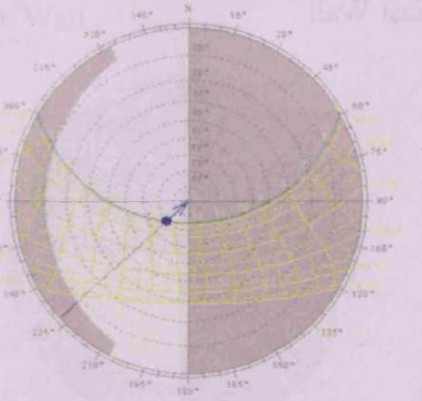

Figure 77. Sun-path diagram and shading for level c on the west wall of the NS H5W10 canyon, Athens

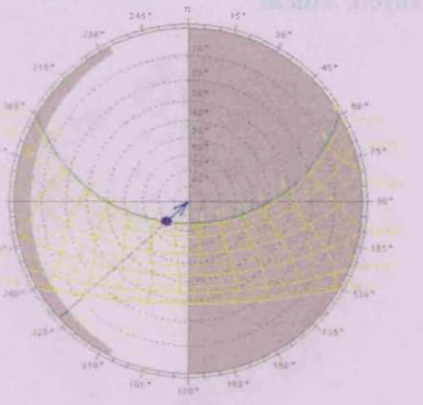

Figure 78. Sun-path diagram and shading for level d on the west wall of the NS H5W10 canyon, Athens

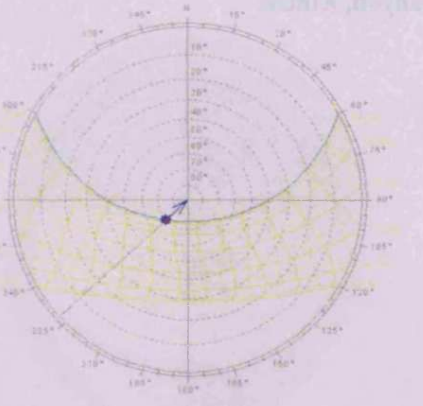

Figure 79. Sun-path diagram and shading for level e on the west wall of the NS H5W10 canyon, Athens

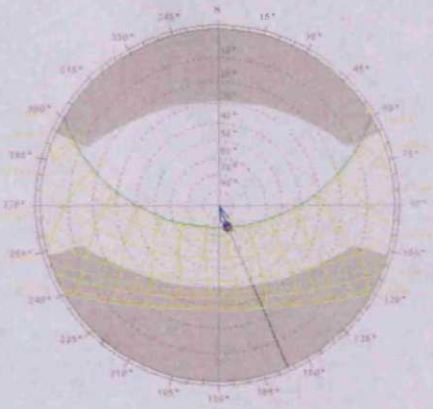

Figure 86. Sun-path diagram and shading for layer IX on the asphalt of the EW H5W15 canyon, Athens

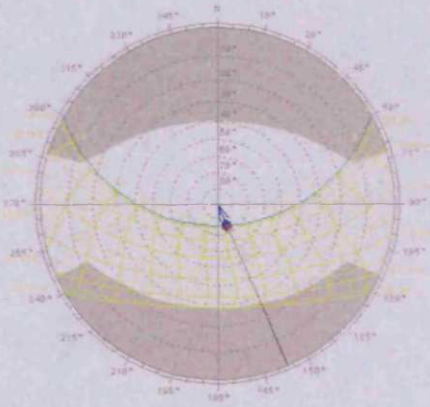

Figure 87. Sun-path diagram and shading for layer X on the asphalt of the EW H5W15 canyon, Athens

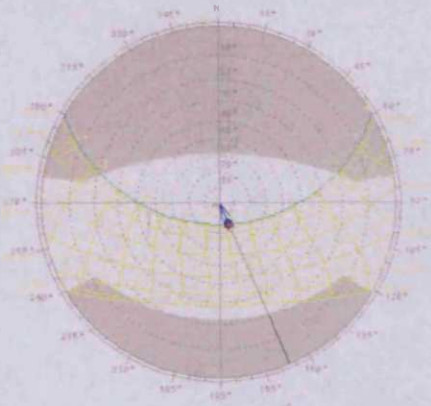

Figure 88. Sun-path diagram and shading for layer XI on the asphalt of the EW H5W15 canyon, Athens

South Wall

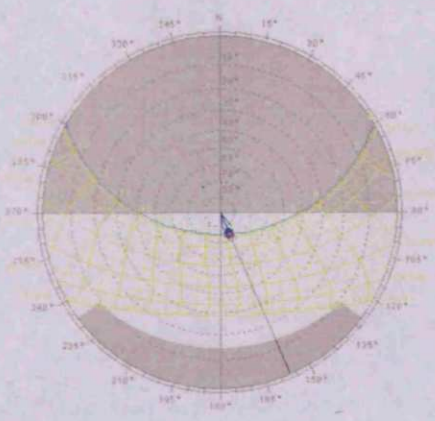

Figure 89. Sun-path diagram and shading for level a on the south wall of the EW H5W15 canyon, Athens

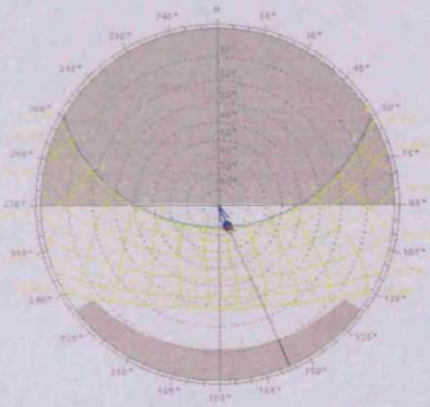

Figure 90. Sun-path diagram and shading for level b on the south wall of the EW H5W15 canyon, Athens

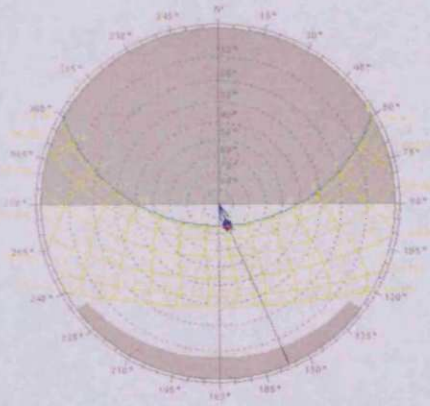

Figure 91. Sun-path diagram and shading for level c on the south wall of the EW H5W15 canyon, Athens

6. Appendix 6: Results

Due to the enormous amount of pages in which the graphs of the results of the 240 runs are presented, appendix 6 is enclosed in the attached cd-rom.